High Q Tunable Filters

by

Fengxi Huang

A thesis
presented to the University of Waterloo
in fulfillment of the
thesis requirement for the degree of
Doctor of Philosophy
in
Electrical and Computer Engineering

Waterloo, Ontario, Canada, 2012

AUTHOR'S DECLARATION

I hereby declare that I am the sole author of this thesis. This is a true copy of the thesis, including any required final revisions, as accepted by my examiners.

I understand that my thesis may be made electronically available to the public.

Abstract

Microwave tunable filters are key components in radar, satellite, wireless, and various dynamic communication systems. Compared to a traditional filter, a tunable filter is able to dynamically pass the required signal and suppress the interference from adjacent channels. In reconfigurable systems, tunable filters are able to adapt to dynamic frequency selection and spectrum access. They can also adapt to bandwidth variations to maximize data transmission, and can minimize interferences from or to other users. Tunable filters can be also used to reduce size and cost in multi-band receivers replacing filter banks. However, the tunable filter often suffers limited application due to its relatively low Q, noticeable return loss degradation, and bandwidth changing during the filter tuning.

The research objectives of this thesis are to investigate the feasibility of designing high Q tunable filters based on dielectric resonators (DR) and coaxial resonators. Various structures and tuning methods that yield relatively high unloaded Q tunable filters are explored and developed. Furthermore, the method of designing high Q tunable filters with a constant bandwidth and less degradation during the tuning process has been also investigated.

A series of novel structures of dielectric resonators have been proposed to realize in a high Q miniature tunable filters. The first type of TME mode DR filter is designed to be tuned by piezoelectric bending actuators outside the cavity, and has achieved a tuning range from 4.97 to 5.22 GHz and unloaded Q better than 536 over the tuning range. The second type of TME mode tunable filters are integrated with various tuning elements: GaAs varactors, MEMS switches, and MEMS capacitor banks are employed. The designed filter with MEMS switches operates at 4.72 GHz, and has achieved a tuning ratio of 3.5% with Q better than 510 over the tuning range. The designed filter with GaAs varactors operates at 4.92 GHz, and has achieved a tuning ratio of 2% with Q better than 170 over the tuning range. Finally, the designed filter with MEMS capacitor bank operates at 5.11 GHz, delivering a tuning ratio of 3.5% with Q better than 530 over the tuning range.

Cavity combline/coaxial resonators are also used in the design of high Q tunable filters. This thesis presents a novel approach to design a tunable cavity combline filter tuned by a MEMS switched capacitor bank. Instead of mechanically moving the tuning disk, the cavity combline filter is tuned with capacitances loading on the tuning disks, which are electrically adjusted by MEMS switched capacitor bank. The assembled 2-pole filter operates at 2.5 GHz with a bandwidth of 22 MHz, a tuning range of 110 MHz and a Q better than 374 over the tuning range. The assembled 6-pole filter operates at 2.6 GHz with a bandwidth of 30 MHz and has a tuning range of 44 MHz.

Finally, the design of high Q tunable filter with constant bandwidth is explored. A 4-pole high Q cavity combline tunable filter with constant bandwidth is demonstrated. The tuning has been realized manually and by using a piezoelectric motor respectively. The designed filter operates at 2.45 GHz and has achieved a stable bandwidth of 30 ±1.1 MHz over a tuning range of 400 MHz and an unloaded Q better than 3000. This design method for a constant bandwidth filter is applicable to both cavity combline filters and dielectric resonator filters.

Acknowledgements

I would like to express my special appreciation and sincere thanks to my supervisor Professor Raafat Mansour for all his support during my time at the University of Waterloo. It would be impossible for me to complete my PhD without his guidance and advice. His advice on both my research as well as on my career development are invaluable. I am also grateful to the members of my committee, Professor Safieddin Safavi-Naeini, Professor Slim Boumaiza, Professor Eihab Abdel-Rahman for the knowledge they provided during my research and Professor Ahmed A. Kishk from the Department of Electrical and Computer Engineering at Concordia University for taking the time to serve as my external examiner.

It was such a great privilege for me to be a member of the Centre for Integrated RF Engineering (CIRFE), which has attracted many talents. Special thanks go to my colleague Dr. Siamak Fouladi Azarnaminy for his help and for sharing his expertise especially in the last two year of my study. I would also like to thank Dr. Mohamed Fahmi and Dr. Dong Yan for their valuable discussions, and Dr. Nino Zahirovic, Dr. Paul Laforge, Mr. Bill Jolley and my colleagues in CIRFE for their assistance, support and friendship.

I would like to acknowledge the financial support from University of Waterloo, Natural Sciences and Engineering Research Council of Canada (NSERC), COM DEV International Ltd., Huawei Technologies Canada Co., Ltd.

Finally, I would like to thank my parents and my sisters for their love and support. I would also like to thank my son, Hanyu, for his love, and he is my pride. Final thanks to my wife, Jin, for all her patience, love, support and encouragement that allowed me to achieve this important goal of my life.

Table of Contents

List of Figures

List of Tables

.

Chapter 1

Introduction

1.1 Motivation

In recent years, the spectrum for wireless communication has become much more crowded, which has made designing radio devices and base station transceivers a great challenge. The high Q tunable filter is a potential solution to solve this kind of challenge in front-end receivers. In modern wireless communication systems, the receivers always operate in the presence of large interfering signals from adjacent channels. A high Q narrow band tunable filter is much more effective for suppressing interference from adjacent channels. A high Q narrow bandpass tunable filter would also suppress Inter-Modulation (IM) signals from interfering with the receiver.

High Q tunable microwave filters can also be used in flexible systems to meet the dynamic requirements. For example, in the Software-Defined Radio (SDR) system, with a high Q tunable filter used after the antenna matching circuits, the RF front-end transceiver is able to dynamically pass the desired signal, suppress undesired signals in the receiving mode; and with a tunable filter employed before the power amplifier, the RF front-end transceiver can synthesize the RF signal in the transmitting mode without introducing noise or spurious emissions at other frequencies [1].

Tunable filters are quite in demand for self-adapted systems, such as the cognitive radio. Based on the active monitoring of several factors in the external and internal radio environment, the cognitive radio can adapt for the spectrum regulator, the network operator, and the user objectives [1]. The tunable filters employed in a cognitive radio are able to dynamically adapt the transceivers' frequency selection, spectrum access, and bandwidth variation for maximizing data transmission, and minimizing the interference from or to other users. Additionally employing

tunable filters in transceivers for both dynamic band selection and noise suppression is an optimal solution for an unfriendly user environment.

Tunable filters are used in systems using multi-band receivers, like the Joint Tactical Radio System (JTRS) [2]. Presently, filter banks are employed to achieve system requirements for all receiving bands due to the limited coverage of a single filter. To improve the system performance, replacing the filter bank with a tunable bandpass filter can significantly reduce the filter volume and the complexity of the whole system. The system's reliability also substantially increases due to fewer components used in the system. Therefore, the whole system's performance can be improved [3].

In most of these applications, the insertion loss of a tunable filter is a key design parameter, which is decided by the unloaded Q of the filter resonator and filter bandwidth. The insertion loss impacts directly the system's noise figure, the transmitted power, and the system's performance. To design a tunable filter with a low insertion loss, both the resonator configuration and the tuning techniques should be considered.

The categories of resonators mainly employed in microwave filters include: lumped element, microstrip, superconductor, coaxial, dielectric resonator, and waveguide. Figure 1.1-1 shows the relationship between the unloaded Q and the relative size of typical microwave resonators [4]. There are a wide range of resonator configurations in each resonator category. The Q value is the key challenge in designing the resonator to meet the requirements, and it varies widely for each resonator category. Once these resonators are loaded with the tuning elements, the overall unloaded Q will be further reduced. Superconductor filters can offer unloaded Q values ranging from 20,000 to 50,000, however, the superconductor filters need to be cooled down to very low temperatures. Three Dimensional (3D) resonators, which include coaxial, dielectric resonator, and waveguide, offer an unloaded Q value ranging from 3,000 to 30,000 at 1 GHz. 3D resonators are widely employed to construct filters for low loss wireless and space communication systems.

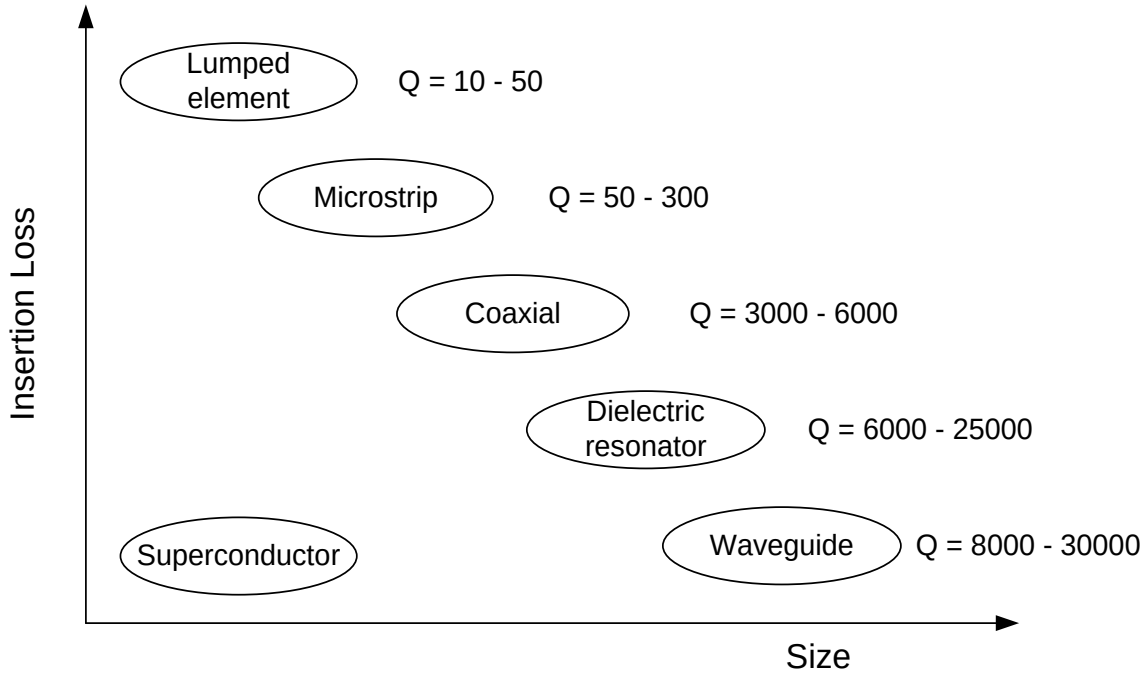

Figure 1.1-1 The relative insertion loss and size of various resonators [4]

Dielectric resonators can operate at various modes, offering tunable filter designers the flexibility to select tuning elements that can easily interact with the field distribution of a particular mode. Dielectric resonators can also be easily machined to various shapes by using low-cost water jet machines, which allow easy realization of various resonator configurations [5, 6]. Therefore, tunable dielectric resonator filters are investigated in this thesis. Tunable coaxial resonator filters are also studied in this thesis due to their low cost and relatively high Q factors.

The tuning technologies currently employed in tunable filters include mechanical tuning, piezoelectric tuning, magnetic tuning, semiconductor varactor tuning, ferroelectric film tuning, and MEMS tuning. Traditional mechanical tuning elements are inexpensive, easy to fabricate, and have very low loss. However, they are large in size and have a rather low tuning speed. Magnetic tunings are realized by using ferrite material to tune the magnetic field in the resonators. Ferrite materials are able to handle large power levels and have a fast switching speed; however, ferrite based circuits are large in size, high in power consumption, and have difficulties in integration. A semiconductor diode consists of a p-n junction; the junction capacitance can be controlled by a reverse bias voltage. Nevertheless, the internal resistance in a diode causes loss and limits its application for high Q microwave filters. Ferroelectric films can

be made as a varactor for a tunable filter since they offer fast tuning speed, low power consumption, and ease of integration. However the Q factor of the ferroelectric film varactor limits its application in high Q tunable filters.

Piezoelectric tuning retains the advantages of mechanical tuning while having a relatively small size. Thus, piezoelectric tuning elements are investigated in the thesis. MEMS tuning circuits are realized by the physical movement of a component, which changes the capacitance or inductance of the device. MEMS tuning devices are investigated due to their properties of low loss, high power handling, and high linearity at microwave frequencies.

The integration of high Q resonators and low loss tuning elements is a key factor in realizing high Q tunable filters. In this thesis, the integration of 3D resonator filters with tuning elements including piezoelectric actuators, semiconductor varactors, and MEMS tuning devices are investigated.

1.2 Objectives

The purpose of this thesis is to investigate the feasibility of designing high Q coaxial and dielectric resonator tunable filters. This includes exploring novel DR configurations that are amenable to integration with high Q tuning circuits. Additionally, techniques to realize high Q tunable filter with constant bandwidth are investigated. The research topics in this thesis are:

- Development of high Q dielectric resonator configurations that are amenable to integration with tuning elements such as piezoelectric devices, MEMS devices, and GaAs varactors.
- Investigation of techniques to increase the tuning range of high Q tunable dielectric resonator filters.
- Investigation of techniques to develop high Q tunable filters with a constant bandwidth.

1.3 Thesis Outline

Following the motivation and objectives presented in Chapter 1, Chapter 2 reviews the literature on tunable filters, tuning elements, tuning methods, and different technologies for maintaining a constant bandwidth for tunable filters. Chapter 3 presents the external tuning of single mode and dual mode DR filters integrated with piezoelectric tuning elements. Chapter 4 introduces a novel structure of DR filter integrated with MEMS switches, GaAs varactors and

MEMS varactors. In Chapter 5, a coaxial tunable filter with a constant bandwidth is illustrated. In Chapter 6, coaxial tunable filters based on MEMS technology for discrete tuning are demonstrated. In Chapter 7, a summary of the research contributions of this thesis and suggestions for future research is provided.

Chapter 2
Literature Survey

In this chapter, a literature survey of tuning technologies for the tunable filter will be presented. The survey includes the tuning mechanism, the tuning method, and the technique of tunable filter with a constant bandwidth. The tuning mechanism is introduced in the first section, and then the updated tuning methods for tunable filters will be listed. The technology used for tunable filter with an absolute constant bandwidth over the tuning range will be presented in the last section.

2.1 Tuning Mechanism

A microwave filter is made up of an input, an output, and some microwave resonators coupled to each other and all resonators operate at the same frequency. In a circuit model, a resonator consists of a resistor (R), an inductor (L) and a capacitor (C). The resistor represents the loss in the resonator, while the inductor (L) and the capacitor (C) decide the resonant frequency of the resonator. Figure 2.1-1 illustrates a circuit model of a two-pole lossless filter. The filter's resonant frequency f_0 equals to $\frac{1}{2\pi\sqrt{LC}}$ ($f_0 = \frac{1}{2\pi\sqrt{LC}}$). Therefore, tuning the filter's center frequency f_0 is equivalent to tuning the capacitance C, or the inductance L, or both the capacitance and the inductance of the entire resonator. The bandwidth is controlled by the inter-resonator coupling and the input/output coupling. So the bandwidth tuning can be realized by changing the input/output coupling and the inter-coupling between the resonators. With the exception of a few publications, most published papers only report tunable filters being realized by tuning the resonant frequency of the resonators, and the constant bandwidth cannot be maintained over the tuning range.

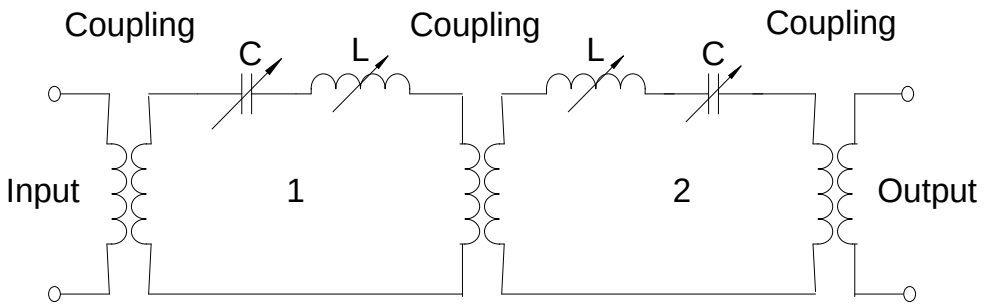

Figure 2.1-1 Circuit model of a two-pole tunable filter

2.1.1 Capacitance Tuning

The most straight forward way of designing a tunable filter is to deploy capacitance tuning elements [7-10]. Figure 2.1-2 illustrates a tunable filter loaded with capacitance tuning circuits [11]. Each microstrip resonator is assembled with a pair of orthogonal bias capacitance banks C_L and C_M to achieve the frequency tuning response. The schematic views of the capacitance banks C_L and C_M are displayed in Figure 2.1-3. The capacitance bank C_L is used for the resonator frequency tuning, and the capacitance bank C_M is designed for the impedance matching of the tunable filter's input/output. The whole capacitance values and the required capacitance values at each tuning step of the tunable filter are obtained by using a full-wave simulation.

The paper [11] shows that when the designed capacitance bank C_L values change from 190fF to 550fF and the capacitor C_M values change from 270fF to 450fP, the filter's center frequencies are tuned from 5.19 GHz to 4.17 GHz. The measured filter tuning responses are shown in Figure 2.1-4, and the data at each step are displayed in Table 2.1-1.

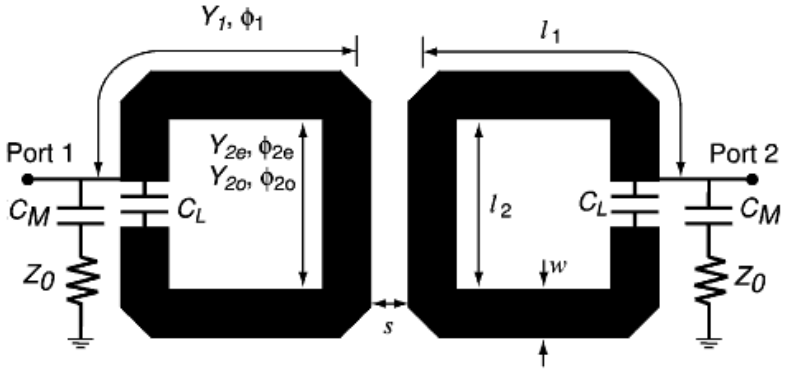

Figure 2.1-2 Schematic view of a filter loaded with a capacitance tuning circuit [11]

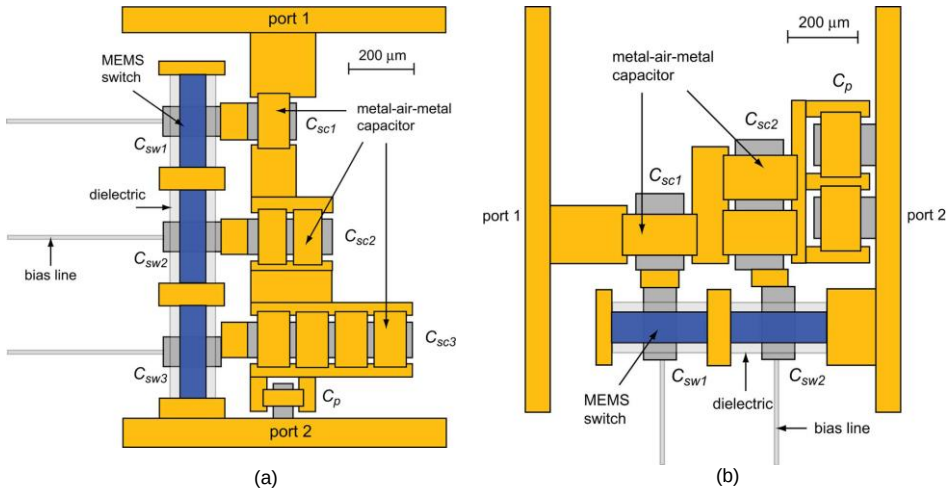

Figure 2.1-3 Schematic view of capacitor banks [11] **: (a) C_L and (b) C_M**

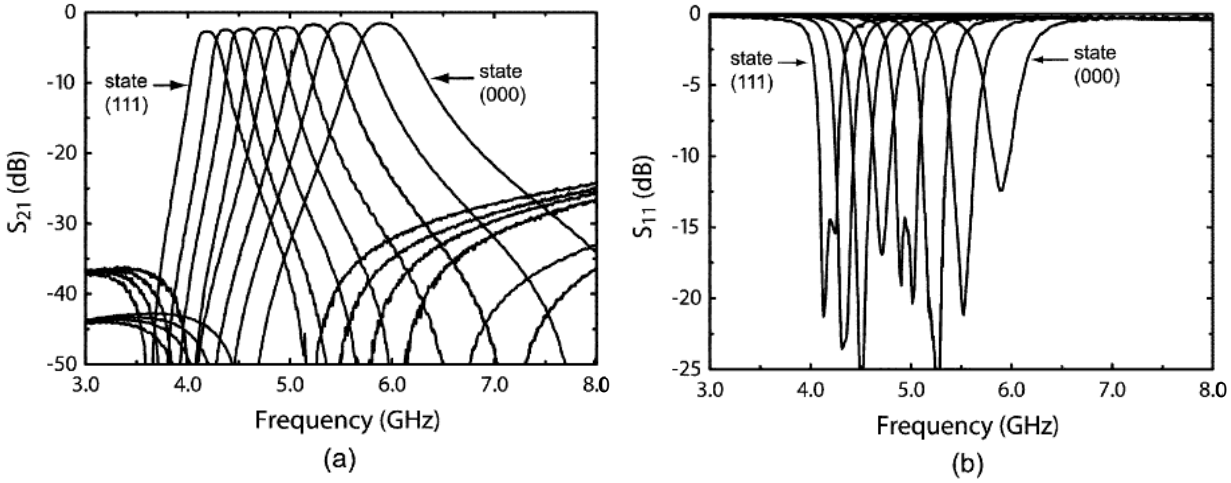

Figure 2.1-4 Measured filter tuning response [11]: (a) insertion loss and (b) return loss

Table 2.1-1 Measured eight states of the RF-MEMS filter [11]

C_L (state)	111	110	101	100	011	010	001	000
in (fF)	550	480	430	380	340	290	240	190
C_M (state)	11	11	10	10	01	01	00	00
in (fF)	450	450	390	390	330	330	270	270
fo (GHz)	4.17	4.38	4.56	4.76	4.97	5.24	5.53	5.91

2.1.2 Inductance Tuning

The circuit model of the resonator illustrates that changing the inductance of the resonator is an alternative solution to design a tunable filter. Compared with the publications on capacitance tuning, there are very limited publications on tunable filters using inductance tuning.

Figure 2.1-5 (a) illustrates a bandpass filter based on inductance change [12]. The filter consists of three resonators and four series coupling Metal-Insulator-Metal (MIM) capacitors. The tuning approach is to change the inductance values of each resonator while all the capacitance values are kept constant. The inductance change is achieved by changing the length of the short-stub using a metal-metal contact switch. The equivalent circuit model of the resonator is shown in Figure 2.1-5 (b), which illustrates the configurations of the inductance tuned resonator. The measurement results plotted in Figure 2.1-6 (a) and (b) show that the center frequency of the tunable filter shifts from 8 to 12.3 GHz, and that the 3dB bandwidth maintains about 10 % over the tuning range. However, the insertion loss varies from 9 dB to 11 dB. The measured single resonator responses are plotted in Figure 2.1-6 (c). Based on the circuits' mode in Figure 2.1-5 (b), the extracted RLC values from the measurements are listed in Table 2.1-2. The circuit simulation results based on the elements' values extracted from the measurements are given in Figure 2.1-6 (c) as well. The quite agreement between the simulations and measurements verifies the validity of the proposed equivalent circuit model. The designed filter is tuned by inductance changing.

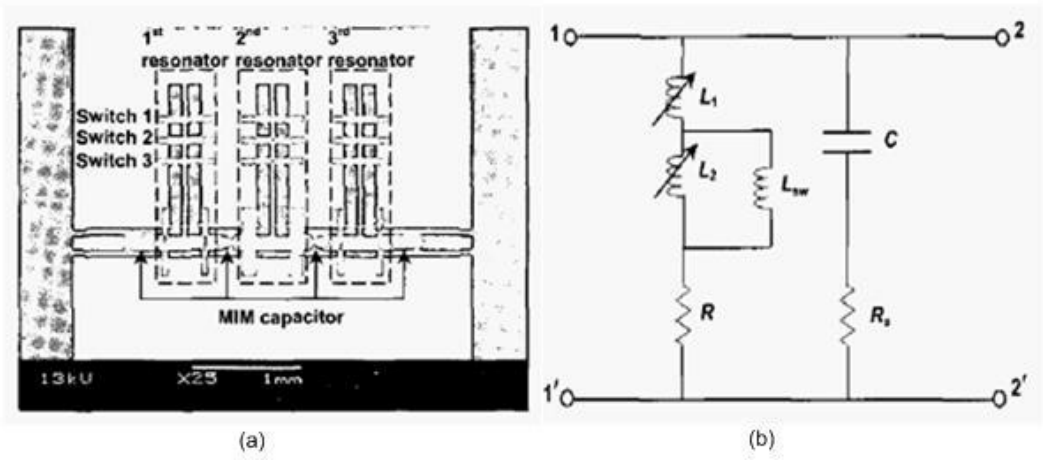

Figure 2.1-5 (a) SEM image of the tunable BPF and (b) the equivalent circuit of the resonator [12]

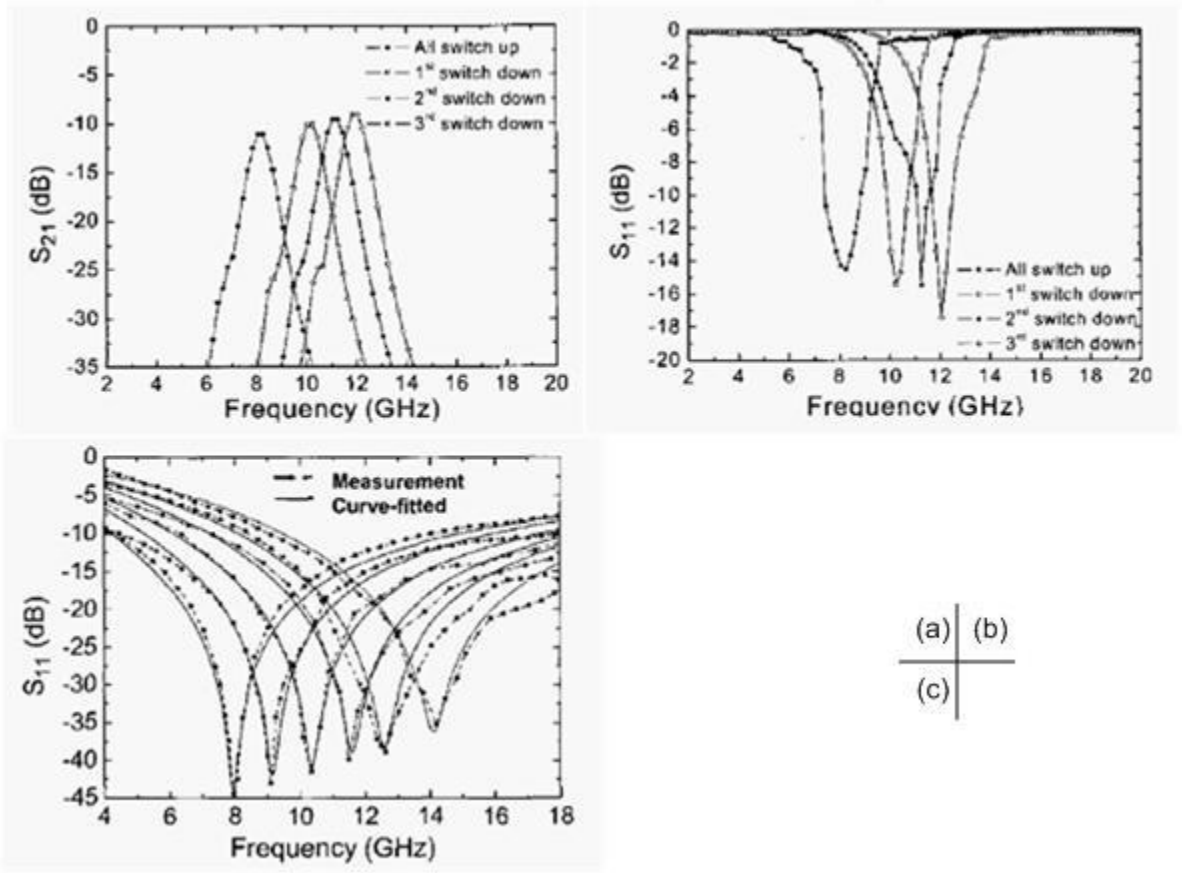

Figure 2.1-6 Measured tuning responses of a MEMS BPF with an inductance change [12]**: (a) insertion loss, (b) return loss, and (c) measurement and curve-fitted results of a single resonator.**

Table 2.1-2 Curve-fitted values of the lumped elements in the tunable resonator [12]

Lumped elements	Curve – fitted values					
F_0(GHz)	8.0	9.2	10.5	11.7	12.8	14.0
C (fF)	190	190	190	190	190	190
L_1 (nH)	2	1.5	1.23	0.98	0.83	0.66
L_2 (nH)	0	0.5	0.77	1.02	1.17	1.34
Lsw (pH)	20	20	20	20	20	20
R (Ω)	1.8	1.6	1.6	1.6	1.4	1.4
Rsw (Ω)	0.8	0.8	0.8	0.8	0.8	0.8

2.2 Tuning Method

Tunable filters are a very attractive choice in radar and communication systems, especially in multiband communication systems. By employing tunable filters, the complexity and cost of the system are significantly reduced, and the overall performance is improved. Overall there are six technologies used in the design of the tunable circuits for tunable filters. They are mechanical tuning, piezoelectric tuning, semiconductor varactor tuning, ferroelectric materials film tuning, ferrite materials tuning, and MEMS tuning.

2.2.1 Mechanical Tuning

The earliest forms of tunable circuits were based upon mechanical tuning, and their design principles are well explained in the literature [13]. Mechanical circuits are inexpensive and easy to fabricate, have very low loss, and possess a high power handling capability. The problem however, is that they are large in size and have a rather low tuning speed. Although the specifications for a compact size, light weight, and fast tuning time have been the driving force for modern communication systems, mechanical tunable filters still attract attention due to their unbeatable power handling capability and high quality factor. Mechanical tuning has been realized in dielectric resonator, coaxial, and waveguide configurations [14-18]. The tunings of such mechanical tunable filters are accomplished by human labour or electrical motors.

Dielectric resonators are widely used in microwave communication systems due to their superior performance over other resonators. They offer a high unloaded Q and have excellent temperature stability. Figure 2.2-1 (a) and (b) demonstrates a configuration of a loaded resonator with its tuning element [19]. The big dielectric ring is the main resonator body, and the dielectric plug is the tuning element. A wide tuning range is obtained while other properties of the resonator are maintained over the whole range. The measured responses of the designed filter are plotted in Figure 2.2-1 (c). As seen from the figure, the filter can be tuned from 1930 to 1990 MHz. The relationship between the unloaded Q and the travel range of the tuning element is plotted in Figure 2.2-1 (d). Such a large travel range of the tuning element, which is more than 600 um, can only be realized by mechanical tuning.

The DR tunable bandpass filter presented in [19] has displayed good tuning properties in terms of the filter size and tuning range, but, the filter's tuning speed is very low due to the large travel distance of the tuning element and screw-like configuration.

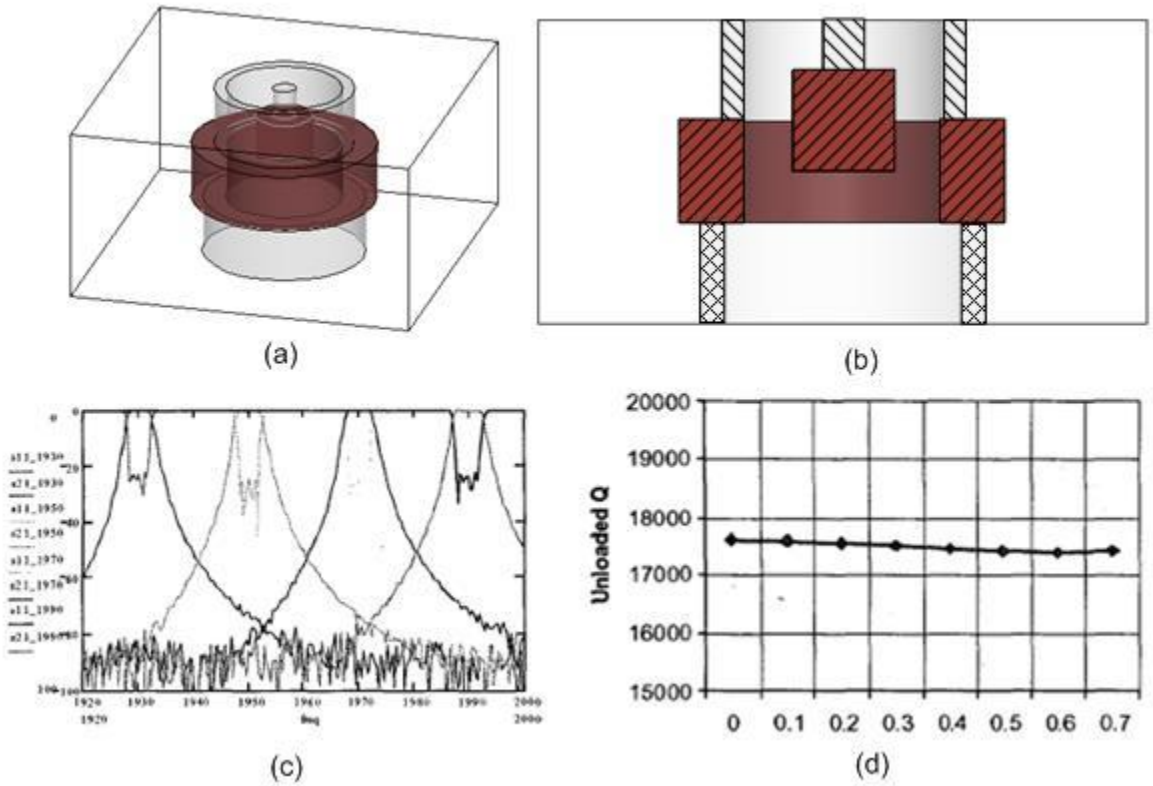

Figure 2.2-1 (a) 3D configuration of a loaded resonator, (b) a cross section view of the resonator, (c) the measured filter tuning response, and (d) the unloaded Q of the resonator versus travel range of the tuning element [19]

2.2.2 Piezoelectric Tuning

Employing a piezoelectric actuator can solve the problem of the tuning speed and retain the advantageous properties of mechanical tuning. Utilizing a piezoelectric actuator in a tuning dielectric resonator filter was first reported by Wakino in 1987 [20]. Since then, piezoelectric actuators have been widely employed in all types of filters, such as in the planar tunable filter [21], the LTCC filter [22], the cavity filter [23], and the dielectric resonator filter [24, 25]. Figure 2.2-2 exhibits the two tunable dielectric resonator configurations in Wakino's patent [20]: (a) an inserted piezoelectric actuator tuning method, and (b) an inserted piezoelectric actuator attached with a DR disk tuning method. The inserted tuning element is placed over the top of the

resonator. The piezoelectric bending actuator is controlled by an applied DC voltage, and the resonant frequency is tuned by controlling the gap between the resonator and the tuning element. When the gap becomes smaller, the loading of the resonator increase. Therefore, the resonance frequency of the DR resonator drops. Wakino reported a tuning range of 8% as the gap varies from 1 to 5 mm (Figure 2.2-2a), and the actuator attached with DR disk reported a 12% tuning range (Figure 2.2-2b).

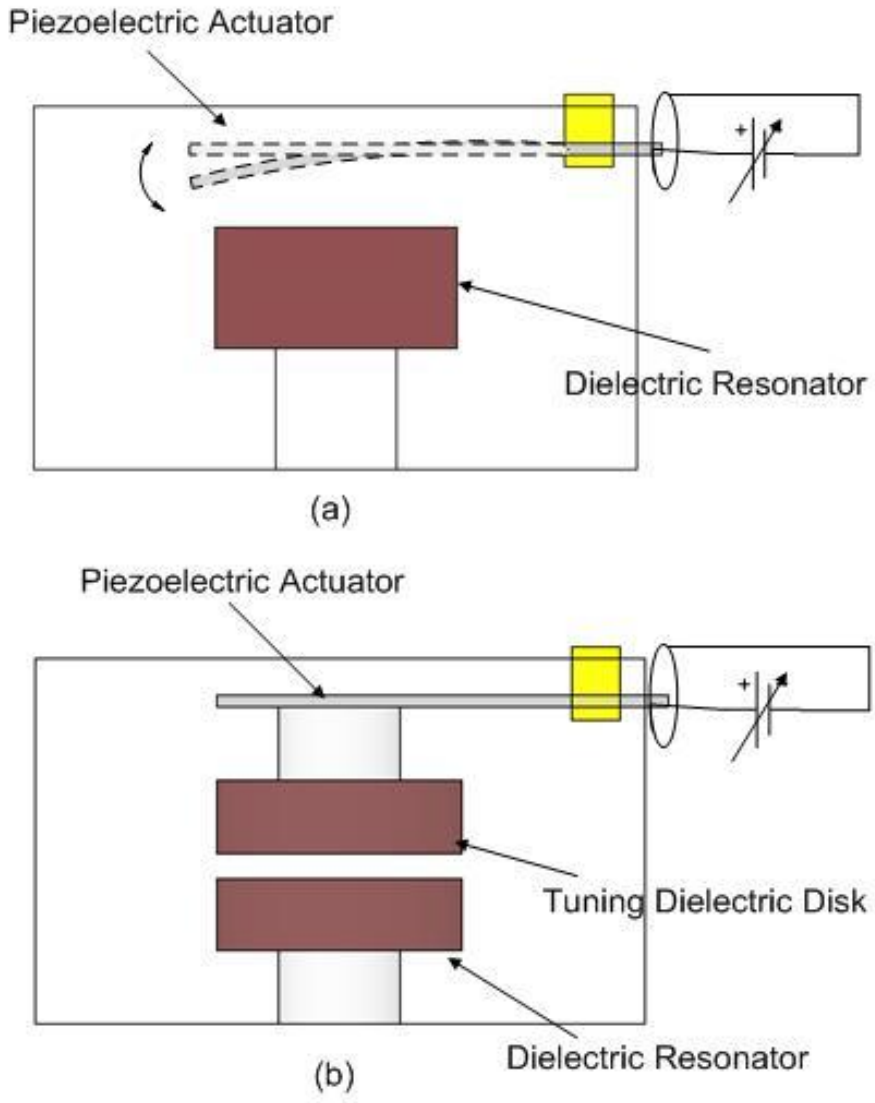

Figure 2.2-2 Tunable dielectric resonators in [20]**: (a) an inserted piezoelectric actuator tuning method, and (b) an inserted piezoelectric actuator attached with a DR disk tuning method.**

Figure 2.2-3 (a) is a schematic view of the tunable dielectric resonator with an application of plate piezoelectric actuated switches [25]. The tunable resonator comprises of three basic

components: a dielectric resonator operating at the TE_{01} mode, a metal disk consisting of a number of radial-arranged quarter-wave slotline resonators, and piezoelectric actuated switches for each slotline resonator. The tunability is obtained by controlling the inter-mode coupling between the dielectric resonator and the slotline resonators. As plotted in Figure 2.2-3 (b), when the switches are at the 'OFF' state, each slotline resonator possesses a strong magnetic coupling with the dielectric resonator. This leads to an increase of the effective room of the resonator and results in a decrease of the resonant frequency of the TE_{01} mode. When the switch is at the 'ON' state, the slotline becomes a half-wave length resonator. Due to the change of the magnetic field in the middle of the slotline, the coupling between the slotline and the dielectric resonator becomes weaker, and the resonant frequency of the TE_{01} mode increases due to the decrease of the effective size of the resonator.

The test results reveal a tuning range of 5 MHz at approximately 2 GHz with a discrete frequency step of 0.25 MHz. This tunable dielectric resonator maintains an unloaded quality factor larger than 12,000 over the whole tuning range. Piezoelectric actuators are employed as switches to close the slotline resonators; and the post-switching oscillation decay within 1 millisecond after the piezoelectric actuators are triggered.

Figure 2.2-4 (a) and (b) exhibit a schematic view of a tunable 2-pole filter based on a dual mode dielectric resonator with a piezoelectric bimorph actuated tuning element [26]. The resonator with a constant of 80, a diameter of 14.2 mm and a height of 7.2 mm is placed in a silver-plated cavity with a diameter of 35 mm and a height of 20 mm. The resonant frequency and Q factor are dependent on the gap between the tuning disk and the resonator. A piezo bimorph actuator is used to accurately control the movement of the tuning disk as shown in Figure 2.2-4 (a). Adjustable screws are used to control the inter-coupling of the dual modes. Input and output connectors are placed at 90 degrees as shown in Figure 2.2-4 (b). The resonator operates at the HE_{11} mode.

A circular piezoelectric bimorph with a diameter of 25 mm and a thickness of 1 mm is used to drive the metal disk towards the dielectric resonator. This displacement at the center of the bimorph is ~ 140 um with a 300 v bias voltage.

The measured results of the insertion loss and return loss of a Ba-La-Ti-O ceramic based 2-pole DR dual mode filter are 1.0 dB and 15 dB respectively, as shown in Figure 2.2-4 (c). When

the filter is tuned from 2.235 to 2.45 GHz, the insertion loss is less than 2.5 dB over the entire tuning range (shown in 2.2-4d). Also reported in [26] is an alternative dielectric resonator, the Ba-Zn-Ta-O ceramic based dielectric resonator. This dielectric resonator achieves a much higher Q, with 3500 at 2 GHz, and a bandwidth of 0.3-0.5%. Its center frequency tuning ($\Delta f/f$) is ~7%.

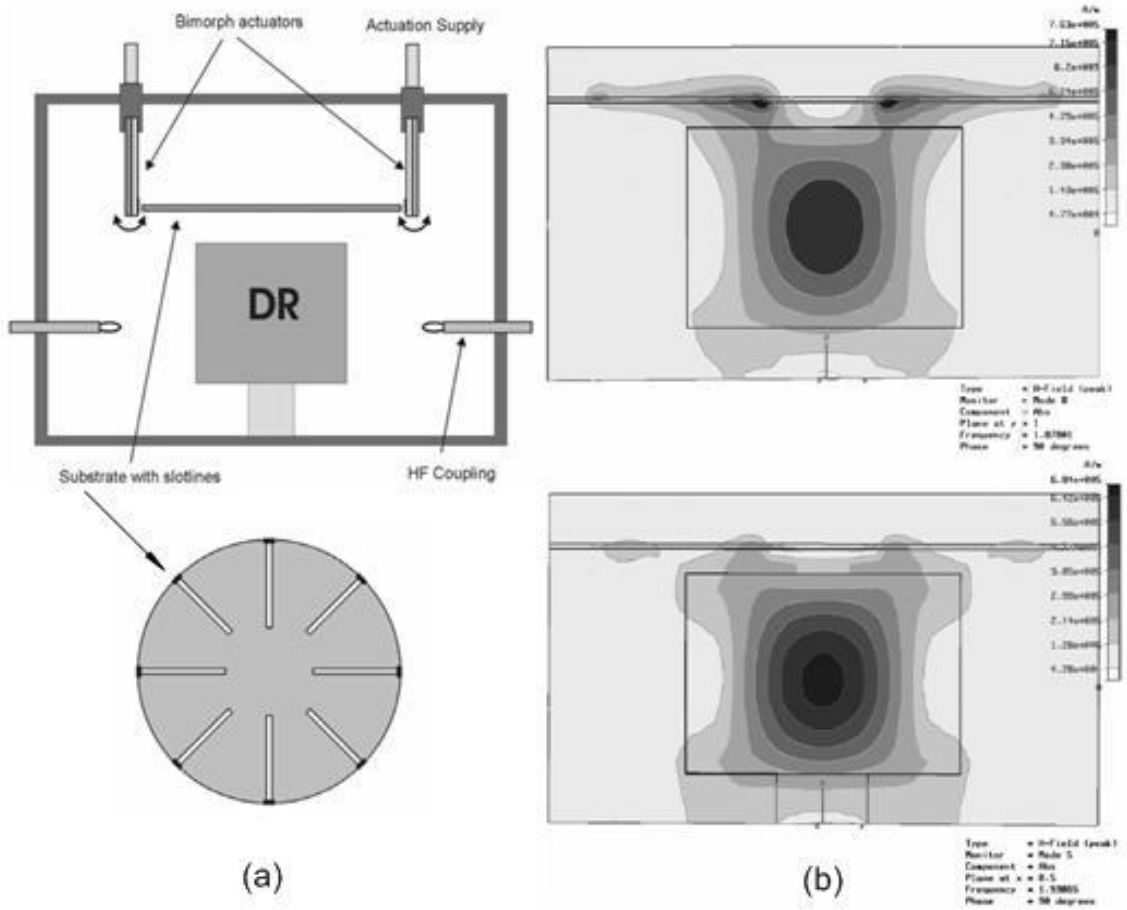

Figure 2.2-3 (a) Schematic view of the test setup for the discrete tuning of a dielectric resonator and (b) the axial magnetic field contours of the resonator with all the slots being in the open state (top) and closed state (bottom)[25]**.**

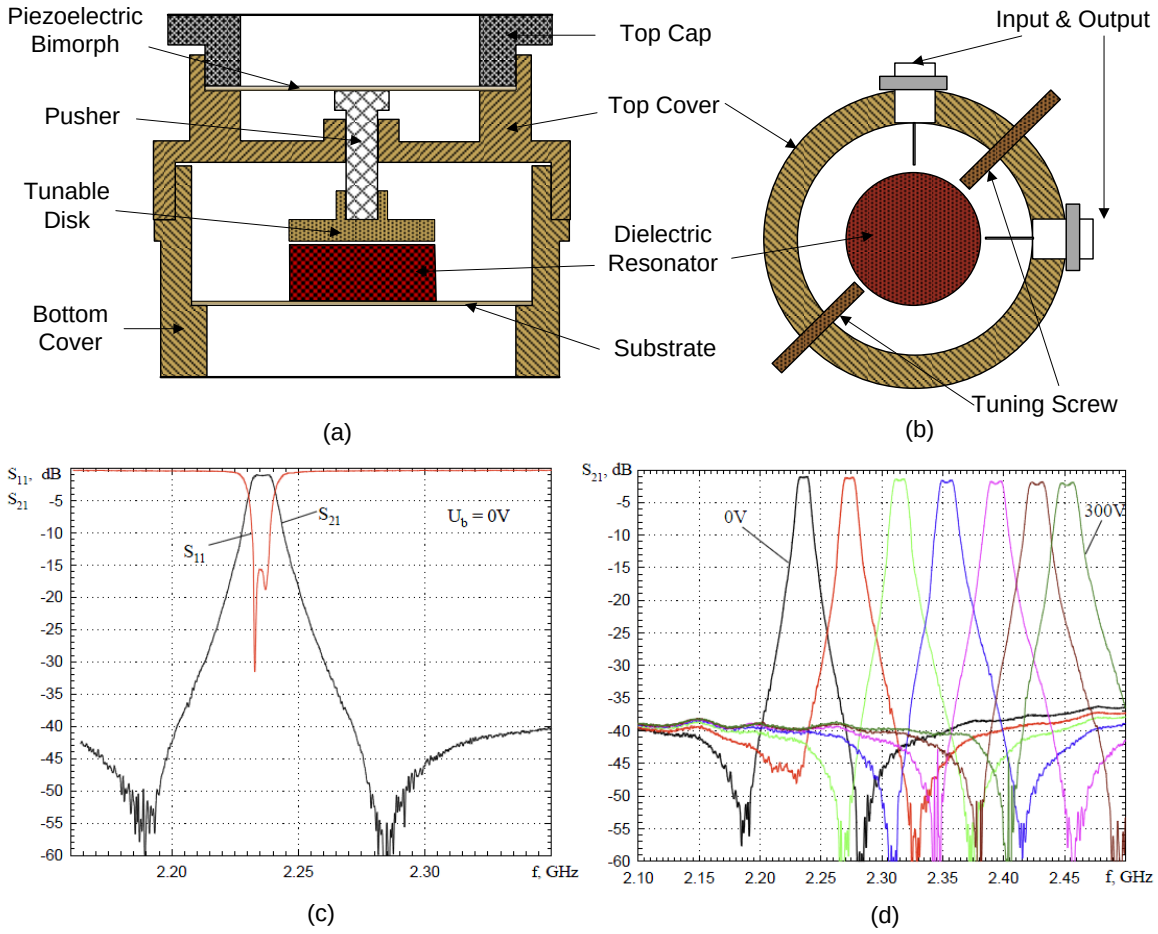

Figure 2.2-4 (a) Cross section of the 2-pole filter in a single cavity with a piezoelectric bimorph, (b) the top view of the cavity with tuning screws and probes, (c) the measured response from the Ba-La-Ti-O ceramic based 2-pole DR dual mode filter, and (d) the tuning response of the Ba-La-Ti-O ceramic based 2-pole DR dual mode filter [26]

2.2.3 Semiconductor Varactor Tuning

A semiconductor diode varactor, or simply called varactor, is operated with reverse-biased voltages without any current flowing through it. The thickness of the depletion zone varies when the bias voltages are applied, which cause changes in the capacitance of the diode. As tuning devices, varactors are widely used in tunable filters.

Figure 2.2-5 illustrates a typical varactor-tuned bandpass filter. The varactor connects each stripline to the ground. Together with the stripline and the varactor, they form a filter resonator. DC voltages are applied on the varactor to change the total capacitance of each resonator; hence

the resonant frequency of the filter changes with the applied voltages. This tuning mechanism is easy to adapt to planar tunable filters, such as microstrip line filters [27-31], suspend stripline filters [32, 33], CPW line filters [34], and Fin line waveguide bandpass filters [35]. The diode varactor has also been employed in bandstop filters and lowpass filters [7, 36-38].

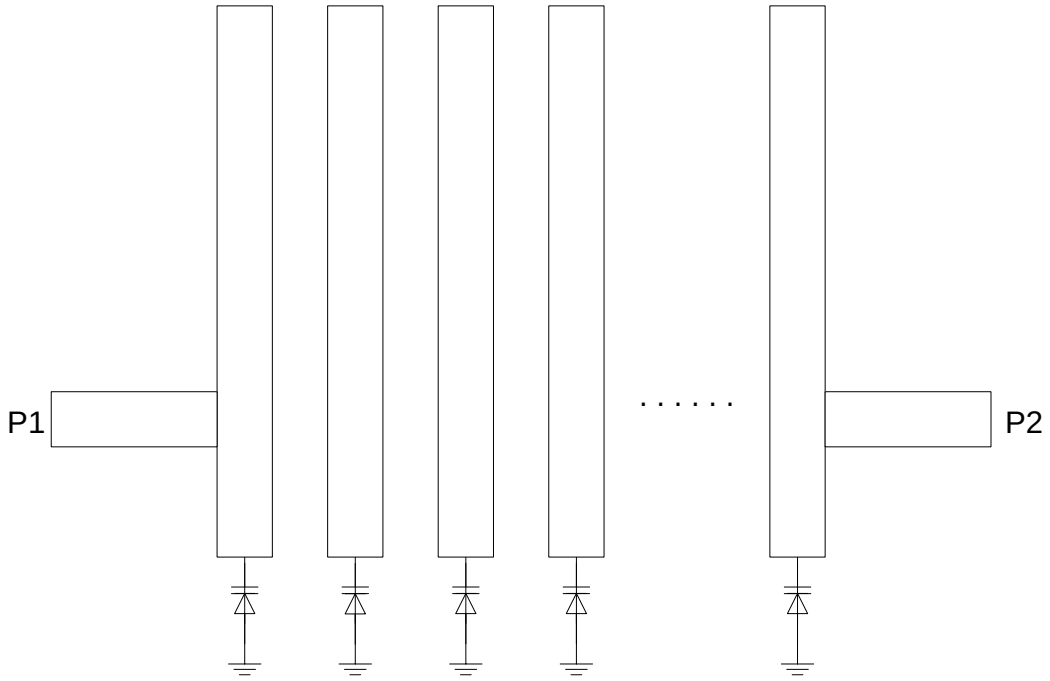

Figure 2.2-5 Schematic view of a varactor–tuned bandpass filter

A varactor can be used to tune not only 2D filters, but also 3D filters. A 3D resonator, which consists of 3D filters, is hard to tuned directly using the varactor. Usually, through the coupling between a 2D circuit and a 3D resonator, tuning the 2D circuit can achieve a tuning of the 3D resonator. 3D dielectric resonators which are tuned by varactors have been reported in [39, 40]. Figure 2.2-6 [39] illustrates a method of tuning a dielectric resonator using a varactor diode. A dielectric resonator is mounted over the top of a microstrip circuit, which affects the dielectric resonator through the coupling between them. Through controlling a microstrip circuit, a varactor can tune the DR resonant frequency. The corresponding tuning circuit is shown in Figure 2.2-6 (c). The center frequency of the dielectric resonator is at 3.318 GHz and the Q is above 9000 without DC voltage being applied to the diode. When the DC voltages are applied at 30 volts, the center frequency is altered by 53.7 MHz, or 1.6%, while the Q is maintained above 7000 over the entire tuning range, as shown in Figure 2.2-6 (d).

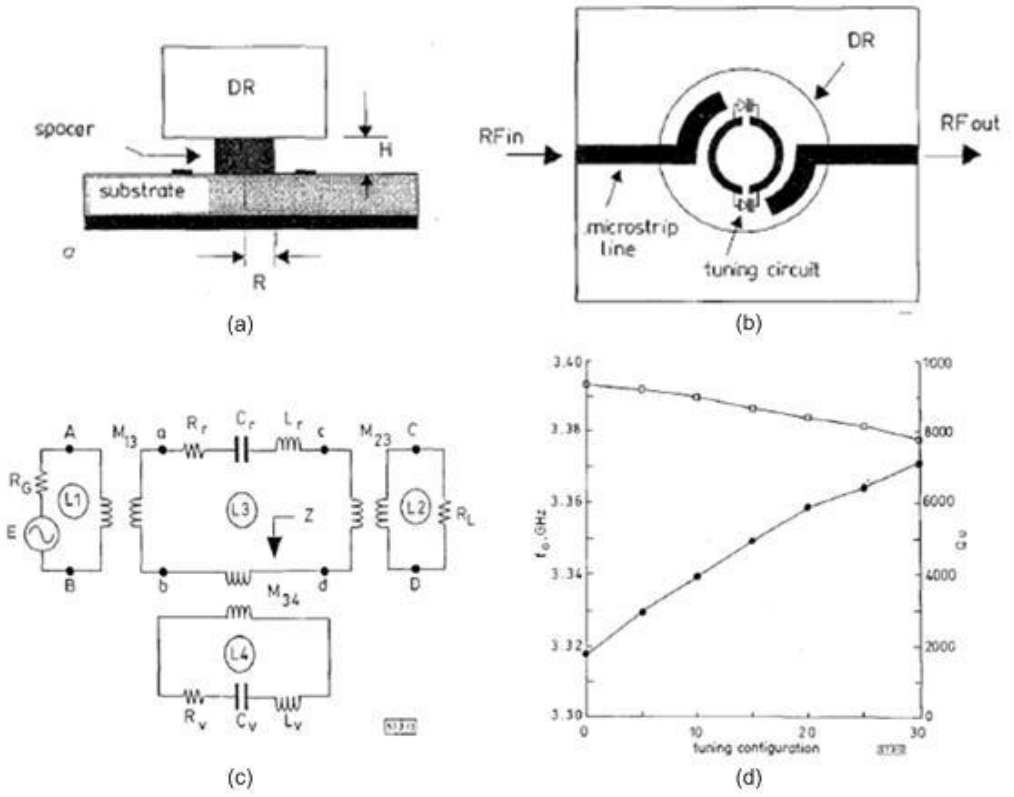

Figure 2.2-6 Tuning configuration [39]**: (a) the structure side view, (b) the structure top view (c) the equivalent tuning circuit, and (d) the resonant frequency and the unloaded Q-factor obtained with tuning configuration**

Figure 2.2-7 displays another method for tuning a dielectric resonator using a varactor [40]. The dielectric resonator, which is supported on low constant dielectric material, operates at $TE_{01\delta}$ mode. Microstrip arc patterns, which are on the top of the substrate material, are used to couple the electromagnetic energy in and out to the resonator structure. The varactor is placed in the DR slot, and the DC anode is connected to the filter base and is therefore grounded. The cathode is connected via a 1 nF feed-through capacitor to prevent the microwave signal from reaching the DC control source of the varactor. The varactor-carrier sides are metalized to ensure that the perturbed field appears uniformly at each side of the slot. This field is then displaced in synchronism by varying the varactor-control voltage. In one design of the center frequency is 4.47 GHz, and the tuning range of the center frequency ($\Delta f/f$) is ~7.1%. The detailed results and analysis are illustrated in [40].

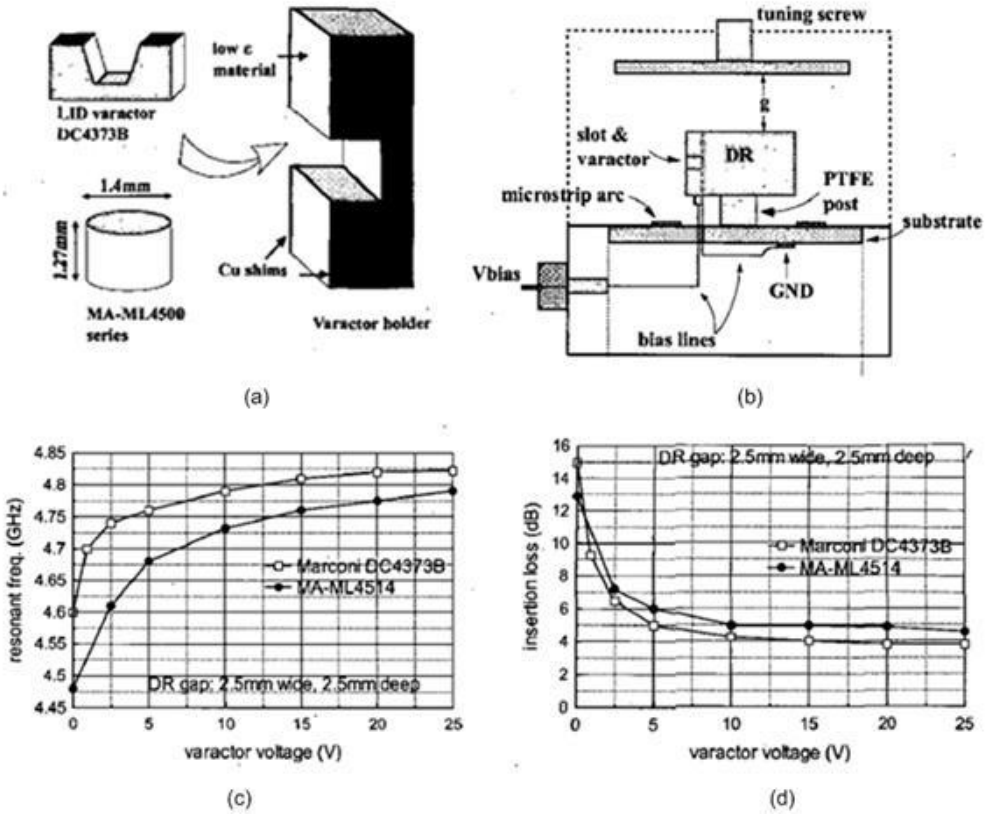

Figure 2.2-7 The slotted DR [40]**: (a) the varactor package and holder layout, (b) the schematic view in cavity, (c) the relationship between the resonant frequency and the reverse-biased voltage of two different varactor types, and (d) the relationship between the insertion loss and the varactor reverse-biased voltage.**

2.2.4 Ferroelectric Film Tuning

BST (Barium-Strontium-Tianate) is a type of ferroelectric film. The film maintains a relative high dielectric constant (eps~300). When a DC voltage is applied to the ferroelectric film, the dielectric constant of the film is changed, which in turn, changes the wavelength in the microwave devices. By exploiting this property of BST, tunable capacitors (varactors) can be fabricated. Figure 2.2-8 is a schematic view of filters whose dielectric resonators are loaded by ferroelectric varactors [41]. As shown in Figure 2.2-8 (a), the resonator is formed on silica substrate, which is placed in the cut off section of the rectangular waveguide. The ferroelectric varactor is connected to the metallic electrodes patterned on silica substrate (Figure 2.2-8b). The resonant frequency is controlled by the DC voltage employed on the ferroelectric varactor. A schematic view and image of the designed 4-pole filter is shown in (c) and (d). The final measured tuning results are plotted in Figure 2.2-9. The detailed data analysis of tuning is in [41].

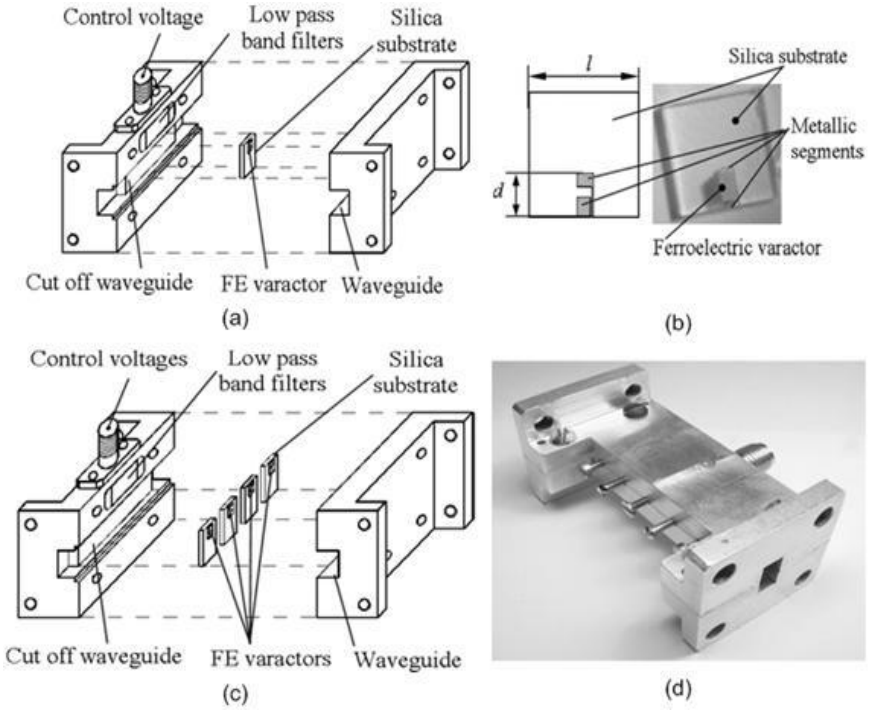

Figure 2.2-8 Schematic view of filters loaded by ferroelectric varactors [41]: (a) the waveguide design of a single dielectric resonator, (b) the design and image of a dielectric resonator supplied with metallic electrodes and ferroelectric varactor, (c) the design of a 4-pole tunable filter based on waveguide dielectric resonators, and (d) the image of a fabricated 4-pole tunable filter

Figure 2.2-10 illustrates a fabricated tunable filter based on the BST film plate capacitor mechanism [42]. A cross section of the BST varactor is shown in Figure 2.2-10 (a). The photo of a fabricated two-pole tunable filter is shown in Figure 2.2-10 (b), and its measured results are plotted in Figure 2.2-10 (c). Based on the same mechanism, a three-pole filter tuned by BST varactor is fabricated, and the measured results of the fabricated three-pole filter are presented in Figure 2.2-10 (d). All these measurements reveal that the designed tunable filter with a BST tunable capacitor can realize a very wide tuning range. These kinds of tunable filters are easy to integrate into an Integrated Circuit (IC).

BST varactors have been widely researched in [43-49] for tunable filters. Compared with other tuning circuits, the main advantages of these devices are their small size and fast tuning speed, as well as their wide tuning range and relatively small DC – bias voltage. In parallel plate capacitors, a tunability greater than 50 % is achievable at DC bias levels as low as 2-5 Volts [50]. Compared with the varactor diode, the BST film varactor can decrease the insertion loss and increase the power handling without reducing the tuning range. The BST varactor can be fabricated either in a parallel plate structure or in an inter-digital configuration. Both types of BST varactors were researched and compared in [51].

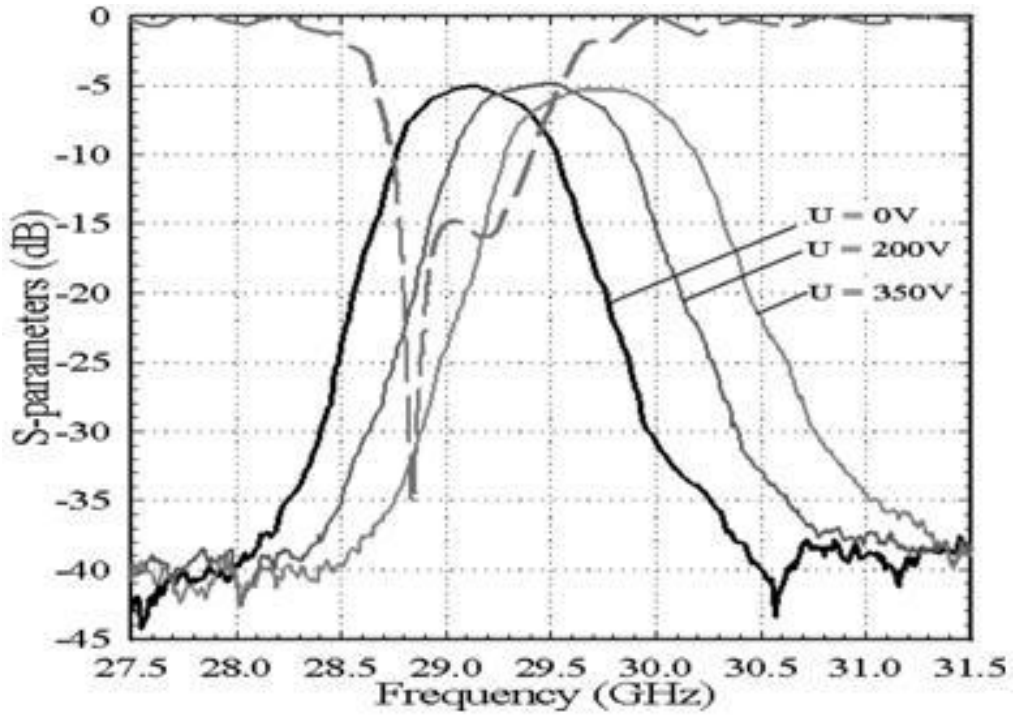

Figure 2.2-9 Measured results of the designed 4-pole tunable filter [41]

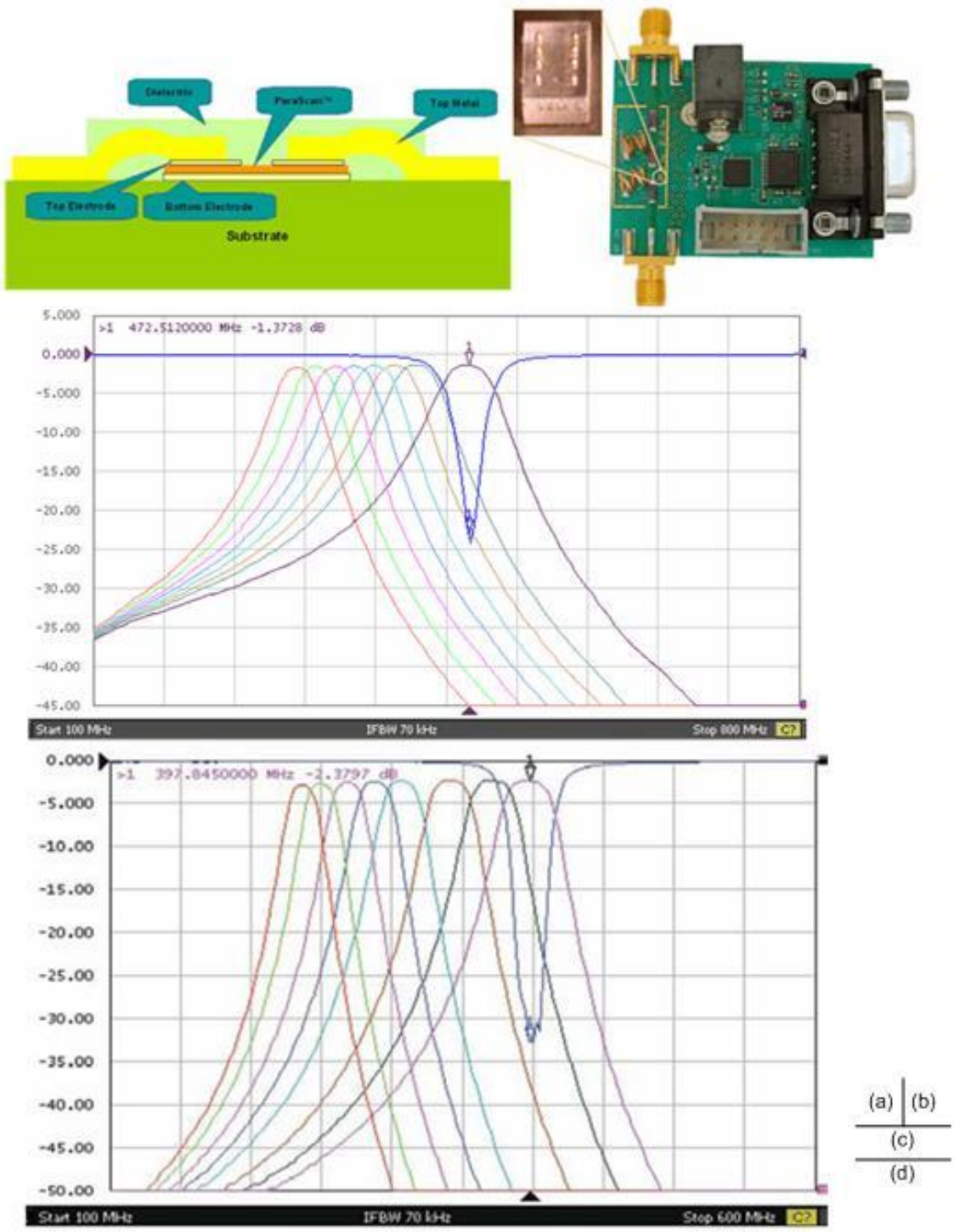

Figure 2.2-10 Broadband tunable filters[42] **(a) a cross section of the parallel-plate BST capacitor, (b) a photo of integrated two pole BST tunable filter, (c) the measurement results of a two pole tunable filter at room temperature, and (d) the measurement results of a three pole tunable filter at room temperature**

2.2.5 Ferrite Material Tuning

The YIG (Yttrium Iron Garnet) is a key tuning element in magnetic tunable filters. The mechanism for ferrite material tuning is the resonance controlled by the ferromagnetic resonance (FMR) frequency which changes with externally applied DC voltages. The YIG magnetically tunable filter plays a dominant role in applications where an ultra-wideband tuning range is required. Tunable microwave bandpass and bandstop YIG filters are reported in [52-56]. They can be used in the front-end receivers for microwave systems, and in electronic counter-measure transceivers. Their traditional power consumption, bulk size, and heavy weight are limiting factors for their applications in modern wireless systems. However, as some novel technologies are developed using YIG material, some new tunable YIG filters are designed to be compact in size and energy efficiency [54, 57]; therefore, it is possible to apply them in RF front-end receiver and other microwave circuits.

Ferrite material tuned dielectric resonators have been reported in [58-60]. The principle is to control the magnetic field pattern in the vicinity of the dielectric resonator using ferrite material whose magnetic intensity is controlled by an external voltage. Figure 2.2-11 illustrates two configurations of magnetic tunable dielectric resonators using ferrite material [59]. The dielectric resonator operates at TEH mode. The tunability is realized by using either the axially magnetized ferrite rod (Figure 2.2-11a), or the circumferentially magnetized ferrite disks (Figure 2.2-11b), which generate a magnetic field in the same or opposite direction of the TEH mode. Therefore, the magnetic field intensity in dielectric resonator changes with the external magnetic field intensity generated by the axially ferrite rod or ferrite disk. Resonators employing these two technologies are fabricated and illustrated in Figure 2.2-12 (a) and (b) respectively. The magnetic tunable two-pole filters adopting these types of resonators are fabricated and shown in Figure 2.2-12 (c) and (d). The measurement results are displayed in Figure 2.2-13 (a) and (b). A tuning range of 20 MHz at 2.22 GHz, and an unloaded Q better than 2,500 are obtained for the filter containing an axially magnetized ferrite rod. While the filter containing the circumferentially magnetized ferrite disks obtained a 28 MHz tuning range at 2.35 GHz and an unloaded Q better than 3,500. To achieve such tuning ranges they need currents of 2.5A and 3A, with power consumption in the tuning circuit of 4.5 W and 3.5 W respectively. The tuning range can be

increased by increasing the tuning power; however, the Q will decrease while the tuning power increases.

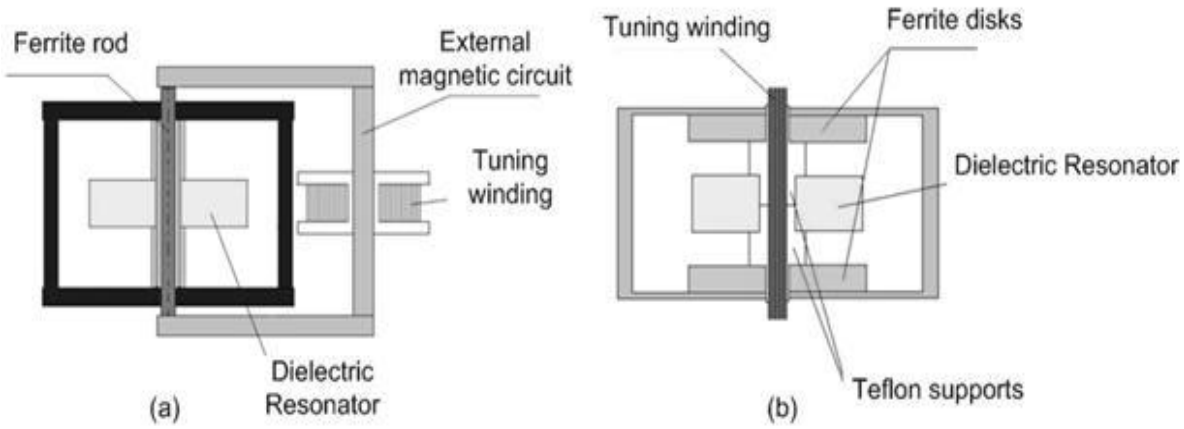

Figure 2.2-11 Schematic diagram of a tunable dielectric resonator containing [59]**: (a) axially and (b) circumferentially magnetized ferrite disks elements**

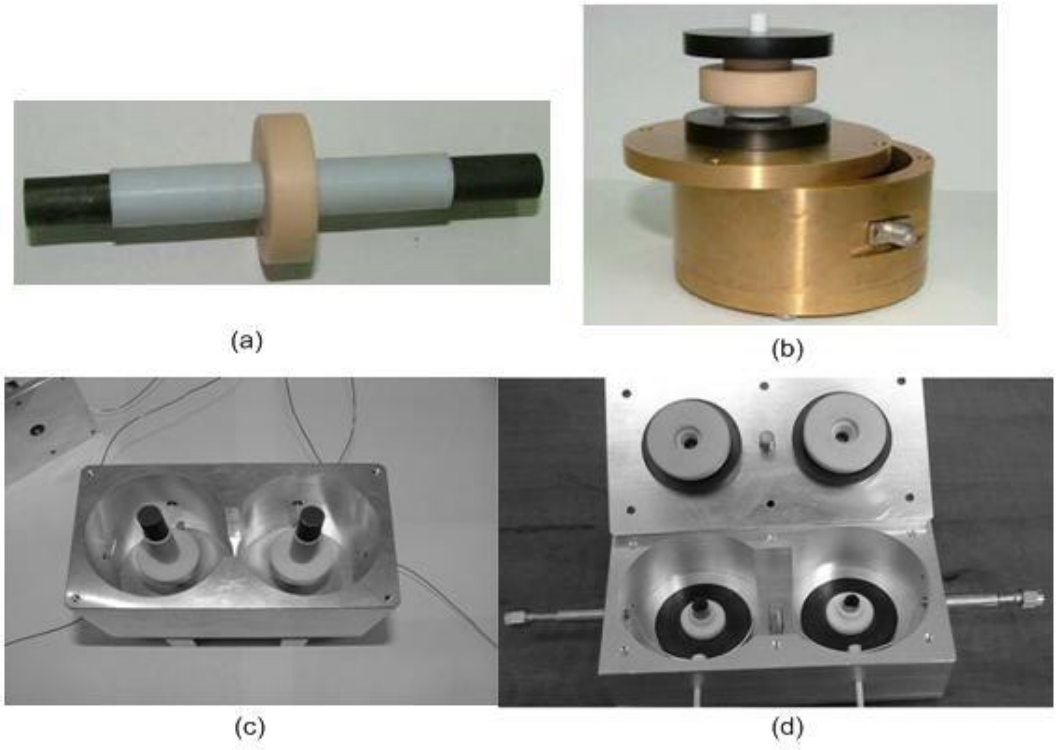

Figure 2.2-12 Pictures of the tunable dielectric resonators and filters[59]**: (a) an axially and (b) circumferentially magnetized resonator, (c) a filter containing axially magnetized ferrite rods and (d) a disassembled filter containing circumferentially magnetized ferrite disks**

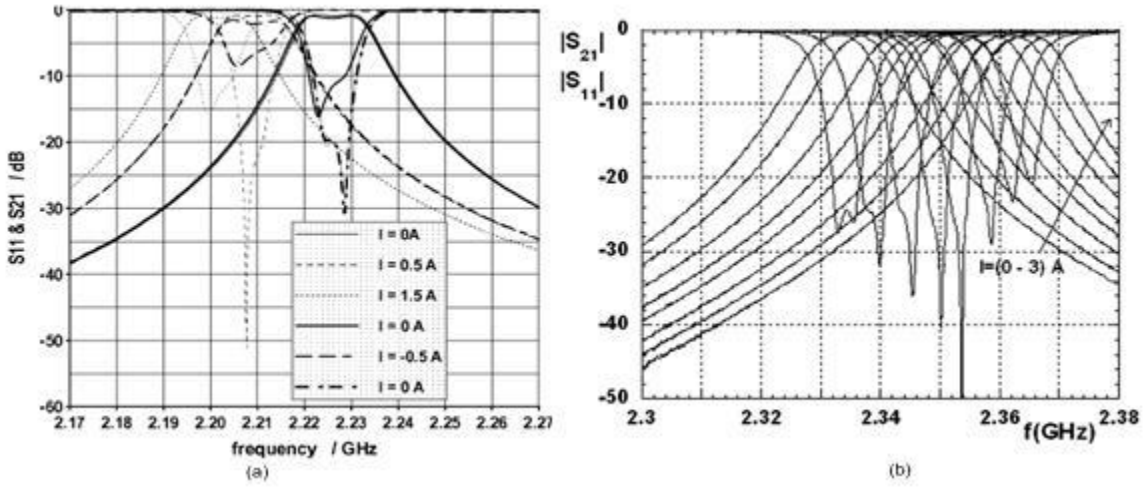

Figure 2.2-13 (a) The measured results for the filter containing axially magnetized ferrite rods ; (b) the measured results for a filter containing circumferentially magnetized ferrite disks [59]

2.2.6 MEMS Tuning

The MEMS (Micro-Electro-Mechanical-Systems) tuning circuit is an electro-mechanical device that is able to mechanically change its switch to the 'on' and 'off' status, or change its capacitance value with an external applied DC voltage. The capacitance change can be digital, analog, or both. The most straight forward way to design a MEMS tunable filter is to replace the traditional multiport switches with MEMS switch counterparts in the switch bank [61, 62], and replace the traditional semiconductor diode varactors with MEMS varactors in the tunable filters [63].

Unlike the diode switch, the MEMS switch itself has a high Q (150-300) at microwave and millimetre wave frequencies, and has a very low distortion level [64, 65]. The MEMS devices can be very small and can use electrostatic, piezoelectric or thermal effects to produce the movement. The switching time of these devices is 0.5-50 microseconds. Hence, the tunable filters using MEMS devices as tuning elements have the advantage of low loss and low distortion levels. Due to their compact size, MEMS switches can be easily integrated with a small Integrated Circuited (IC). While the electronics are fabricated using IC process sequences, the micro-mechanical components are fabricated using compatible "micro-machining" processes that

selectively etch away parts of the silicon wafer or add new structural layers to form the mechanical and electro-mechanical devices.

In general, MEMS switches have been employed in all kinds of tunable filters. Some of the examples are microstrip tunable filters [9, 66], CPW filters [67, 68], lumped element filters [69, 70], tunable micro-machined filters[71-75], and tunable DR filters [76-78].

Figure 2.2-14 (a) and (b) illustrate the schematic view of a W–band MEMS tunable filter [74]. The Chebyshev inductive iris-coupled waveguide filter consists of two cavities with two circular membranes on the top surface of each cavity. The whole device is made of a plastic structure while the internal wall of the waveguide is electroplated with a 3-um thick gold layer. All the initial design parameters of the waveguide filter were obtained from a K-impedance inverter circuit model, $\lambda/2$ resonator, and the EM simulation using HFSS. The circular membrane will deform when the DC voltage is applied. The deformed cavities cause the load of the resonator to change; as a result, the filter is tuned.

The measurements from the fabricated filter reveal that the designed filter operates at 94.79 GHz with a bandwidth of 4.05 GHz, and an insertion loss better than 2.37 dB over the tuning range. The filter is tuned from 94.0 to 96.59 GHz with a membrane deflection from -50 um to +150 um, as shown in Figure 2.2-15. The detailed results are listed in Table 2.2-1.

Figure 2.2-16 shows MEMS actuators implemented in a DR filter [76], each resonator of the designed filter includes a dielectric resonator with an operating mode of TEH, a tuning disk, and a MEMS thermal actuator that connects between the tuning disk and the cavity wall. A cross section view of the proposed tuning mechanism is exhibited in Figure 2.2-16 (a). Each MEMS actuator is connected with a DC voltage. When the DC voltage is applied on the MEMS actuator, it will push the disk towards the top of the dielectric resonator, and the extra capacitance load is applied on the dielectric resonator. Therefore, the filter tuning is realized. The thermal actuator design and fabricated tunable filter are shown in Figure 2.2-16 (b)-(d).

The measurements of the filter's tuning responses are plotted in Figure 2.2-16 (e) and (f). The figures show that the insertion loss of the filter at the mid-band is better than 1.5 dB, and the unloaded Q is above 1300 at the initial status. When tuned to a high frequency the filter degrades and the Q decreases. The measured results show the filter tuned from 15.6 GHz to 16.0 GHz. The bandwidth change is about 2.6%. The detail analysis and results are exhibited in [76].

In short, employing MEMS devices in a tunable DR filter is a challenge, especially at a low frequency. The DR filter is relatively larger, whereas the MEMS switch is very small. If both parts are fabricated separately, the process to assemble them will be very costly and difficult.

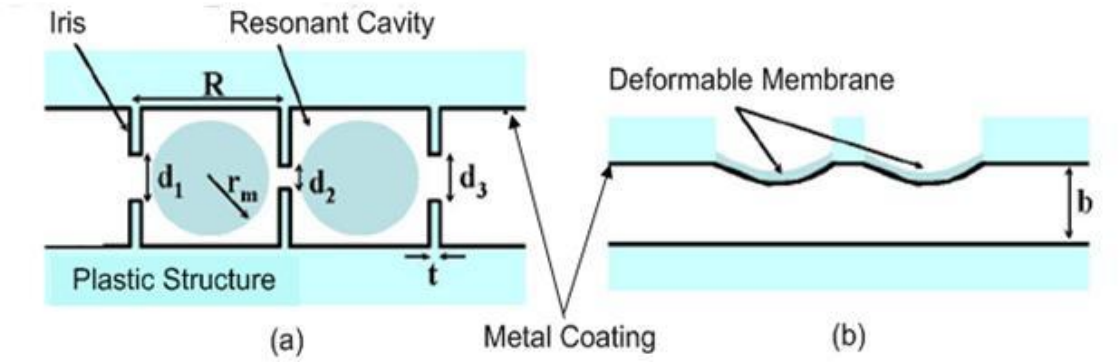

Figure 2.2-14 Schematic view of a W-band tunable filter [74]**: (a) the top view, and (b) the side view**

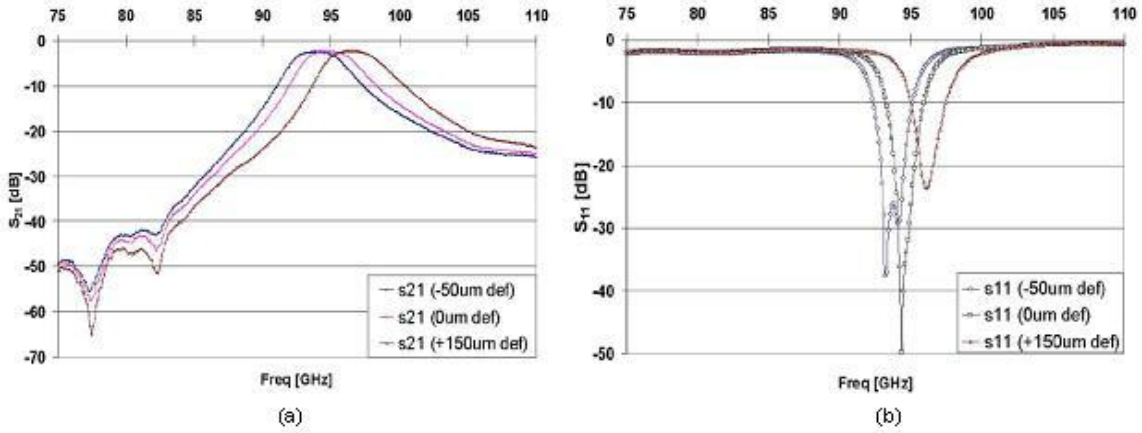

Figure 2.2-15 Measurements of a tunable 2-pole filter [74]**: (a) the insertion loss and (b) the return loss**

Table 2.2-1 Filter performance due to membrane deflection [74]

Deflection(um)	**-50**	**0**	**+150**
f_{c1} [GHz]	92.00	92.79	94.48
f_{c2} [GHz]	96.05	96.84	98.75
f_c [GHz]	94.00	94.79	96.59
IL [dB]	2.4	2.37	2.36
BW [GHz]	4.05	4.05	4.27
%BW	4.31	3.27	4.42

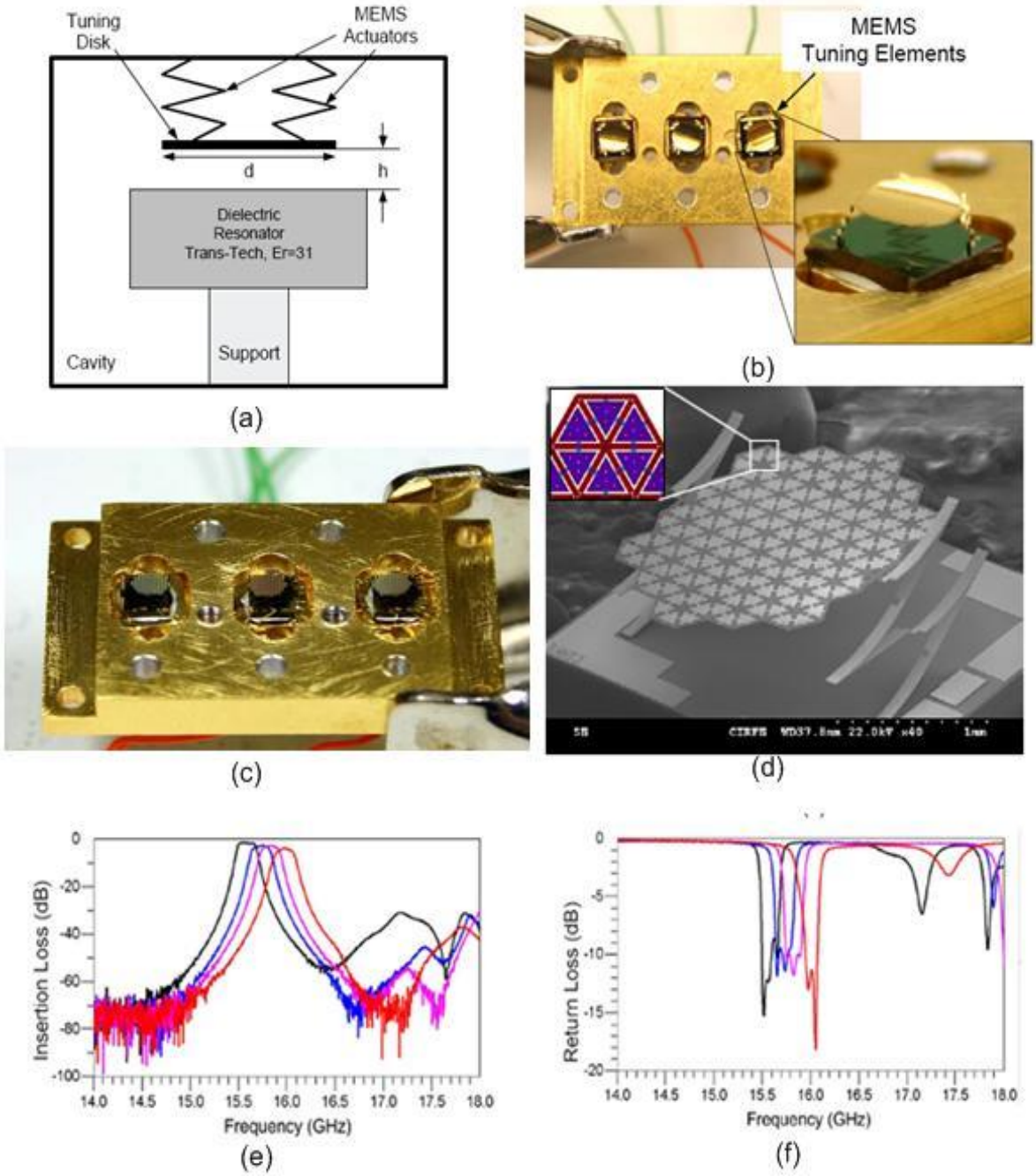

Figure 2.2-16 DR filter tuned by MEMS actuators[76]**: (a) schematic view of the proposed tuning structure, (b) MEMS tuning elements: a solid circular disk with a warpage, (c) a hexagonal tuning disk without warpage, (d) a fabricated DR filter embedded with MEMS tuning elements, (e) the comparison of measured results of the insertion loss, and (f) the comparison of measured results of the return loss**

2.3 Tunable Filters with Constant Bandwidth

The main drawbacks of typical tunable filters are the changing bandwidth and the degrading return loss during the tuning process. This issue is attributed to the changes of the inter-resonator coupling and the input/output coupling as a function of the filter's center frequency when the filter is being tuned over the tunable frequency. To maintain a constant bandwidth, the coupling coefficients should vary inversely with the tuning frequency, and the external loaded Q_e should vary directly with the tuning frequency [13]. Most publications on tunable filters only report employing tuning elements for the center frequency and few for the couplings [14, 29, 79-85]. However, if all the couplings need adjusting during the tuning process, the tunable filter will become too complex, and it will lose the advantage over the filter bank. So, ideally designing a constant bandwidth tunable filter means not just designing the tunable resonator. It also means designing coupling coefficients that can automatically vary inversely with the resonator's center frequency, and the input/output coupling which the external loaded Q_e can vary directly with the center frequency.

2.3.1 Tunable 3D Filter with Constant Bandwidth

In [14], a Ku-band high-Q tunable filter with a stable bandwidth was presented; the designed filter and its schematic view are shown in Figure 2.3-1. The filter employs two dual-mode cylindrical cavities operating in the TE_{113} mode. The frequency tuning of this cavity is realized by adjusting the cavity length through the compression or expansion of a flexible bellows, which is mounted on the top of the cavity. To maintain the bandwidth stability, an extended-double-slot iris is designed for the input/output coupling (Figure 2.3-2 (a)), and the inline iris is designed for inter-resonator coupling (Figure 2.3-2 (b)). All the positions and dimensions of these irises are designed based on the optimum simulations of the tunable filter responses over the tuning range. Detail design analyses are illustrated in [14]. The final filter's tuning responses are displayed in Figure 2.3-3. The figure shows that this designed tunable filter operates at 12 GHz, with a tuning range of 460 MHz; the bandwidth changes from 156 MHz to 166 MHz; and the filter's unloaded Q is better than 10,000 over the tuning range. However, the return loss degrades after the filter is tuned.

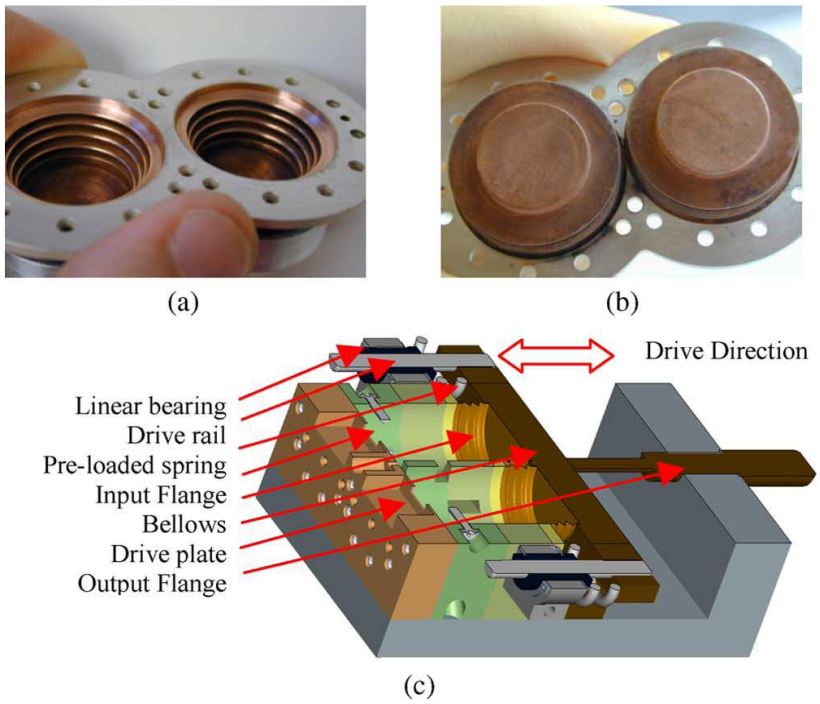

Figure 2.3-1 Fabricated Ku-band tunable filter [14]**: (a) & (b) tapered bellows attached to the flange, and (c) filter structure**

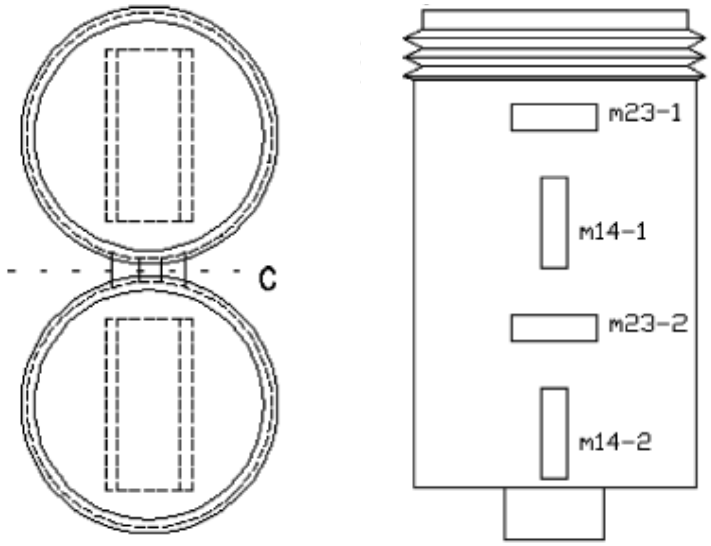

Figure 2.3-2 Input/output iris and inline iris coupling [14]**: (a) the input/output iris from top view and (b) the inline iris coupling from side view**

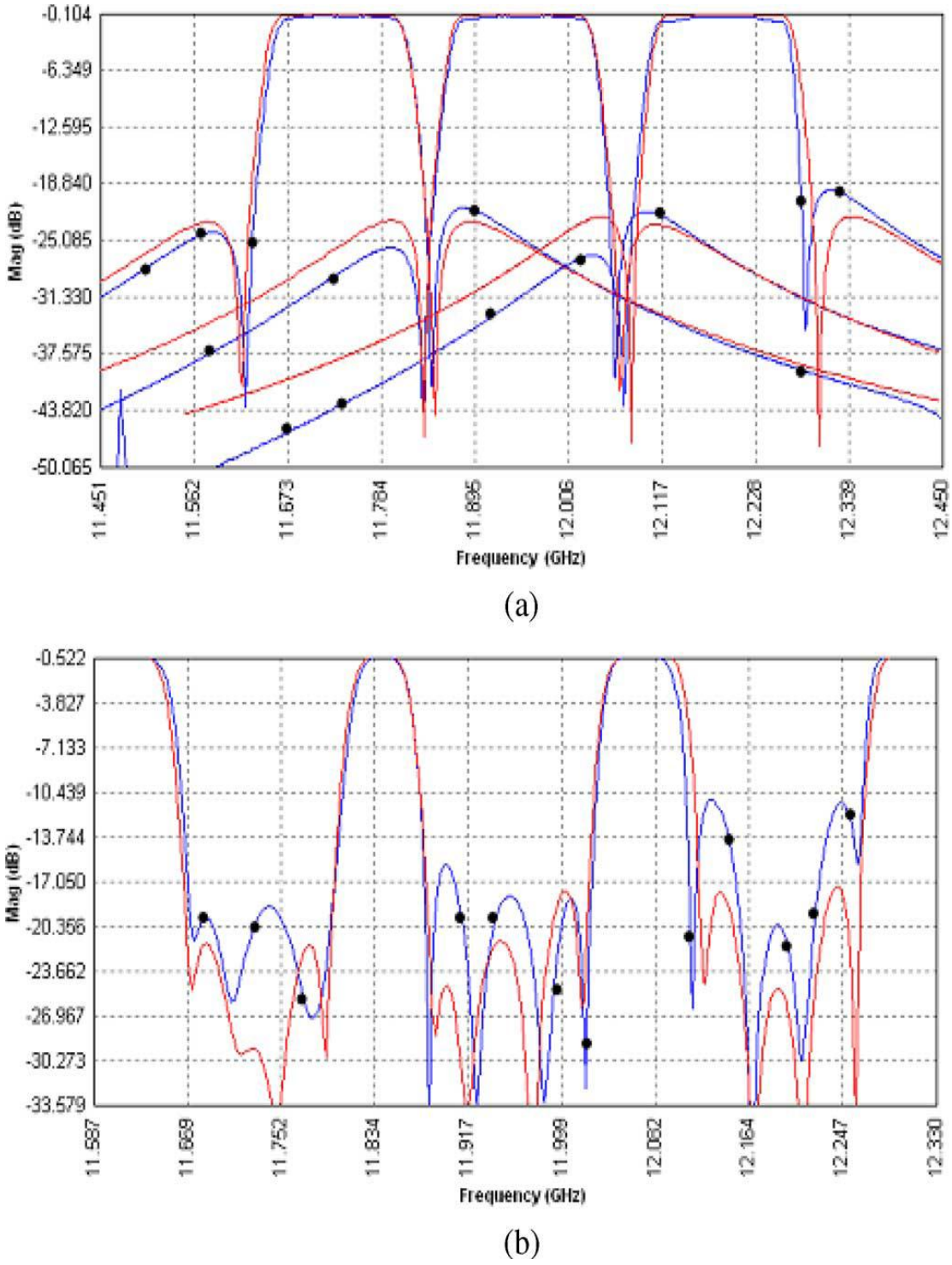

Figure 2.3-3 Measurements (blue line) and simulations (red line) of the filter's tuning response [14]**: (a) the insertion loss, and (b) the return loss**

2.3.2 Tunable 2D Filter with Constant Bandwidth

Figure 2.3-4 illustrates a two pole zig-zag hairpin-comb filter. The HTS tunable capacitance is realized by fabricating a long interdigital capacitor with a tunable capacitor lumped over the gap in top of the interdigital capacitor [79]. Special circuits are added in series with the input and output of the filter, as shown in Figure 2.3-4. These added circuits consist of an interdigital capacitor in parallel with meander inductors which are tapped for input/output coupling of the filter. This configuration can reduce the effect of the input coupling when the resonator's frequency is tuned. This design also ensures that the input coupling and inter-resonator coupling are stable with the filter tuning process. The measured results are displayed in Figure 2.3-5.

In [29], step-impedances are introduced to design the microstrip tunable filter (in Figure 2.3-6). To keep a constant bandwidth over the tuning range, the step-impedances are implemented to reduce the magnetic coupling near the short ends of the microstrip lines. Thus, the coupling values between resonators can vary inversely with the tuning frequency. The input coupling is determined by the lumped input inductor and its position. The lumped input inductor allows the external Q_e to vary directly with the tuning frequency. Therefore, a constant bandwidth over the tuning range can be realized. The simulations and measurements are illustrated in Figure 2.3-7.

In [85], a 2-pole microstrip tunable filter with a constant bandwidth is demonstrated and shown in Figure 2.3-8 (a). In the design, a mixed electric and magnetic coupling that was extracted at various frequencies are displayed in Figure 2.3-8 (b) and (c) respectively. The mixed coupling is used for the inter-resonator coupling, which makes the coupling coefficient meet the specifications of a constant bandwidth over the tuning range. The simulations and measurements are exhibited in Figure 2.3-9. The results show that constant bandwidth is well maintained over the tuning range.

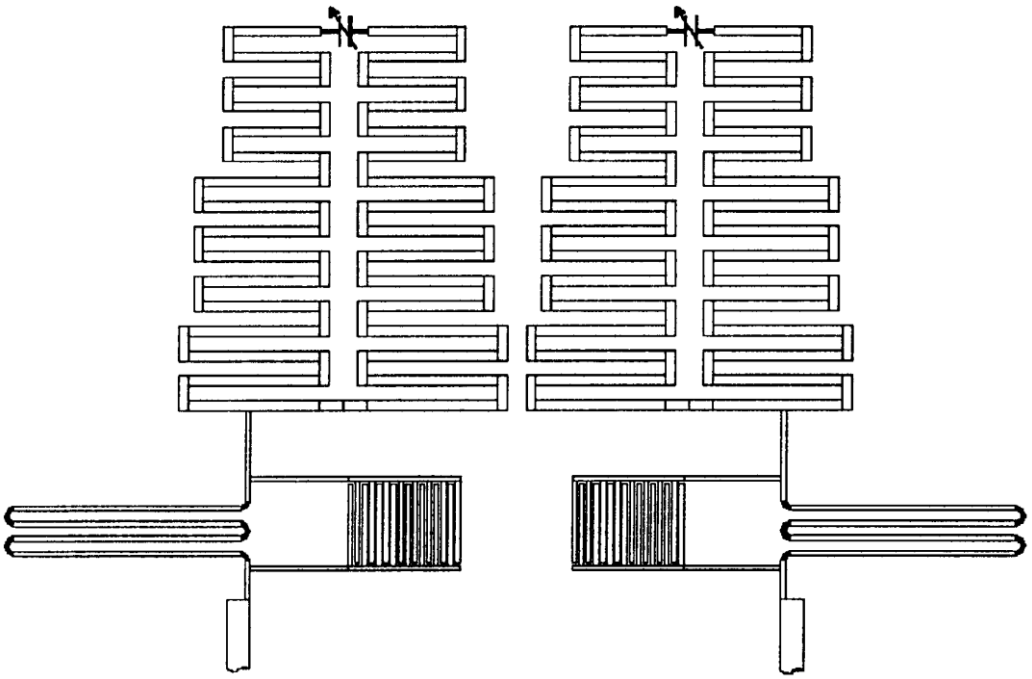

Figure 2.3-4 Tunable two pole zig-zag hairpin-comb filter with inductive tap input couplings [79]

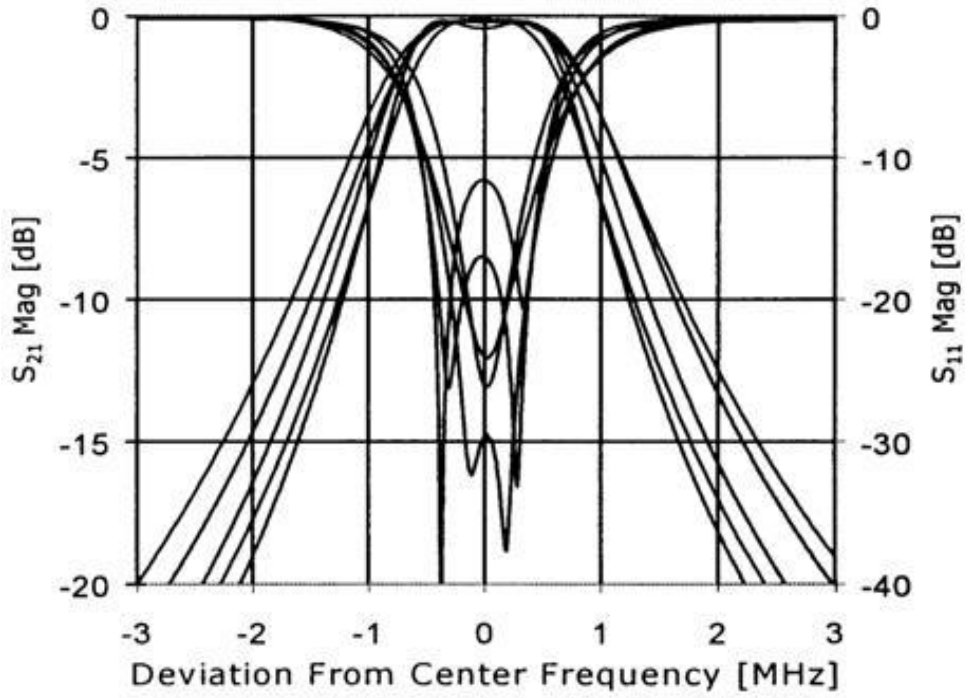

Figure 2.3-5 Superposition of the measured results of the two pole zigzag hairpin-comb filter for center frequencies of 0.498, 0.555, 0.634, 0.754 and 0.948 GHz [79]

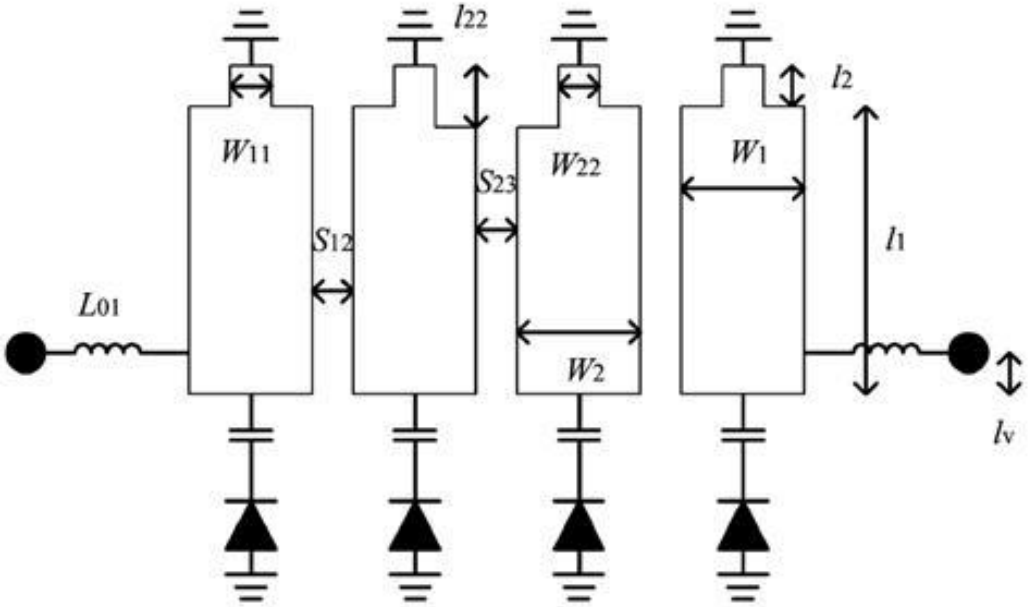

Figure 2.3-6 Diagram of a tunable combline bandpass filter with a step-impedance microstrip [29]

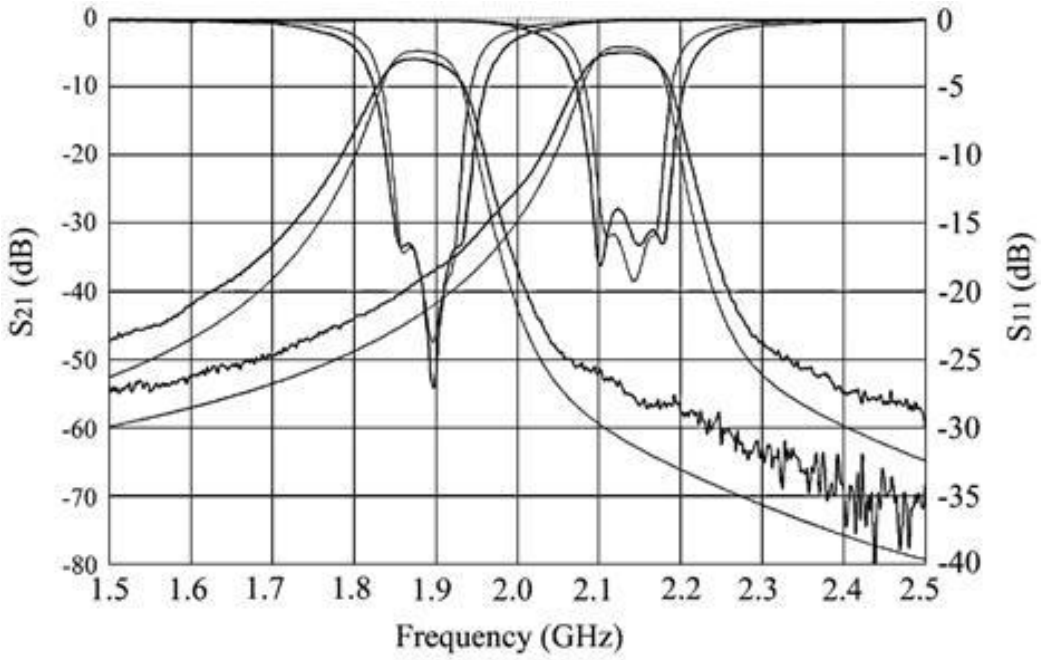

Figure 2.3-7 Simulated (thinner lines) and measured (thicker lines) results of the tunable combline filter with step-impedance microstrip lines [29]

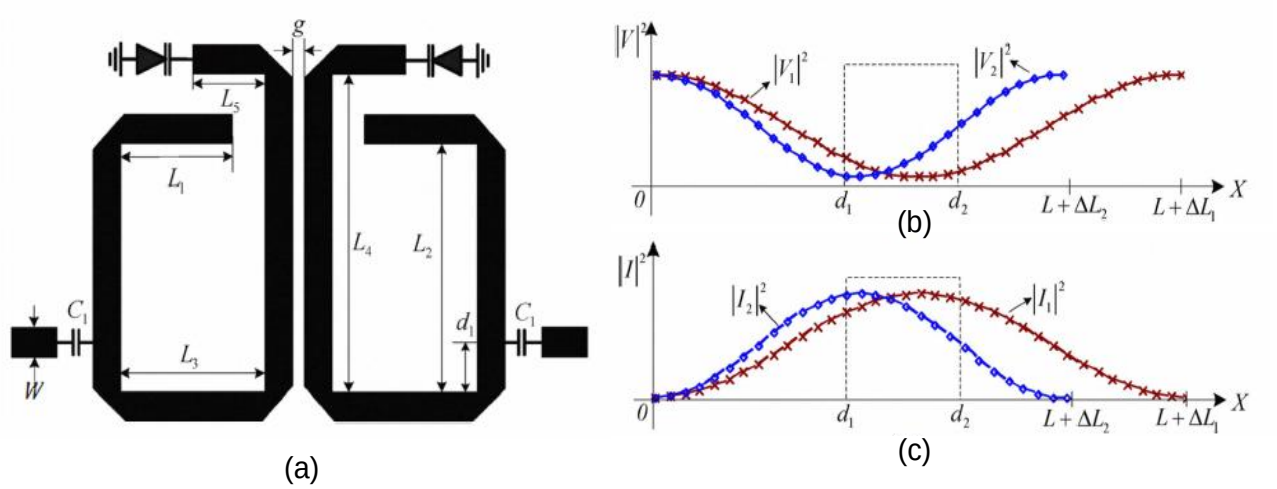

Figure 2.3-8 (a) The filter configuration, (b) the electric coupling at various frequencies, and (c) the magnetic coupling at various frequencies [85]

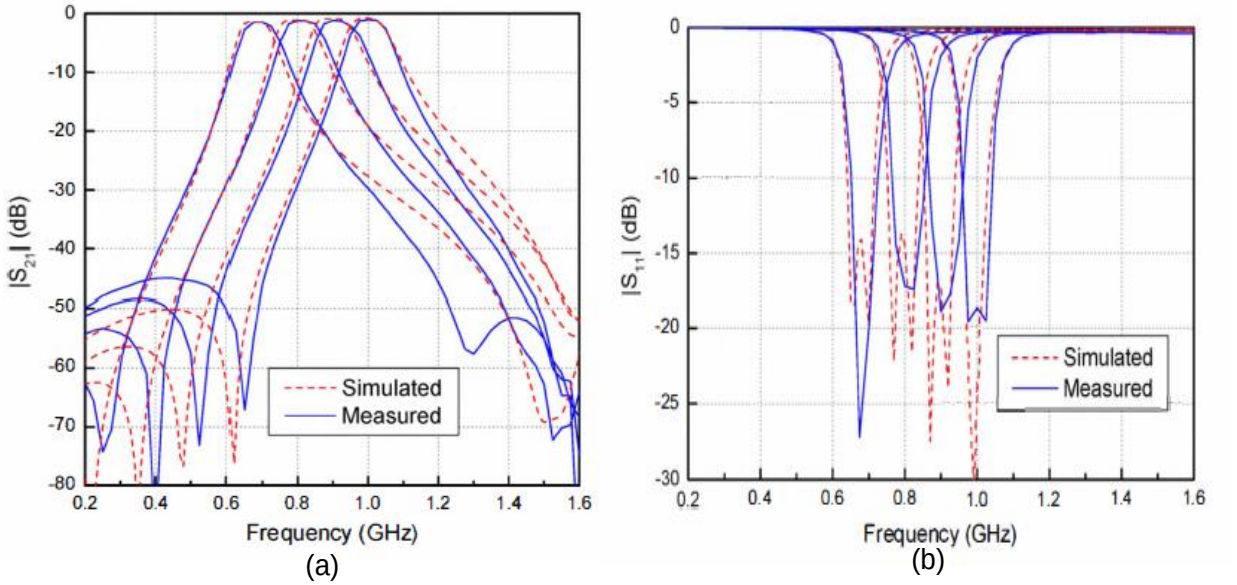

Figure 2.3-9 Tuning responses of the tunable filter [85]**: (a) S_{21}, and (b) S_{11}**

2.4 Summary

Three dimensional (3D) cavity resonators are necessary in the design of a high Q tunable filter at a normal temperature. The Q factor of the tuning circuit itself and the method of integration of the tuning circuit with the 3D cavity resonator should be considered as well.

To design a constant bandwidth tunable filter, the key technique is to design an input/output external loaded Q_e that varies directly with the center frequency, and to design inter-resonator couplings that vary inversely with the center frequency. The filter performance degradation and bandwidth variation are reported in most tunable filters published in literatures. Therefore, designing a high Q tunable filter with constant bandwidth is a challenge.

Chapter 3
Compact Tunable DR Filters Using Piezoelectric Actuator

Emerging reconfigurable systems demand the use of low-loss narrow-band filters. Such requirements cannot be met by low-Q planar-type filters. On the other hand, 3D compact filters offer relatively high Q values and can potentially be integrated with tuning elements to achieve low loss tunable filters.

In this chapter, a compact dielectric resonator structure is used in the design of a high Q tunable filter. The behaviours of the dielectric resonator modes are investigated. A TME mode dielectric resonator filter tuned by a piezoelectric actuator is fabricated and tested. For further study, a compact dual mode dielectric resonator structure is also investigated for the design of compact high Q tunable filters.

3.1 Introduction

With the rapid development of modern communication networks, compact high Q tunable bandpass filters are in high demand in modern wireless communication systems. A high Q filter reduces the insertion loss in the receiver. As a result, it increases the link budget in radio systems. In addition to reconfigurable systems, the bandpass tunable filter is typically employed in front-end of receivers [86], cognitive radios [87], and software defined radios [88-90]. They are frequently used in other applications such as frequency hopped receivers, Doppler radar, and troposcatter [17].

A micro-machined ridge waveguide with built-in tuning elements have been reported in [75], but the achievable Q is relatively low. This is the result of the limited number of layers in the majority of micromachining process, which limits the filter's cavity height, and in turn reduces

the Q value. A dielectric resonator filter integrated with MEMS actuators has been reported in [76]. The Q value demonstrated in the filter is quite high. However, a filter with this structure is limited to applications in high frequencies (X-band and up). In [91], piezoelectric tunable dielectric resonator filters are reported, but these filter structures [91] are relatively large in size requiring the use of large-size piezoelectric actuators. Miniature high Q tunable filters at low frequencies remain elusive.

3.2 Compact Tunable Dielectric Resonator Filter

Dielectric resonator filters are preferable for wireless base stations due to their superior features of high Q value and small size. Typically, the achievable unloaded Q of a dielectric resonator is not only determined by the material loss tangent, operating mode, and frequencies, but also affected by other factors such as the size of the enclosure, the conductivity of the enclosure, the support structure, and the tuning elements.

3.2.1 Dielectric Resonator

A traditional dielectric resonator filter consists of high-K dielectric resonators supported by low constant dielectric material, and is enclosed in a metallic cavity. These resonators usually operate at the TEH mode. However, a DR resonator that operates at TEH mode generally has a relatively large cavity size in order to keep the TEH mode as the dominant mode. As a result, it is not as compact as required.

In order to design a compact dielectric resonator, high-K dielectric material with a novel structure is investigated. Then tunability of modes in the dielectric resonator with an unloaded Q value of 10,000 at 5 GHz, a permittivity of 45, and a thickness of 2.54 mm is investigated. In the design proposed here, we use a dielectric resonator mounted directly on the cavity wall. Thus, the dominant mode of the resonator is the TME mode where the gap between the resonator and the cavity lid is small enough. The schematic view of the cavity DR structure is displayed in Figure 3.2-1, along with the electric field vector in the DR resonator for the TME mode. The total height of the cavity is the height of the DR plus the gap. In this design, the gap is considered as a parameter for simulating the frequency changes of the first two modes. The simulation results using HFSS software for this structure are shown in Figure 3.2-2. The figure shows that the frequency of the TME mode shifts from 4.43 GHz to 8.39 GHz with the gap increasing from

0.1 to 2mm. The TME mode frequency is much more sensitive when the gap is smaller, and both frequencies of the TME mode and the HEE mode have intersected when the gap is about 0.65 mm. Thus, if the TME mode is considered for designing a tunable filter, the gap should be smaller than 0.5 mm over the tuning range of the resonator structure. Figure 3.2-3 displays the unloaded Q of the first two modes varying with the gap change. The figure shows that the TME mode maintains a relatively acceptable high Q-value (>2000), even when the gap between the dielectric resonator and the cavity lid is very small. Therefore, the TME mode can be used to design a high Q tunable filter if the gap between the resonator and the cavity lid is controllable.

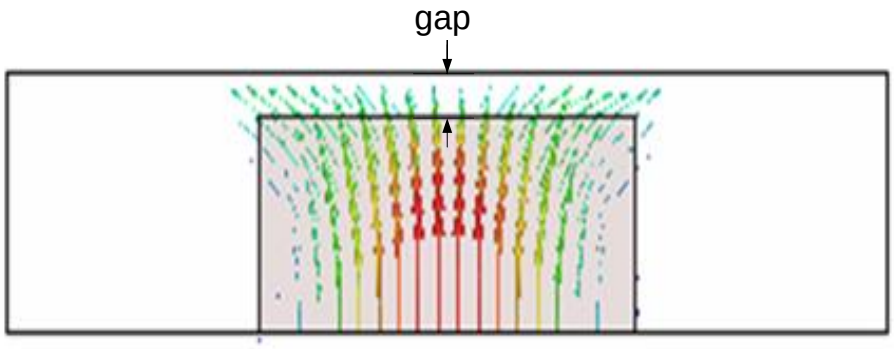

Figure 3.2-1 Cavity DR structure with electric field vector in the DR resonator for the TME mode

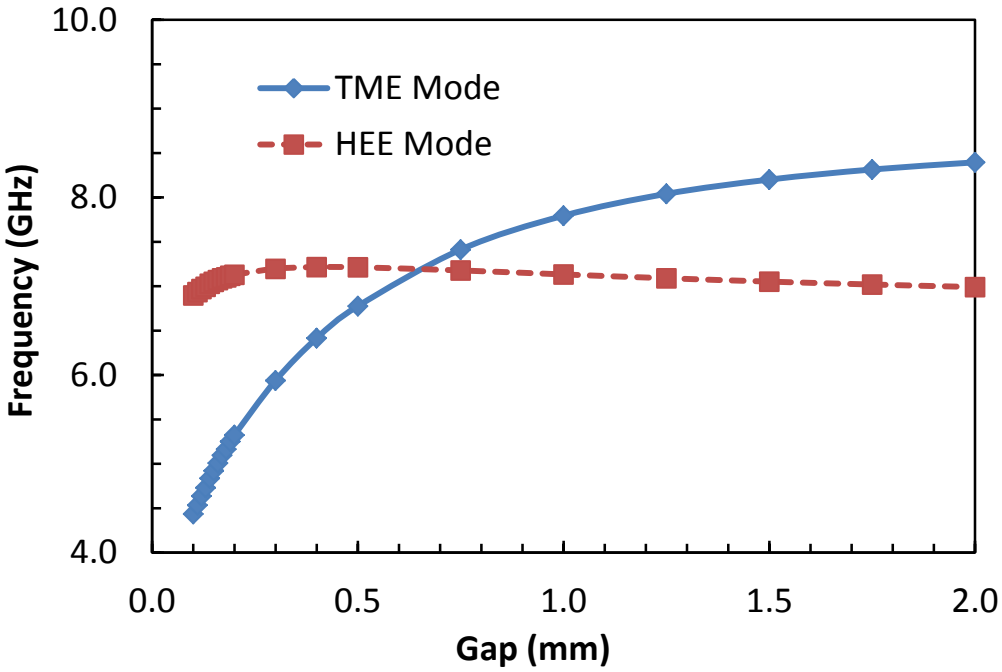

Figure 3.2-2 Resonant frequency of TME, HEE modes versus the gap between the resonator and the top cavity wall

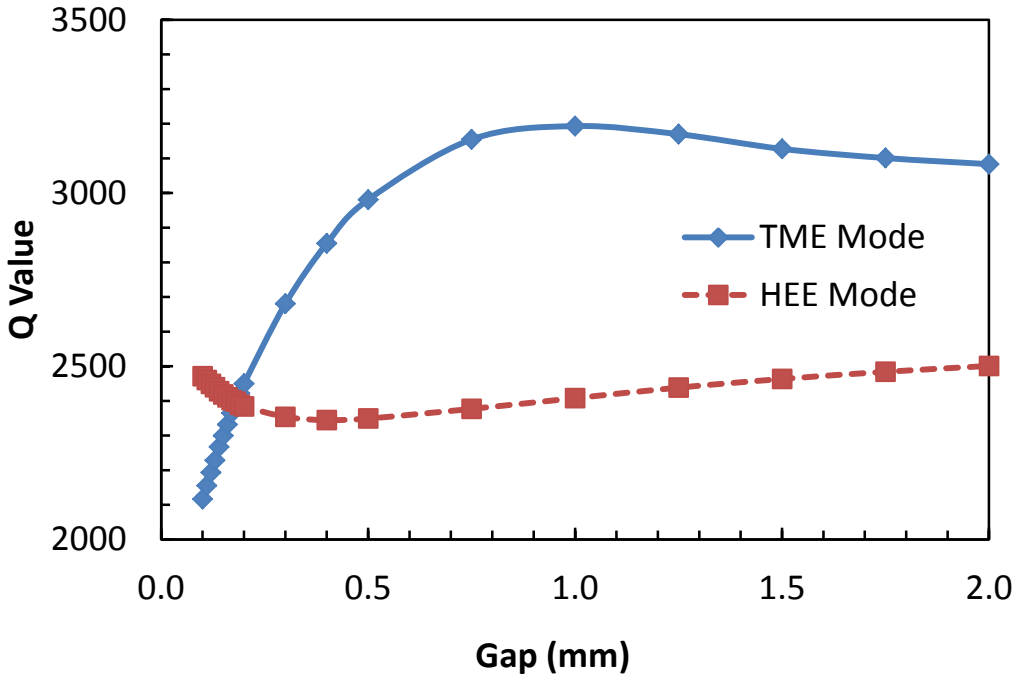

Figure 3.2-3 Unloaded Q of TME, HEE modes versus the gap between the resonator and the top cavity wall

3.2.2 Piezoelectric Bending Actuator

Piezoelectricity is the property to become electrically charged when subjected to mechanical stress. These material also shows the reverse effect, it will deform with the application of an electric field. Owing to this property, piezoelectric transducers can be designed and realized in many forms and shapes. The most widely used piezoelectric transducers are in the form of a thin sheet that can be bonded to, or embedded in a composite structure. Piezoelectric actuators are also available in the form of “stacks”, where many layers of piezoelectric materials and electrodes are assembled together. These stacks generate large forces but small displacements.

The working principle of the piezoelectric actuators is based on the reverse piezoelectric behaviour, which means that mechanical movement is generated when an external electric field is applied. A piezoelectric bending actuator consists of a thin flexible substrate laminated by piezoelectric ceramic material. When an electric field is applied, the laminated piezoelectric material expands or compresses. This expansion or compression of the piezoelectric component is restricted by the elastic substrate. As a consequence, an internal piezoelectric horizontal momentum arises and deforms the actuator. This leads to an up-and-down movement at the free end of the actuator. The total displacement in the z-direction (up and down) is much larger than the deformation of the piezoelectric component in the x-direction, as shown in Figure 3.2-4. Thus, it is possible to generate a large displacement in the z-direction, even when the actuator is driven by low electric voltages (24-200 V).

Hysteresis is a natural property that exists between the polarization and the applied electric field of a piezoelectric material, which depends on the previous history of the piezoelectric ceramics and the external voltage change. The hysteresis phenomenon appears between the deflection of the piezoelectric actuator and the applied voltages are shown in Figure 3.2-5. Therefore, the hysteresis effect needs to be considered when using the piezoelectric actuator at low-voltage levels.

The piezoelectric actuator’s switching speed is limited by its mechanical resonant frequency. The relation between the deflection amplitude of the piezoelectric actuator and the frequency of the applied voltage is shown in Figure 3.2-6. When the applied voltage frequency is below the actuator resonant frequency, the amplitude of the actuator deflection is almost constant. When the applied voltage frequency equals to the resonant frequency of the piezoelectric actuator, the

actuator deflection reaches maximum. Frequency of the applied voltage should be considered when using a piezoelectric actuator in the design of the tunable filters.

Some typical commercial piezoelectric actuators are displayed in Figure 3.2-7. The deflection of these commercial piezoelectric actuators ranges from micrometre to millimetre and their blocked force is larger than 10 Newton when a DC volts is applied. The deflection, blocked force, and capacitance of these actuators vary with dimensions and configurations. In the stacked actuators (Figure 3.2-7 (d)), the blocked force can reach 800 Newton at 100 volts.

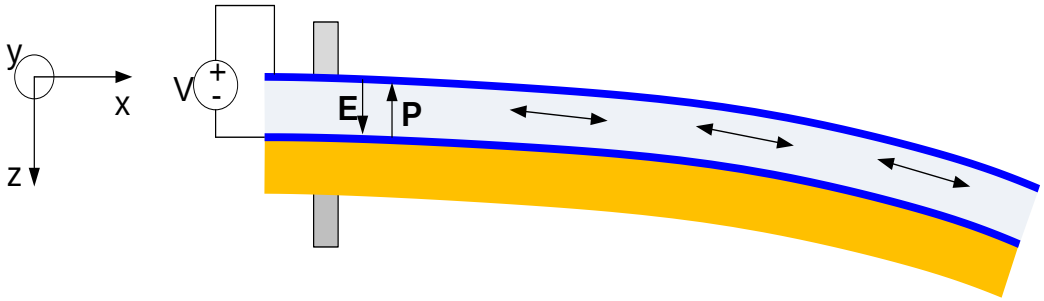

Figure 3.2-4 Schematic view of the behavior of a mono morph subjected to an electrical voltage

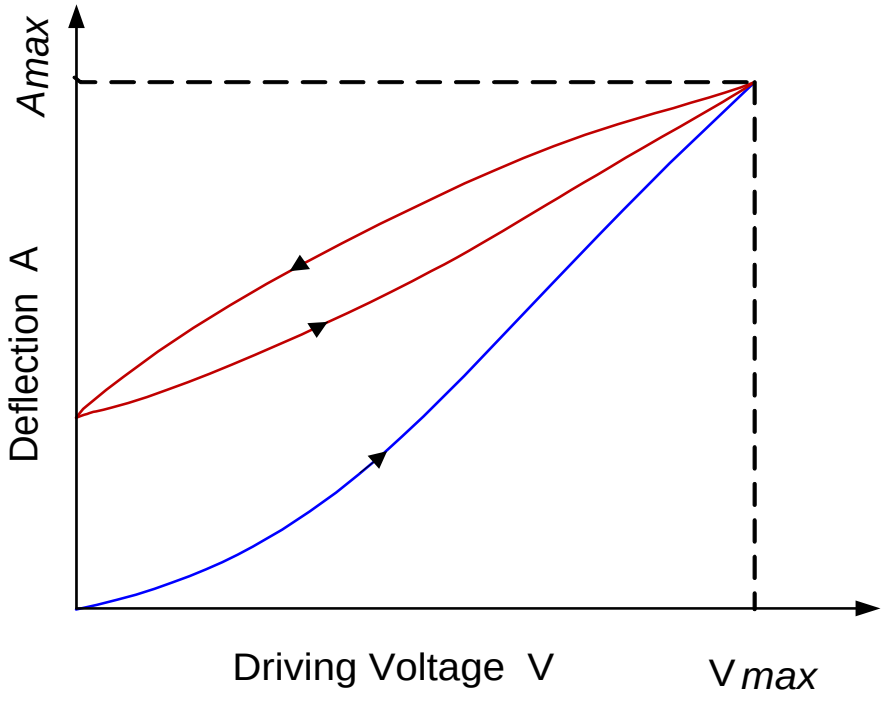

Figure 3.2-5 Deflection of the piezoelectric actuator versus the driving voltage

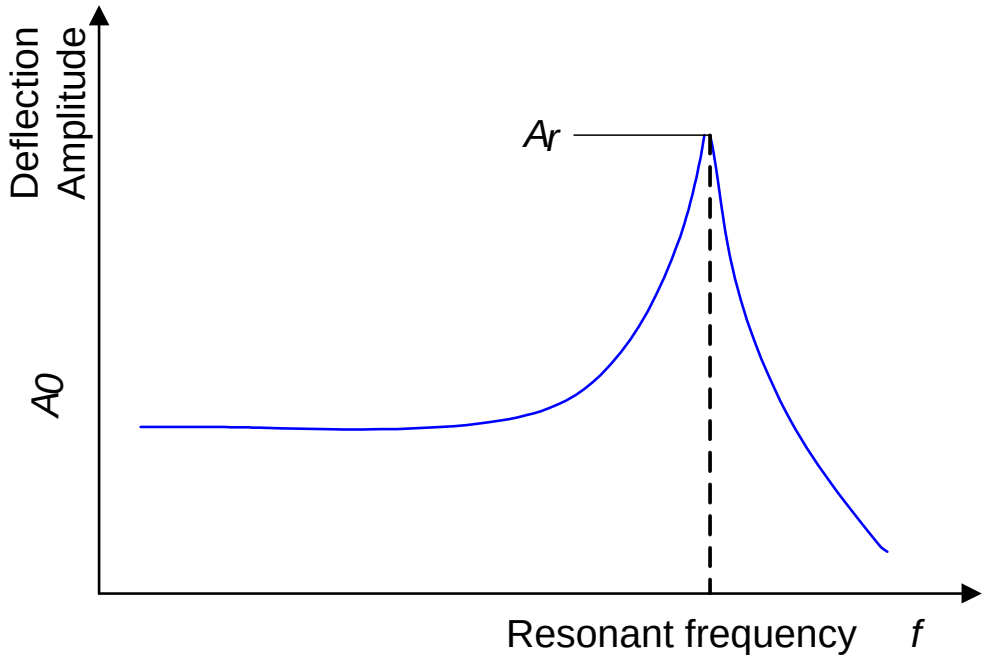

Figure 3.2-6 Amplitude of the piezoelectric actuator versus the electric field frequencies of the controller

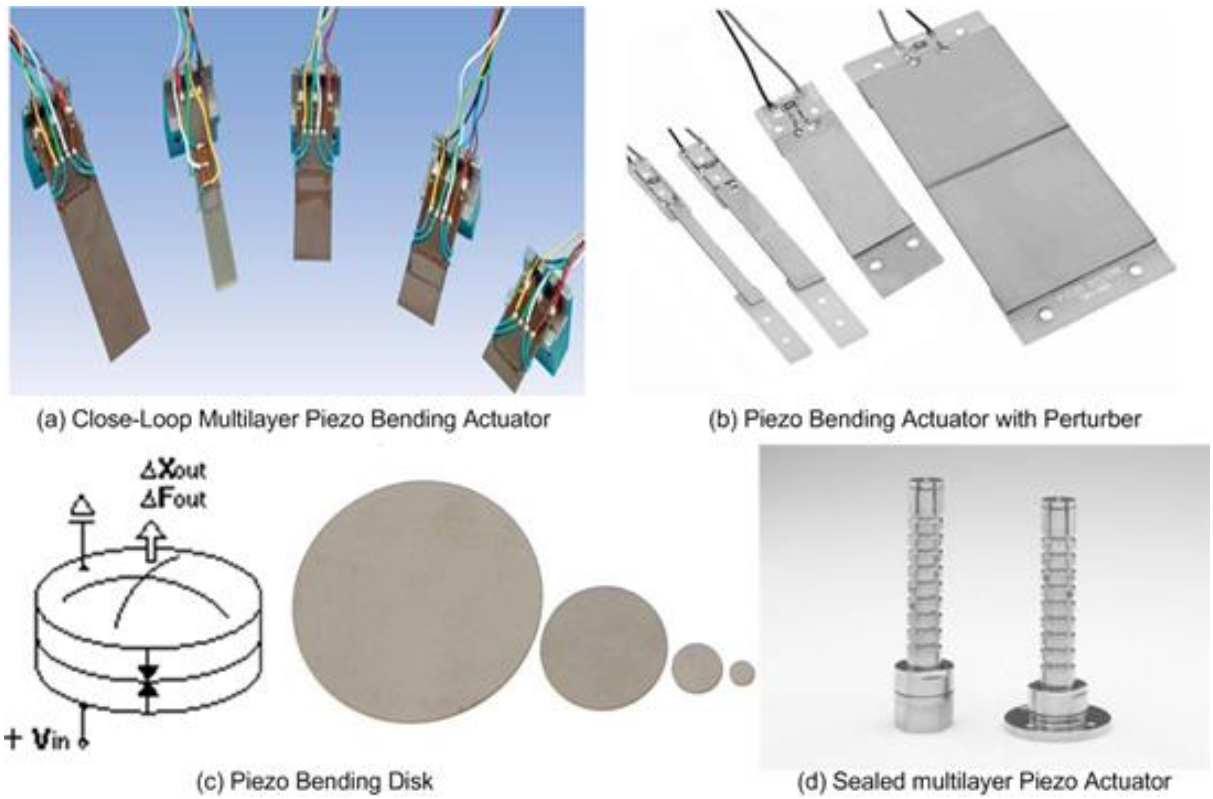

Figure 3.2-7 Samples of commercial piezoelectric actuators

3.2.3 Configuring the Resonator with the Piezoelectric Bending Actuator

In this design, the dielectric resonator is cut from a low loss high K dielectric ceramic with a thickness of 2.54 mm, ε_r=45 and a loss tangent of 10^{-5}, as supplied by Trans Tech Inc. A dielectric resonator that is 6 x 6 x 2.54 mm^3 in size is employed, and placed in contact with the metal cavity bottom to reduce the filter size. The dimensions of a single resonator cavity are 14 x 14 x 2.7 mm^3. The EM simulation results of a single resonator are shown in Table 3.2-1. It tabulates the frequency and the Q factor of the designed single resonator as the gap is changed from 160 μm to 130 μm. The table illustrates that the frequency shifts down by 5.6% from 5 GHz to 4.71 GHz, and the unloaded Q factor stays above 2000 when the gap is reduced by 30 μm.

Each resonator cavity is integrated with a thin film and piezoelectric transducer, as shown in Figure 3.2-8. A flexible thin copper coated polyflon sheet covers the top of the metallic cavity. A multilayer piezoelectric actuator with perturbers attached to each end is mounted on the polyflon film. One perturber is fixed on the cavity, and the other flexible peturber is located on the film right above the cavity center as shown in Figure 3.2-8. The two electrodes are connected to a DC voltage source for actuation. When the DC voltage is applied, the piezoelectric actuator will bend and generate a force on the flexible perturber, which will push the polyflon film's deflection towards the dielectric resonator. Thus, the gap between the DR and the lid decreases while the loading on the resonator increases. Therefore, the frequency of the TME mode shifts down. When the DC voltage is removed, the polyflon film will return to its original shape because of the elastic force of the material itself. As a result, the resonator frequency can be tuned within a range.

Table 3.2-1 Simulation results of a single resonator frequency and Q factor

Dielectric Resonator		
gap(μm)	**Frequency (GHz)**	**Q factor**
160	4.991	2326
155	4.946	2309
150	4.900	2292
145	4.861	2277
140	4.809	2258
135	4.756	2239
130	4.709	2222

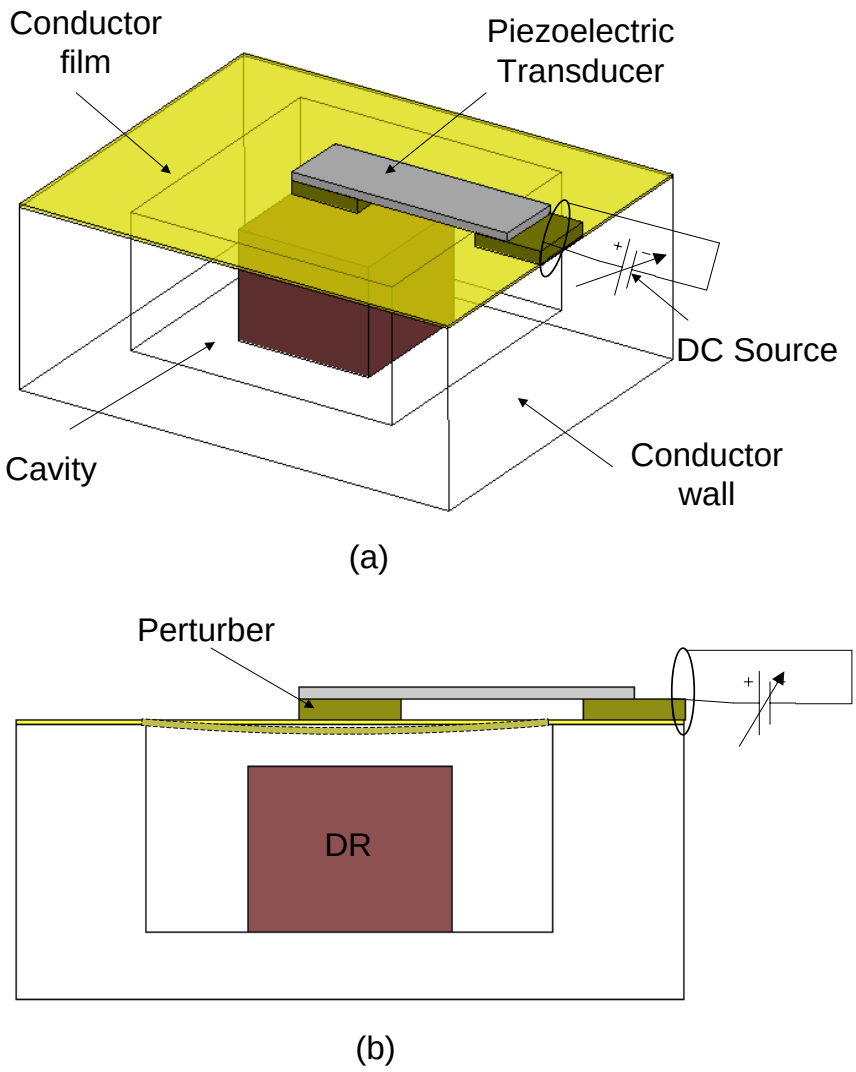

Figure 3.2-8 Mechanism of the tuning cavity: (a) the 3D view of a single cavity tunable resonator and (b) the side view of the deflected cavity of a resonator

3.2.4 TME mode Four-pole DR Filter Design

Figure 3.2-9 shows a schematic structure of a TME mode 4–pole DR filter. The size of the dielectric resonators, the width of the iris, and the input/output coupling are calculated by HFSS simulation. The dimensions of a single resonator cavity are 14 x 14 x 2.7 mm^3. The height of the dielectric resonator is 2.54 mm, and the initial gap between the resonator and the cavity lid is 160 μm. Based on the calculated values, the filter is optimized to achieve a good response for a center frequency of 5.0 GHz and a bandwidth of 50 MHz. The optimized filter results are

displayed in Figure 3.2-10 and Figure 3.2-11. These results show that before tuning, the filter's center frequency is at 5.0 GHz with a bandwidth of 50 MHz, an insertion loss of 1.14 dB, and a return loss of 17.5 dB. Simulation results of the filter as the gap changes from 160 μm to 150 μm and 140 μm are displayed in Figure 3.2-10 and 3.2-11 as well. The results show that with a gap shift between 150 μm and 140 μm, the filter's center frequency shifts from 4.91 and 4.83 GHz. The insertion loss increase from 1.48 to 1.75 dB, and the return loss degrades from 13.5 to 9.5 dB respectively.

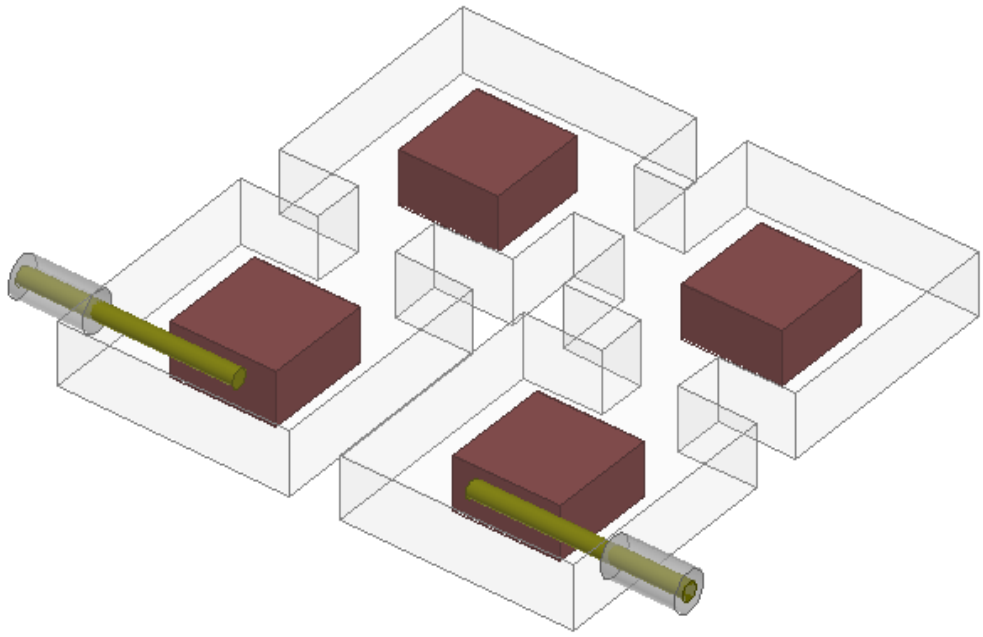

Figure 3.2-9 A schematic structure of a TME mode 4-pole filter

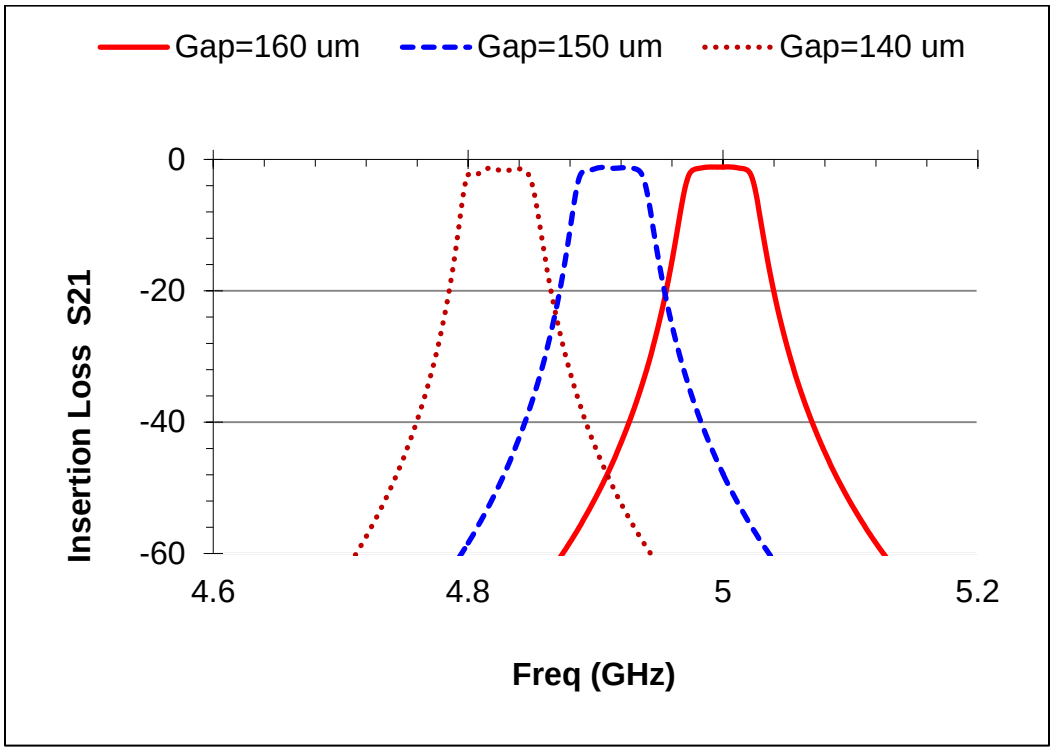

Figure 3.2-10 Simulated tuning response: insertion loss of the 4-pole tunable filter

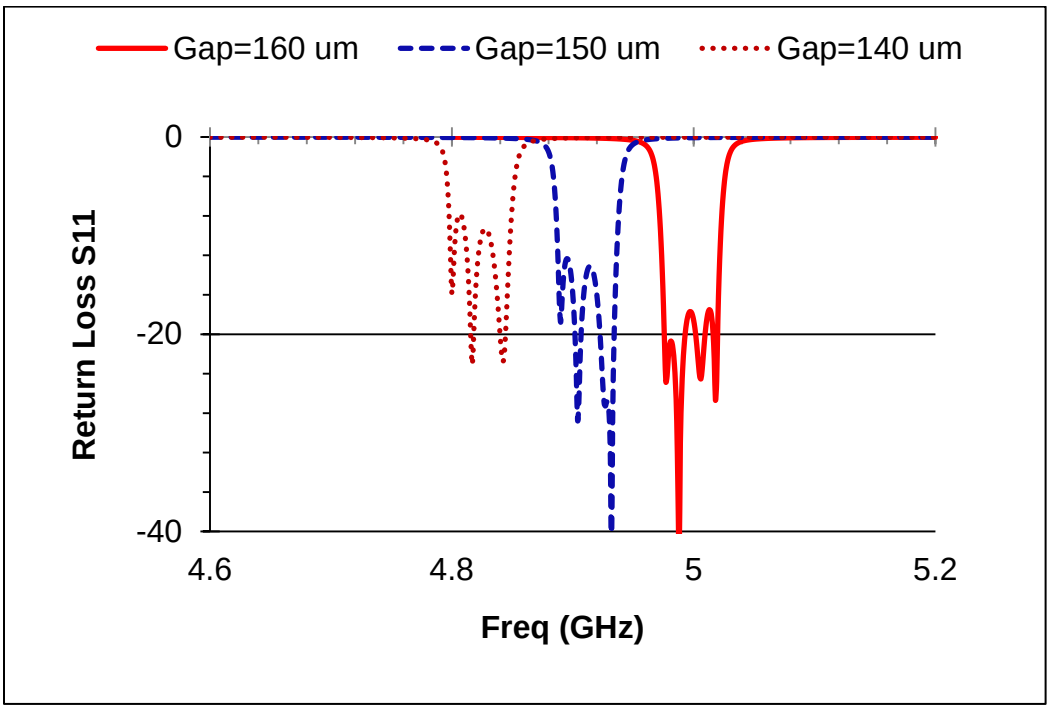

Figure 3.2-11 Simulated tuning response: return loss of the 4-pole tunable filter

Figure 3.2-12 shows pictures of the fabricated 4-pole filter. The measured results of the fabricated filter without tuning are shown in Figure 3.2-13. The figure shows that the filter operates at 5.22 GHz with a bandwidth of 67 MHz. The change in the center frequency is due to the tuning screws used in the cavity's initial tuning. The filter exhibits a mid-band insertion loss of 3.9 dB. The high of the insertion loss achieved in this prototype unit is attributed to many factors including the high loss adhesive materials used to support the dielectric resonator in the cavity, the oxidation of the copper cavity, and the uneven surface of the input/output probes.

Figure 3.2-14 illustrates the unloaded Q extracted from the measurement of the single dielectric resonator tuned at different frequencies. The method used to extract the unloaded Q can be found in [4]. As shown in Figure 3.2-14, when the DC voltage applied to the piezoelectric actuator increases, the DR resonant frequency decreases from 5.15 GHz to 4.94 GHz and the unloaded Q varies from 548 to 536.

When a DC voltage of 180 volts was applied to the piezoelectric actuator, the piezoelectric actuator bent and pushed the copper coated polyflon film, causing the film to deflect towards the dielectric resonator. The measured results are displayed in Figures 3.2-15. The center frequency moves from 5.22 GHz to 4.97 GHz demonstrating a 250 MHz tuning range. The bandwidth changes from 67 MHz to 65 MHz, which is relatively stable. A return loss better than 11.5 dB and an insertion loss better than 4.4 dB are achieved over the tuning range. The differences between the simulated and measured results are due to the fact that the HFSS simulation assumes the copper coated film has a uniform flat surface deflection. However, in reality the copper film does not deflect uniformly.

One feature of this designed filter is that the tuning elements are located outside the cavity. The advantage of such a design is that there is a minimum impact on the resonator's unloaded Q. Another feature is that the dielectric resonator is mounted directly on the cavity wall and operates at TME mode, so that the filter cavity is only 2.7 mm in thickness. This is similar to the microstrip filter, but the unloaded Q is much higher than that of a microstrip filter. The third feature of the designed DR filter is the large spurious free window, which is greater than 2 GHz, and much larger than that achieved by traditional dielectric resonator filters, which are typically several hundred MHz. In addition, since the piezoelectric elements are not in the main electrical path, the power-handling capability in this design can be maintained at a high level.

Nevertheless, because of the need to use a small gap and the nature of the flexible lid used, the structure poses great challenge in assembling and tuning. The initial tuning in particular must be capable of dealing with imperfections in assembling.

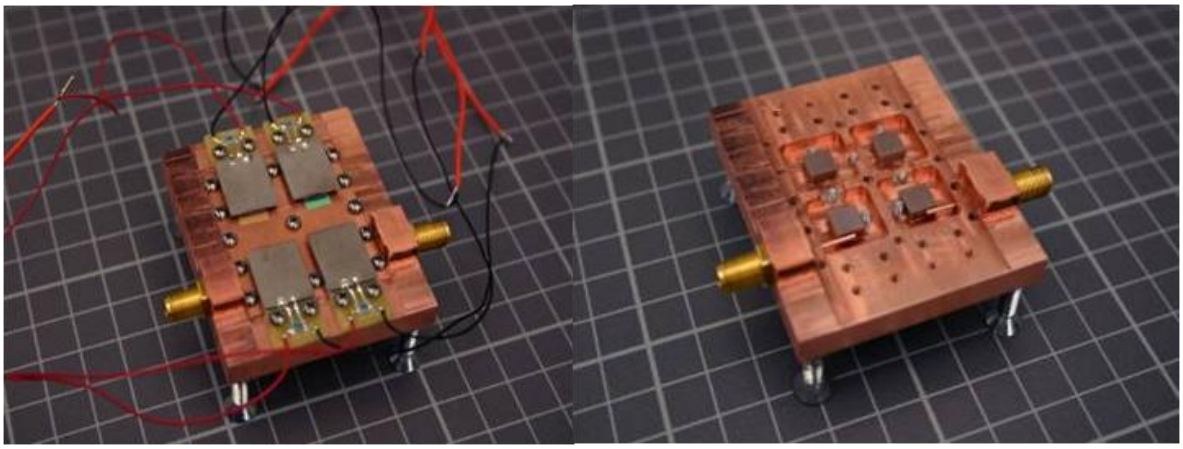

Figure 3.2-12 Fabricated four-pole tunable filter: (left) the 4-pole tunable filter integrated with a piezoelectric actuator and (right) the 4-pole tunable filter with the cover open

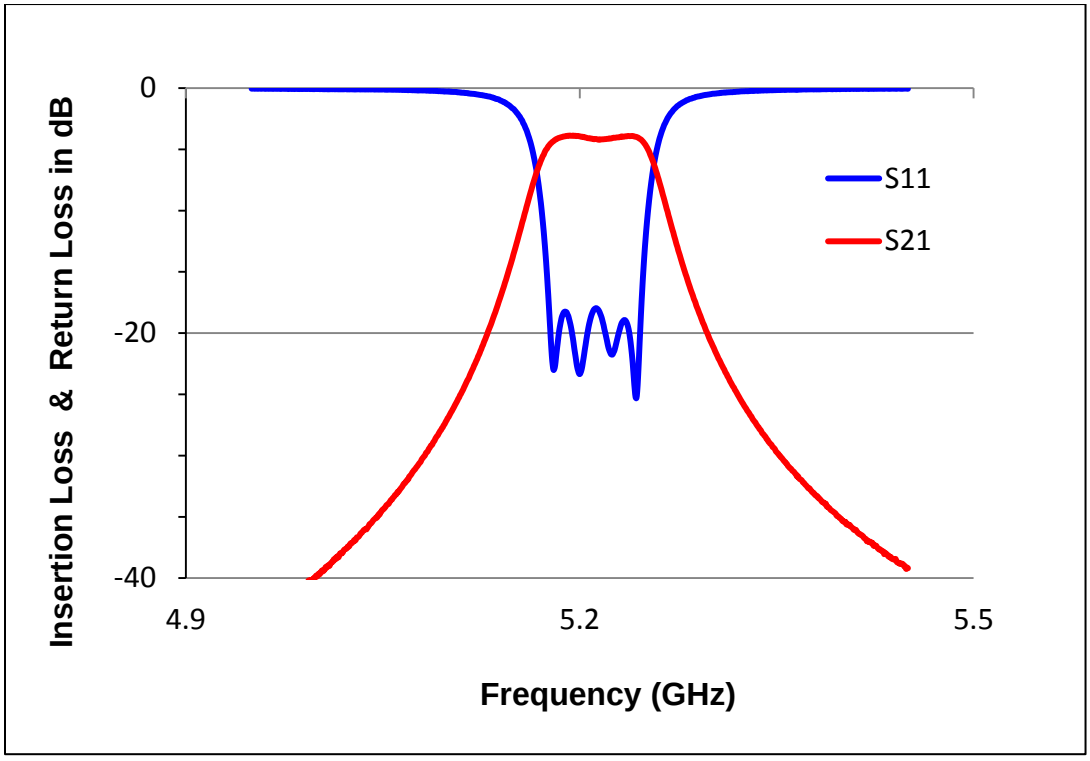

Figure 3.2-13 Measured results of the 4-pole filter before tuning

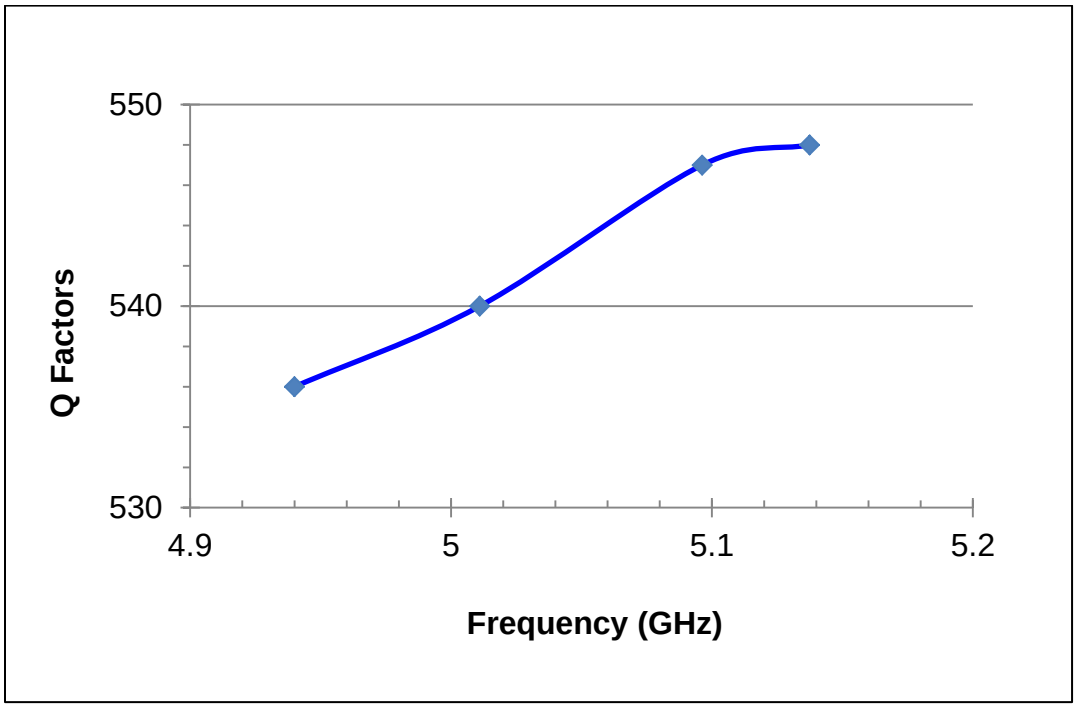

Figure 3.2-14 Extracted Q factors of the single dielectric resonator tuned at different frequencies

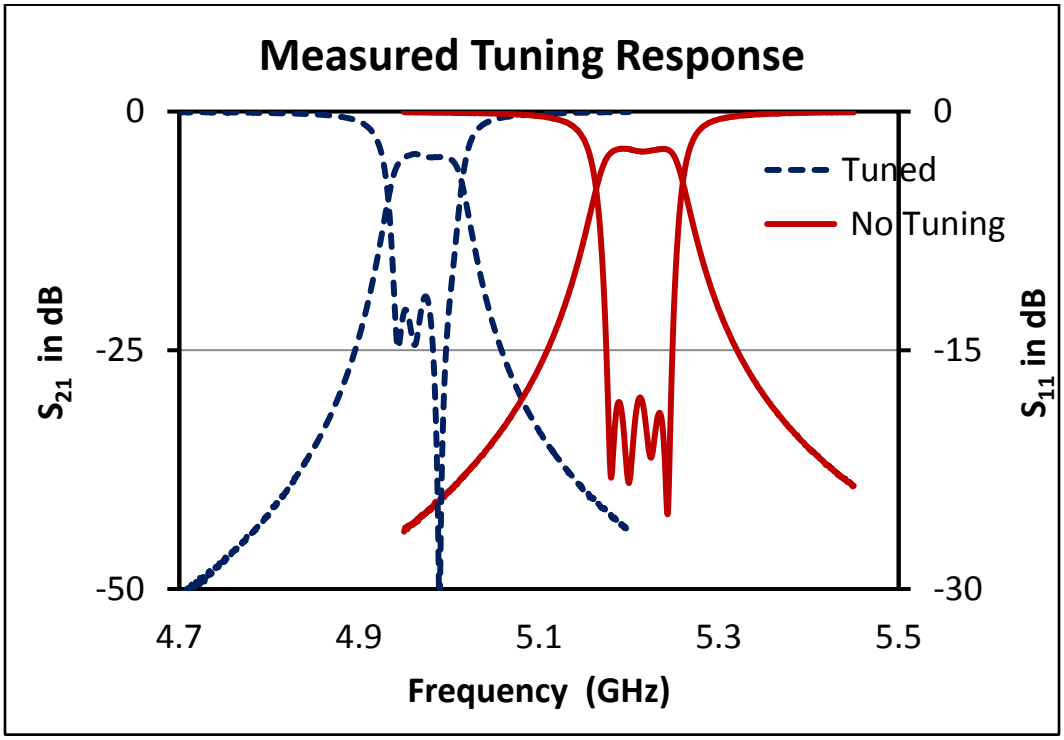

Figure 3.2-15 Measured tuning response of the 4 – pole filter before and after tuning

3.3 Compact Tunable Dual Modes DR Filter

In general, dual-mode filters are smaller by 30% in volume in comparison with single mode filters. In this section, a dual-mode dielectric resonator tunable filter employing a simular concept to that used in section 3.2 is investigated.

3.3.1 Dual Modes Resonator

A high-K ceramic material with a permittivity of 45, a loss tangent of 0.0001, and 12.5 x 12.5 x 2.54 mm^3 in size has been explored as a dielectric resonator. It is placed on a thin metal square support in the metallic cavity, which is 17.5 x 17.5 x 3 mm^3. The metallic support is used to align the position of the dielectric resonator. The structure of the single resonator is illustrated in Figure 3.3-1. If the resonator operates at HEE dual hybrid mode, the frequency of the HEE mode is roughly at 5 GHz. The electric field distributions of the HEE hybrid dual-mode are plotted in Figure 3.3-2. Table 3.3-1 lists the discrete values of the resonant frequencies of the dielectric resonator's first three modes in the given structure. It can be seen that the resonant frequency of the second mode, HEE (hybrid dual mode), shifts by approximately 200 MHz as the gap is changed from 0.15 mm to 0.2 mm. The 50 micrometre deflection is achievable with the use of a piezoelectric bending actuator. If the gap changes further, a larger tuning range can be achieved. The simulation results also demonstrate that the unload Q of the HEE mode of the resonator is better than 2000 over the whole tuning range (as shown in Figure 3.3-4). Figure 3.3-3 illustrates the resonant frequencies of the dielectric resonator's first three modes as simulated by HFSS. The results reveal that the spurious window, before and after the HEE hybrid dual mode, is larger than 1 GHz over the whole tuning range, which makes this dual-mode an acceptable candidate for designing compact high Q tunable bandpass filters.

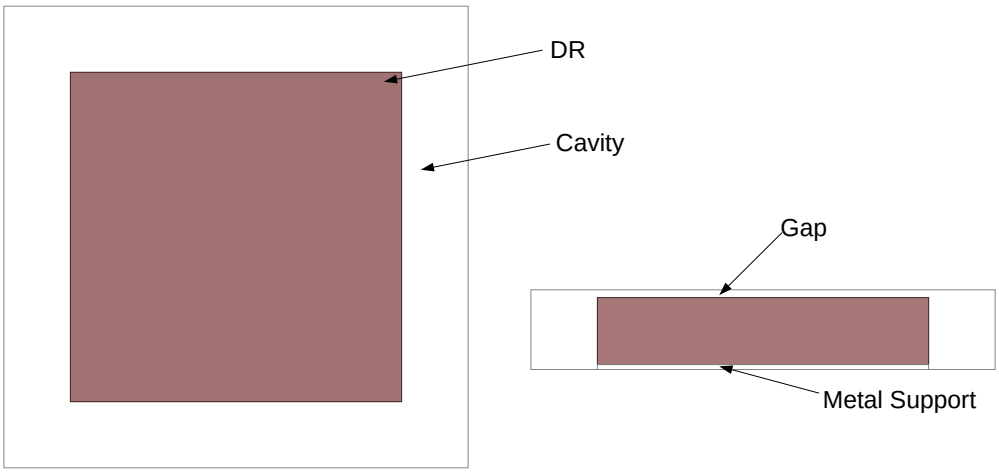

Figure 3.3-1 Structure of a single cavity dielectric resonator: (a) the top view and (b) the side view

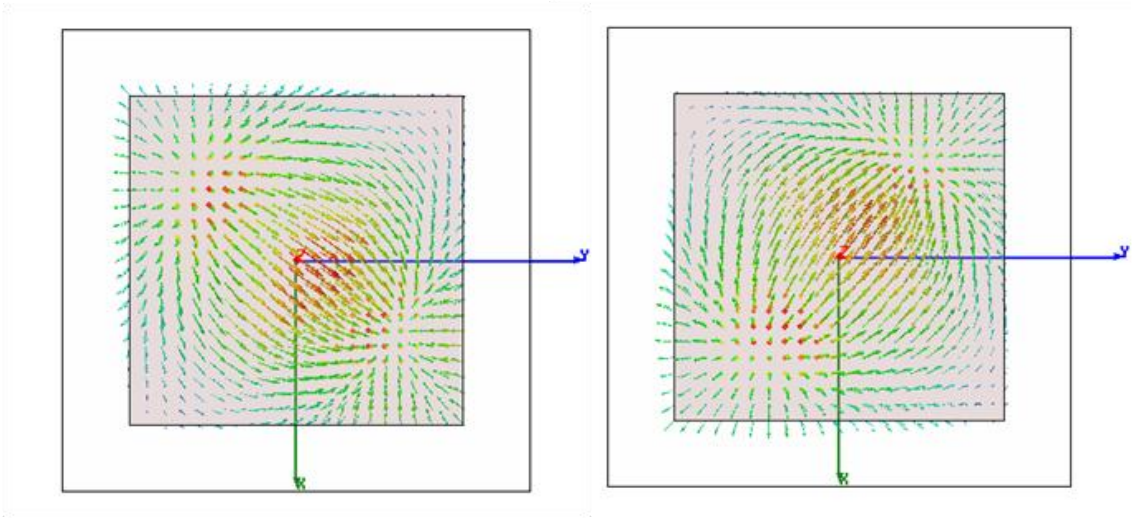

Figure 3.3-2 Electric field distributions of the HEE mode (top view)

Table 3.3-1 Resonance frequency of first three modes in the dielectric resonator

Gap (mm)	TME (Single Mode)	HEE (Dual-Mode)	HEH (Hybrid-Mode)
0.13	3.08	4.62	5.60
0.15	3.23	4.78	5.85
0.17	3.35	4.88	5.92
0.2	3.51	5.01	6.00
0.3	3.94	5.30	6.28
0.4	4.27	5.47	6.30
0.5	4.50	5.56	6.32

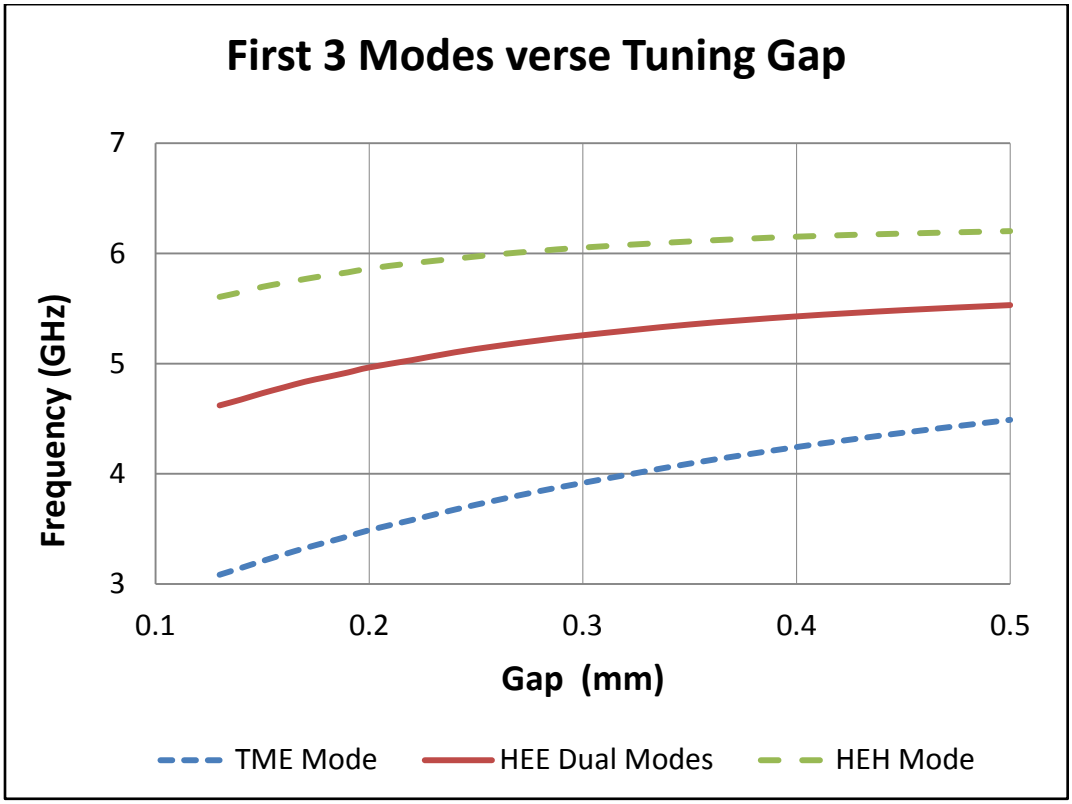

Figure 3.3-3 The mode chart for the first three modes of the dielectric resonator (based on Table 3.3-1)

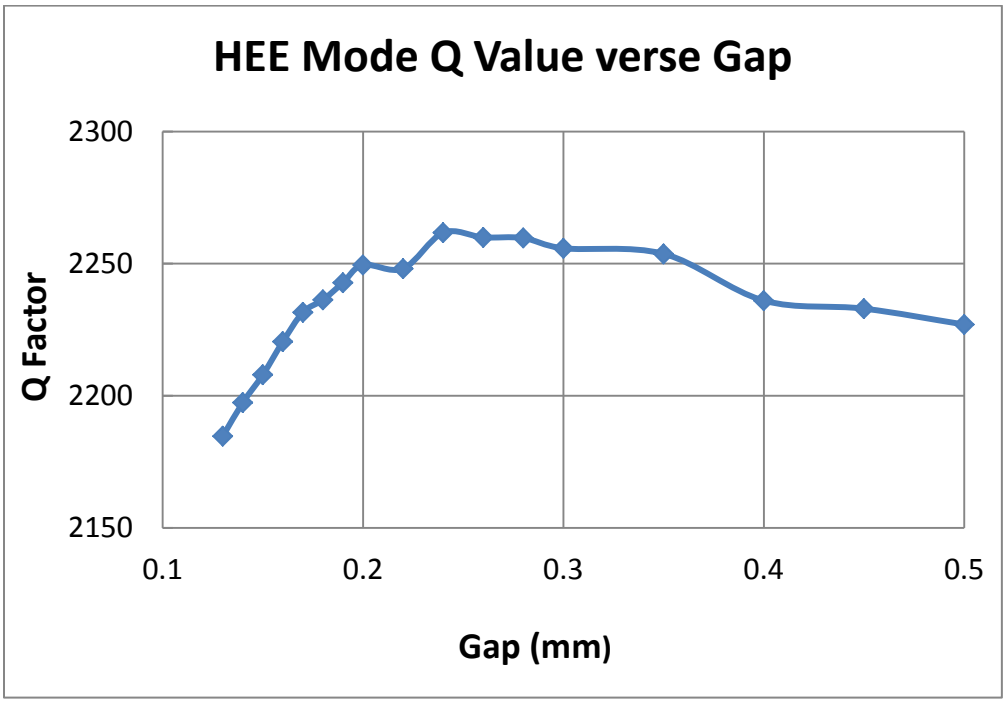

Figure 3.3-4 Q value of the HEE mode versus the gap between the resonator and the cover

3.3.2 Design of Four-pole Dual-mode Filters

Based on the simulation and analysis, a 4-pole dual-mode filter was designed as shown in Figure 3.3-5. It consists of two dual-mode dielectric resonators placed in rectangular metal cavities and separated by an iris window. In the figure, the tuning screws are used to control the coupling between the dual modes in each resonator, and the iris is used to control the coupling between the two resonators. The width of the iris, the position and length of internal tuning screw, the resonator size, and the input probes are obtained by HFSS simulation of the structure at 5.0 GHz with a bandwidth of 50 MHz. After optimization, the 4-pole filter's responses are plotted in Figure 3.3-6. The figure shows that the designed filter operates at 5.0 GHz with a bandwidth of 53 MHz, and exhibits a return loss better than 24 dB, and an insertion loss less than 1.09 dB at the initial status. All the parameters from the initial optimization simulation are kept, simulating the 4-pole filter with the gap decreased by 20 μm and 40 μm respectively. The filter's tuned responses are shown in Figure 3.3-7 and Figure 3.3-8. The corresponding filter center frequencies are located at 5 GHz, 4.905 GHz, and 4.785 GHz, and their bandwidths are 53 MHz,

56 MHz, and 59 MHz, and their insertion loss is 1.09 dB, 1.31 dB, and 1.59 dB respectively. The return loss, however degrades from 25 dB to 10 dB over the tuning range.

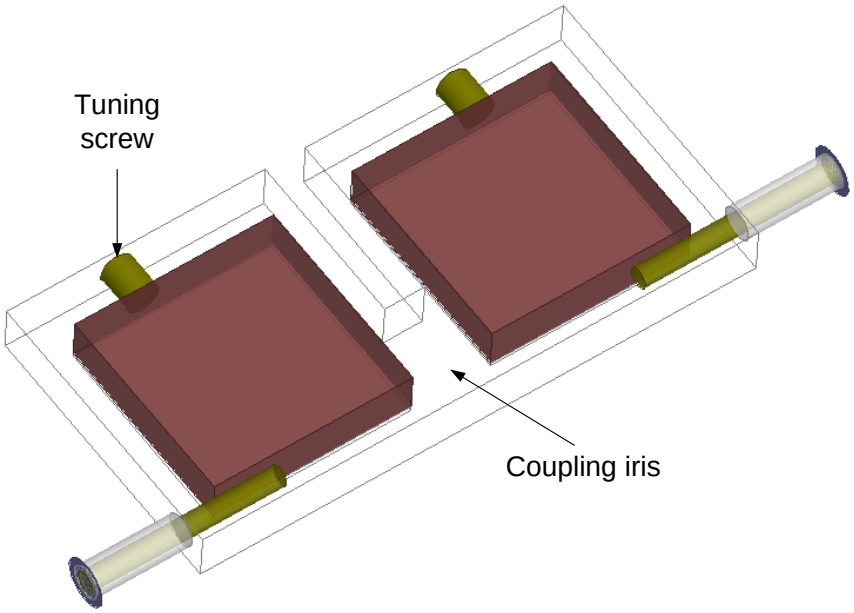

Figure 3.3-5 Structure of a dual-mode four-pole DR filter

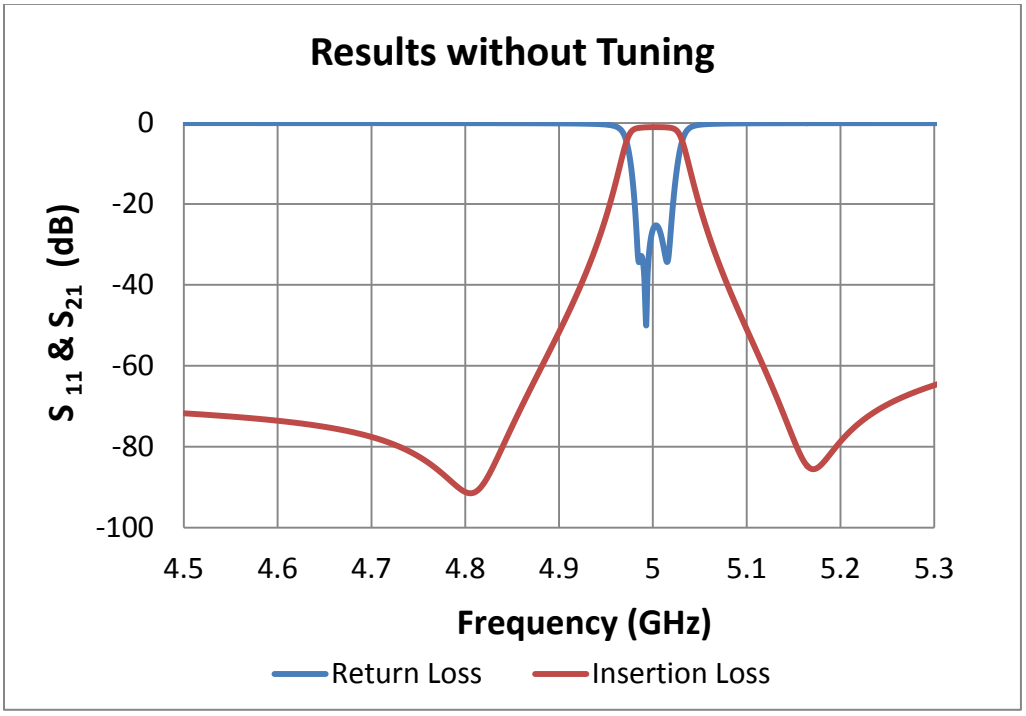

Figure 3.3-6 Simulation results of the four-pole filter without tuning

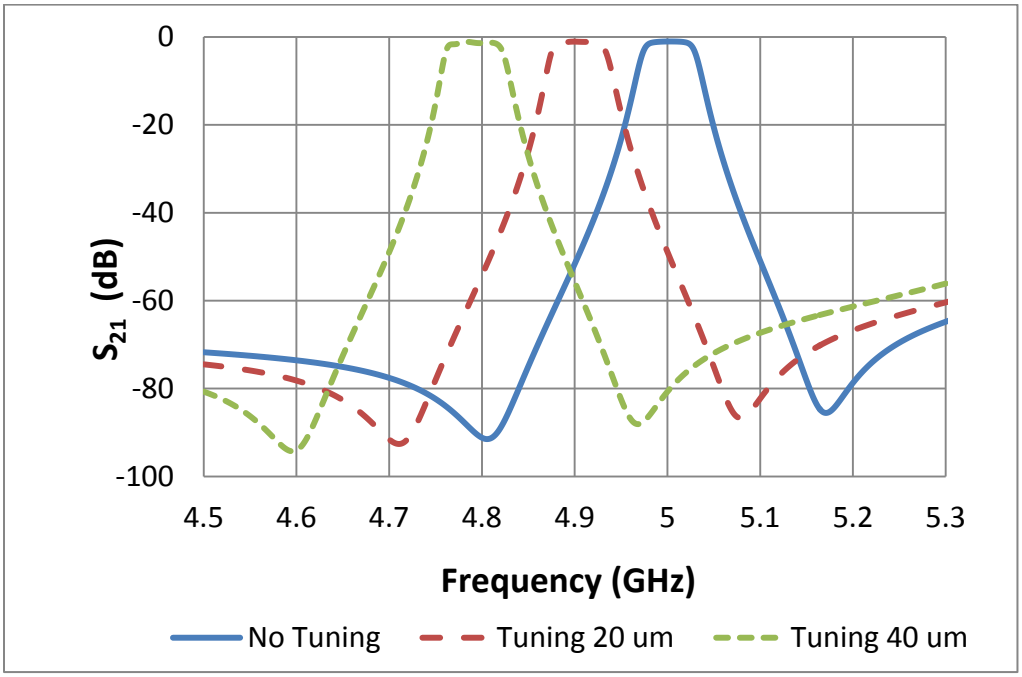

Figure 3.3-7 Simulated tuning performance of S_{21}

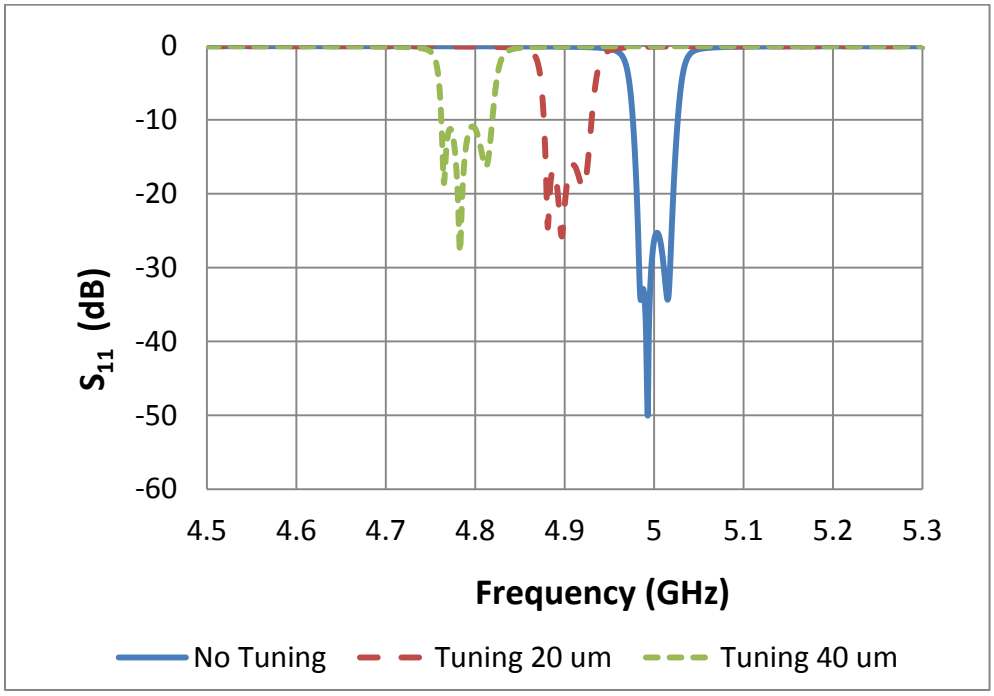

Figure 3.3-8 Simulated tuning performance of S_{11}

3.4 Summary

In this chapter, a new approach to designing a compact high Q tunable dielectric resonator filter based on a piezoelectric bending actuator has been presented and discussed. By placing dielectric resonators made of high-K ceramics directly on the cavity wall, a highly miniature tunable filter with a relatively high Q value was achieved. Both the single mode filter and the dual mode filter were capable of achieving a theoretical Q of 2000 with a cavity height of less than 2.7 and 3.0 mm at 5 GHz respectively. A careful assembly procedure, however, is needed to obtain the experimental Q that matches the theoretical Q. A single mode 4-pole filter has been designed, fabricated and tested to validate the tuning mechanism. A similar approach could be used for compact high Q dual-mode filters, which can even provide more volume reduction in comparison with a single-mode tunable DR filter.

Chapter 4
Tunable Dielectric Resonator Filters Using MEMS Technology

In this chapter, a novel structure of a dielectric resonator filter integrated with MEMS devices and GaAs varactors is presented. By using the coupling that exists between the dielectric resonator and a circuit controlled by MEMS devices or GaAs varactors, the resonant frequency of a dielectric resonator is tuned. The proposed resonator is employed to realize high-Q tunable dielectric resonators.

4.1 Introduction

Dielectric resonator filters are widely used in wireless and satellite communication systems. A variety of approaches have been devised in order to make tunable dielectric resonator filters with a low insertion loss [24, 76, 92-94]. The major conventional tuning method is mechanical tuning, such as in [18, 95], where the density or distribution of the electric field in the dielectric resonator is altered via elements or mechanisms external to the dielectric resonator. Magnetically tuned dielectric resonator filters can also achieve high-Q values[76, 96]. Although mechanically and magnetically tuned dielectric resonator filters can maintain high-Q values, they are bulky in size.

Another technique that has been employed in the past to achieve a fast tuning speed while maintaining a high-Q is the use of MEMS elements as controllable tuning screws. A tunable dielectric resonator filter using embedded MEMS actuators and tuning disks to perturb the electric and magnetic fields has been reported in [76]. This type of filter achieves a relatively high-Q value; however, the proposed tuning method is limited to high frequency applications (X-band or above). Dielectric resonator filters operating at the C-band and tuned by employing

piezoelectric actuators are also reported in chapter 3 [24]. The use of piezoelectric actuators leads to complicated assembly and increased size of the fabricated dielectric resonator filters.

In this chapter, a tuning approach employing MEMS switches on DR filters for low frequency applications is proposed. The proposed tuning concept to tunable DR filters is expanded to employ GaAs and MEMS capacitor banks as the tuning elements. By using varactors and MEMS switched capacitor banks a better performance is achieved in terms of tuning range.

4.2 Tunable DR Filter with MEMS Switches

4.2.1 Proposed Tuning Concept

The dielectric resonator modes are determined by both the structure of the resonator and its boundary conditions. The main two modes of a cylindrical dielectric resonator, typically used to design DR filters for wireless applications, are the TEH and TME modes. Attempts have been made to down shift the TME mode in a dielectric resonator by reducing the height of the cavity as reported in [8]. For the designs presented in this thesis, disk shaped dielectric resonators cut from a high k dielectric material with thickness of 4.7 mm, a relative permittivity of ε_r=38 and a loss tangent of 10^{-4} are used. Figure 4.2-1 shows the schematic diagram of the dielectric resonator. The dielectric disk is supported inside the cavity by a Teflon material with a low loss and low dielectric constant. There is a hole with a diameter of 3 mm inside the dielectric material. This hole can be used to improve the spurious window between the main mode, and the higher order modes of the dielectric resonator. It is also used to provide the room to place the tuning elements inside the resonator as will be explained later. This configuration of the tunable dielectric resonator is quite compact.

Both the TME and TEH modes can be used to design tunable DR resonators. For the TME mode this can be achieved by placing a conductive metal strip inside the center hole within the dielectric material. The conductive strip is connected to the cavity wall and it can act as a tuning element. The surface current on the conductive strip and also the electric field for the TME mode are presented in Figure 4.2-2. The direction of the surface current is parallel to the TME mode's electric field inside the dielectric resonator as seen in this figure. Therefore, there is a coupling between the conductive gold strip and the TME mode. By varying the surface current on the

conductive strip, the TME mode can be tuned. This allows tuning of the resonance frequency by varying the length of the metal strip inside the dielectric resonator. Figure 4.2-3 shows the simulation results for the resonance frequency and the Q-value of the TME mode versus the length of the conductive strip. A wider tuning range can be achieved using a longer conductive strip. However, for the proposed tuning concept, the ohmic loss of the conductive strip is dominant and it will degrade the Q of the resonator. A center hole with a bigger diameter along with a wider conductive strip will also improve the tuning range at the expense of a reduced Q value.

A similar approach is applicable for the TEH mode. The resonance frequency can be tuned by employing a conductive ring on the dielectric material and a varactor as the tuning element as depicted in the inset of Figure 4.2-4. Based on the simulation results in Figures 4.2-3 and 4.2-4, a wider tuning range can be achieved using TME mode. However, a higher Q-value is obtained for the TEH mode. Figure 4.2-5 shows the EM simulation results for the resonance frequencies of the TME and TEH modes versus the cavity height, H . Based on the simulation results in Figure 4.2-5, a cavity height less than 6 mm is required to make the TME mode dominant.

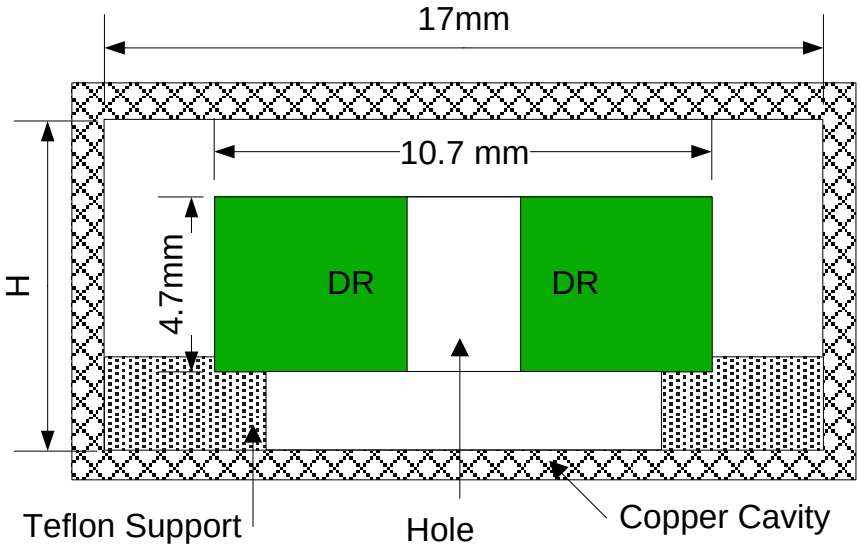

Figure 4.2-1 Schematic diagram of the dielectric resonator

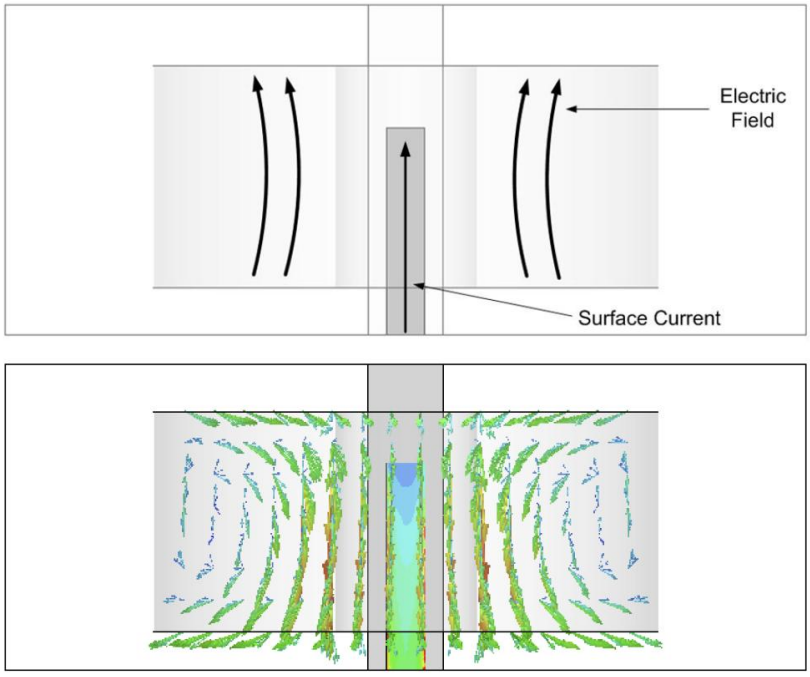

Figure 4.2-2 Electric field for the TME mode and the surface current on the conductive

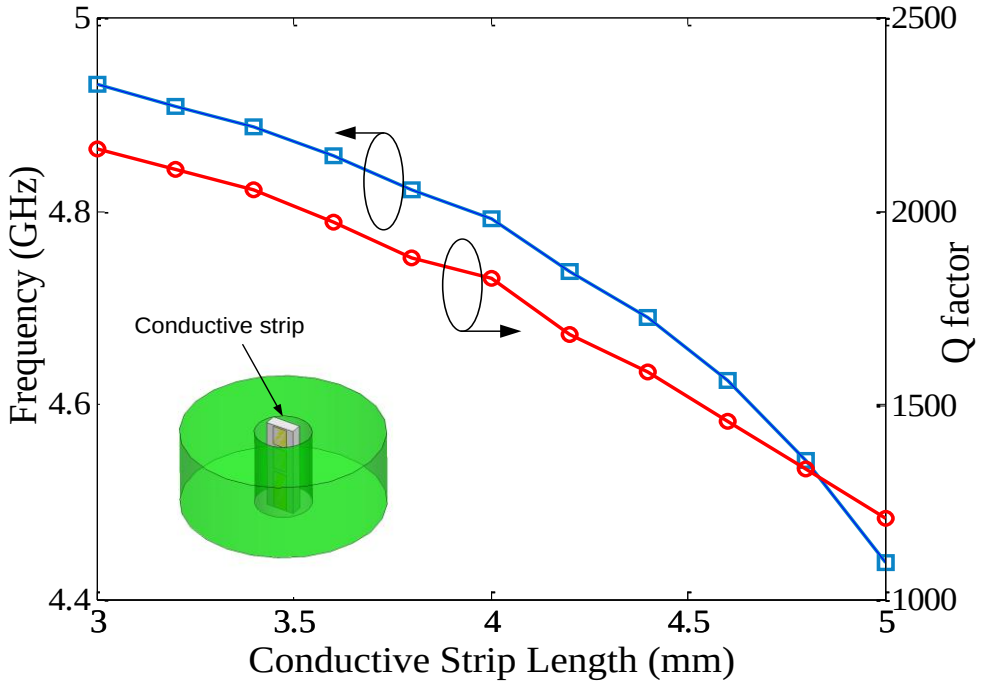

Figure 4.2-3 Simulated resonance frequency and Q versus the length of conductive strip (TME mode)

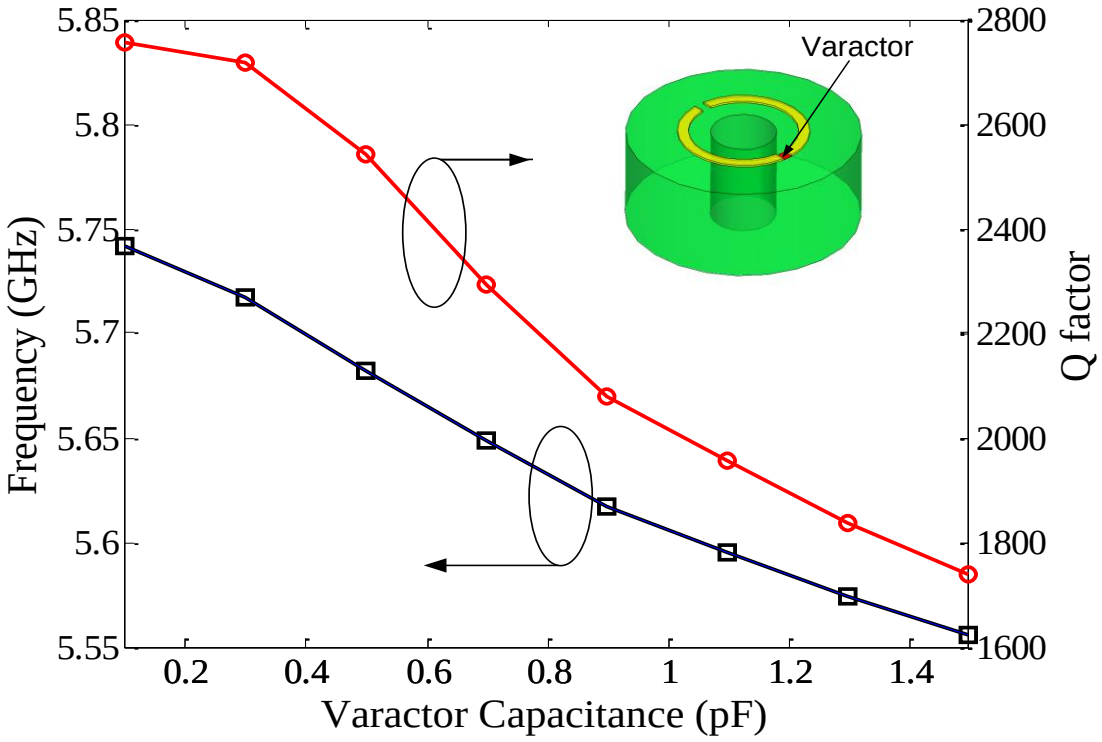

Figure 4.2-4 Simulated resonance frequency and Q versus the capacitance value (TEH mode)

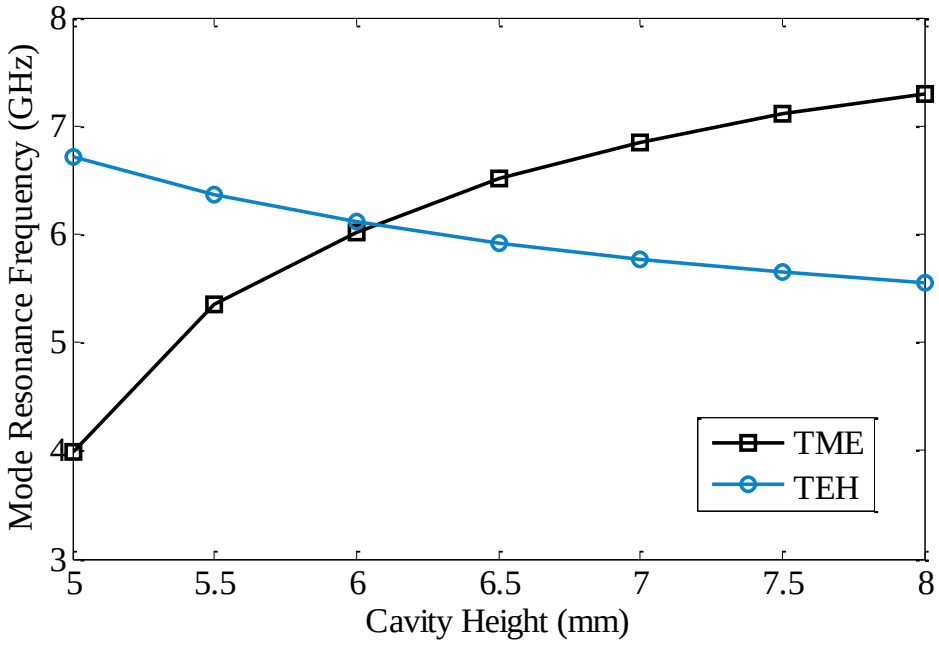

Figure 4.2-5 Simulated resonance frequency versus cavity height for TME and TEH modes

4.2.2 Tunable Dielectric Resonator with MEMS Switches

The cross sectional schematic view of the proposed tunable dielectric resonator and the layout of the tuning circuits are shown in Figure 4.2-6. The tuning circuit with MEMS contact-type switches is fabricated on an alumina substrate and is assembled inside the circular hole within the dielectric material in a way that the conductive strip is connected to the cavity wall and makes a ground connection. The tuning circuit, as shown in Figure 4.2-6 (b), consists of three segments of conductors made of 1.2 μm thick gold on a 625 μm alumina substrate. Each section has a different length (L_1, L_2 and L_3) separated by a 100 μm gap from each other. Two sets of contact type MEMS switches are utilized over the 100 μm gap between these sections. The MEMS switches are fabricated using the UW-MEMS fabrication process at the University of Waterloo. The bias lines are made of SiCr with a high sheet resistance in order to reduce the loss and maintain a high Q value. A SEM image of the fabricated cantilever type MEMS switches is presented in Figure 4.2-7.

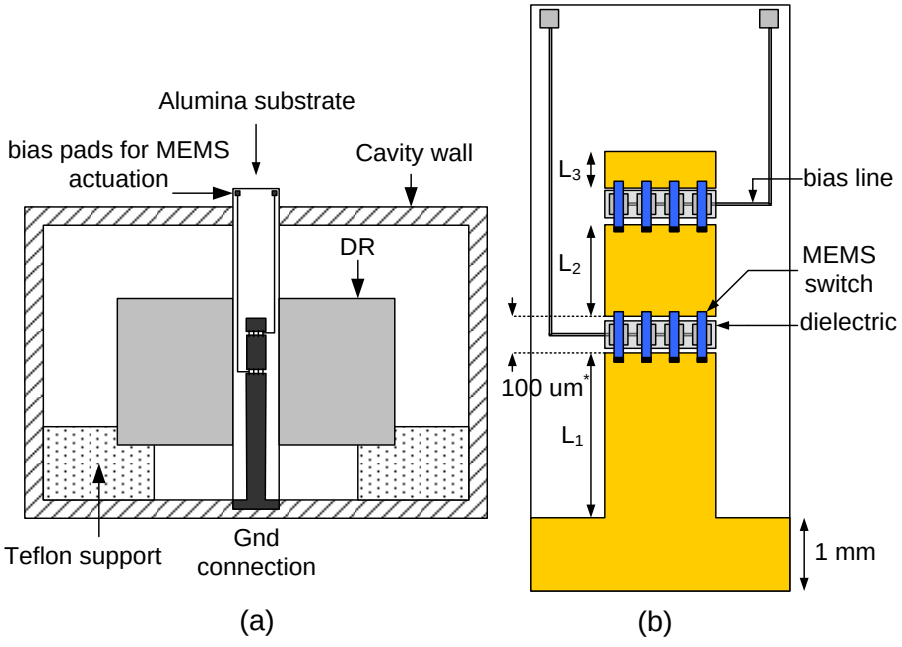

Figure 4.2-6 (a) Cross sectional view of the dielectric resonator with the tuning element inside and (b) schematic view of the alumina substrate with the tuning circuit (dimensions not to scale)

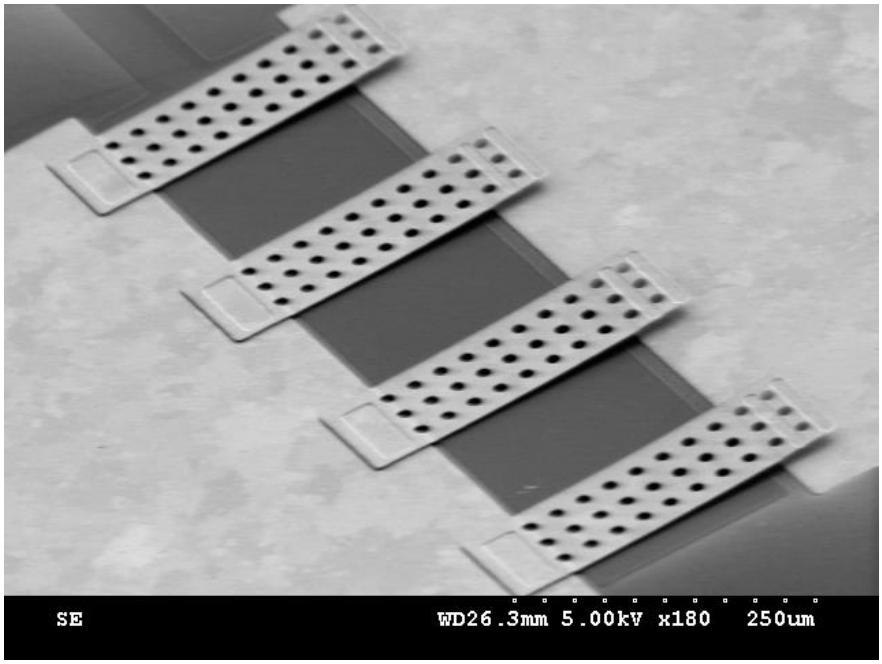

Figure 4.2-7 SEM image of the fabricated contact type MEMS switches

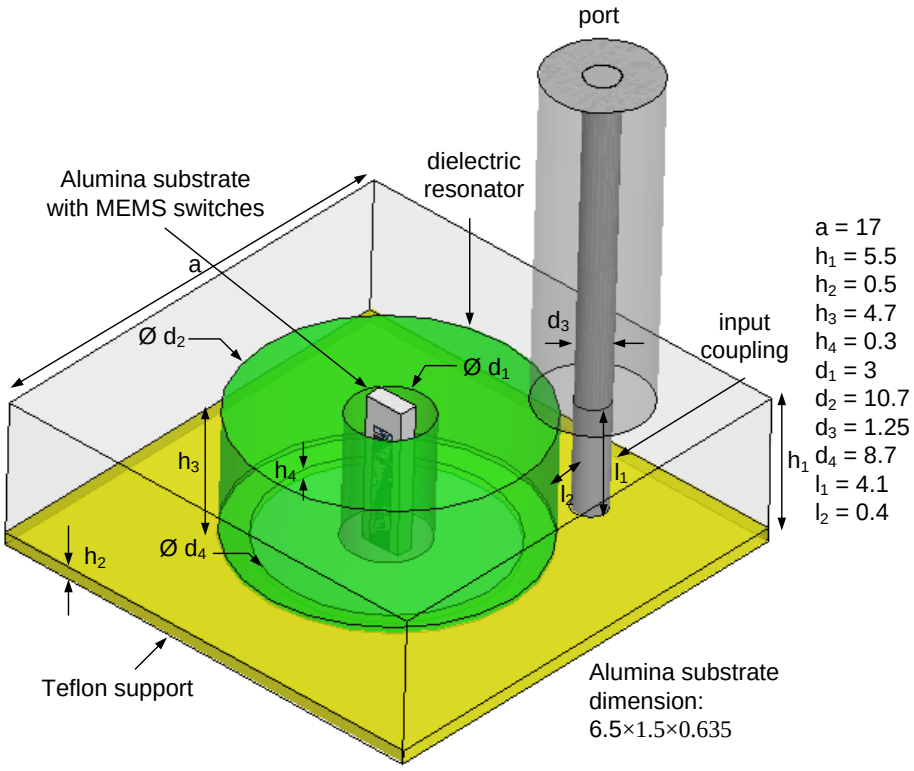

Figure 4.2-8 EM model for the proposed tunable dielectric resonator using MEMS switches as tuning elements (unit: mm)

Figure 4.2-8 shows the 3D EM model for the tunable dielectric resonator. Based on EM simulations with HFSS, the first two modes of the resonator are the TME mode at 5.17 GHz and the TEH mode at 6.37 GHz with unloaded Q values of 2700 and 3470, respectively. The length of the conductive strip is tuned by employing two sets of MEMS switches as shown in the schematic view of the proposed tuning circuit in Figure 4.2-6(b). Each set of MEMS switches has a separate bias line connected to bias pads outside the cavity and can be actuated independently. When the bias voltage on the MEMS switches is zero, the effective length of the conductive strip is $L = L_1$. When the first set of switches are actuated to the down state, the second segment of conductive strip (L_2) is electrically connected to the first strip and the total length of the strip is increased to $L = L_1 + L_2$ tuning the resonance frequency of the resonator. A third state can be achieved by simultaneously actuating both sets of the MEMS switches. For this particular design, using two sets of MEMS switches, three different resonant frequencies are achieved. Higher number of MEMS switches along with more conductive strips on the alumina substrate can be used to obtain finer tuning steps with lower Q.

4.2.3 Two-pole Tunable Dielectric Resonator Filter

Employing the designed tunable dielectric resonator, a two-pole DR filter is designed and simulated using HFSS. Figure 4.2-9 shows the full-wave simulation model of the filter. For EM simulation, each set of the MEMS switches is modeled with a series capacitor and resistor for the off and on states, respectively. The conductivity of the gold metal layer for the MEMS tuning circuit is assumed to be 4.1×10^7 s/m. Based on the simulation results, the final lengths of the conductive strips are L_1=3.3 mm, L_2=0.75 mm and L_3=0.25 mm separated by a 100 μm gap for the MEMS switches.

Figure 4.2-10 shows the simulated S-parameters of the designed filter for different tuning states. Simulation results demonstrate that the filter operates at 4.82 GHz with a bandwidth of 20 MHz and a return loss better than 20 dB. It exhibits an insertion loss of 0.42 dB for the first state, when no bias voltage is applied on the MEMS switches. The center frequency can be tuned to three different values f_1=4.82 GHz, f_2=4.73 GHz and f_3=4.65 GHz while the bandwidth for a return loss better than 18 dB is 20 MHz for all three states as listed in Table 4.2-1.

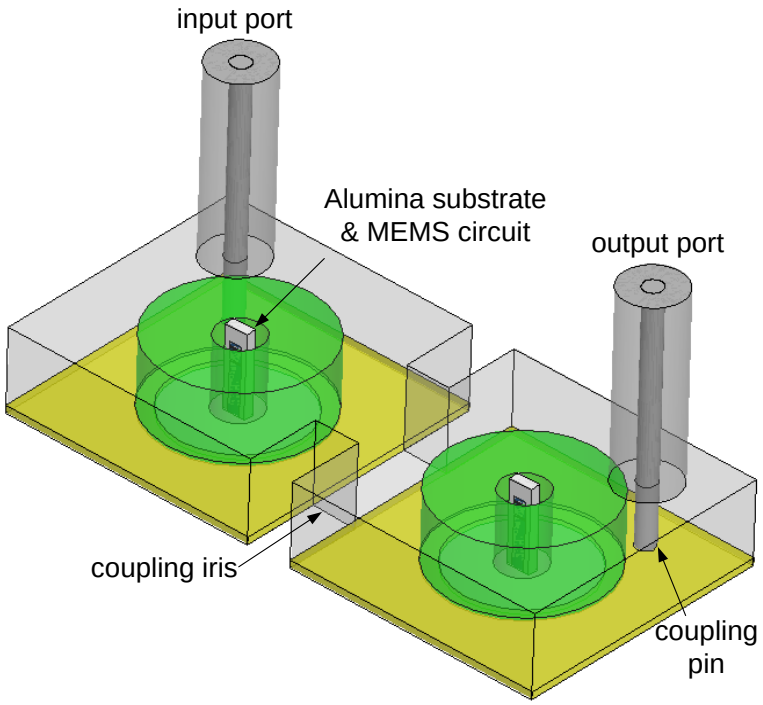

Figure 4.2-9 Full-wave HFSS simulation model of the two-pole tunable dielectric resonator filter

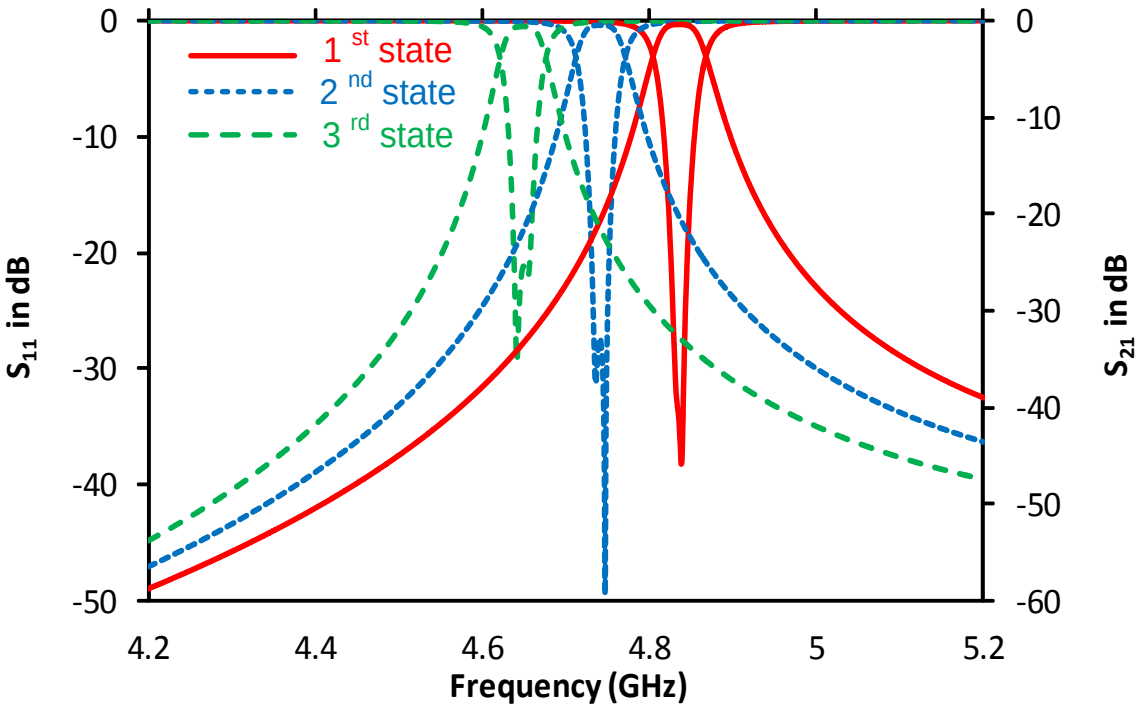

Figure 4.2-10 Simulated S-parameters of the tunable dielectric resonator filter with MEMS switches

Table 4.2-1 Summary of simulation and measured results

Tuning State	1^{st}	2^{nd}	3^{rd}
f_o (sim/meas) (GHz)	4.82/4.80	4.73/4.71	4.65/4.64
BW (sim/meas) (MHz)	20/21	20/21	20/23
IL (sim/meas) (dB)	0.42/1.03	1.01/1.63	2.01/2.10

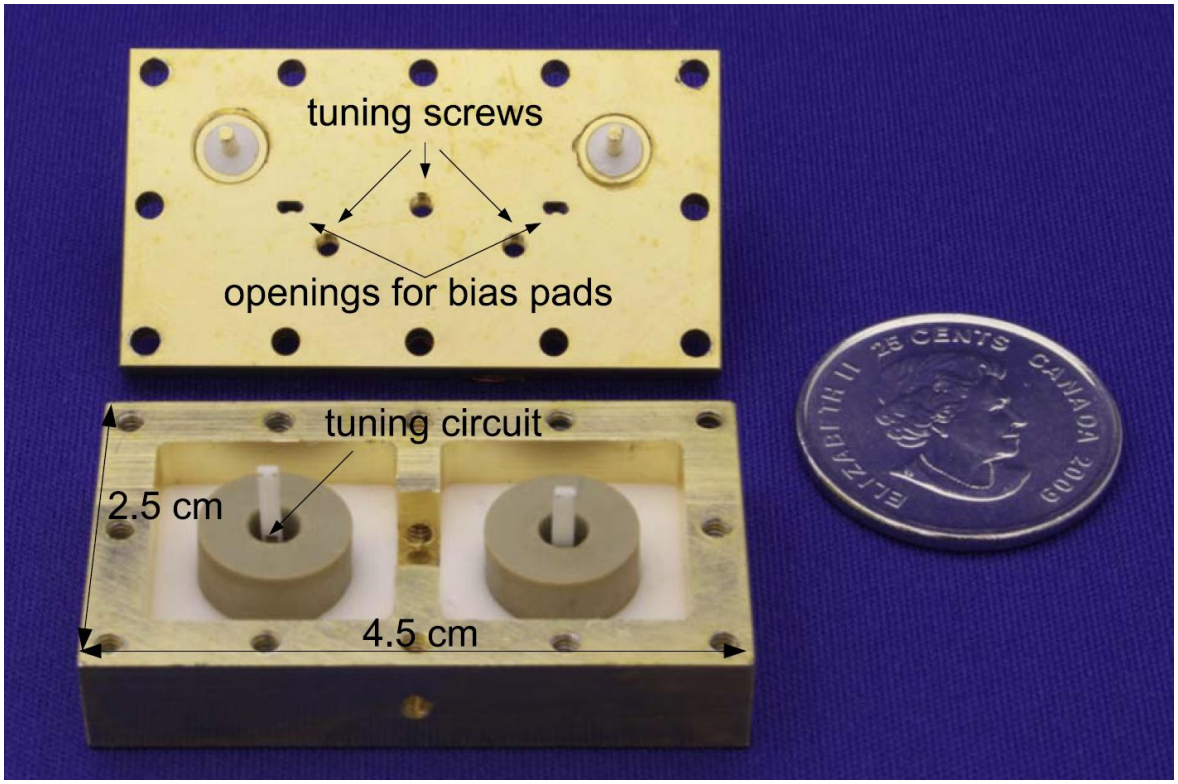

Figure 4.2-11 Image of the two-pole tunable dielectric resonator filter

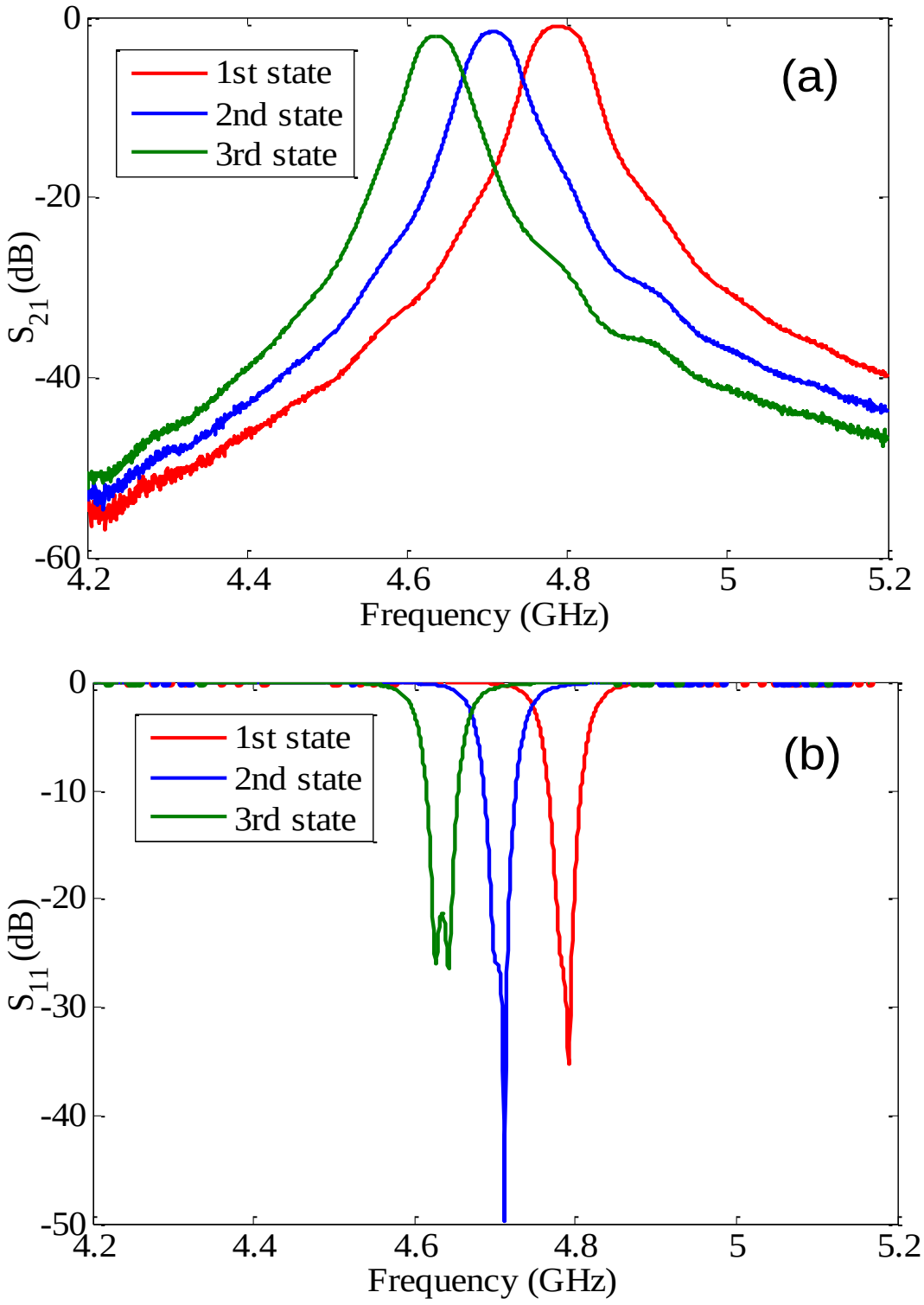

Figure 4.2-12 Measured (a) insertion loss S_{21} and (b) return loss S_{11} of the tunable dielectric resonator filter

A 2-pole tunable dielectric resonator filter is fabricated and tested. The aluminum housing is gold plated for improved performance. The tuning circuits with MEMS switches and the final filter is assembled as shown in Figure 4.2-11 with the lid open. There are openings on the lid for tuning screws and also for the bias wires for the MEMS switches. For electrostatic actuation of the MEMS switches, a 60 V bias voltage is applied between the bias pads for each set of the MEMS switches and the DC ground which is the cavity walls in this case. Measurement results are presented in Figure 4.2-12. As shown in this figure, the filter operates at 4.80 GHz with a 21 MHz bandwidth and 1.03 dB insertion loss for the first state. A maximum tuning range of 160 MHz from 4.80 GHz to 4.64 GHz is achieved using the MEMS switches. The return loss is better than 20 dB and the insertion loss is less than 2.1 dB for all three tuning states as listed in Table 4.2-1. The measured Q values for different tuning states are presented in Table 4.2-2. The measurement results match with the simulations and validate the feasibility of using the proposed tuning approach for dielectric resonator filters.

Table 4.2-2 Measured effective loaded Q values

Without Tuning Circuit	1^{st} state	2^{nd} state	3^{rd} state
1900	1220	690	510

4.3 Varactor Tuned Dielectric Resonator Filter

To obtain continuous tuning, a second 2-pole tunable dielectric resonator filter based on GaAs hyperabrupt varactors is designed. Figure 4.3-1 shows the schematic diagram of the tuning element. The circuit consists of two segments of conductor made of 5 μm thick gold on alumina substrate. Each section has a different length of L_1=3.9 mm and L_2=4 mm separated by a 100 μm gap from each other. A commercial GaAs varactor from Aerolex is mounted over the 100 μm gap between the two conductors. The first conductive section (L_1) is placed inside the hole within the dielectric resonator that can alter the electric field. The second section (L_2) makes contact with the cavity lid and establishes a ground connection. A 300 kΩ bias resistor is used to reduce the leakage of the RF signal through the DC bias lines for varactors and maintain a high Q value. The surface current density on L_1 varies with the capacitance value of the GaAs varactor which can be used to tune the resonance frequency of the TME mode for the proposed

filter. Figure 4.3-2 shows the simulation results for the proposed tunable DR filter with GaAs varactors, for C_{var}=0.3, 0.4, 0.6, 0.8 and 1.1 pF. The simulated maximum tuning range is from 4.999 to 4.861 GHz (138 MHz) while the insertion loss is better than 2.73 dB over the tuning range. Using GaAs varactors a continuous tuning range can be achieved as will be presented in the measurement results.

The measured capacitance of the GaAs varactor varies from C_{var}=1.1 pF to C_{var}=0.32 pF with a change in the reverse bias voltage (V_{bias}) from 0-10 volts. The measured Q-factor of the GaAs tuning element changes from 2.7 to 46 over the tuning range. Figure 4.3-3 shows the measured S-parameters of the fabricated tunable dielectric resonator filter for different DC bias voltages. A continuous tuning range from 4.87 GHz to 4.97 GHz (100 MHz) is achieved using GaAs varactors as tuning elements. The maximum insertion loss is 4.6 dB when C_{var}=1.1 pF. The high insertion loss is due to the low Q-factor of the GaAs varactors when V_{bias}=0 V. The minimum measured insertion loss of the filter is 1.17 dB when V_{bias}=10 V. Figure 4.3-4 shows the variations in the measured Q value and also bandwidth of the filter over the tuning range. It can be seen from the measurement results that the bandwidth of the filter, for a return loss better than 12 dB, is almost constant within a range from 60 to 70 MHz while the Q value varies from 660-170. The lower Q value for this filter is due to the lower Q-factor of the GaAs varactors. This issue is addressed by utilizing MEMS varactors with a higher Q-factor in the next section.

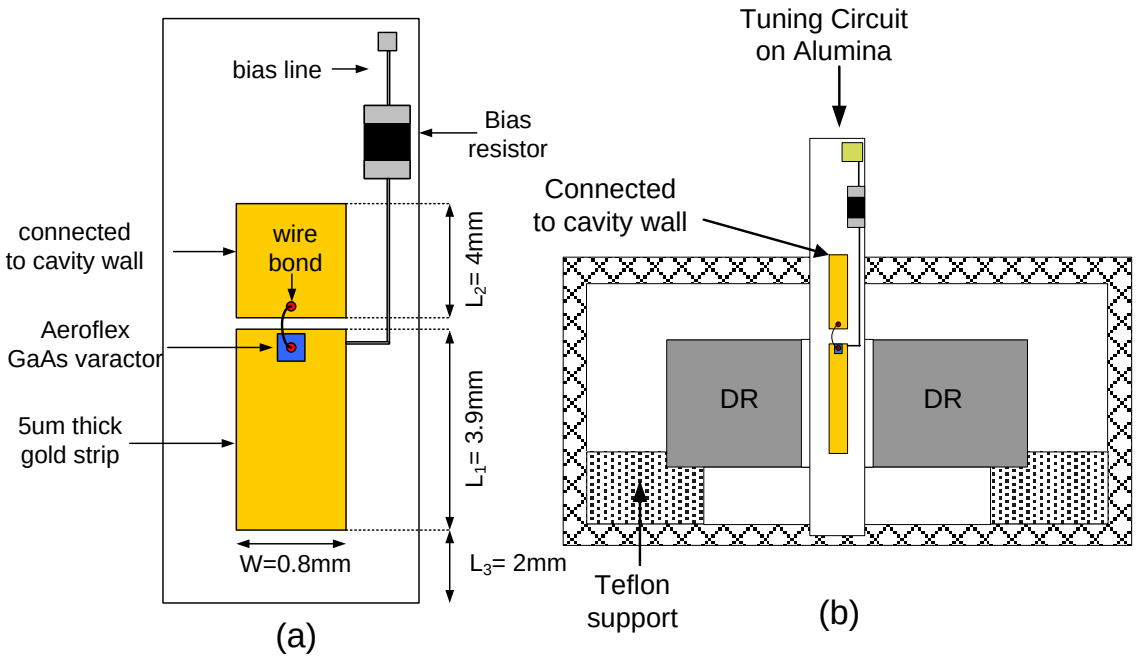

Figure 4.3-1 Schematic diagram of the (a) tuning element and (b) tunable dielectric resonator based on GaAs varactor

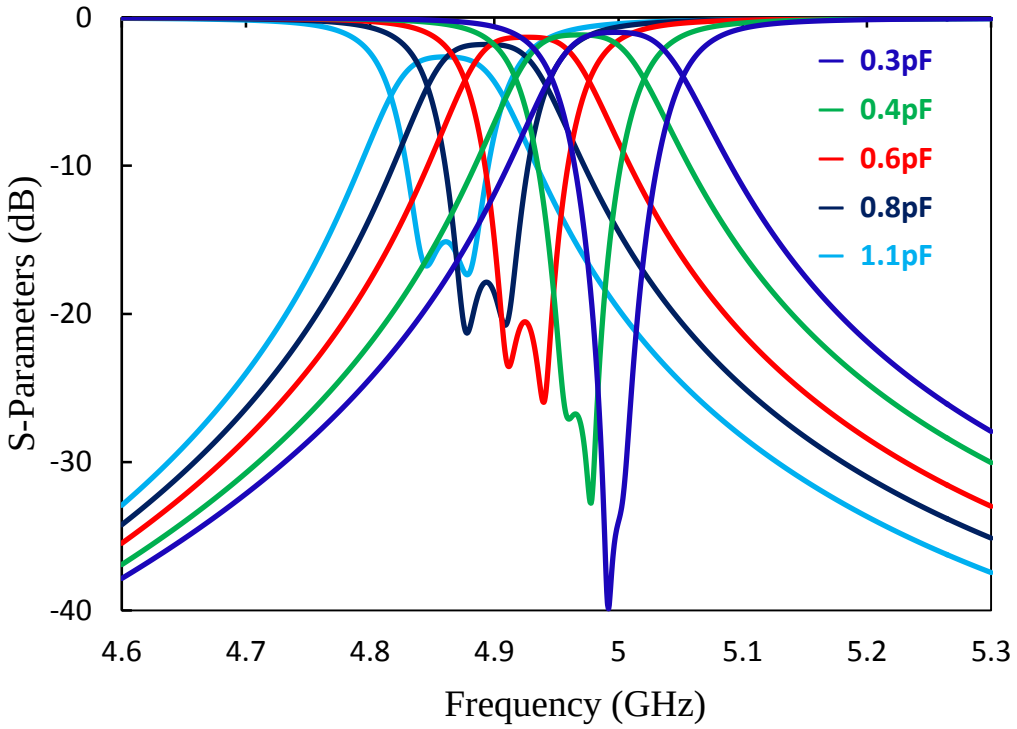

Figure 4.3-2 Simulated S-parameters of the tunable DR filter with GaAs varactors

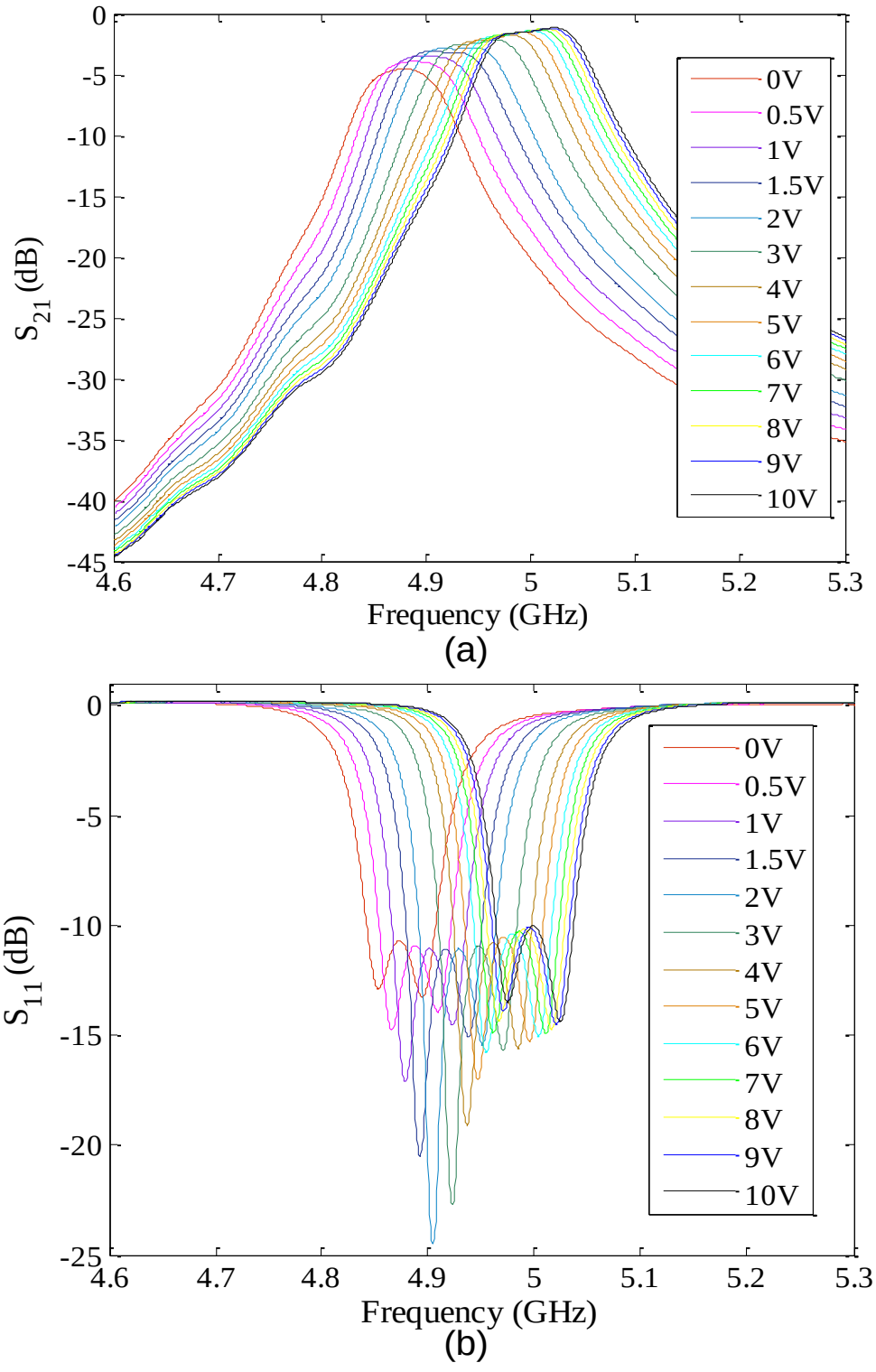

Figure 4.3-3 Measured responses (a) and (b) of the tunable DR filter with GaAs varactors

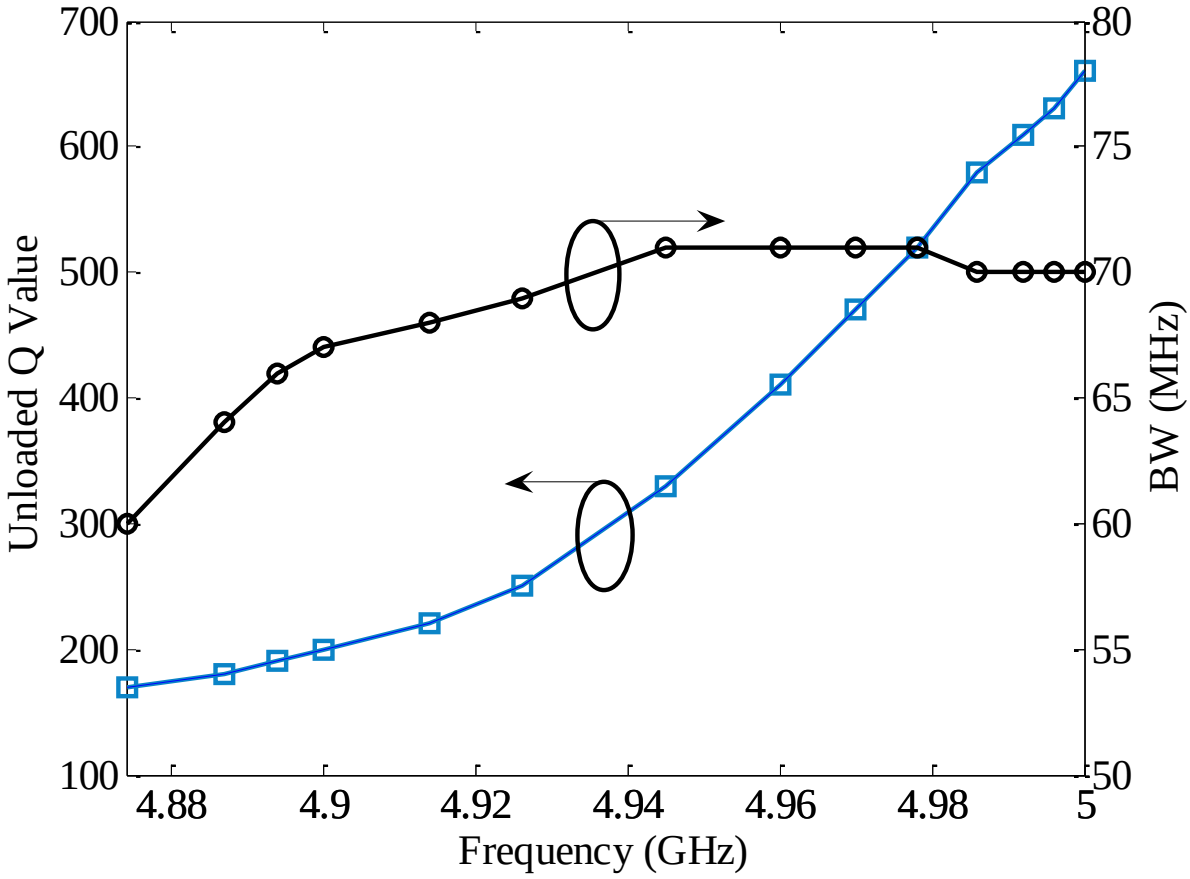

Figure 4.3-4 Variations in the Q value and bandwidth of the filter

4.4 Tunable Dielectric Resonator Filter with MEMS Capacitor Bank

In order to improve the performance of the proposed tunable dielectric resonator filter in terms of tuning while maintaining a high Q value, a third tuning circuit utilizing 4-bit RF MEMS switched capacitor banks is designed and fabricated using the UW-MEMS fabrication process. Figure 4.4-1 shows the schematic diagram of the tuning circuit. Similar to the tuning circuit for the GaAs varactors, there are two conductive strips, one connected to the cavity wall and the other placed inside the hole within the dielectric resonator. The length of the strip inside the resonator is L_1=4.5 mm. A higher tuning range can be achieved by employing a longer strip

length inside the resonator at the expense of a lower Q value. The surface current density on the conductive strip L_1 is tuned by a 4-bit RF MEMS varactor. The schematic circuit diagram of the MEMS varactor is illustrated in Figure 4.4-2. It consists of four Metal-Insulator-Metal (MIM) capacitors ($C_1...C_4$) and four capacitive RF MEMS switches with up-state and down-state capacitance values of C_u and C_d, respectively. The actuation voltage of these capacitive switches is 40 volts while the required DC current is zero due to electrostatic actuation mechanism. As shown in the tuning characteristic of the MEMS capacitor bank in Figure 4.4-3, the capacitance value changes from 347 fF to 744 fF while the Q-factor is better than 69 for all the 16 states. A higher Q-factor is expected for this type of MEMS capacitor bank. The relatively lower Q-factor is attributed to the loss from the DC bias lines. A Titanium-Tungsten (TiW) resistive material with a sheet resistance of 40 Ω/□ is used here. A resistive material with a higher sheet resistance value, such as SiCr, will result in a higher Q-factor. The circuit is fabricated on a 625 μm thick alumina substrate and measures 1.6 mm × 12 mm. An SEM image of the MEMS capacitor bank is presented in Figure 4.4-4. The extracted capacitance values of the 4-bit MEMS capacitor bank are used in the HFSS EM model to simulate the tuning range of the designed filter. According to simulation results, as shown in Figure 4.4-5, the center frequency is tuned from 5.205 to 5.036 GHz (169 MHz) while the insertion loss varies between 1.1 and 2.39 dB. The simulated bandwidth is 26 MHz for a return loss better than 15 dB.

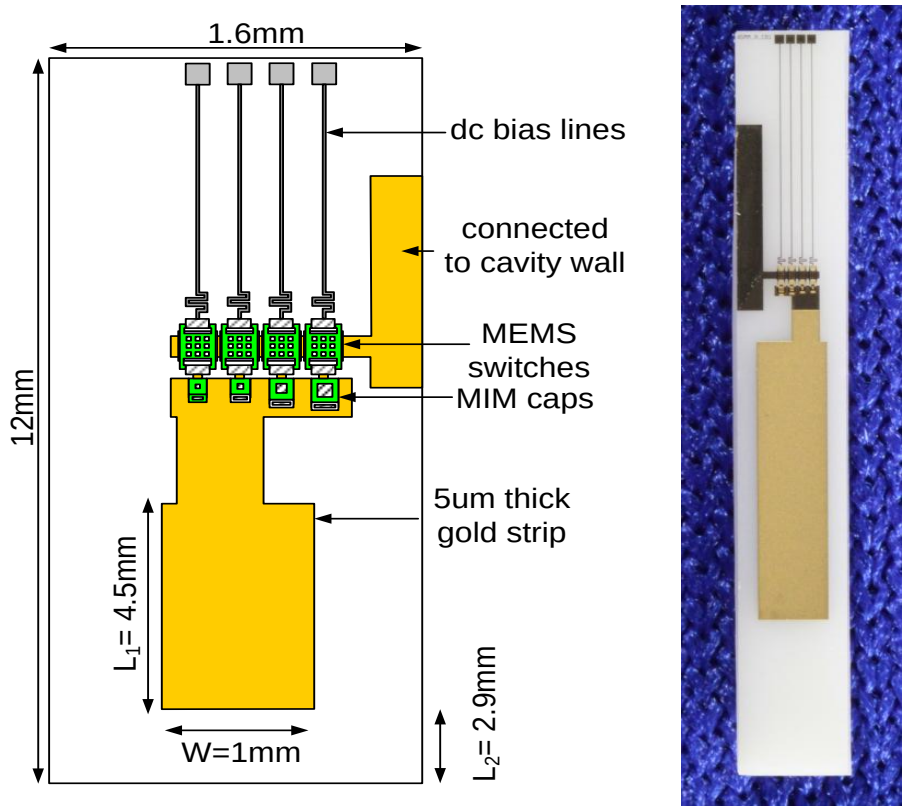

Figure 4.4-1 Schematic diagram and image of the fabricated tuning circuit with 4-bit RF MEMS capacitor bank

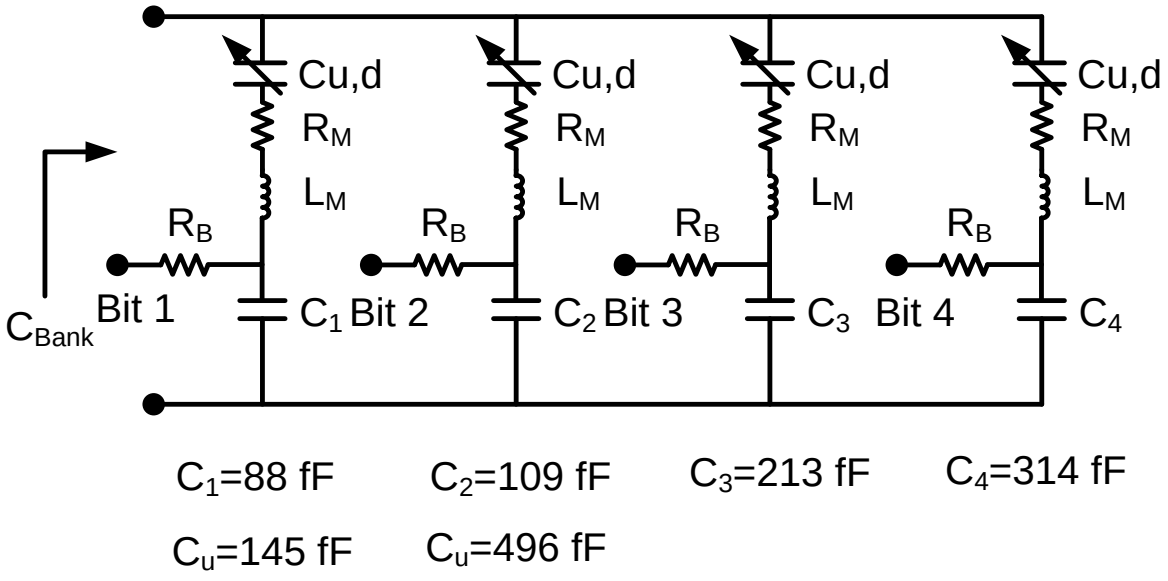

Figure 4.4-2 Schematic circuit diagram of the 4-bit RF MEMS capacitor bank

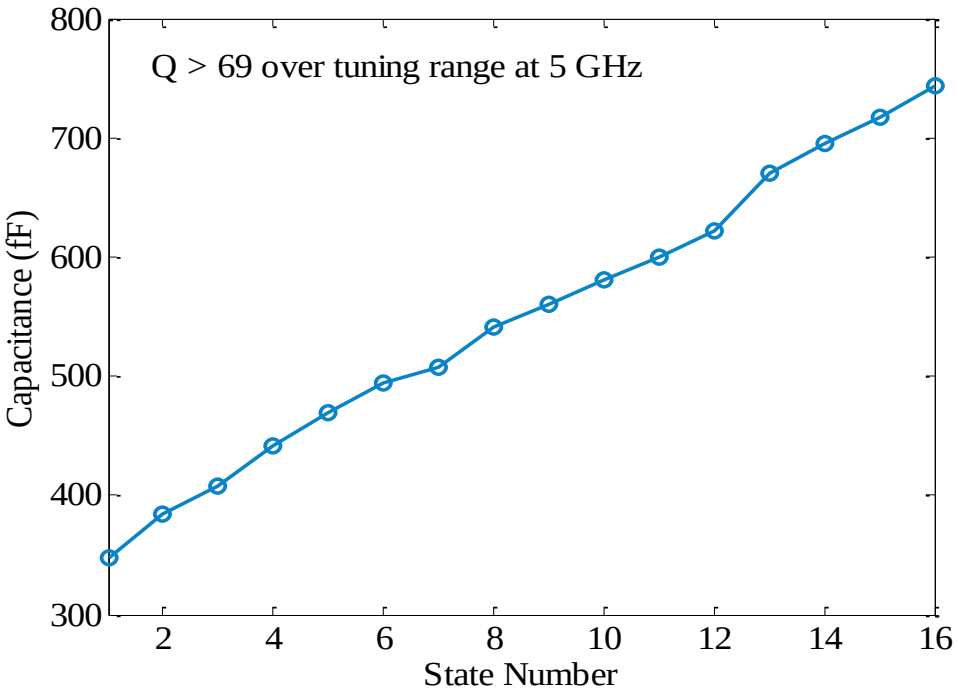

Figure 4.4-3 Tuning characteristic of the RF MEMS capacitor bank

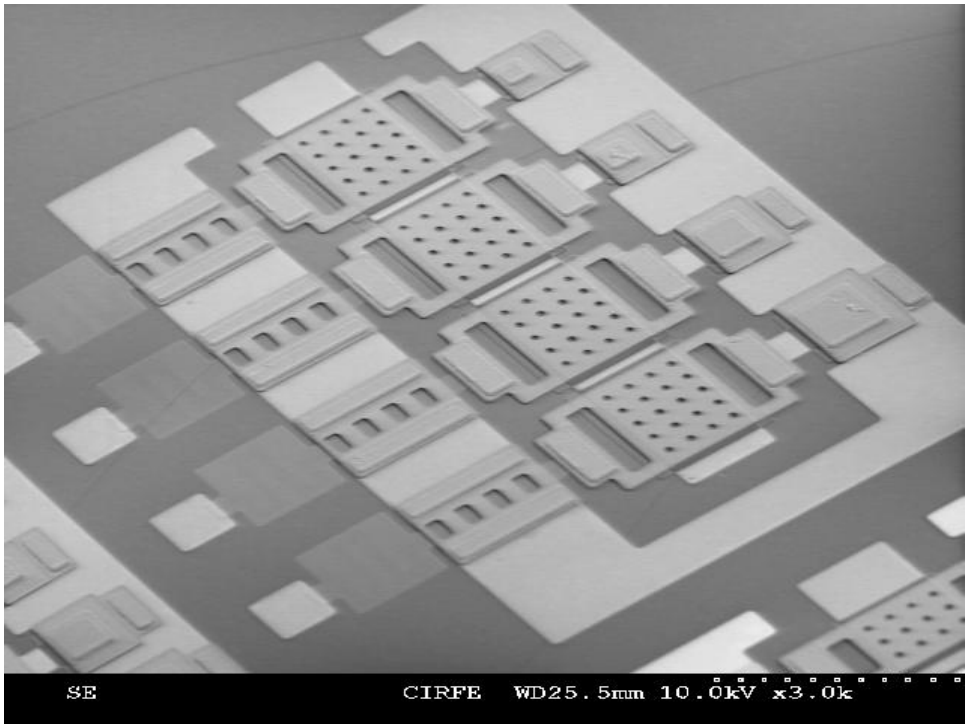

Figure 4.4-4 SEM image of the fabricated RF MEMS capacitor bank

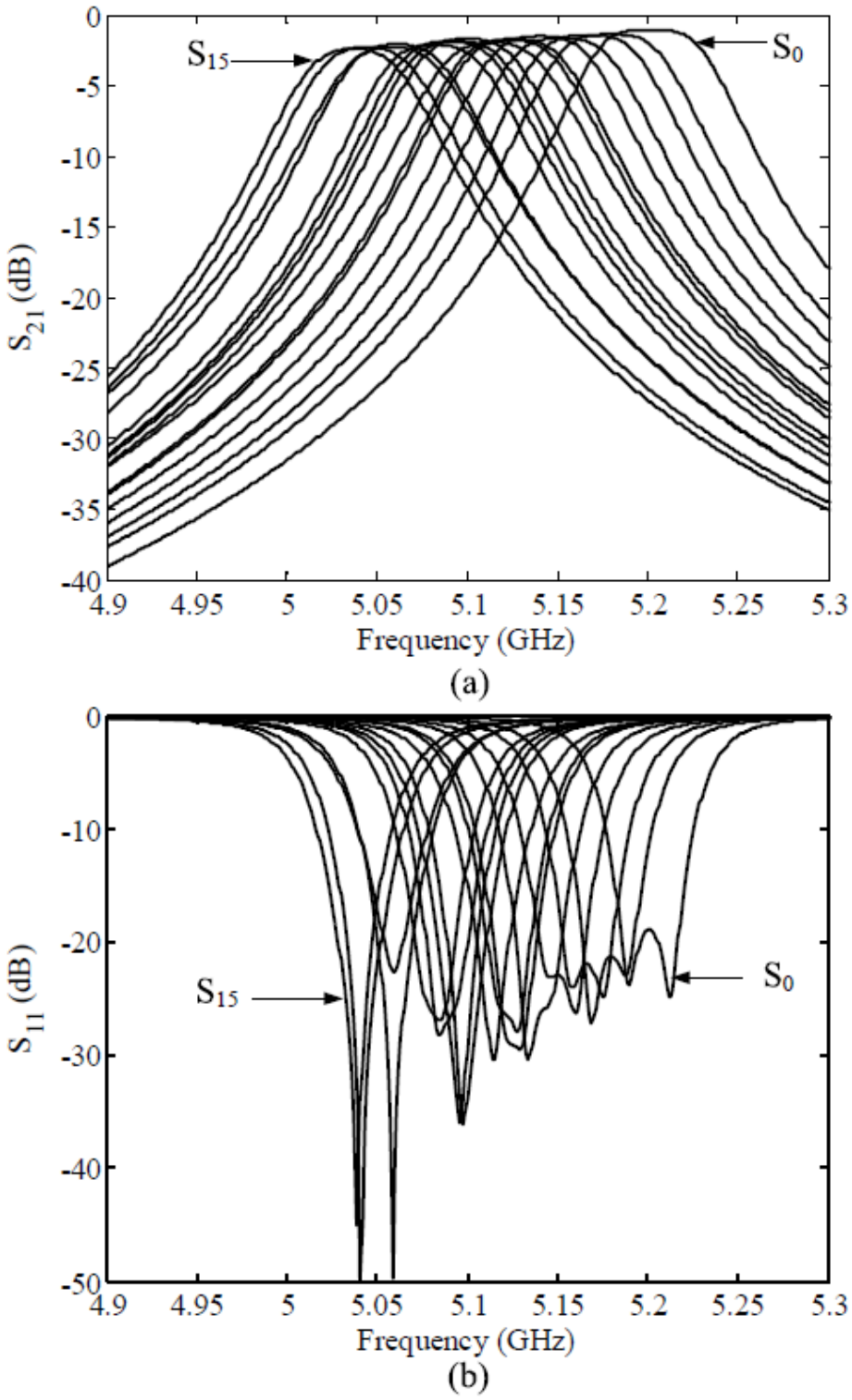

Figure 4.4-5 Simulated (a) and (b) of the tunable dielectric resonator filter with MEMS capacitor banks

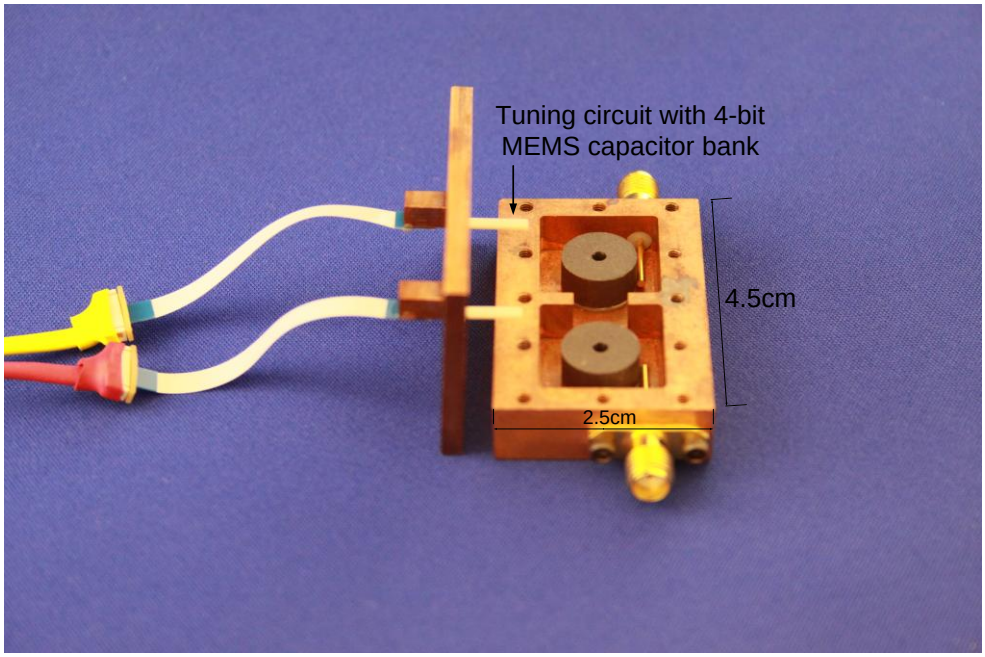

Figure 4.4-6 Fabricated tunable dielectric resonator filter with MEMS switched capacitor banks

The third tunable dielectric resonator filter assembled with MEMS switched capacitor banks is shown in Figure 4.4-6. The cavity is made of copper to obtain a higher Q value. The height of the cavity is 6.5 mm and all the other dimensions are the same as the cavity in Figure 4.2-8. A new dielectric material from Trans-Tech with ε_r =35, an inside diameter of d_1 =2 mm, an outside diameter of d_2 =11.5 mm and a height h_3 =5.1 mm is used for this filter. Thus, the center frequency is slightly higher than the previous two designs.

The measured S-parameters for all the 16 tuning states of the filter with MEMS switched capacitor banks are presented in Figure 4.4-7. A tuning range from 5.20 GHz to 5.02 GHz (180 MHz) is achieved. The maximum insertion loss is better than 2.8 dB. The measured Q value and the bandwidth for a return loss lower than 15 dB over the tuning range are presented in Figure 4.4-8. As shown in this figure, the bandwidth is almost constant around 25-30 MHz. The measured Q value changes from 800 for the first state when all the MEMS switches are up (S_0) to 550 when all the MEMS switches are actuated to the down state position (S_{15}).

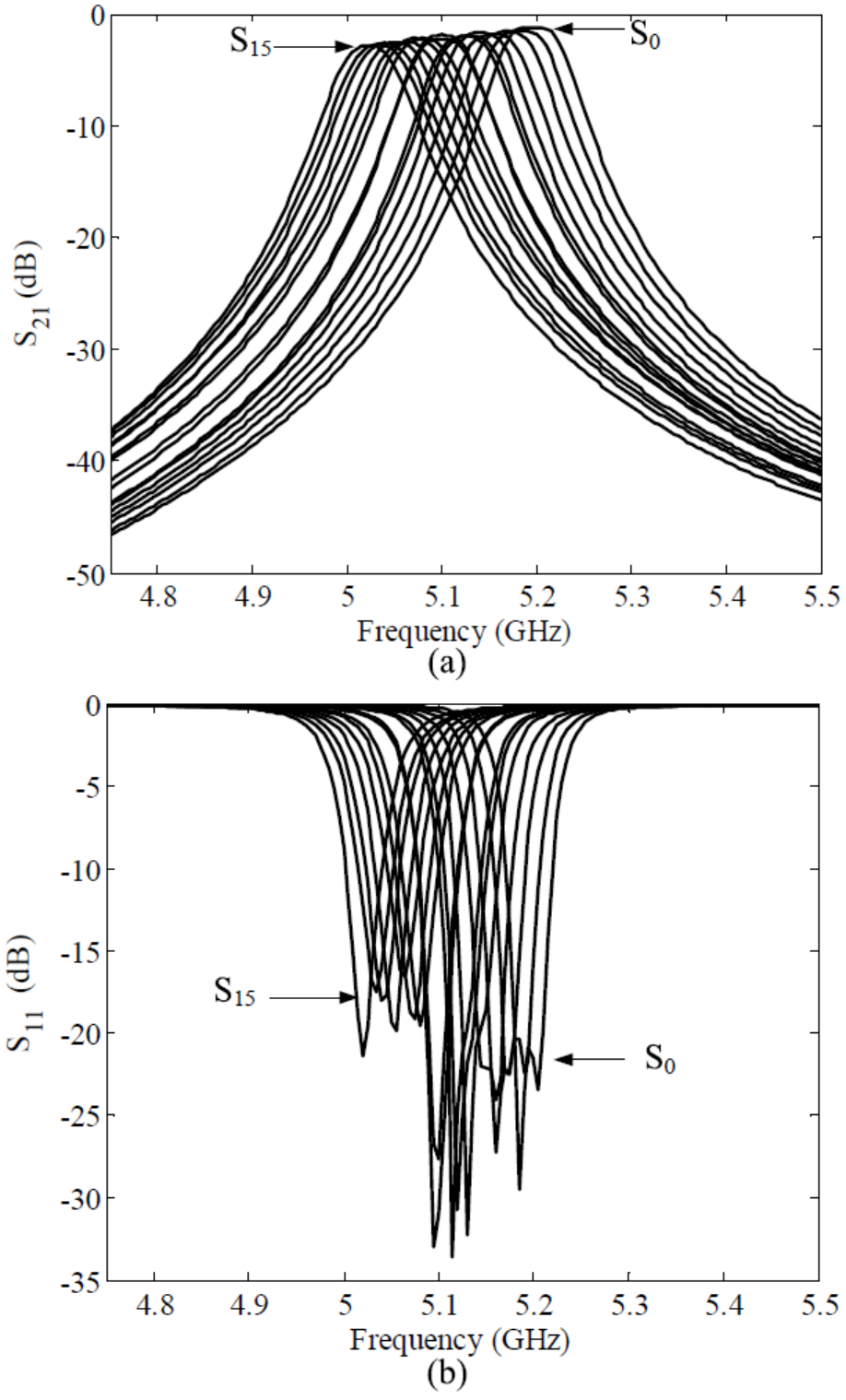

Figure 4.4-7 Measured (a) and (b) of the tunable dielectric resonator filter with MEMS capacitor banks

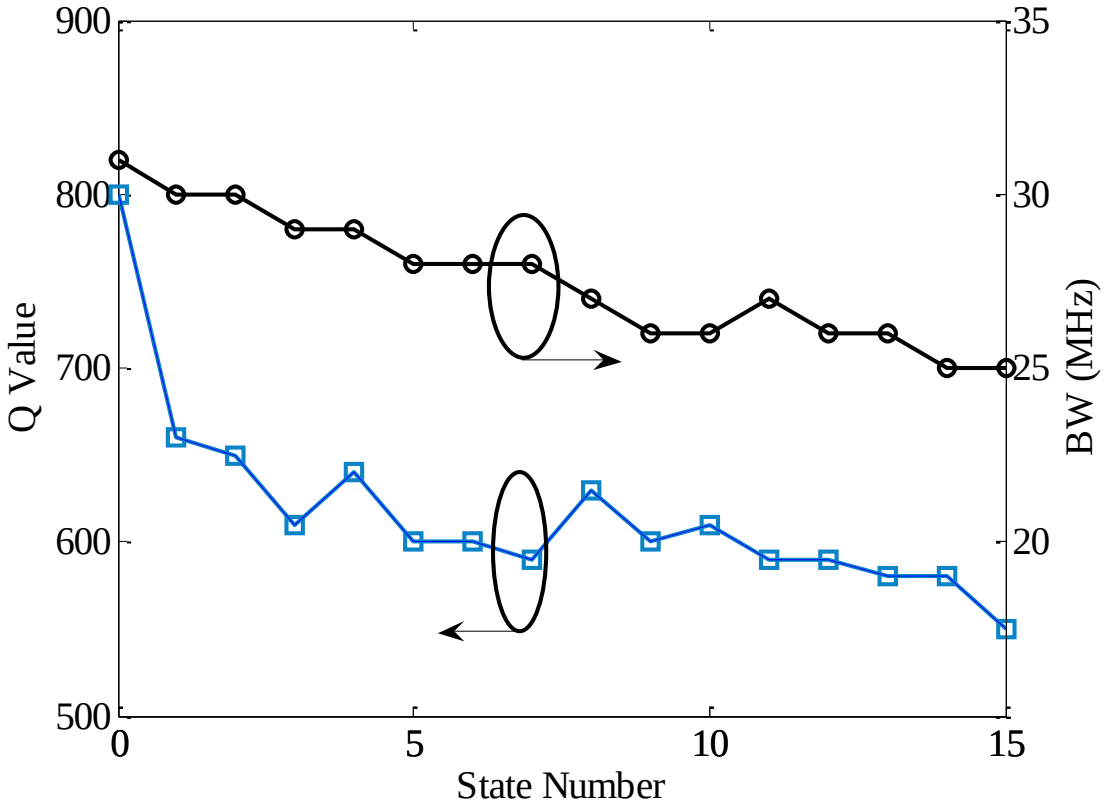

Figure 4.4-8 Measured Q value and bandwidth over the tuning range of the tunable filter with MEMS capacitor bank

A summary of the measurement results for all three filters based on different tuning elements is listed in Table 4.4-1. The tunable dielectric resonator filter with MEMS contact-type switches has the highest Q value with a discrete tuning characteristic. The tunable filter with GaAs varactors has the lowest Q value and a continuous tuning range. The tunable filter with MEMS capacitor bank has a better performance in terms of both tuning range and also Q value. A higher Q value can be achieved for this design by improving the Q-factor of the MEMS capacitor banks through the use of a higher resistive bias lines. The filters presented in this thesis are also compared with other MEMS-based tunable filters in Table 4.4-1. To our knowledge the tunable dielectric resonator filters with MEMS contact-type switches and MEMS capacitor banks reported in this thesis achieve the highest reported Q value at this frequency range for a tunable filter using MEMS technology. The achieved tuning range is smaller than the other MEMS based approaches due to the degradation of Q with increasing the tuning range. This can be improved

by reducing the loss associated with the tuning elements in the proposed approach. For example, by increasing the thickness of the conductive metal strips.

Table 4.4-1 Comparison of different tunable filters

Design	Center Frequency	Tuning Ratio	Q Value
This work (MEMS Switch)	4.72 GHz	3.5%	1220-510
This work (MEMS Varactor)	5.11 GHz	3.5%	800-550
This work (GaAs Varactor)	4.92 GHz	2%	660-170
Ref. [71]	4.95 GHz	23.7%	511-273
Ref. [76]	15.5 GHz	3%	1600-400
Ref. [97]	3.85 GHz	44%	650-300

4.5 Summary

In this chapter, a novel tuning approach for dielectric resonator filters is presented. The tuning is based on the interaction between the electric field and the surface current on a tuning circuit inside the dielectric material. Three tunable filters are implemented using different tuning elements including contact-type RF MEMS switches, GaAs varactors and RF MEMS switched capacitor banks. The filter based on MEMS contact-type switches has a tuning range from 4.80-4.64 GHz while the Q value is from 1220-510 which to our knowledge is the highest reported Q value at this frequency range for a MEMS-based tunable filter. A continuous tuning range from 4.97-4.87 GHz is achieved by employing GaAs varactors. To maintain a high Q value while improving the tuning performance, a third tunable dielectric resonator filter utilizing MEMS capacitor banks is implemented. The measured Q value varies from 800-550 over a tuning range from 5.20-5.02 GHz.

Chapter 5
A Tunable Filter with Constant Bandwidth Based on Balanced EM Couplings

3D cavity combline resonator filters are widely used in communication systems due to their relatively high Q value and small temperature drift. Many techniques were investigated in designing combline tunable filters [23, 98-101]. In this chapter, a bandpass tunable combline filter with a constant bandwidth is demonstrated. The design method for constant bandwidth tunable filter will be explained.

5.1 Introduction

High Q constant bandwidth tunable filters are in high demand in any flexible transceiver, such as cognitive radios, software defined radios, and WiMAX systems. The tunable filter is a key block in the front-end of a transceiver. In these systems, a reconfigurable filter with an absolute constant bandwidth is essential for high speed data exchanging. A switched filter bank is an alternative solution for a tunable filter that offers a discrete flexibility, however this type of filter bank usually suffers from a large size.

High Q constant bandwidth is a target for designing tunable filters. The Q value is determined by the resonator, the tuning element, and the tuning method itself. The bandwidth during the tuning process usually changes with the coupling method in most cases. A variety of tuning technologies have been reported in order to design filters that maintain a constant bandwidth during the tuning process. Low Q planar tunable filters employed with varactors and MEMS varactors to maintain a constant bandwidth have been reported for years [36, 80, 83, 84, 102].

The main problems of these filters are low Q factors and poor transmission responses during the tuning process. In [79, 103], techniques were reported to design superconductor tunable filters with constant bandwidth. These techniques however are not easily amenable to high-Q 3D filters.

A mechanically tunable waveguide has both high-Q and high-power-handling capabilities. A high-mode tunable filter with four cylindrical cavities was reported in [104]. The tuning is accomplished by a movable plunger with a disk located in the cavity. An unloaded Q better than 9000 was reported in [104] for a filter operating at *Ku*-band. The narrow spurious free window and the limited tuning range is the main drawback of these types of filters. A tunable TE_{113} dual-mode cavity filter was reported in [14]. The tuning method is based on the cylindrical cavity mounted bellows that function as the tuning element and building block. The bellows is a flexible electroformed copper structure with a thin-walled metallic closed-end piston and a number of convolutions. A high Q with ± 1.9% of the tuning range at *Ku*-band was reported. However, this design also suffers from a variation of the bandwidth response. Its bandwidth variation reaches ± 3.1% in such a small tuning range.

In this chapter, a method of designing a constant bandwidth tunable filter is demonstrated by using balanced electric and magnetic couplings. Based on this method, a cavity combline tunable filter is designed. The unloaded Q of the designed filter is above 3000 over the tuning range. The bandwidth varies from 28.9 to 31.1 MHz, 30 ± 1.1 MHz (less than ±3.7%) over a tuning range of 430 MHz at a center frequency of 2.45 GHz.

5.2 Constant Bandwidth Tunable Filter Design

5.2.1 Theory Fundamentals

Techniques derived from a coupling matrix based synthesis can be used to design filters [4]. The S-parameters of a filter in terms of the coupling matrix *M* are given by

$$S_{11} = 1 + 2jR(\lambda I - jR + M)^{-1}_{1,1}$$
$$S_{21} = -2jR(\lambda I - jR + M)^{-1}_{N,1} \qquad 5.1$$

where I is an n x n identity matrix, R is an n x n matrix with all elements zero except the input and load impedance $R_{1,1}=R_{n,n}=R$, and M is an n x n symmetric coupling matrix, and the variable

$$\lambda = \frac{f_0}{BW}\left(\frac{f}{f_0} - \frac{f_0}{f}\right) \qquad 5.2$$

where f_0 is the nominal center frequency, f is the bandpass frequency variable, and BW is the bandwidth.

The elements of the coupling matrix M and input impedance R are independent of the filter center frequency and bandwidth since they are all expressed in terms of the low pass prototype. Therefore, the design of a constant bandwidth tunable filter requires to maintain the normalized compling matrix M and the normalized impedance R.

5.2.2 Tunable Resonator Design

The proposed tunable resonator structure is shown in Figure 5.2-1. The combline resonator consists of a cylindrical post with a diameter of W_D=12 mm and a height of H_D=21 mm inside a cavity with dimensions of H x C x D = (30 mm)^3. The tuning element consists of a disk with a diameter of 12 mm. and a threaded rod connecting the tuning disk to the cavity lid or ground. The resonator can be simply tuned by adjusting the gap between the tuning disk and the cylindrical post (*Gap*). EM simulation results for the tuning range and the unloaded Q values of the proposed resonator are presented in Figure 5.2-2. The center frequency can be tuned from 2.24 GHz to 2.71 GHz (470 MHz running) by varying the gap from 3 mm to 8 mm while the Q value is maintained well above 4000 over the entire tuning range.

5.2.3 Coupling Iris Design for Constant Bandwidth

Figures 5.2-3 (a) and (b) illustrate the magnitude of electric field and magnetic field at cavity side wall respectively. Figure 5.2-3 (a) shows that the maximum electric field is at the center of the side wall, and it decreases from center to sides. Figure 5.2-3 (b) shows that the maximum magnitude magnetic field is at the bottom center of the side wall, and it decreases from bottom to top. This means that both electric coupling and magnetic coupling exist between two adjacent resonators if a horizontal slot is used at the side wall between them. The electric coupling and the magnetic coupling vary with the slot vertical position changing. Therefore, horizontal slot can be

used for inter-resonator coupling, which can be used to balance the electric and magnetic coupling to maintain the normalized coupling value constant over the tuning range.

Figure 5.2-4 demonstrates a horizontal slot opening at the side wall of the cavity. The resonant frequencies of f_e and f_m are obtained with the iris boundary condition set as the electrical wall (PEC) and the magnetic wall (PMC) respectively. This is equivalent to even and odd model of coupled pair resonators. Therefore, the physical coupling between two resonators k can be calculated through

$$k = \frac{f_e^2 - f_m^2}{f_e^2 + f_m^2} \tag{5.3}$$

The normalized coupling matrix M can be calculated as:

$$M = \frac{f_0}{BW} \cdot k \tag{5.4}$$

Equation 5.4 shows that in order to design a constant bandwidth tunable filter, its physical coupling value k should be inversely varying with the center frequency f_0 of the tunable filter during the tuning process.

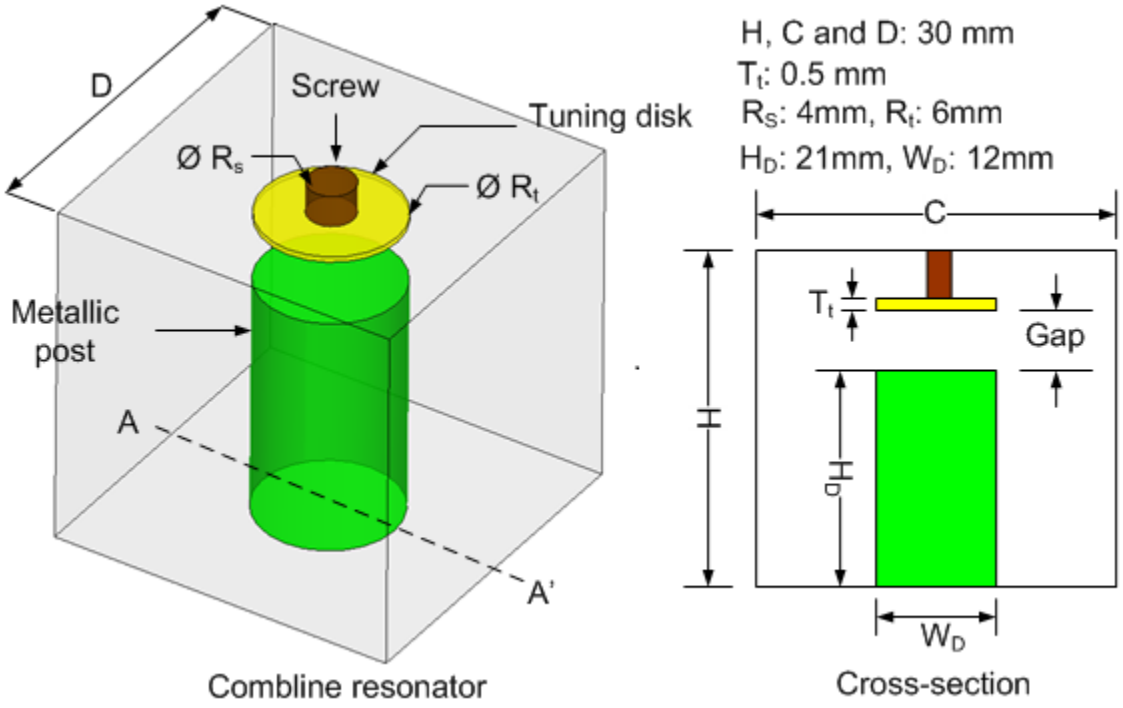

Figure 5.2-1 (a) Schematic view of the resonator, and (b) equivalent circuit model of the resonator

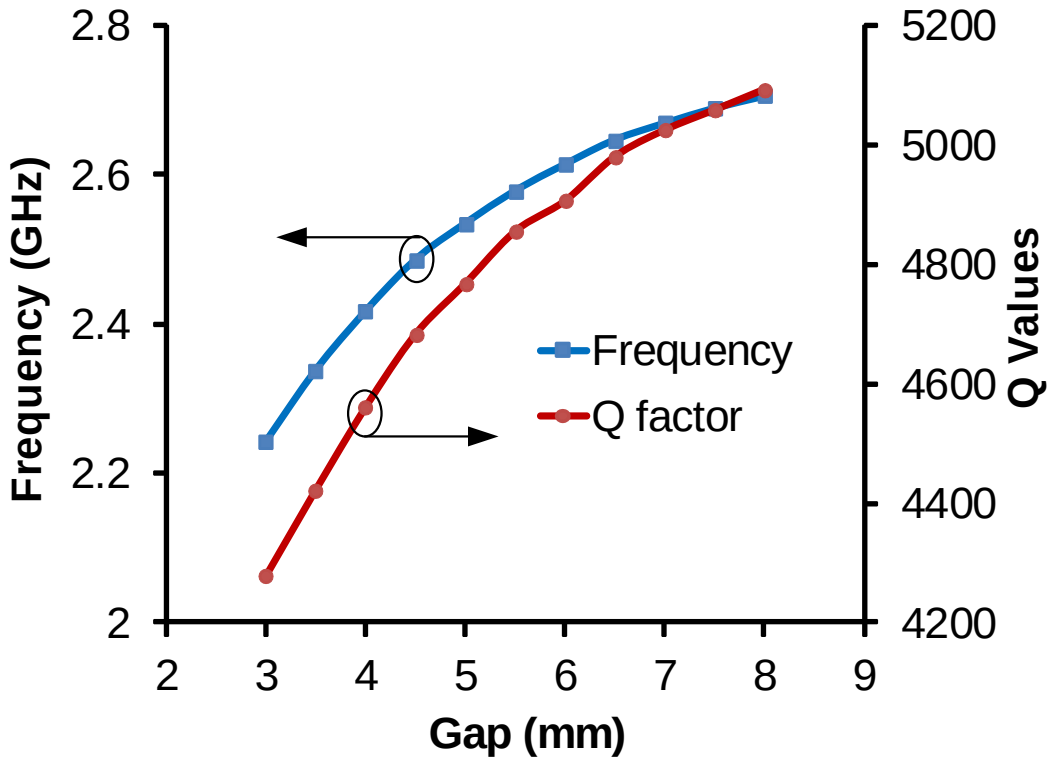

Figure 5.2-2 Simulation results of the tunable resonator

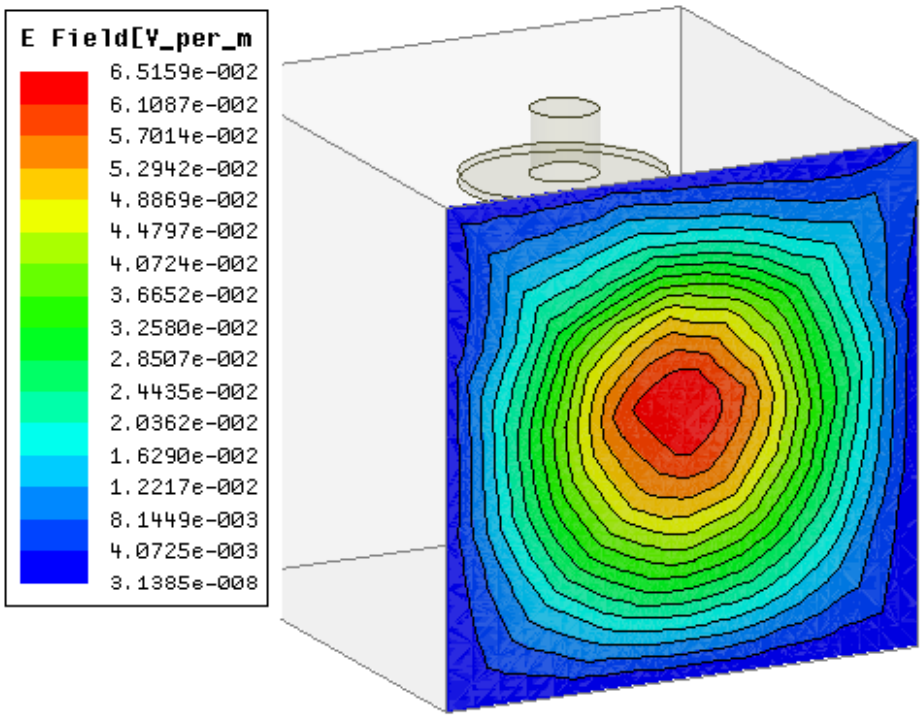

(a)

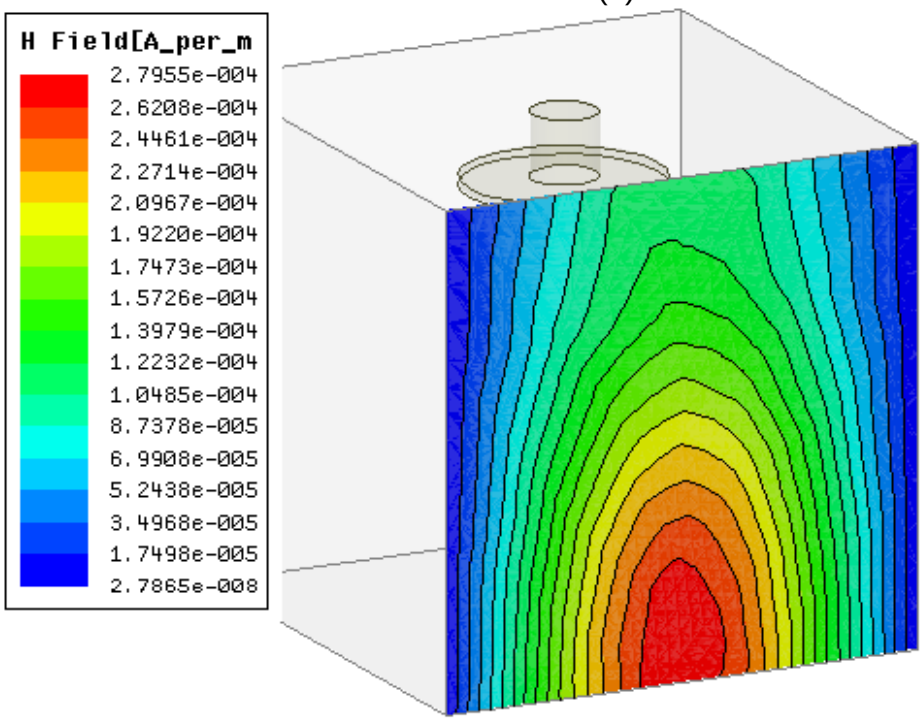

(b)

Figure 5.2-3 Magnitude of EM field at side wall of cavity: (a) electric field and (b) magnetic field

The investigation of the relation between the center frequency f_o and the normalized coupling M_{ij} is illustrated in Figure 5.2-4 and Figure 5.2-5. The center frequency is tuned by the gap, and the normalized coupling M is derived from the physical coupling k, which is varied by the slot configuration. The resonator with a 20 mm x 4 mm slot, which is located at H=4 mm and H=24 mm from the cavity bottom respectively, is simulated by HFSS with an electrical wall (PEC) boundary condition set on the slot, as shown in Figure 5.2-4. The resonant frequency f_e is plotted in Figure 5.2-5 using a blue dotted line and a blue solid line for H=4 mm and H=24 mm respectively. Alternatively, for calculation f_m a magnetic wall (PMC) boundary condition is set on the slot. The resonant frequency f_m is plotted in Figure 5.2-5 using a red dotted line and a red solid line for H=4 mm and H=24 mm respectively. Using Equation 5.3 and 5.4 with assumed bandwidth of 30 MHz, the normalized coupling can be obtained, and its values are plotted as a green dotted line and a green solid line for H=4 mm and H=24 mm respectively in the same figure. The green dotted line shows that the normalized coupling value M_{ij} increases as the center frequency grows with the slot position H=4 mm. The green solid line shows that the normalized coupling value M_{ij} decreases as the center frequency grows with the slot position H=24 mm.

Since the normalized coupling value M_{ij} has opposite variation trends with the center frequency at the two different positions, it must be between these two positions that the normalized coupling value M_{ij} has a stable value as the resonant frequency changes. The variable H with values from 4 to 24 mm is simulated, and the normalized coupling values are extracted and shown in Figure 5.2-6. The H=17.2 mm is finally selected for the tunable filter since it can maintain a stable coupling as the resonant frequency changes. Figure 5.2-7 displays the simulation results of the required coupling values between resonator R_1 and R_2 over the tuning range. The figure shows that the normalized coupling is a constant when the resonator frequency changes. The figure implies that the couplings slot can maintain the constant bandwidth if selected properly.

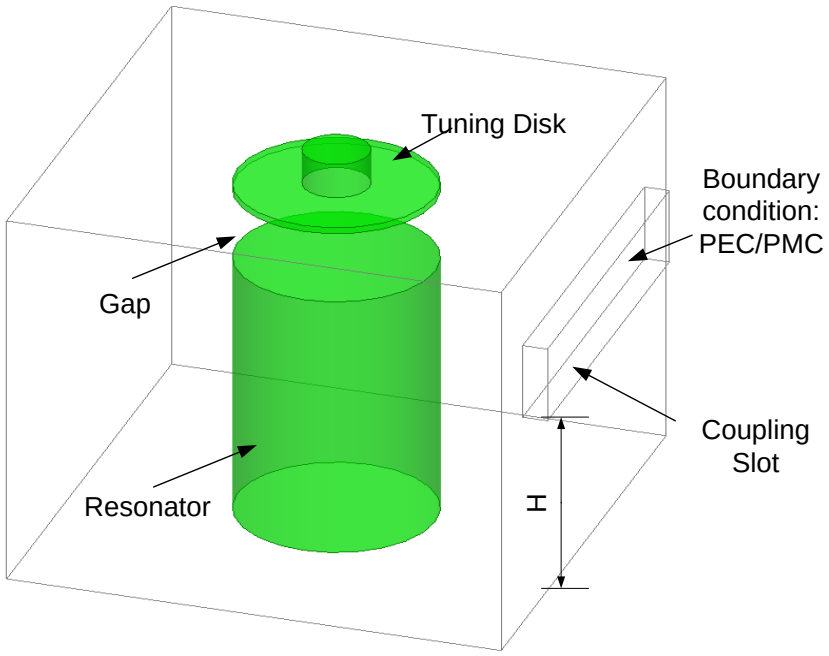

Figure 5.2-4 Single resonator with coupling slot

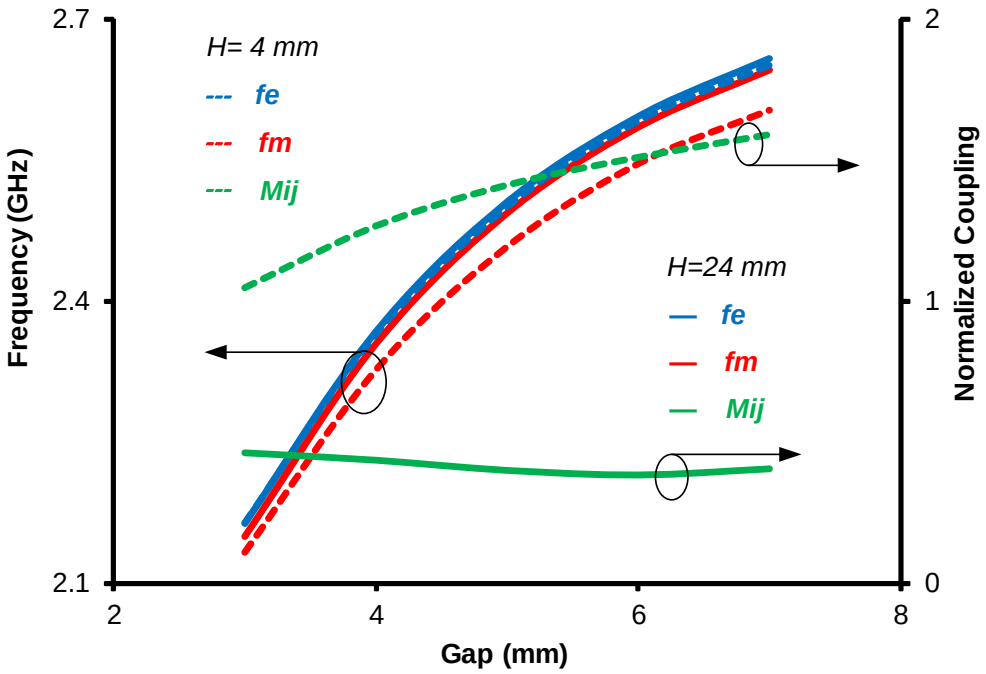

Figure 5.2-5 Frequencies and normalized coupling that varies with the gap, the dotted line plots the results of the slot at 4 mm to the bottom, and solid line plots the results of the slot at 24 mm to the bottom

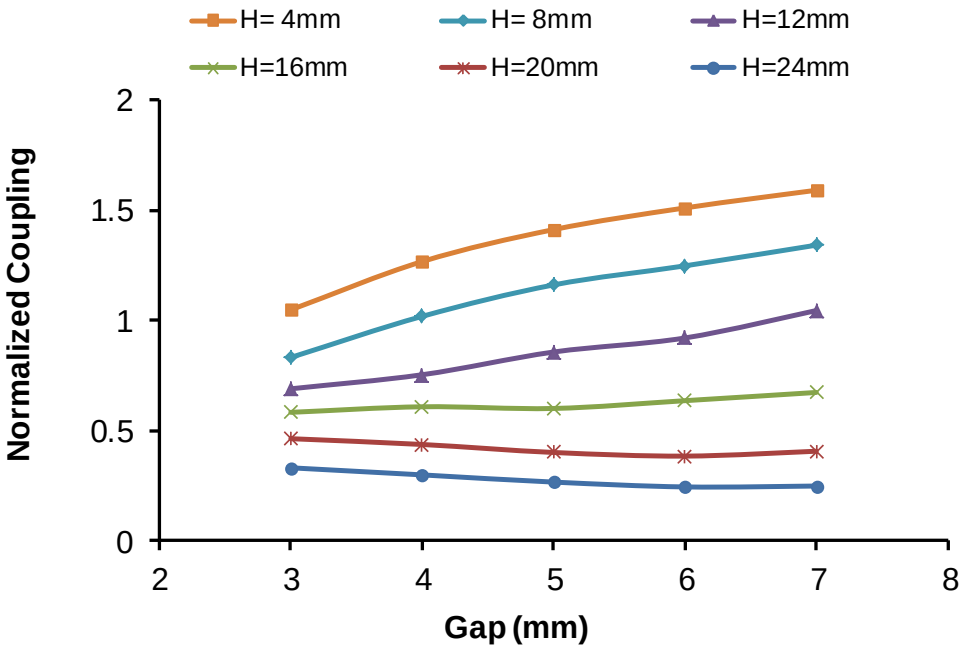

Figure 5.2-6 Simulation results of the normalized coupling with the gap at different H values

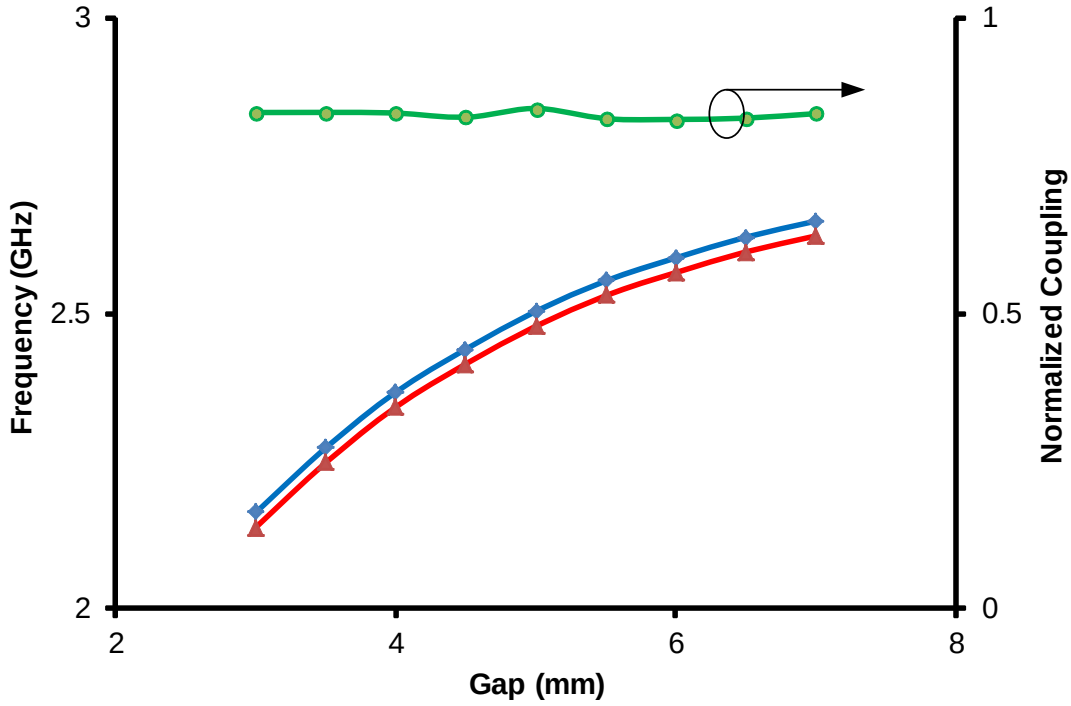

Figure 5.2-7 Achieved constant coupling over the tuning range between resonator 1 and 2

5.2.4 Input Coupling Design for Constant Bandwidth

The filter input coupling Q_e can be calculated from the normalized input/output resistance $R=R_{1,1}=R_{n,n}$ [4]

$$Q_e = \frac{f_0}{BW \times R} \qquad 5.5$$

where f_0 is the nominal center frequency and BW is the bandwidth.

Equation 5.5 shows that if a tunable filter maintains a constant bandwidth (BW) during the tuning process, its input coupling Q_e should be proportionally changing with the center frequency f_0 during the tuning process.

The relation between filter input coupling Q_e and group delay peak value $\tau(f_0)$ can be expressed as

$$\tau(f_0) = \frac{4 \times Q_e}{2\pi \times f_0} \qquad 5.6$$

From Equation 5.5 and 5.6, R is expressed in terms of group delay as:

$$R = \frac{4}{2\pi * BW * \tau(f_0)} \qquad 5.7$$

Equation 5.7 shows that in order to keep the constant bandwidth, the maximum value of the group delay $\tau(f_0)$ over the tuning range should be a constant value. The group delay can be obtained by using a simulation of a loaded first resonator with an input probe, as shown in Figure 5.2-8.

The simulation results of the group delay versus with the resonant frequency are plotted in Figure 5.2-9 for two values of probe length L. The solid lines and the dot lines in Figure 5.2-8 illustrate the results of the group delay for a probe length of L=20 mm and L=25 mm respectively. As the frequency tuned from 2.31 to 2.62 GHz, the peak values of group delay vary from 25.4 to 9.74 ns (ratio is 2.6) and 14.5 to 6.9 ns (ratio is 2.1) for L=20 mm and L=25 mm respectively. This simulation results imply that the normalized input impedance changes more with frequency for a short probe than for a long probe over the same tuning range. Therefore, an increase in the length of the input probe can reduce the normalized impedance deviation over the

same tuning range. Figure 5.2-10 displays the simulation results of the group delay with a probe length of 29.3 mm. This figure shows that the peak value of each group delay is almost constant at each resonant frequency during the resonator tuning process. For that reason, a long input probe is a good choice for designing constant bandwidth combline tunable filters.

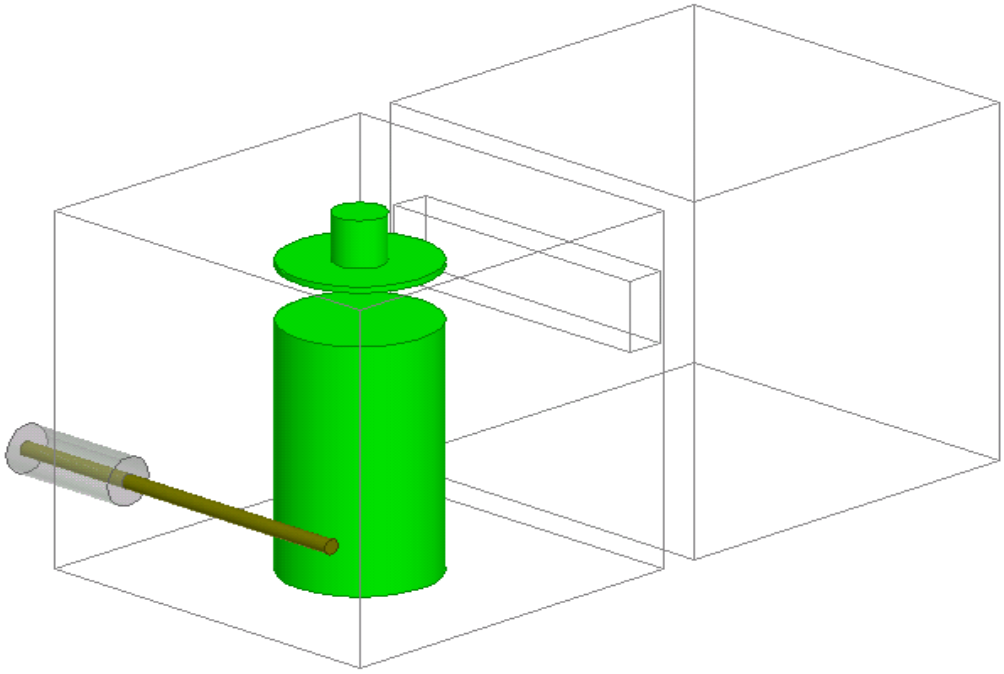

Figure 5.2-8 A loaded resonator with input probe

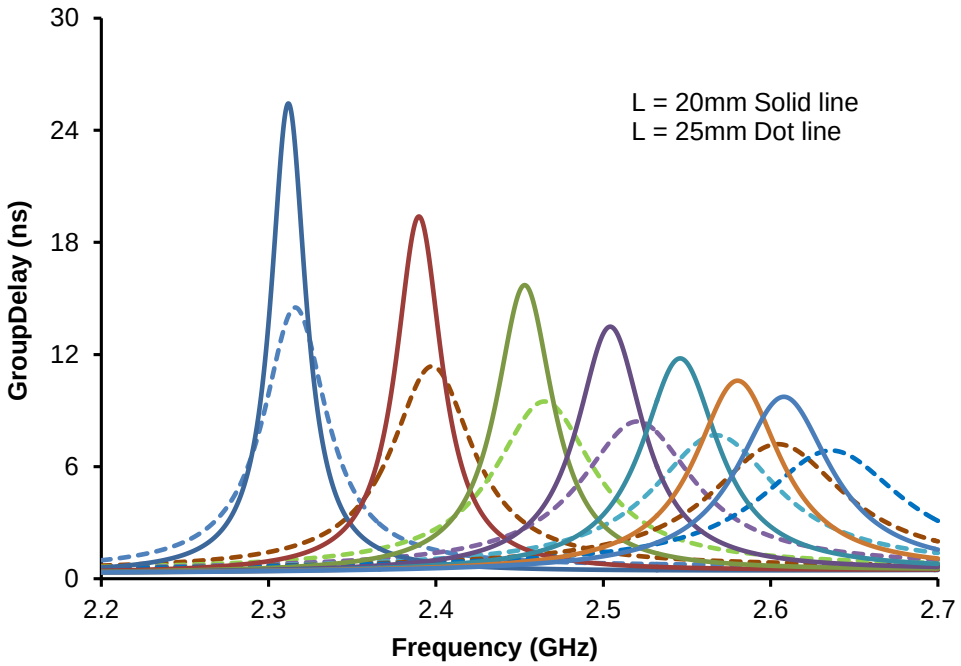

Figure 5.2-9 Simulation results of group delay with a resonator frequency change, the solid lines are the simulation results with the probe length *L*=20mm, and dotted lines are the results with the probe length *L*=25mm

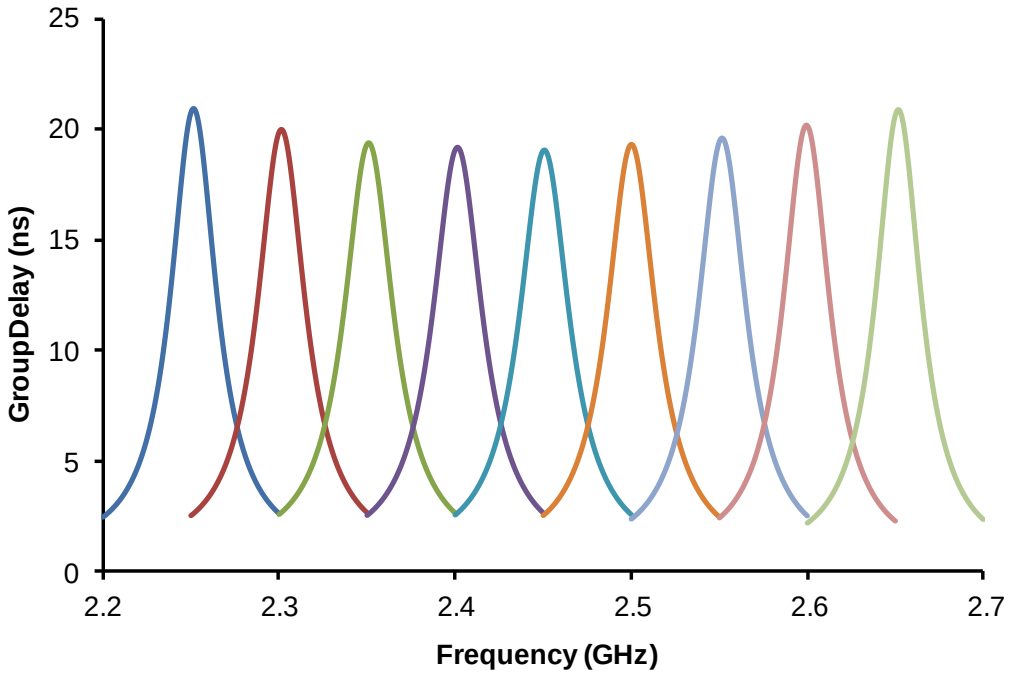

Figure 5.2-10 Simulated results of the group delay with the probe length 29.3 mm

5.2.5 Four Pole Filter Design

A 4-pole Chebyshev filter with operating frequency of 2.45 GHz, a bandwidth of 30 MHz, and a return loss of 20 dB is synthesized. The filter topology and its coupling values are displayed in Figure 5.2-11. A schematic of the 4-pole filter is illustrated in Figure 5.2-12. In this figure, long input probes are used; all the coupling slots are designed to be 17.2 mm from the cavity bottom with a slot height of 6mm. The same position and same height of these coupling slots are used to ensure ease of fabrication and assembly.

Using the design method given in [4] the initial values of all parameters are calculated. These parameters are then optimized to obtain the required filter response at 2.45 GHz. The final optimized results show that the filter's bandwidth at a return loss of 20 dB is 30 MHz, with an in-band insertion loss of better than 0.56 dB. By adjusting the gaps between the tuning disks and the resonators, the filter's center frequency tuning from 2.25 to 2.65 GHz is realized. The simulation results of tuning responses are displayed in Figure 5.2-13. The simulation results show that the designed filter can be tuned over a tuning range of 400 MHz with a stable bandwidth. An insertion loss better than 0.9 dB and a return loss better than 18 dB are achieved over the tuning range. Figure 5.2-13 shows that the center frequency of the filter changes by ±8.16% at 2.45 GHz, and the bandwidth varies from 29.5 MHz to 30.5 MHz, ± 0.5 MHz (less than ±1.7%) over the tuning range. The simulation results reveal that the filter degradation is very limited, and the absolute bandwidth is well maintained over the tuning range.

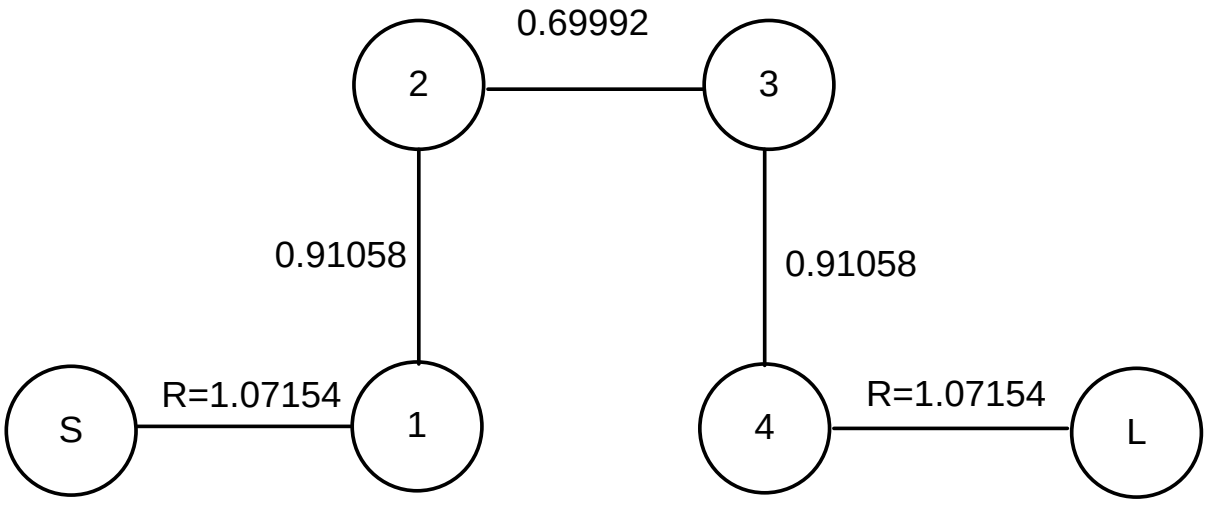

Figure 5.2-11 Topology and coupling values of the synthesized filter

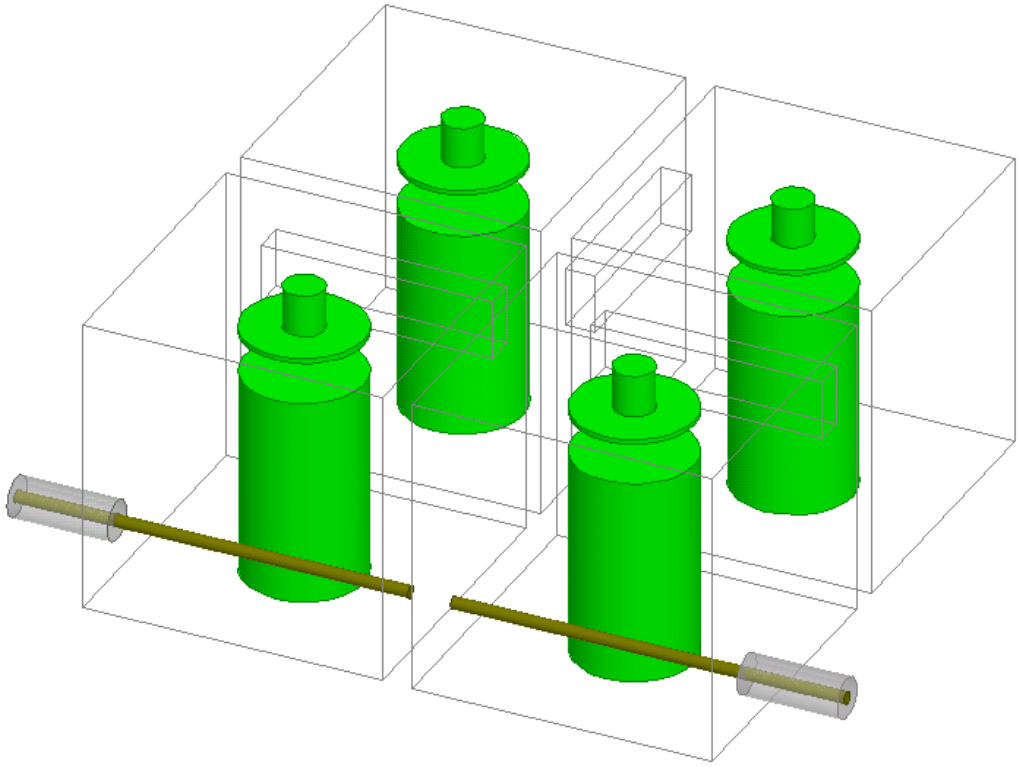

Figure 5.2-12 A schematic view of the tunable 4-pole filter

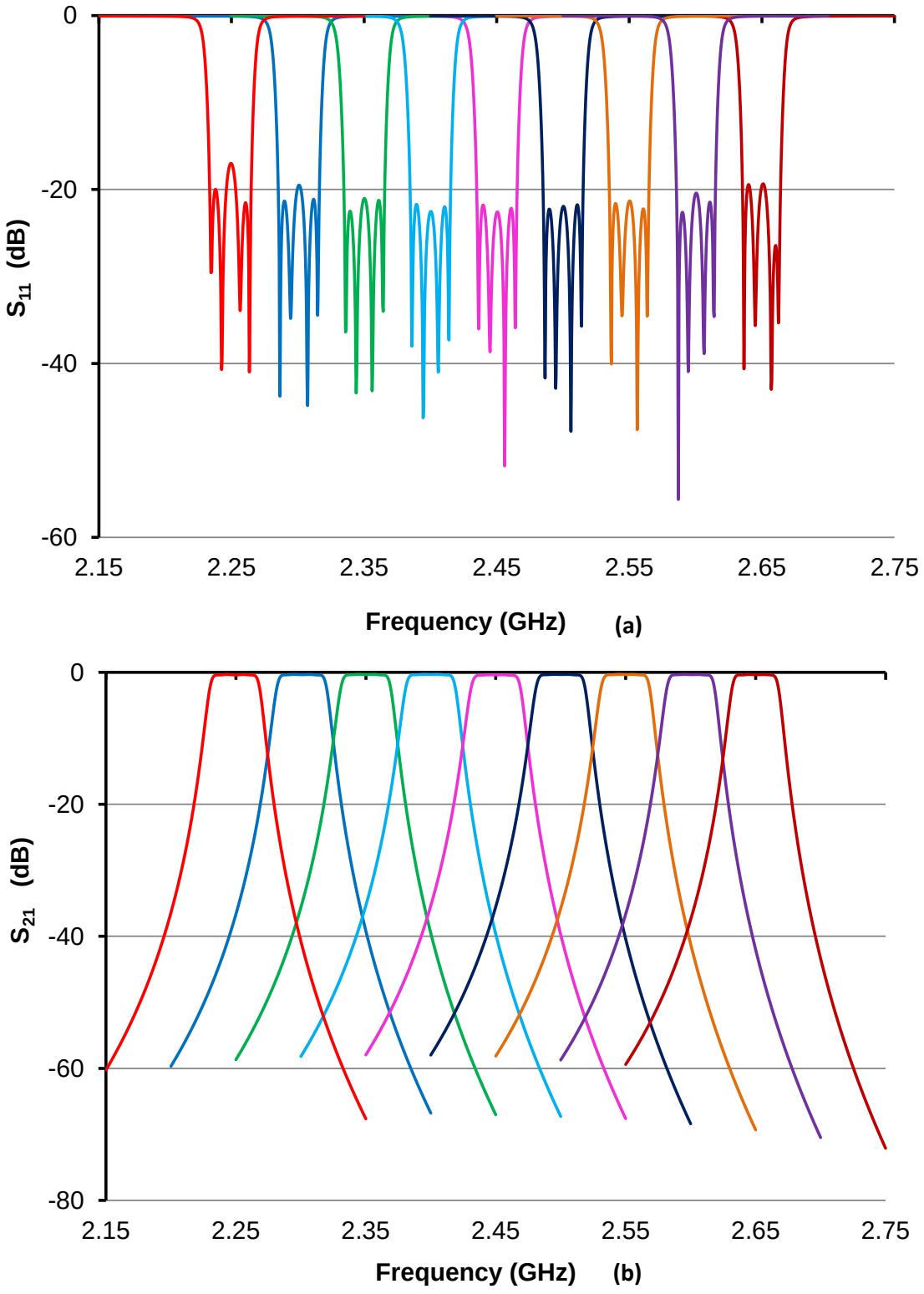

Figure 5.2-13 Simulation of the tuning response of the 4-pole filter: (a) the return loss S_{11}, and (b) the insertion loss S_{21}

5.3 Measurement of Designed Filter

Based on the simulation results, a prototype of a 4-pole tunable filter made of copper is fabricated and tested. As shown in Figure 5.3-1, the coupling slot is just below the filter lid. The filter tuning is realized by the turning disks located above the resonators. The measurements of the filter tuning responses are shown in Figure 5.3-2. At the center frequency of 2.45 GHz, the measured filter bandwidth is 30 MHz, with return loss of 20 dB and insertion loss of 0.65 dB. This figure shows that the filter is able to be tuned from 2.25 to 2.65 GHz (400 MHz). All the in-band return loss is better than 15 dB over the tuning range. The insertion loss at each band center changes from 1.04 – 0.53 dB over the tuning range, and the bandwidth changes from 31.1 – 28.9 MHz, ±1.1MHz (less than ±3.7%). A measured relative tuning range is close to ± 8.5%. The simulation and measured responses are well matched. Figure 5.3-2 also exhibits nine separate bands obtained with 10 dB of insolation between each other over the tuning range. A constant bandwidth is well maintained during the tuning process.

The extracted Q from the single resonator is displayed in Figure 5.3-3. The figure shows that measured unloaded Q values are better than 3000 over the tuning range.

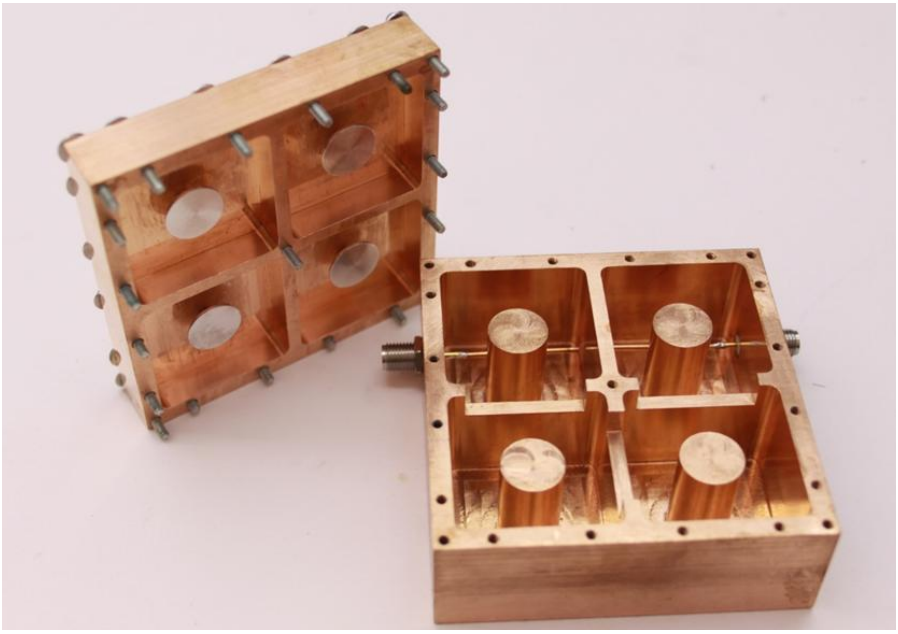

Figure 5.3-1 Picture of the fabricated tunable filter

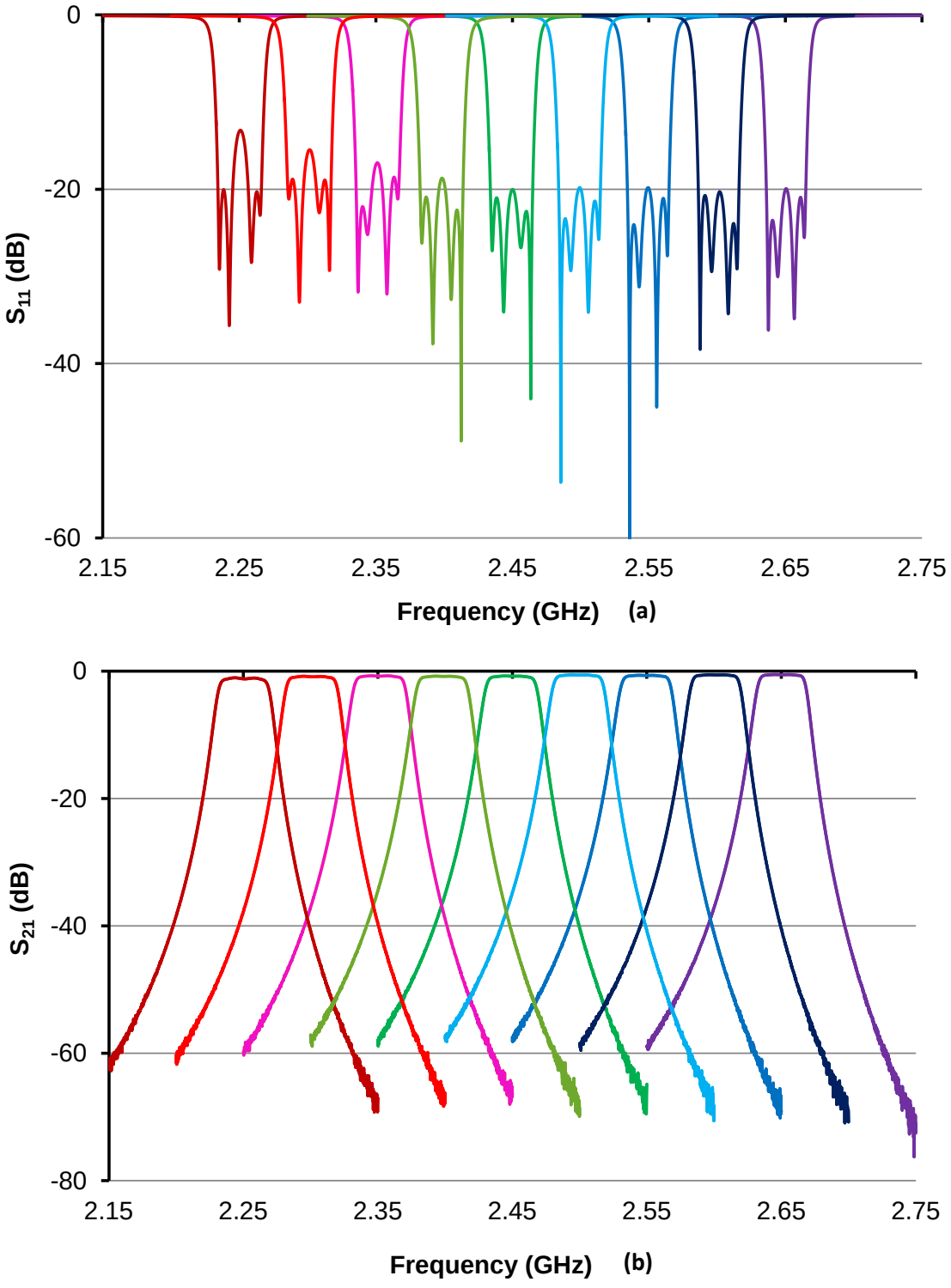

Figure 5.3-2 Measurements of the tuning response of the 4-pole filter: (a) return loss S_{11}, and (b) insertion loss S_{21}

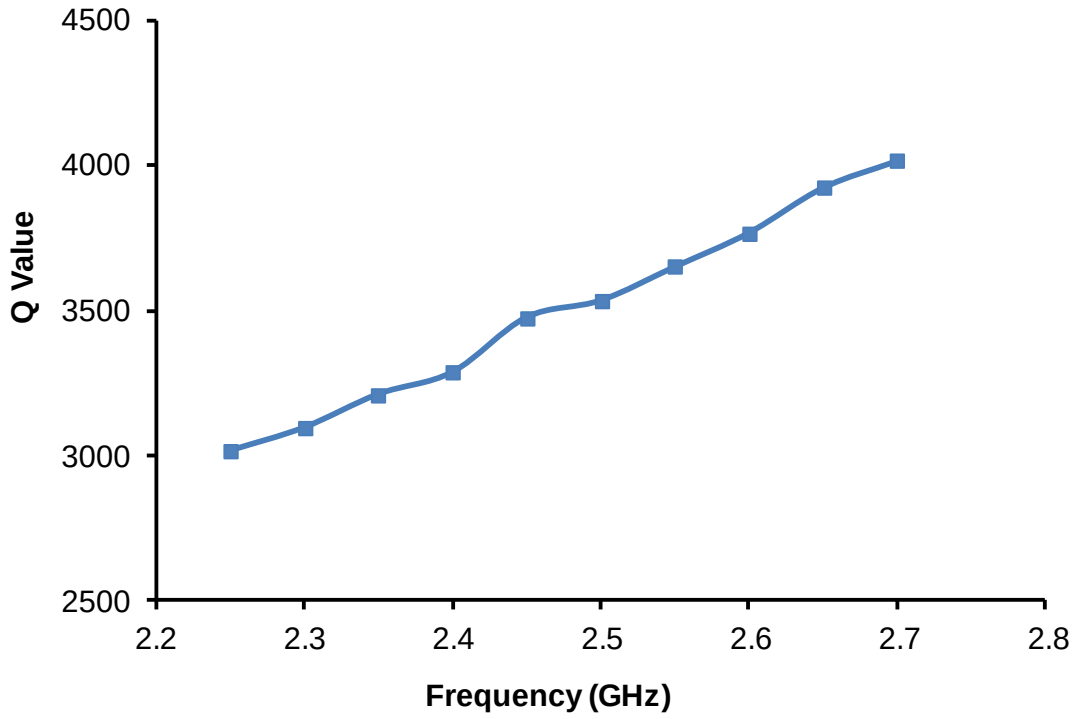

Figure 5.3-3 Extracted Q values from a single cavity resonator

5.4 Filter Assembled with Piezoelectric Motors

In order to make this designed filter practically controllable, piezoelectric driven motors are used in this tunable filter. Each tuning disk is individually controlled by a piezoelectric motor. A picture of the tunable filter assembled with piezoelectric motors is shown in Figure 5.4-1. An enlarged control element of tunable filter is illustrated in Figure 5.4-2.

Piezoelectric motors are vertically fixed in supports located on the top of each cavity. The motor rod connects the disk shaft to the motor itself. By applying an AC triangle wave voltage, the motor rod can move up and down. Thus, the tuning disk can be controlled by moving it towards and away from the post resonator, subsequently, the loading of the resonator changes. Copper beryllium gasket is used to ensure a good contact between the tuning disk and the ground (cavity), as shown in Figure 5.4-2.

The measured results of the motor tunable filters are exhibited in Figure 5.4-3. The motor tunable filter can obtain similar responses to the simulation results. The tuning range is limited by the cavity height since the tuning disks are almost touching the cavity lid. Increasing the

height of the cavity is necessary to achieve a higher frequency and a wider tuning range. The motor tunable filter could be tuned to a frequency as low as 2.25 GHz; further tuning to a lower frequency will degrade the filter return loss performance.

Because of the symmetric structure of the tunable filter, there are only two parameters used for tuning the four-pole filter. One parameter is the gap between resonator R_1, R_4 and their tuning disks, the other parameter is the gap between resonator R_2, R_3 and their tuning disks. It is not difficult to find the coefficient between these two parameters. Accordingly, ratio gears can be potentially used to realize the synchronous tuning of the four-pole filter. Figure 5.4-4 illustrates a synchronous tuning gear. All the gears are mounted on top of the filter lid. Four small gears are connected to the tuning disk by threading rod through the taped hole in the lid individually. Theoretically, by turning the driving gear, the 4-pole filter can be tuned synchronously using a single motor.

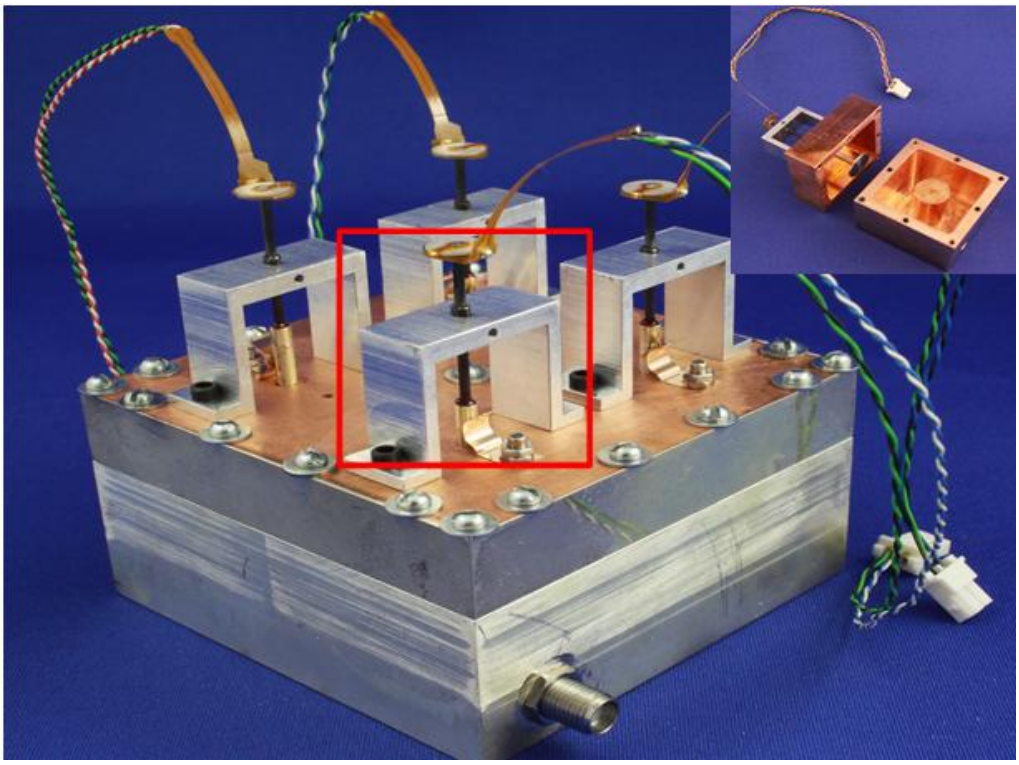

Figure 5.4-1 Picture of the tunable resonator and the tunable filter assembled with piezoelectric motors

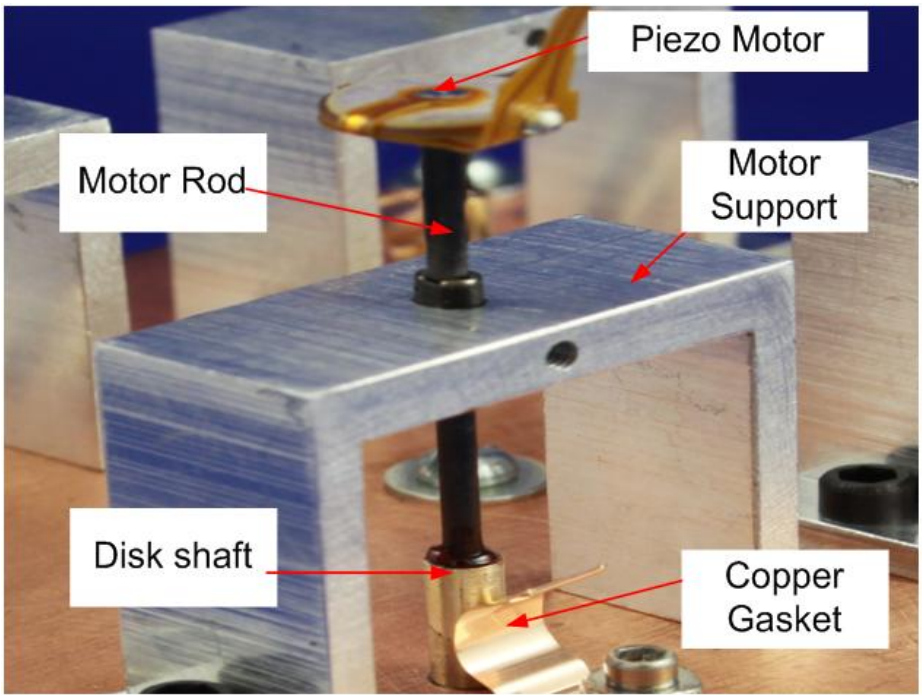

Figure 5.4-2 Enlarged control element of the tunable filter

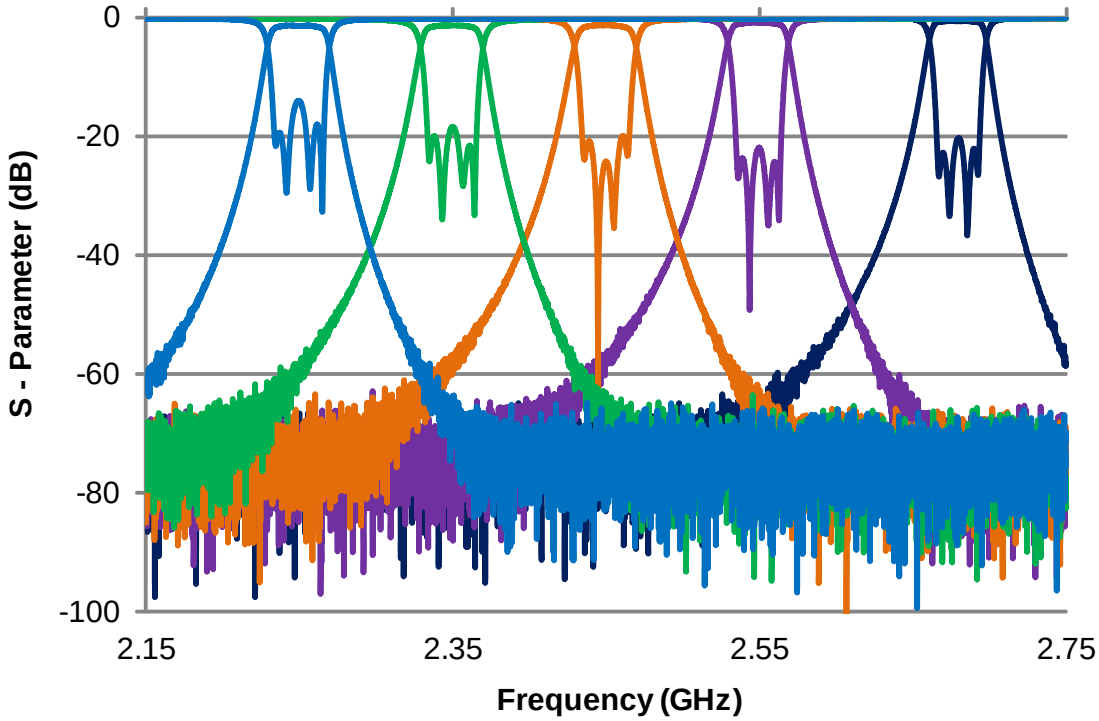

Figure 5.4-3 Selected tuning responses by motor tuning

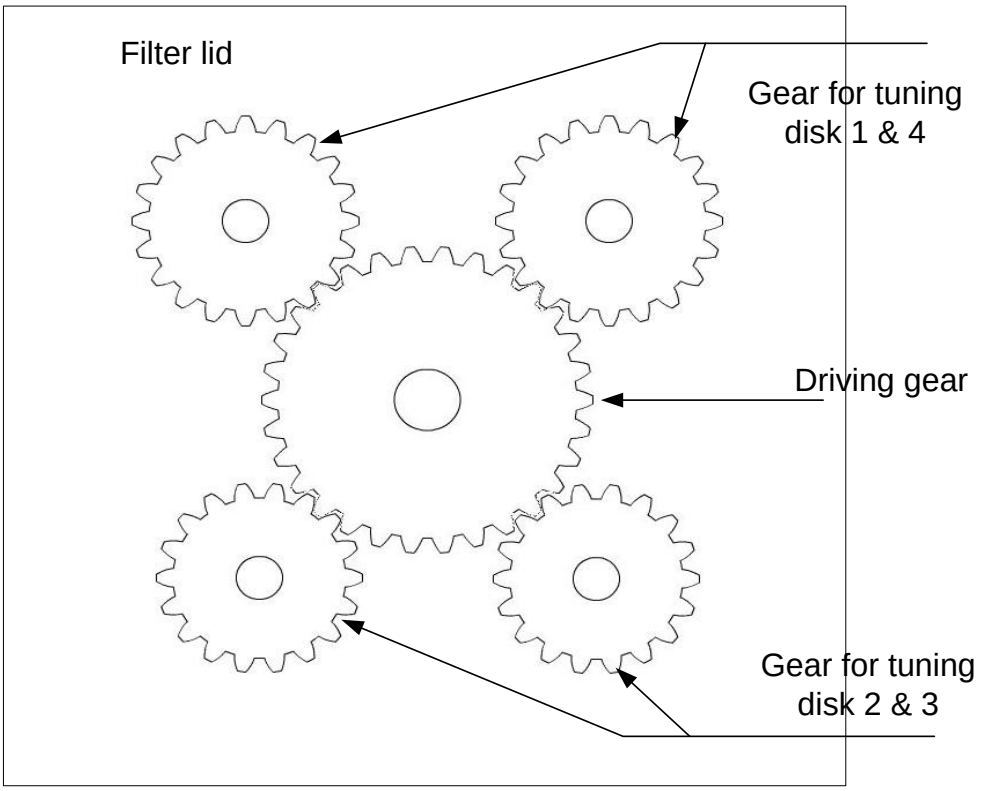

Figure 5.4-4 Synchronous tuning gear

5.5 Summary

In this chapter, a method to design a constant bandwidth tunable filter has been presented. A four-pole Chebyshev cavity combline tunable filter based on the proposal method has been designed. This designed tunable filter is realized by changing the resonator's load using tuning disks. Prototype units of the designed tunable filter, tuned manually and by piezoelectric driven motor, are assembled and measured. The measurements show that the inter-resonator coupling and the input/output coupling of the designed filter are well maintained for an absolute constant bandwidth without extra circuits being used. The measured results show that the prototype filter maintains high Q (Q >3000 over the tuning range), has a very stable bandwidth 30±1.1 MHz (less than ±3.7%), and has a wide tuning range of 2.25-2.68 GHz (close to ±8.5%). The return loss is better than 15 dB over the tuning range. For improving the filte design, it is suggested that a ratio gear for synchronous tuning is applied to the tunable filter. This designed filter is

potentially applicable for use in base station for mobile communication or WiMAX system applications. This design methodology also can be employed to other tunable filter structures.

Chapter 6
High-Q Tunable Combline Filter Using MEMS Switched Capacitor Banks and Piezoelectric Motors

In this chapter, filter structures are proposed consisting of combline resonators with tuning disks that are either mechanically moveable using piezomotors or are loaded with RF-MEMS capacitor banks. 2-pole and 6-pole tunable bandpass filters are designed and measured based on the proposed tuning concept.

6.1 Introduction

As wireless devices become more and more compact, the development of inexpensive and miniaturized tunable filters with a superior performance is crucial not only to mobile handheld devices, but also to wireless infrastructure equipment. It can benefit from tunable filter technologies in three different areas; first, installing wireless infrastructure equipment, such as remote radio unit (RRU) on the top of a 15-storey high communication tower is a very costly job. By using tunable filters, one installation can serve many years since if there is a need to change the frequency or bandwidth, it can be done through remote electronic tuning, rather than installing a new filter. Secondly, in urban areas, there is very limited space for wireless service providers to install their base stations due to expensive real estates and/or maximum weight loading constrains on certain installation locations such as light poles or power lines. Therefore, once an installation site is acquired, it's natural for wireless service providers to stuff as many functions, such as multi standards, and multi bands, into one site as possible. Tunable filter is a

key element to enable such possibility. Finally, frequency spectrum is a very limited and expensive resource. To construct a wireless network that covers large geographic locations, it's not quite unusual for one wireless service provider to use different frequency spectrum and bandwidth at different locations, even within one single network. This complex frequency spectrum allocation will require many different fixed filters to be built. However, by using tunable filters, it's quite possible to just use one type of filter to construct the whole network.

Various tuning techniques have been developed to construct tunable filters. Mechanical tuning [16, 18], magnetic tuning [59], and electrical tuning [29, 32] are the most commonly used. In terms of quality factor, power handling capability, and linearity, mechanical tuning is superior to the other two tuning techniques. Unfortunately, due to their bulky size, heavy weight, and low tuning speed, mechanically tunable filters have limited applications. MEMS technology has the potential to produce highly miniaturized tunable filters [71, 78, 97]. However, most of the MEMS tunable filters reported so far have a relatively low quality factor and require complicated MEMS fabrication and filter assembly. A novel tuning approach of cavity combline filters using RF-MEMS capacitor banks is reported in [105]. A 2-pole tunable bandpass filter is demonstrated that achieve a high-Q above 374 over an entire tuning range from 2.503 GHz to 2.393 GHz. In this chapter, the concept is thoroughly analyzed and also expanded to higher order combline filters with more stringent requirements for WiMAX applications. For the first time, 6-pole tunable filters are presented using both MEMS tuning circuits and piezoelectric motors with superior performance in terms of Q values.

6.2 Two-pole Combline Tunable Filter with RF-MEMS Switched Capacitor Bank

6.2.1 Proposed Tuning Concept

Figure 6.2-1 shows the 3D view and the cross-sectional view of a conventional tunable combline resonator. The resonator can be tuned by adjusting the gap between the tuning disk and the metal post, as presented in chapter 5. This can be achieved by manual tuning using a screw or by automatic tuning using a driving mechanism such as motors. The use of conventional

mechanical tuning using stepper motors can result in fine tuning steps, high-power handling, and high-Q; however, these motors are usually very expensive and bulky, which increase the total weight and size of the tunable filter. Here we are proposing an inexpensive tuning mechanism based on RF-MEMS switched capacitor banks and also piezoelectric motors.

Figure 6.2-2 demonstrates the structure of the proposed tunable resonator based on RF-MEMS switched capacitor banks. As shown in this figure, the tuning disk is isolated from the cavity wall with a Teflon spacer. An RF-MEMS capacitor bank is implemented on a printed circuit board (PCB) and is assembled on top of the cavity. The tuning disk is connected to the PCB board through a threaded insert on the PCB board. The variable loading effect of the capacitor bank on the tuning disk is used to tune the resonator. A simplified schematic view and the equivalent circuit diagram of the RF-MEMS tuning circuit is presented in Figure 6.2-3. The switched capacitor bank consists of high-Q capacitors in series with RF-MEMS contact type switches. By turning the MEMS switches on and off, using a DC actuation voltage, it is possible to change the value of the capacitor bank and adjust the resonant frequency of the cavity. The use of RF-MEMS switched capacitor bank results in improved performance in terms of Q, insertion loss, power handling and linearity for the proposed tunable filter.

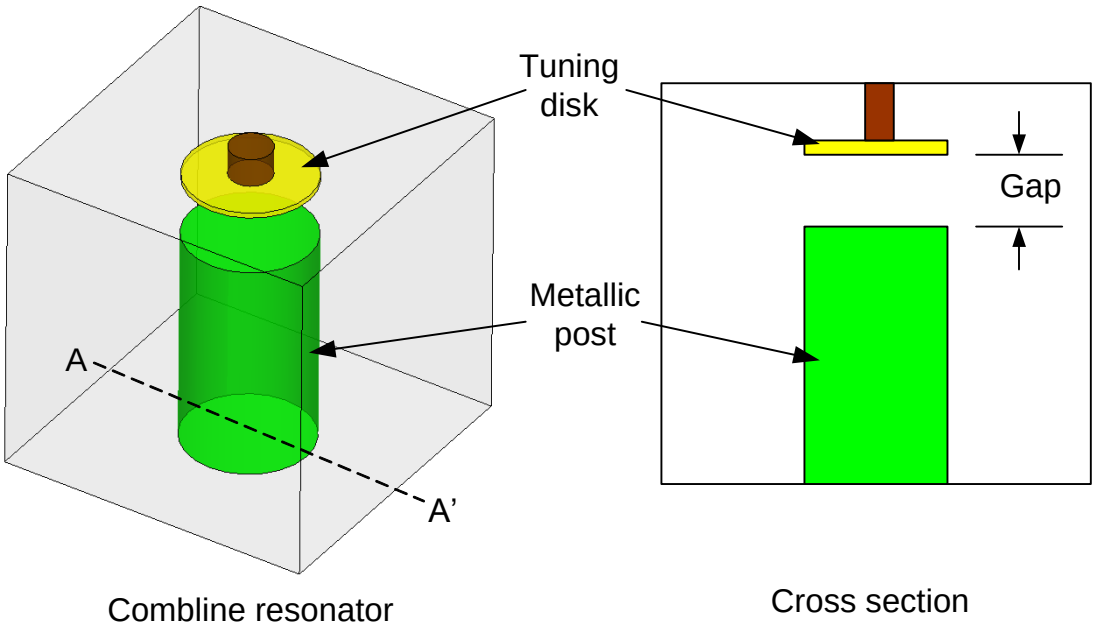

Figure 6.2-1 Combline tunable resonator with tuning disk

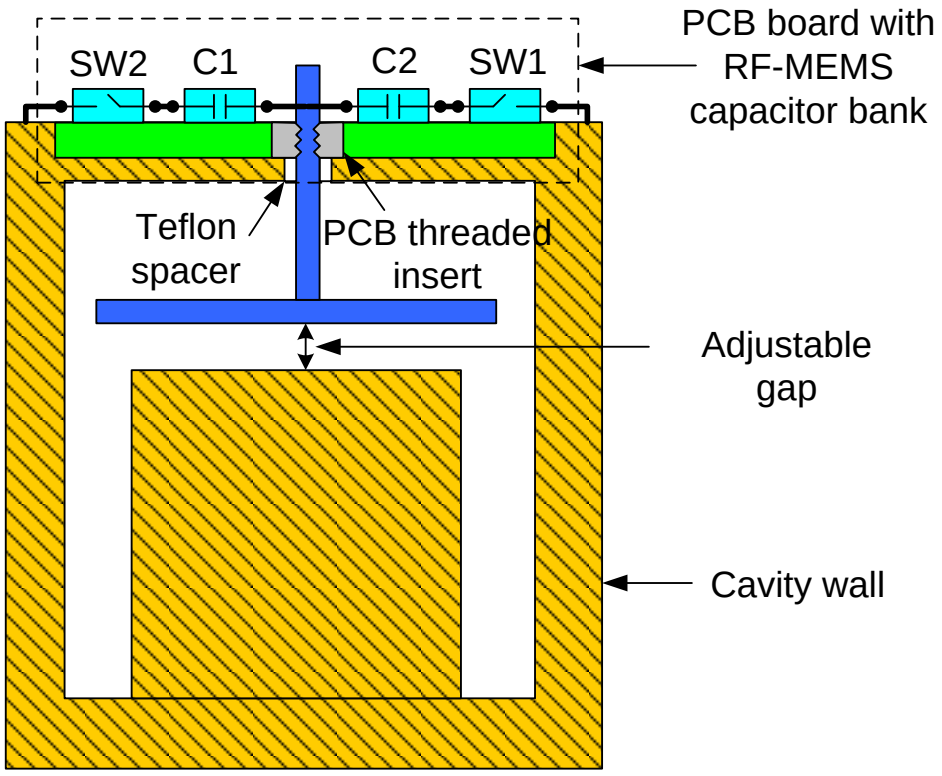

Figure 6.2-2 Schematic drawing of the proposed tunable resonator

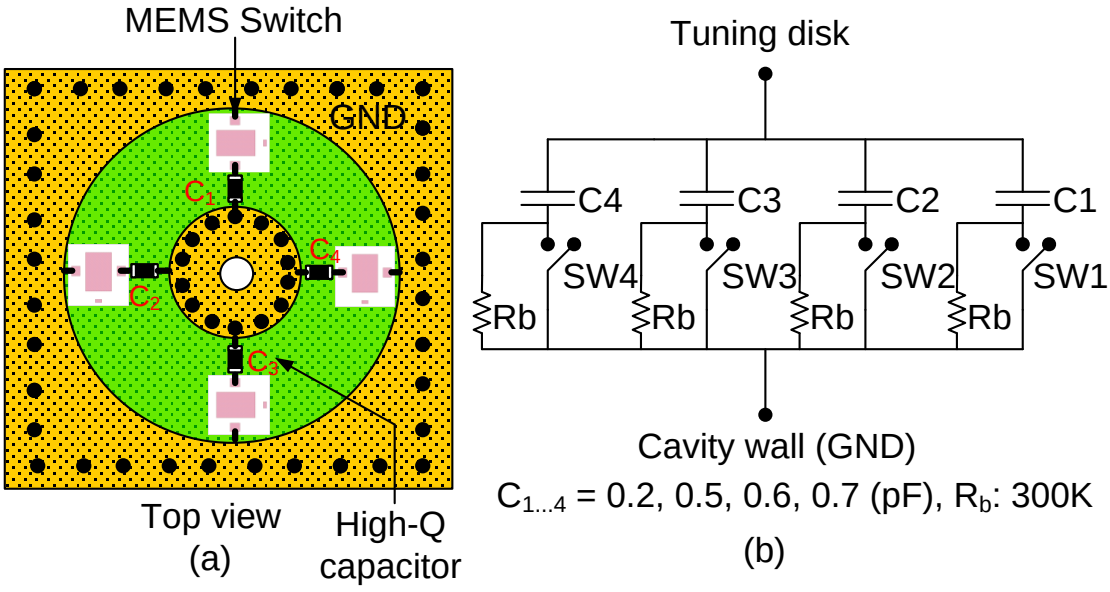

Figure 6.2-3 (a) Schematic diagram of the RF-MEMS tuning circuit and (b) the circuit model

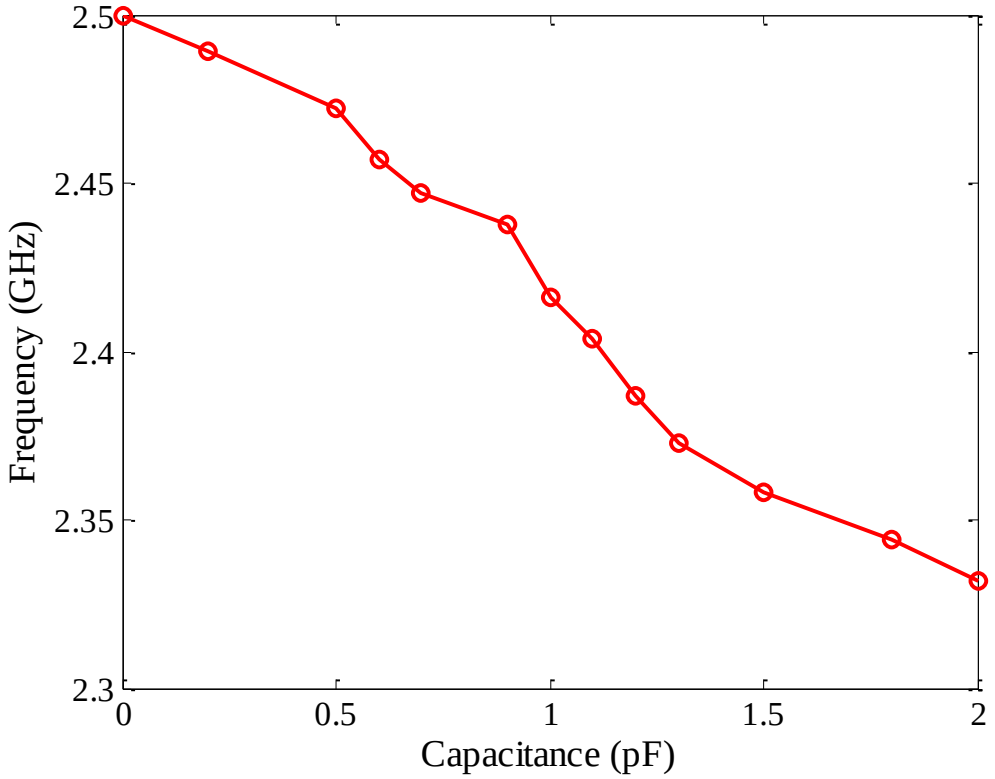

Figure 6.2-4 Simulated resonance frequency versus capacitance value

6.2.2 Tunable Resonator

A tunable resonator is designed using the proposed structure and the tuning circuit shown in Figure 6.2-3. The capacitor bank consists of four high-Q capacitors C1 to C4 in series with four RF-MEMS switches. Each one of the MEMS switches has a separate bias voltage and can be actuated separately. Using this circuit, the resonator can be tuned to 16 different states based on the value of the capacitor bank. Figure 6.2-4 shows the simulated resonance frequency of a single resonator for different values of the capacitor bank (C_1=0.2pF, C_2=0.5pF, C_3=0.6pF, and C_4=0.7pF). As seen in this figure a tuning range of 168 MHz from 2.5 GHz to 2.332 GHz is achieved.

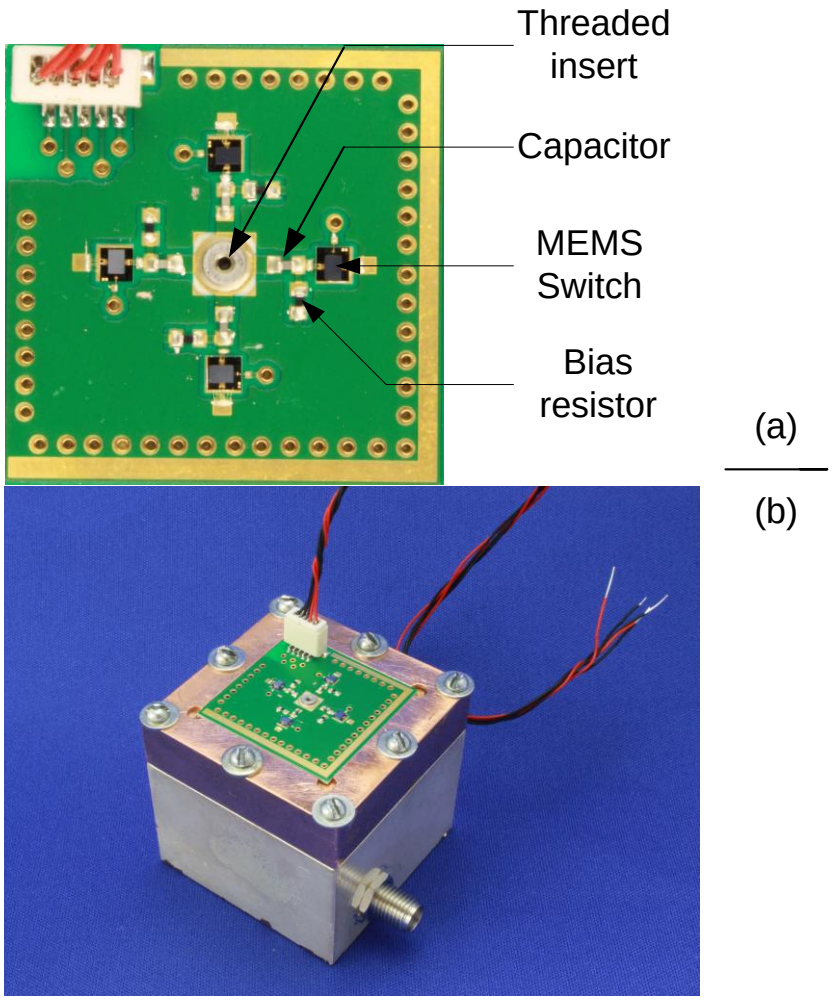

Figure 6.2-5 (a) Assembled circuit capacitor bank, and (b) tunable resonator with RF-MEMS switched capacitor bank

A photograph of the switched capacitor bank circuits and the assembled tunable resonator is shown in Figure 6.2-5. The resonator is machined from copper and inside the cavity is Silver plated for a higher Q value. The tuning circuit is mounted on top of the lid and glued with silver epoxy. High-Q (Q>150 at 2.5 GHz) multi-layer ceramic capacitors from Johanson Technology and Radant single-pole single-throw (SPST) RF-MEMS switches (RMSW101) are mounted on a Rogers RO4350 PCB board. Each MEMS switch is actuated separately with an actuation voltage of 90 volts and zero DC current (near to zero DC power consumption). The measured tuning response of the resonator is presented in Figure 6.2-6. The resonator is tuned from 2.503 GHz to 2.393 GHz (110 MHz) while the measured Q value is from 1301 to 374 for all the tuning range.

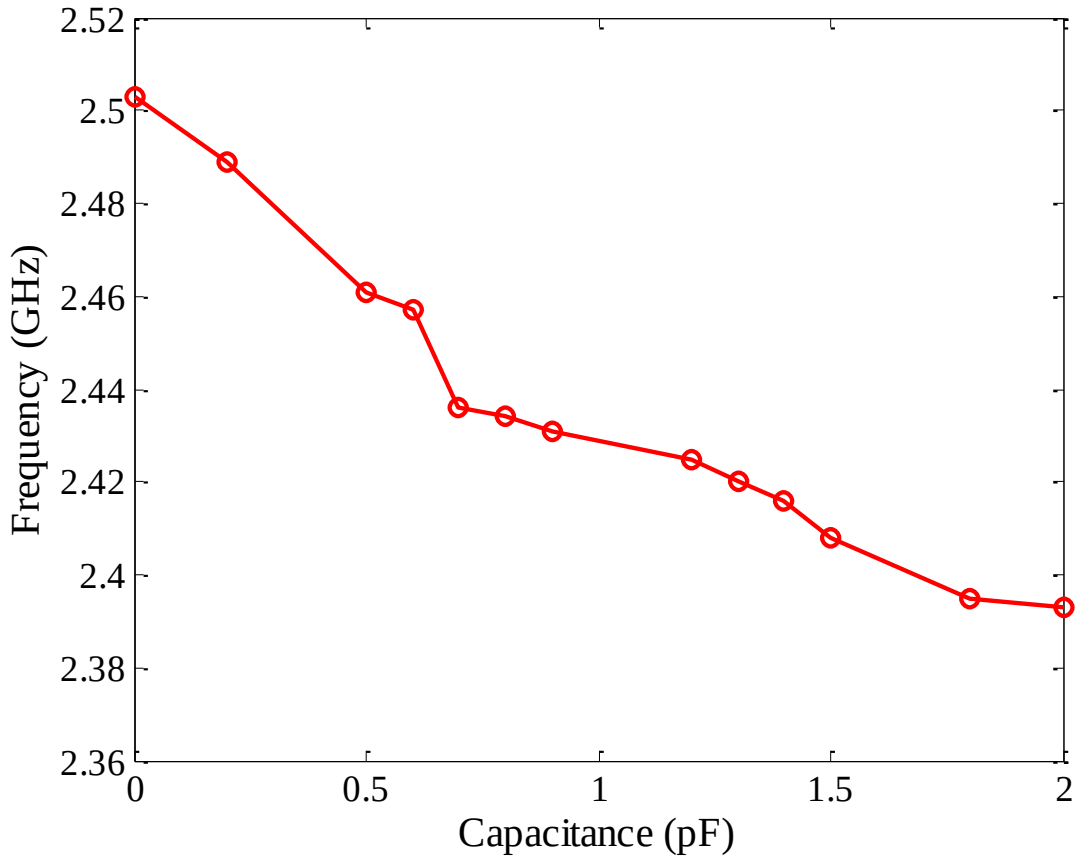

Figure 6.2-6 Measured resonance frequency versus capacitance value

6.2.3 Two-pole Tunable Filter

Employing the designed tunable resonator, a two-pole filter is designed and simulated using HFSS. Figure 6.2-7 shows the full-wave simulation model of the filter. For EM simulation, the MEMS tuning circuits are included in the model. A Q factor of 150 at 2.5 GHz is assumed for the fixed ceramic capacitors. The MEMS switch is modeled with a small series capacitor and resistor for the 'off' and 'on' states respectively. Figure 6.2-8 shows the simulated S-parameters of the designed tunable filter for three different tuning states. Simulation results demonstrate that the filter operates at 2.5 GHz with a bandwidth of 22 MHz (0.9%) and a return loss better than 20 dB. It exhibits an insertion loss of 0.44 dB for the first state, when all the switches are 'off' and the capacitive loading on the tuning disk is almost zero. The center frequency can be tuned to different states from 2.5 GHz to 2.345 GHz while the bandwidth varies from 20 to 22 MHz and the return loss is better than 12 dB.

A two-pole tunable combline filter was fabricated and measured. The aluminum housing is plated with copper for improved performance. The tuning circuits with RF-MEMS capacitor banks are assembled on the lid of the housing as shown in Figure 6.2-9. There are screws connected to the tuning disks. These screws are used only for the initial tuning of the filter after assembly. There are biasing wires for each one of the capacitor banks and each set of MEMS switches. The MEMS switches are tuned on and off in a way that the two capacitor banks have the same capacitance values and the two resonators are tuned synchronously. Measurement results for the two-pole tunable filter are presented in Figure 6.2-10. As shown in this figure, for the first state, the filter operates at 2.5 GHz with a 23 MHz bandwidth and a 1.32 dB insertion loss. A maximum tuning range of 110 MHz from 2.503 GHz to 2.393 GHz is achieved using the RF-MEMS tuning circuit. The return loss is better than 14 dB and the insertion loss is less than 2.4 dB for all the tuning states.

The measured return loss when $C_{total}=C_3=0.6$ pF ($S_{1,2,4}$ are 'off') shows that the two resonators are not completely tuned to the same frequency. This is due to the tolerance in the capacitance value of the fixed capacitor (C_3) which was not accounted for in the simulations. For this type of discrete tuning it is necessary for the two capacitor banks to have exactly the same capacitance values. The measurement results validate the simulations and the feasibility of using the proposed tuning approach for combline filters.

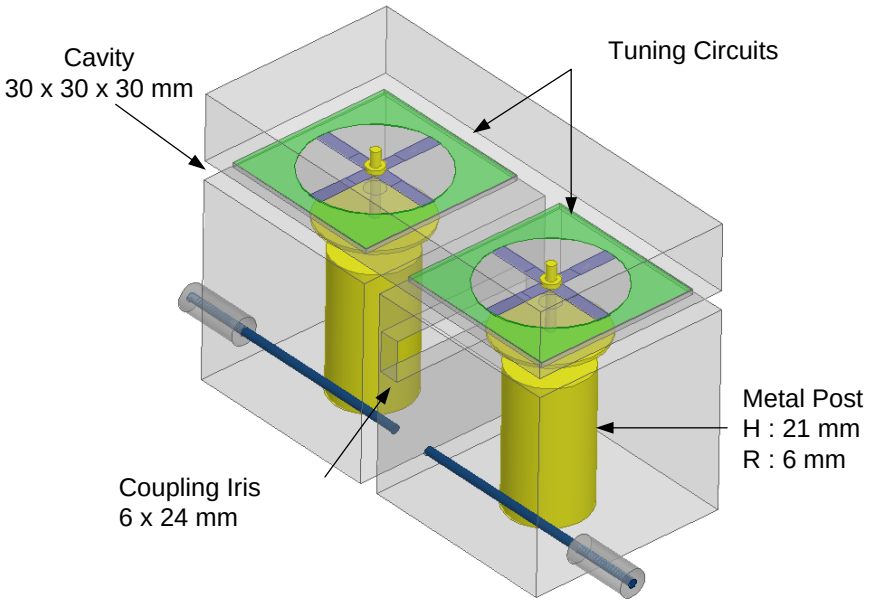

Figure 6.2-7 3D EM model of the two-pole tunable filter

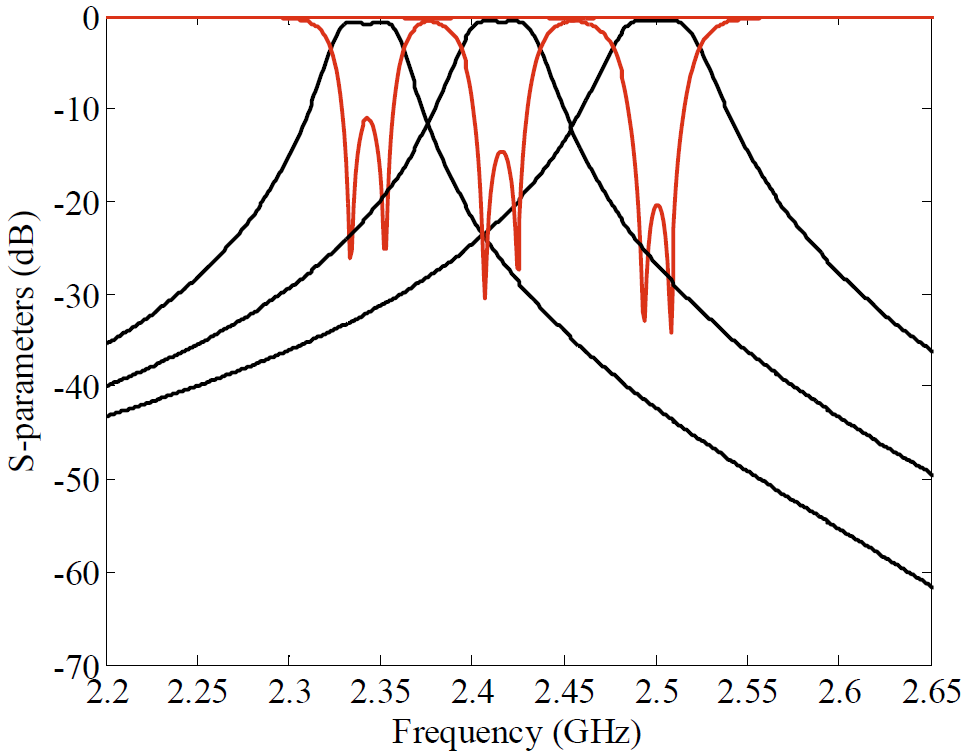

Figure 6.2-8 Simulated S-parameters of the designed filter

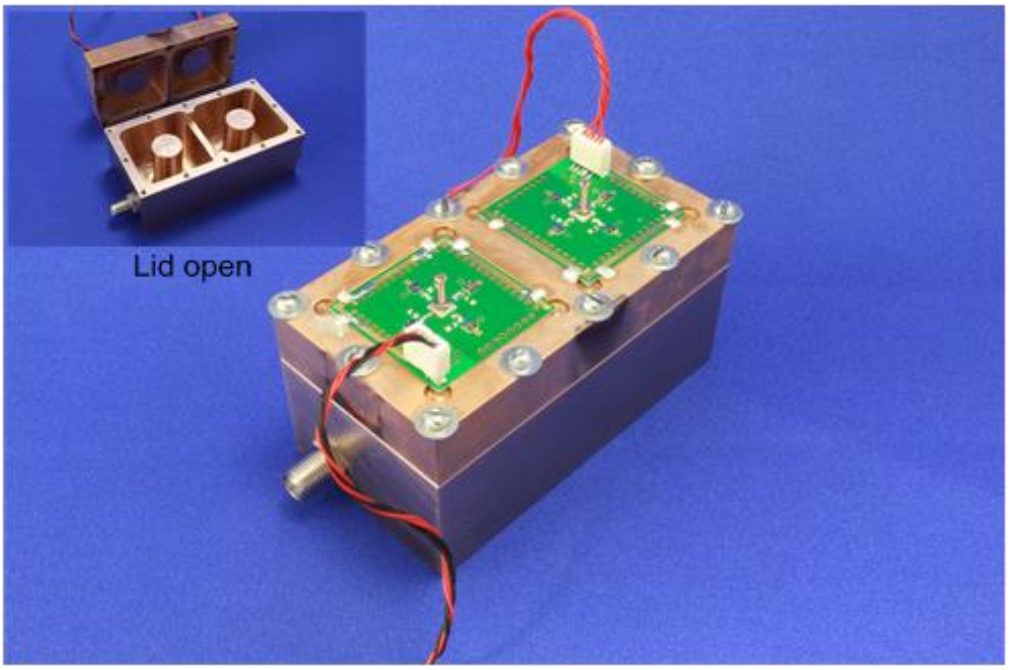

Figure 6.2-9 Assembled two-pole tunable filter

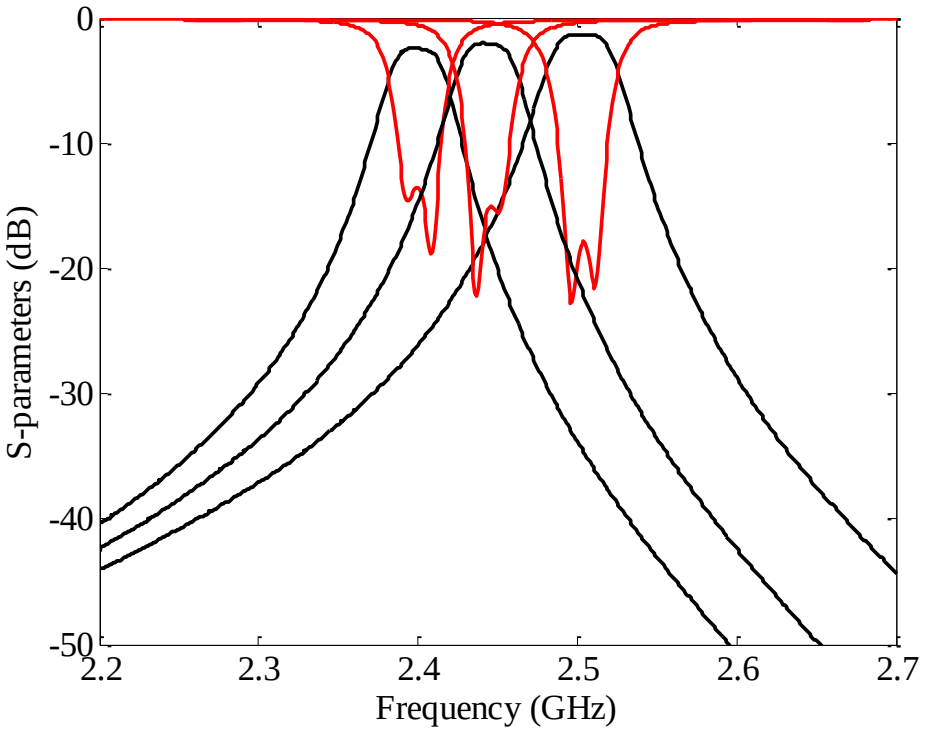

Figure 6.2-10 Measured S-parameters of the two-pole tunable filter

6.3 Application of Tunable Bandpass Filter in WiMAX System

To expand the tuning concept to a more stringent requirements application, a six-pole combline tunable filter is built and investigated for WiMAX application. Table 6.3-1 displays the key specifications of tunable bandpass filter in WiMAX system.

Table 6.3-1 Key specifications of the WiMAX tunable filter

Items	Frequency Band	Specifications
Frequency Center (FC)	2565 ~ 2635 MHz	70 MHz Tuning
Working Band	2550 ~ 2650 MHz	30 MHz Bandwidth
Return Loss	FC ± 15 MHz	≥ 18 dB
Insertion Loss	FC ±15 MHz	≤ 1.8 dB
Rejection	5 MHz offset from passband	≥ 25 dB

6.3.1 Filter Synthesis

To meet these specifications, a 6-pole elliptic filter is synthesized to operate in the WiMAX band. Figure 6.3-1 illustrates the response of the synthesized 6-ploe elliptic filter at low band, middle band, and high band with a rejection mask, a return loss mask and an insertion loss mask. An unloaded Q of 4000 is required to synthesize the filter response to meet the WiMAX system specifications. The topology scheme of the synthesized 6-pole ellipital filter is displayed in Figure 6.3-2. The numbers exhibited on the line of the scheme are the normalized coupling value between the adjacent resonators.

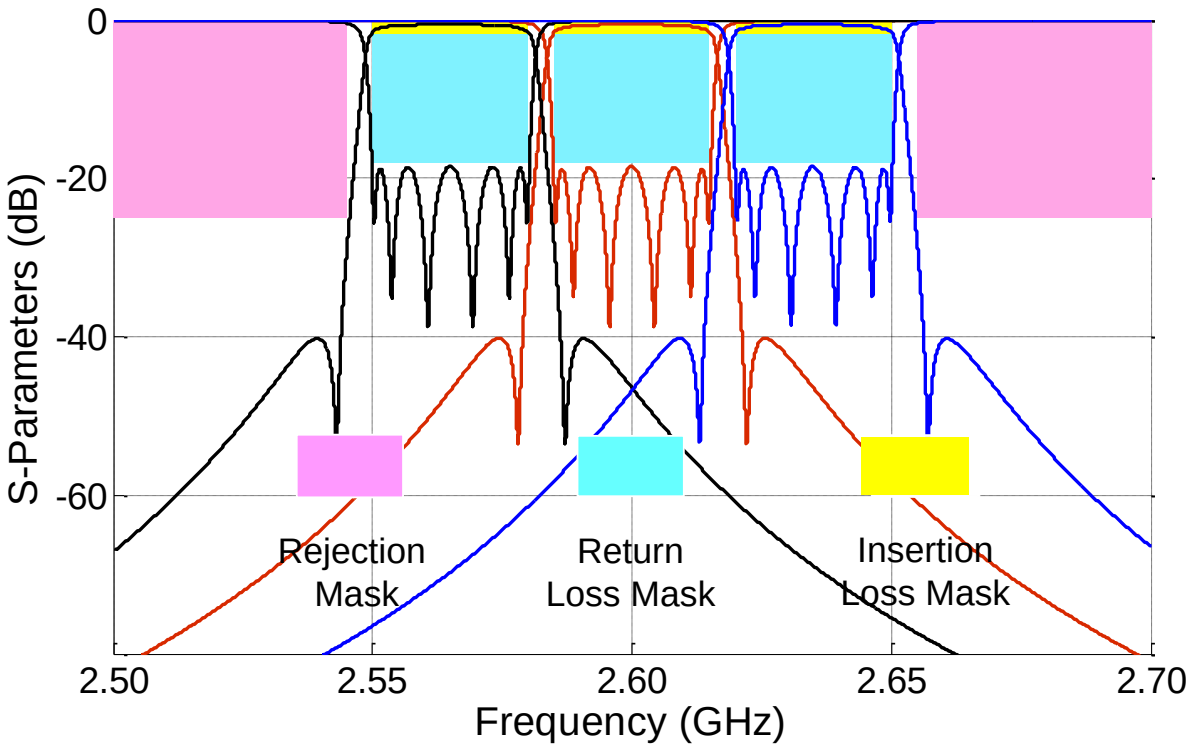

Figure 6.3-1 Synthesized 6-pole elliptical filter at low, middle, and high band with a rejection mask, a return loss mask, and an insertion loss mask

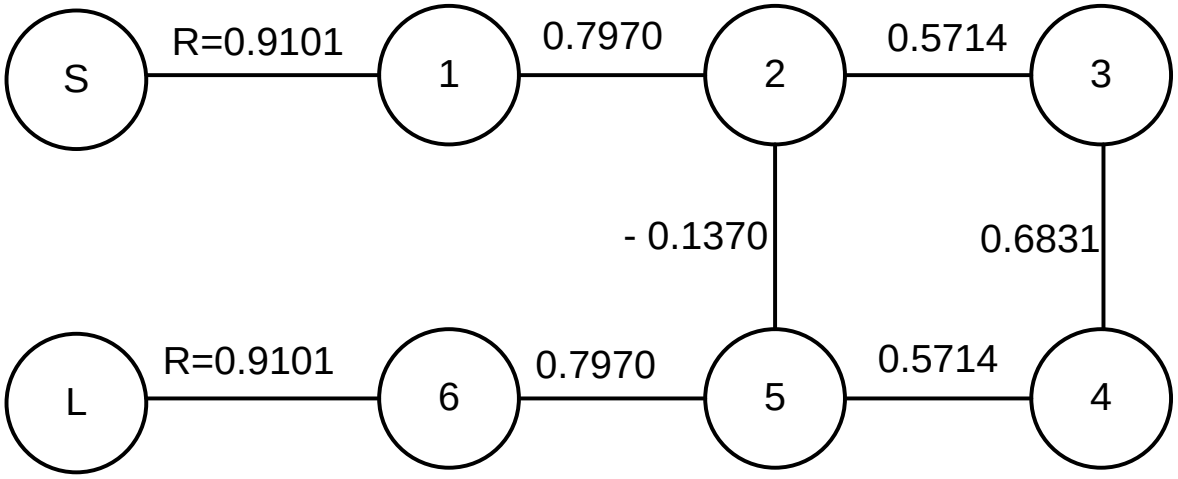

Figure 6.3-2 Six-pole elliptic filter topology scheme

6.3.2 Six-pole Filter with Piezoelectric Motor Tuning

In the previous chapter, a combline cavity resonator tuned by disk was presented. The initial resonator structure is shown in Figure 6.3-3. The dimensions of the combline resonator and its simulated tuning results are exhibited in Table 6.3-2. The table shows that a tuning range from 2.669-2.535 GHz is achieved for a gap variation of 5 to 7 mm. The unloaded Q is better than 4750 over the tuning range and a resonant frequency at 2.6 GHz can be achieved when the gap is 5.718 mm. These simulated results of the single resonator show that the cavity combline resonator can meet the specifications of the WiMAX tunable bandpass filter if their gaps are tuned theoretically.

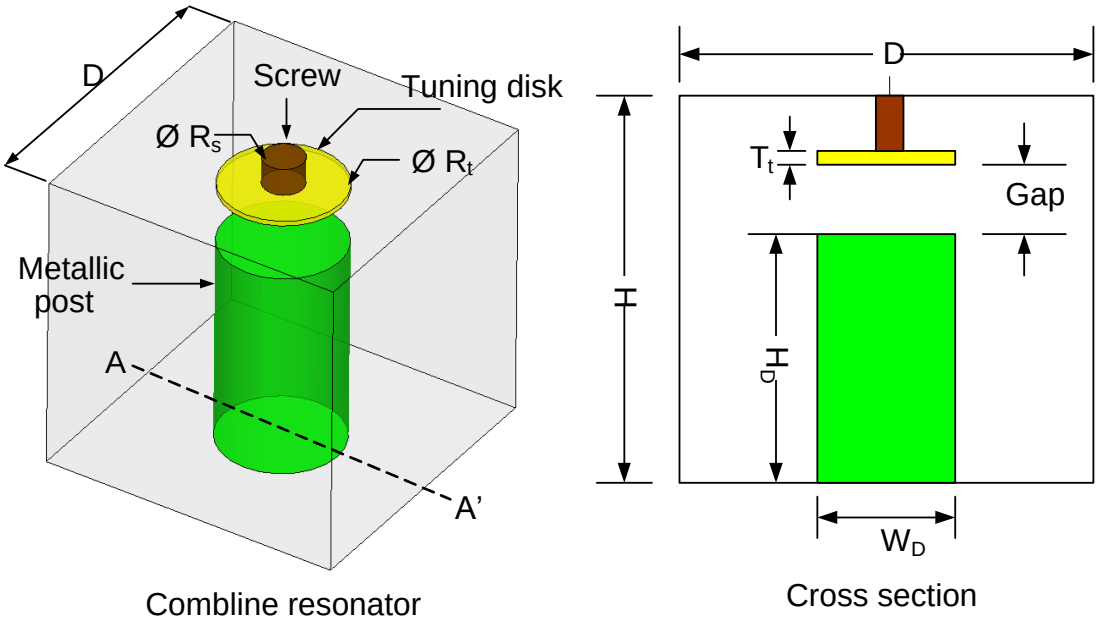

Figure 6.3-3 Structure of the tunable resonator

Based on the coupling scheme of the 6-pole filter in Figure 6.3-2, EM optimization with HFSS is used to find the dimensions of the coupling iris in order to achieve the normalized coupling values listed in Figure 6.3-2. For positive coupling values, as shown in Figure 6.3-4 (a), a rectangular iris with width of W=6 mm and height of H=17.2 mm is used and the parameters L_{ij} are optimized to obtain the different coupling values between resonators. For negative coupling value between resonators R_2 and R_5 a probe with a length L_p is used as shown in Figure 6.3-4 (b). Based on these initial values, all the final values, which include every iris length, every probe length and position, and each gap value G_i (i=1…6) between the posts and the tuning disks, can

be obtained by optimizating the 3D EM model of 6-pole filter (as shown in Figure 6.3-5) to achieve a good response at a center frequency of 2.60 GHz with a bandwidth of 30 MHz. Simulated results of the filter's middle band is shown in Figure 6.3-6, and the geometric dimensions are listed in Table 6.3-3. The low band and high band responses are obtained by optimizing the gaps G_i (i=1…6) between the resonators and their tuning disks based on the other parameters achieved from the optimized middle band filter. The low band and high band responses are shown in Figure 6.3-6 with their gaps values G_i (i=1…6) at three tuning states as listed in Table 6.3-3 as well.

Table 6.3-2 Dimensions of the resonator and its tuning results

Component	Dimensions (mm)	
Cavity	D x D x H (30 x 30 x 30)	
Combline Post	H_D x W_D (21 x 12)	
Tuninng Disk	R_t = 12 T_t = 0.5	
Screw	R_S = 4	
Tuning		
Gap	Frequency (MHz)	Q
5 mm	2535	4767
6 mm	2614	4906
7 mm	2669	5024
5.718 mm	2600	4898

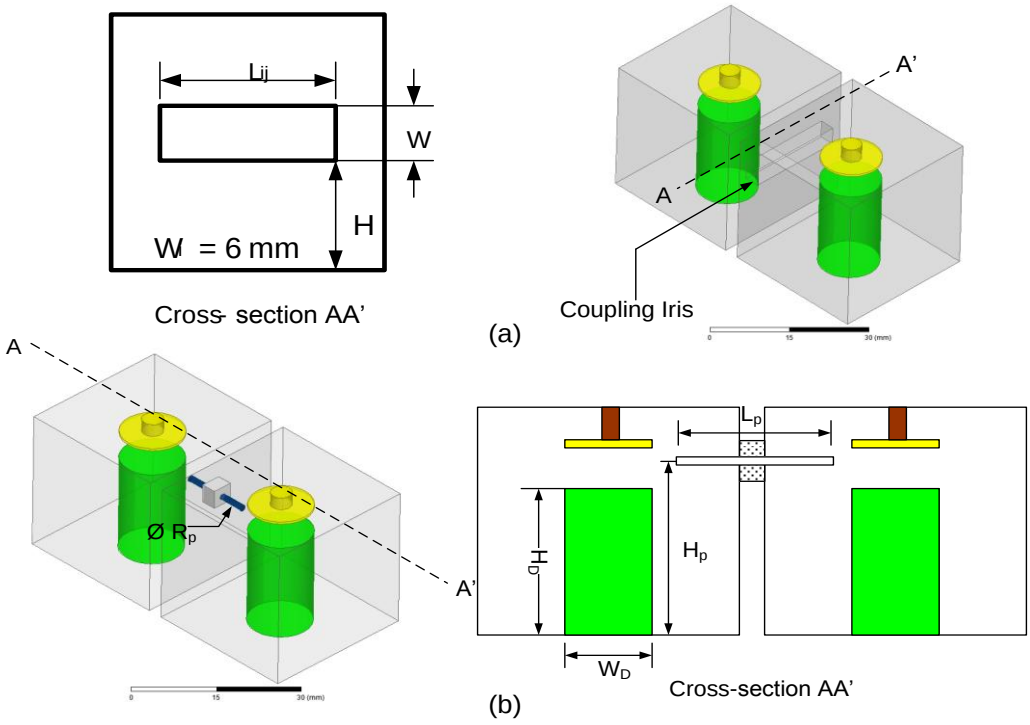

Figure 6.3-4 EM models to find (a) positive coupling and (b) negative coupling between the combline resonators

Table 6.3-3 Optimized dimensions for the 6-pole tunable filter

Parameter	Value (mm)
Iris Height, Width	H=17.2, W = 6
Iris Length	L_{12}= L_{56}= 22.48, L_{23}= L_{45}= 19.08, L_{34}=20.47
Negative Coupling Probe Length, Height	L_p=13.4, H_p = 20.375
Input/Output probe Length, Height	L=29.28, H=4.2
Tuning Disk Gap Values at 2.565 GHz	G_1= G_6=5.29, G_2= G_5=5.53, G_3 =5.47
Tuning Disk Gap values at 2.600 GHz	G_1= G_6=5.71, G_2= G_5=6.01, G_3 =5.93
Tuning Disk Gap values at 2.635 GHz	G_1= G_6=6.22, G_2= G_5=6.61, G_3 =6.52

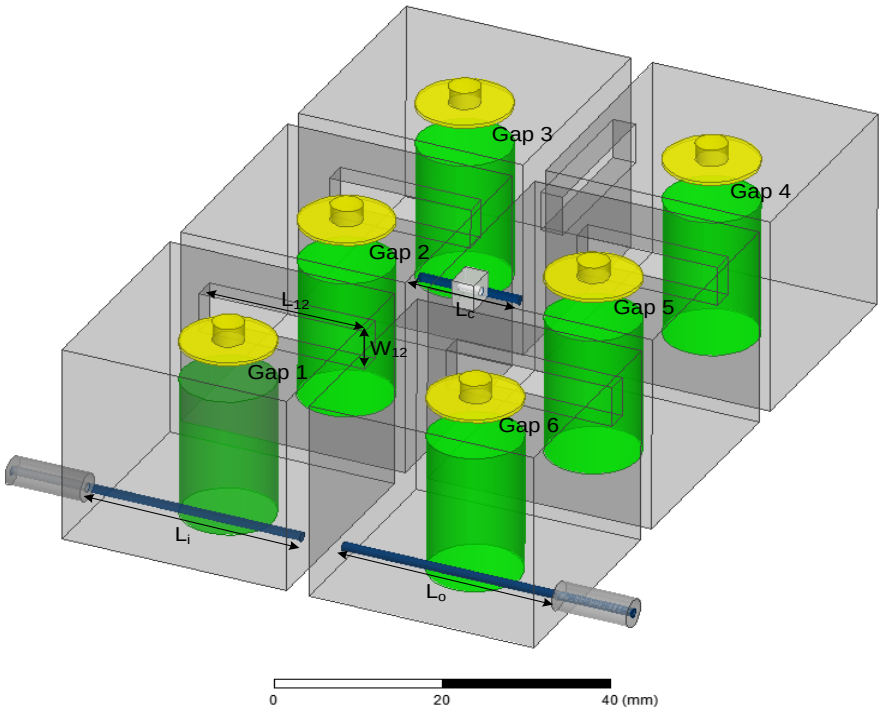

Figure 6.3-5 EM model of the six-pole tunable filter

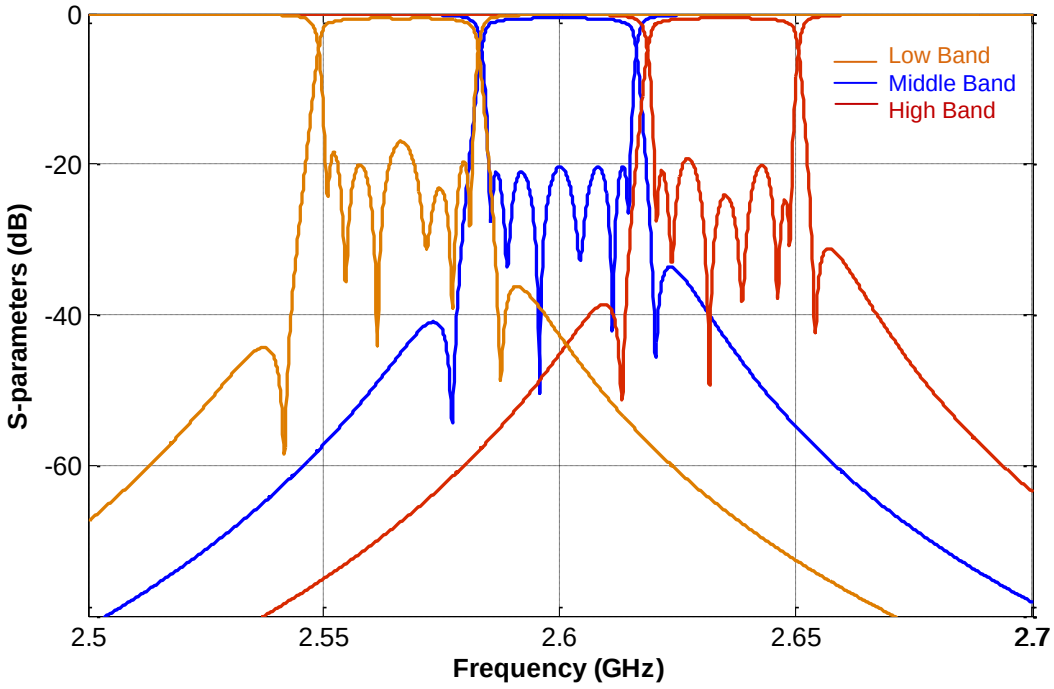

Figure 6.3-6 Simulated results with the tuning response

For automatic tuning of the designed filter, a compact size piezoelectric motor known as tiny ultrasonic linear actuator[106] is used for tuning driver. The pictures of the fabricated tunable filter are displayed in Figure 6.3-7. Each motor is assembled with each tuning disk on the cavity lid. The disks can be moved both directions by the motor by switching the polarity of applied AC trangluar voltages. The initial tuned results at middle band of f_1=2.600GHz are obtained and displayed in Figure 6.3-8. The middle band results show that the insertion loss is between 0.75 to 1.79 dB, the return loss is larger than 18 dB, and the 5 MHz offset from passband boundary rejection is larger than 26 dB, which meet the filter's specifications. The tuned response of the filter at low band of of f_1=2.565GHz and high band of f_1=2.635GHz are exhibited in Figure 6.3-8 as well. In the low band, the insertion loss is between 0.9 to 2.15 dB, the return loss is better than 16.1 dB, and the 5MHz offset from passband boundary rejection is 21.4 dB. In the high band, the insertion loss is between 0.77 to 1.95 dB, return loss is better than 16.2 dB, and 5 MHz offset from passband boundary rejection is 34 dB. The bandwidths of the tunable filter at low band, middle band, and high band are 30.5 MHz, 30 MHz, and 29.6 MHz respectively. A tuning range of required 70 MHz (2.565 GHz-2.635 GHz) is obtained. Merasured results also show that the low band and high band results are not a perfect match for the specifications. This is due to the filter bandwidth changing and degrading during the filter tuning process.

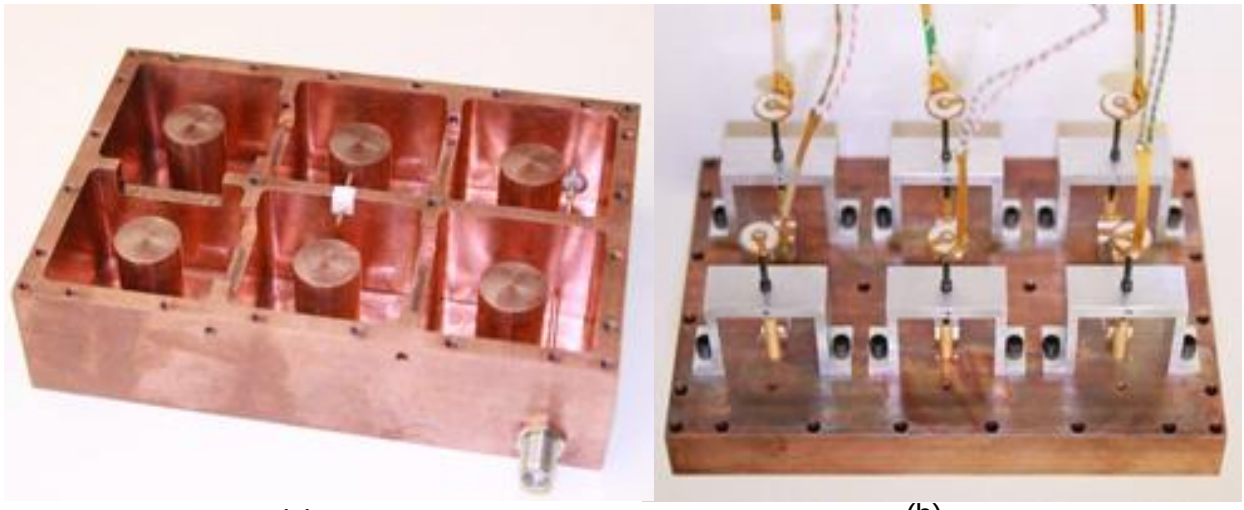

(a) (b)

Figure 6.3-7 Pictures of fabricated filter: (a) housing, and (b) lid assembled with motors

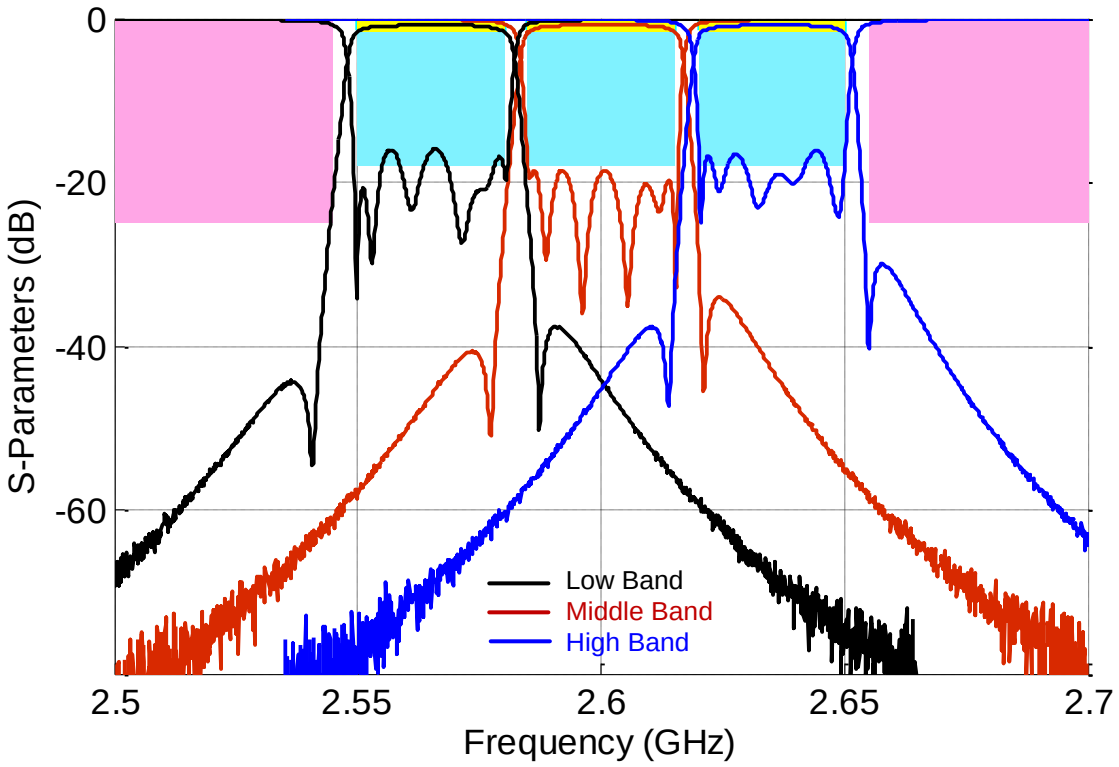

Figure 6.3-8 Measured results with motors tuning

6.3.3 Six-pole Filter with MEMS Switched Capacitor Banks Tuning

Based on the tuning techniques of MEMS switched capacitor bank for a 2-pole filter in section 6.2 and the designed six-pole motor tunable filter in section 6.3.2, a six-pole tunable filter using MEMS switched capacitor bank is assembled. The housing of 6-pole filter, displayed in Figure 6.3-9 (a), is identitical to the housing fabricated for the piezoelectric motor tuned filter in section 6.3.2. Details of the lid structure are shown in Figure 6.3-9 (b), (c), and (d). For the MEMS tuning circuit the same capacitor bank as in Figure 6.2-3 is used with different capacitance values: C_1=0.2, C_2=0.3, C_3=0.5 and C_4=0.7 pF. Because of the symetric structure of 6-pole filter, the capacitor banks for the resonators R_1 and R_6 have the same values; $C_{total,1}=C_{total,6}$, and in a same way $C_{total,2}=C_{total,5}$ and $C_{total,3}=C_{total,4}$. The final optimization of the 6-pole EM model was performed with HFSS and for $C_{total,1}=C_{total,2}$ $=C_{total,3}$=0.7pF to achieve a good response at 2.6 GHz with a bandwidth of 30 MHz. The only parameters that optimized are the gap values for each resonator G_i (i=1…6). The optimized simulation results at 2.6 GHz are demonstrated in

Figure 6.3-11. After optimizating the response at 2.6 GHz, the filter can be tuned only by adjusting the capacitance values of the capacitor banks on each resonator.

The assembled 6-pole filter is shown in Figure 6.3-12. The tuning screws are used for initial tuning at 2.6 GHz and when $C_{total,1}=C_{total,2}=C_{total,3}=0.8$ pF. In order to maintain a high Q and low insertion loss for the assembled filter it is very important to establish a good ground contact between the MEMS capacitor banks and the cavity wall. For this reason, sufficient number of via holes between the bottom ground plane of the printed circuit board and the top ground plane of the MEMS capacitor bank are required as shown in Figure 6.3-12. After assembly, the DC bias voltage is applied to S_2 and S_3 ($C_{total}=0.8$ pF on each resonator) and the filter is manually tuned with the tuning screws to achieve the desired filter response, as shown in Figure 6.3-13. The manually tuned initial results are that filter center frequency is at 2.605 GHz, the best insertion loss is 2.2 dB, the in-band return loss is better than 16.5 dB, and the 3 dB band width is 29 MHz. If switches S_1, S_2, S_3, and S_4 have DC voltages alternatively applied on each resonator simultaneously, the total capacitance on each resonator is synchronously changed. Then the filter responses are tuned with a combination status of different switches. The measured transmission responses of the tunable filter are exhibited in Figure 6.3-14 when the value of the capacitor banks is changed from 0 to 1.7 pF. A maximum tuning range from 2634 MHz to 2590 MHz (44 MHz) is achieved while the insertion loss varies between 2.2-4.25 dB over the tuning range. The 3 dB band width changed from 29 to 31 MHz. The measured responses of return loss are exhibited in Figure 6.3-15. The measured results show that the filter degradation is significant during the filter tuning process.

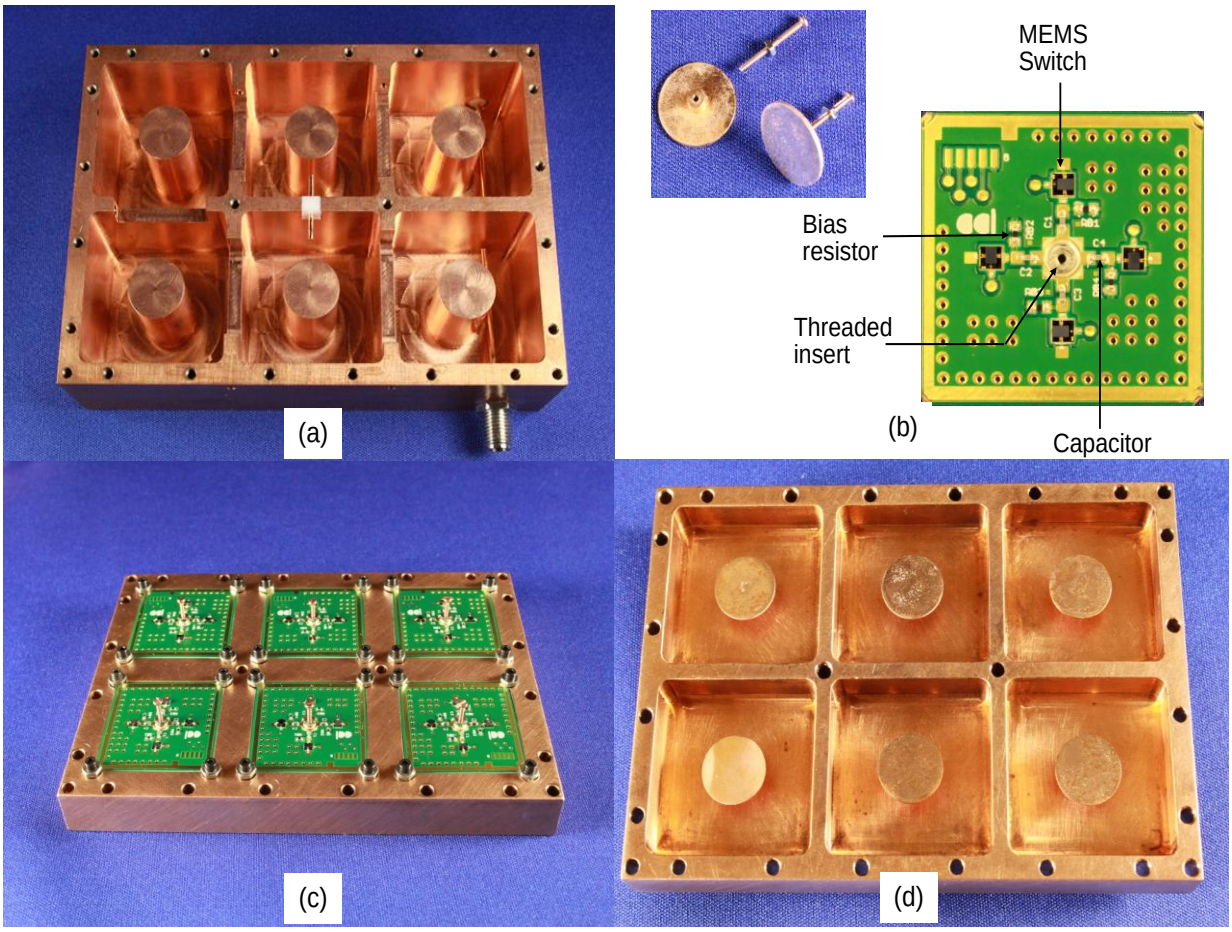

Figure 6.3-9 Picture of the fabricated filter: (a) the housing, (b) the components of the tuning disk and the circuit assembled with MEMS switches capacitor bank, (c) the top view of filter lid assembled with tuning circuits, and (d) the bottom view of lid assembled with tuning disks

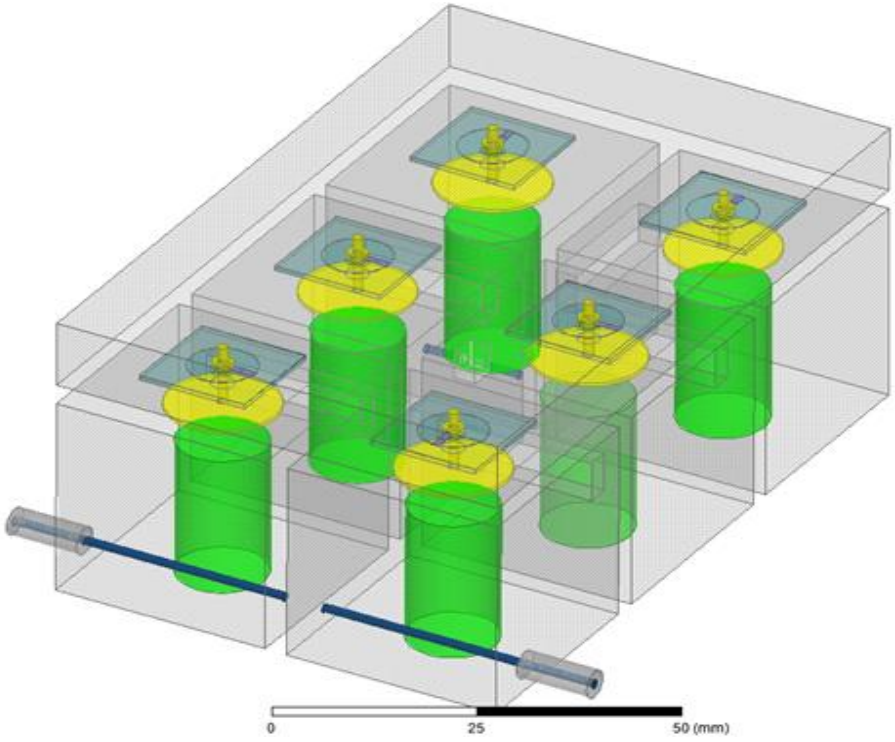

Figure 6.3-10 EM simulated model of a 6-pole filter with lumped capacitors

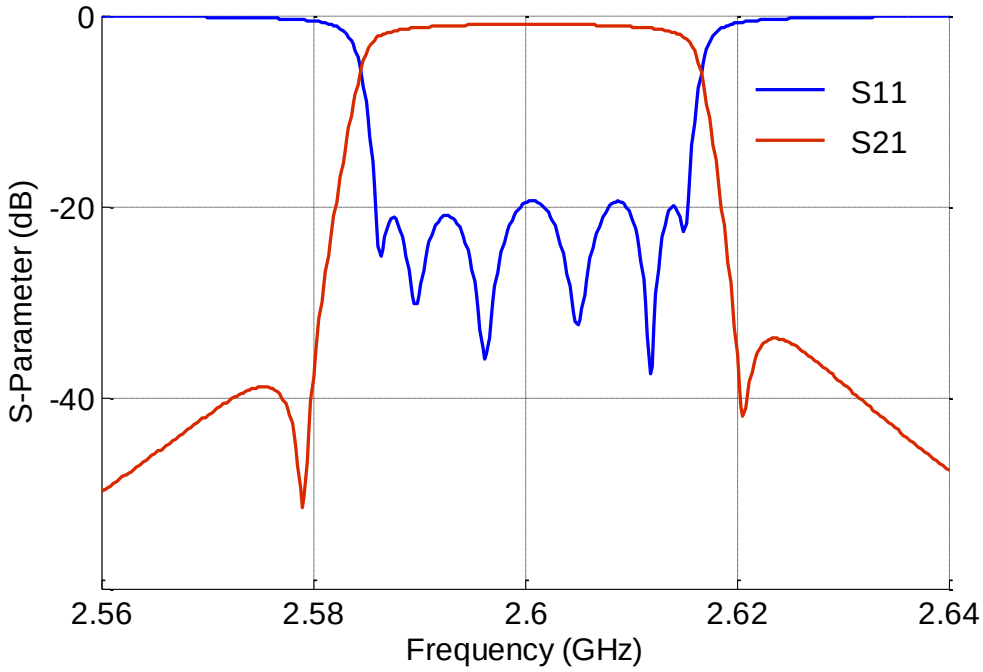

Figure 6.3-11 Simulation results of the 6-pole filter with lumped capacitance of 0.7pF on each circuits

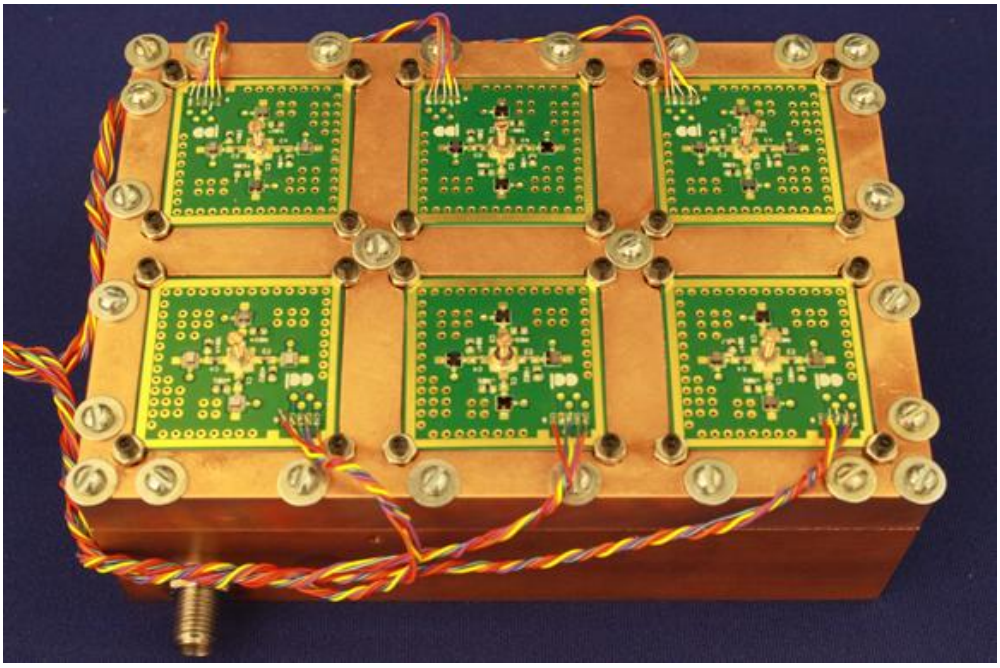

Figure 6.3-12 Picture of the assembled tunable filter with MEMS Switched Capacitor Bank

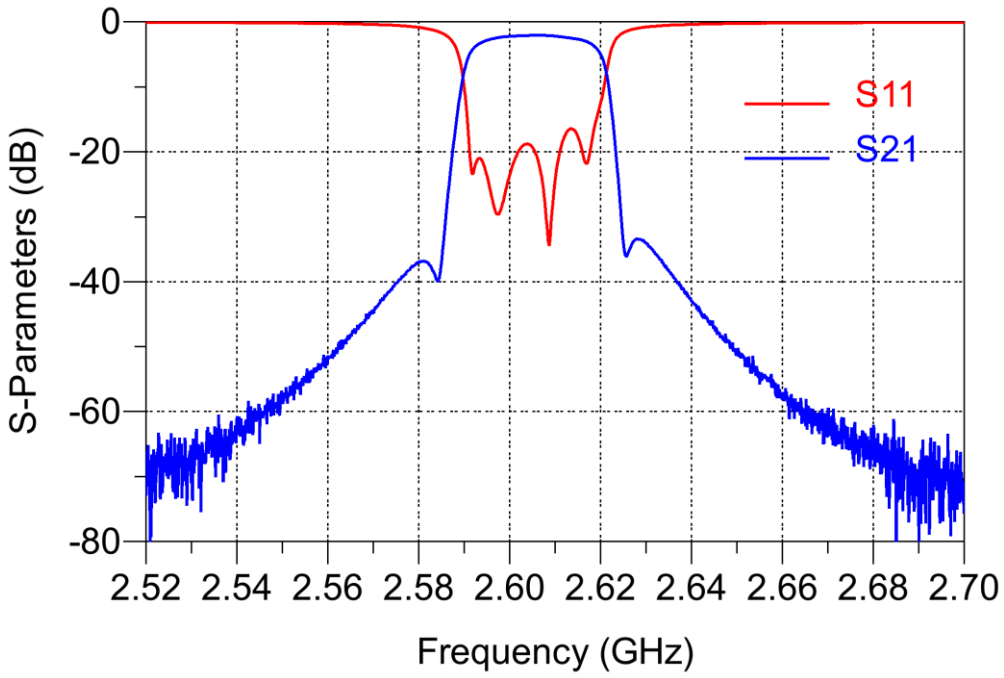

Figure 6.3-13 Initial tuned responses of the tunable filter with MEMS switches S2 and S3 on each resonator

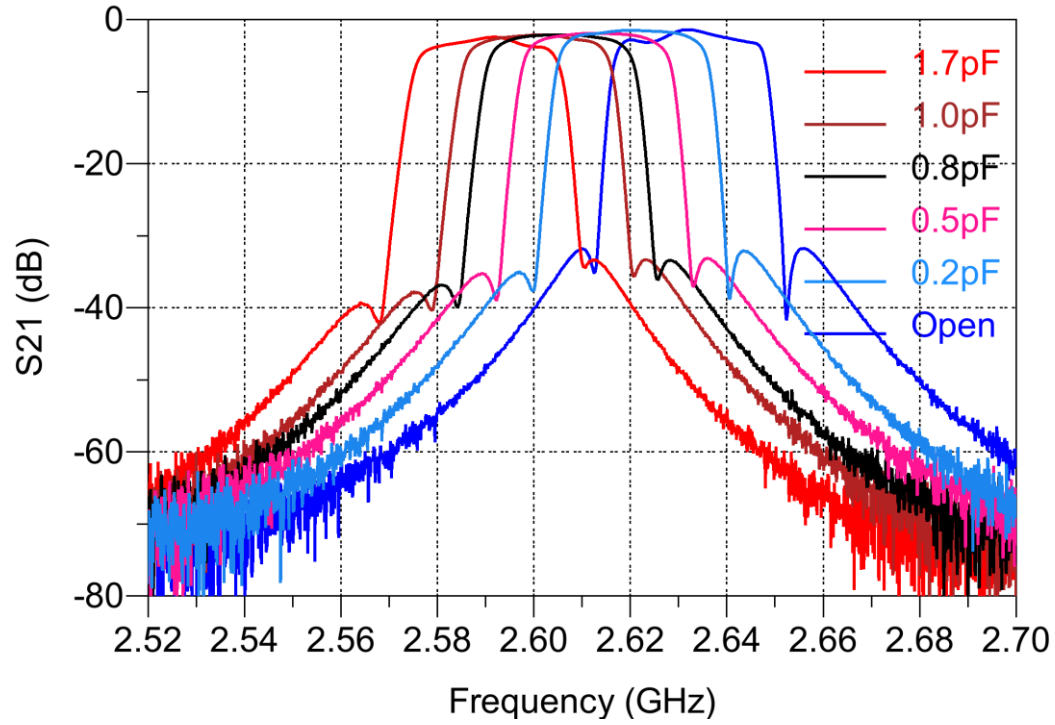

Figure 6.3-14 Measured tuning transmission responses of insertion loss

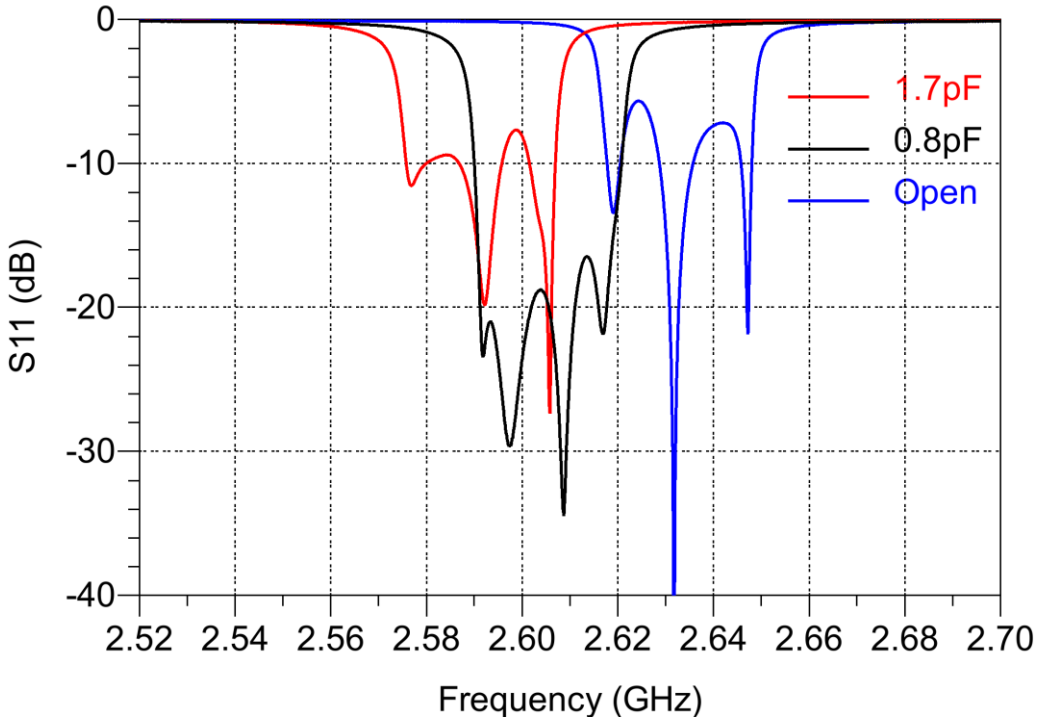

Figure 6.3-15 Measured tuning response of return loss

To solve the degradation problem of the 6-pole filter, an asynchronous tuning method is suggested. In order to tune the center frequency of the proposed filter, the total capacitance value of each resonator $C_{total,i}$ (i=1 to 6) must be tuned. Since the same capacitance values is used on each resonator $C_1 \ldots C_4$, when tuning the filter $C_{total,i}$ is the same for each resonator, the result is synchronous tuning of the resonators. However, based on the results of Figure 6.3-11, which is derived from optimized gaps with 0.7 pF capacitance loading on each resonator, the loaded capacitance are optimized to achieve a good response for the required low band at frequency of 2.565 GHz and the high band at frequency of 2.635 GHz. The achieved responses of asynchronous tuning are shown in Figure 6.3-16. The loaded capacitances from the simulation results are exhibited in Table 6.3-4. The table shows that for a 6-pole filter and in order to have a reasonable return loss (S_{11} & S_{22}) it is required to asynchronously tune each resonator and $C_{total,i}$ is different for i=1 to 6.

To realize asynchronous tuning, the MEMS switched capacitor bank with GaAs varactors shown in Figure 6.3-17 is a suggested replacement for the existing circuit. To tune the center frequency, the same MEMS switched capacitor bank is used as before. Addition of the GaAs varactor in parallel to the MEMS capacitor bank allows for fine tuning of $C_{total,i}$ for the resonators. The GaAs varactor does not require a wide tuning range (0.05~0.3 pF) and usually for these small capacitance values, GaAs varactors have a decent Q. However using this circuit, Q value, power handling and linearity of the proposed filter will be limited by the performance of the varactor.

Table 6.3-4 Simulation results of the loaded capacitance at different frequency

Loaded Capacitance	Low Band 2.565 GHz	Middle Band 2.6 GHz	High Band 2.635 GHz
$C_{total,1}=C_{total,6}$	1.135pF	0.7pF	0.276 pF
$C_{total,2}=C_{total,5}$	1.239 pF	0.7 pF	0.136 pF
$C_{total,3}=C_{total,4}$	1.187pF	0.7pF	0.199 pF

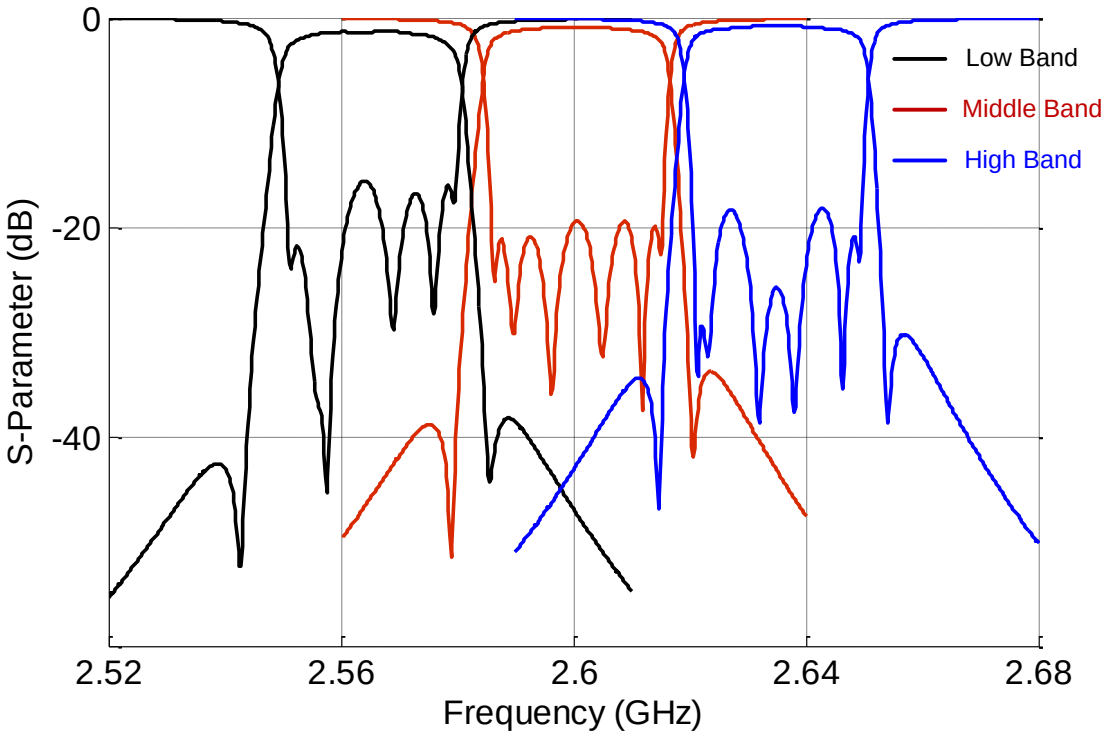

Figure 6.3-16 Simulation results of asynchronous tuning of the capacitance loading

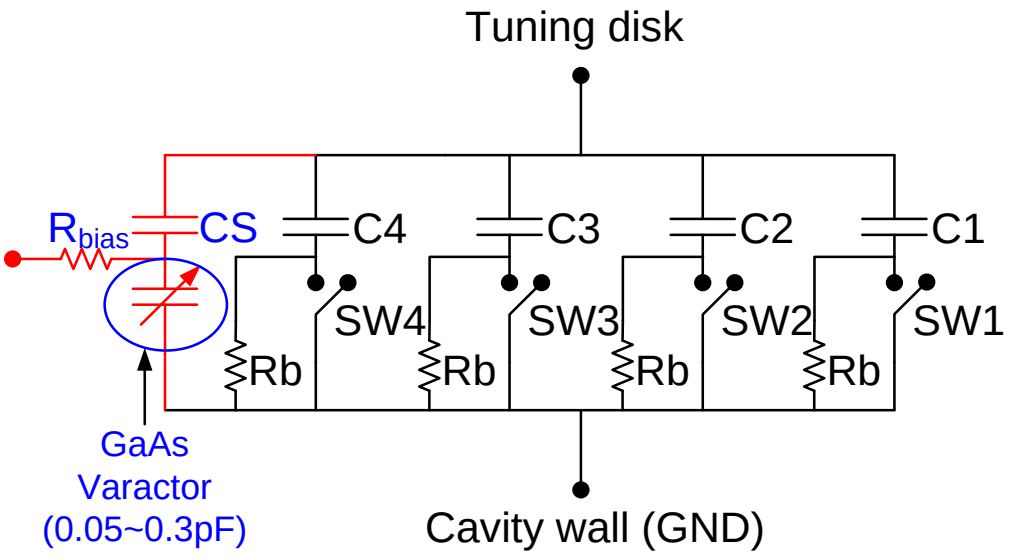

Figure 6.3-17 Schematic view of MEMS switched capacitor bank with a GaAs varactor

6.4 Summary

In this chapter, a novel electronic tuning approach to design tunable cavity combline filter is presented. The tuning is based on the capacitive loading instead of the mechanical movement of the tuning disk. The capacitive loading and as a result the center frequency can be adjusted by using RF-MEMS switched capacitor banks. The use of commercially available SPST contact type RF-MEMS switches makes the tunable resonator extremely compact, with near to zero dc power consumption for tuning and gives the resonator a fast tuning speed. In addition it also maintains a high-Q value of the filter over the entire tuning range by placing the tuning elements outside the cavity. Different filter prototypes are presented with two poles and six poles filter. The 2-pole tunable filter achieves a tuning range of 110 MHz with a Q value higher than 374 (1300-374) over the entire tuning range. The 6-pole filters are implemented using both MEMS tuning circuits and piezoelectric motors. The tunable filter with piezoelectric motors demonstrates superior RF performance with 70 MHz tuning range, insertion loss less than 2.2 dB and a rejection level better than 25 dB. The 6-pole filter with MEMS tuning circuits achieves a tuning range of 44 MHz while the insertion loss is better the 4.25 dB over the tuning range. To our knowledge this is the first implementation of a tunable bandpass filter with an order higher than two using commercially available RF-MEMS tuning circuits. The performance of the proposed filters can be further improved by utilizing asynchronous tuning of the resonators and also by using integrated RF-MEMS switched capacitor banks.

Chapter 7
Conclusions

The main focus of this thesis is on the development of high Q tunable filters based on 3D cavity resonators. The major contributions of this research are summarized below. Some of the research problems and issues will be addressed as a future work and are also listed in this chapter.

7.1 Contributions

The major contributions of this thesis are outlined as follows:

- A new approach for designing a compact high Q tunable dielectric resonator filter has been presented in the thesis [24]. The TME mode of a dielectric resonator is investigated to realize highly compact tunable dielectric filters. A customized design for a dielectric resonator is used to ensure the dominant mode of the DR would operate at TME mode. The mechanism used to tune the TME mode is based on varying the gap between the dielectric resonator and the cavity lid, since the TME mode is sensitive to this specific gap size. To miniaturize the tunable filter, the resonator is directly placed cavity bottom, which does not significantly change the resonant frequency of the TME mode. In this design, a piezoelectric bending actuator is used and placed outside the cavity; a flexible polyamide film laminated with copper is employed as the filter lid. The lid approaches the DR with the external force applied on the lid, and returns to its original position when the force is removed. A miniature piezoelectric tuning circuit is directly mounted on a polyamide surface to control the vertical deflection of the flexible lid. A similar approach can be applied to dielectric resonator dual-mode filters, which can result in an even more compact size in comparison with single-mode tunable DR filters.

- To design a miniature high Q tunable DR filter, methods of integrating DR resonators with tuning elements such as GaAs varactors, MEMS switches, and MEMS capacitor banks are investigated in the thesis [77, 78]. In this design, a disk type dielectric resonator with a hole in the center is employed in the tunable filter. Tuning circuits, which are made of printed metal integrated with

GaAs varactors, MEMS switches, or a MEMS capacitor bank, are placed in the center hole of the dielectric resonator. A coupling exists between the circuits and DR TME mode; thus the mechanism for tuning the DR TME mode is through the existing coupling from the circuits, which can be controlled by GaAs varactors, MEMS switches, or a MEMS capacitor bank. This novel design can maintain a relatively high Q over the tuning range without increasing the volume of the cavity size. This tuning philosophy can be expanded to other frequencies and other dielectric resonator modes.

- In majority of applications, the tunable filter needs technique to have a constant bandwidth over the tuning range. In this thesis, a method to design a tunable 3D cavity filter with constant bandwidth is presented [107]. The main idea in this design is to have a balanced electric and magnetic coupling for both input coupling and inter-resonator coupling over the tuning range. Therefore, the coupling matrix of the designed filter is identical when the filter's operating center frequency changes. Based on this idea, a four-pole evanescent mode combline tunable filter is designed and demonstrated with manually and piezoelectric motor tuning. This design can be expanded to other frequencies of 3D cavity tunable filters for a constant bandwidth.
- A novel approach to design a tunable cavity combline filter tuned by a MEMS switched capacitor bank is presented in the thesis [105, 108, 109]. Each MEMS switched capacitor comprises a plurality of fixed-value capacitors, switches, and direct current bias circuits. Each tuning disk loading on each resonator of the combline filter and the ground (filter cavity) is connected by a MEMS switched capacitor bank. The total capacitance loading on the tuning disk varies with the combination of MEMS switches at the 'ON' or 'OFF' status. Thus, the frequency of each resonator can be adjusted by the capacitance loading on its tuning disk. As a result, the combline filter can be tuned by a MEMS switched capacitor bank. This novel tuning device paves the way for cavity combline filter to be easily tuned electrically. This tuning can be extended to other frequencies of cavity combline filters and cavity dielectric resonator filters.

7.2 Future Work

The most critical components which affect the Q values in tunable filters are the resonator Q and the Q of the tuning element. The high Q 3D cavity resonator integrated with low Q tuning elements would results in a lowered total Q, thereby limiting its application as tunable filters in transceiver systems. For more extensive research and a wider range topic in designing electrical

tunable 3D cavity filters, there are some related research topics in this area that can be possibly explored in the future:

- **Integration of 3D Cavity filters with thick metal circuits:** Compared to the thin metal circuits, thick metal has less resistance. To increase the tuning range, the tuning circuits are usually located in the place where the electric fields are dense; the Q value of the cavity resonator is sensitive to the resistance of the tuning circuit. Therefore, tunable thick metal circuits can improve the Q of the 3D tunable cavity filter.
- **The use of a tuning circuit on high – K material:** Typically, the tuning circuits comprise of metal circuits and substrate. Compared to the high-K DR material, the substrate of the tuning circuits is loss. If tuning circuits are directly built on the dielectric resonator, the loss caused by the substrate can be ignored. As a result, the Q value of the tunable resonator will improve.
- **Development of tunable dual mode or dual band filters:** To further improve the performance of the tunable dielectric resonator filters, tunable dual mode and tunable dual band filters can be considered.

Bibliography

[1] Bruce A. Fette, "Connitive radio technology," 2nd ed, Oxford, UK: Elsevier, 2009.

[2] S. Sarraf and L. Rulli, "Low cost, broadband tunable ferroelectric filters for JTRS Cluster 5 applications," *Ferroelectrics*, vol. 342, pp. 129-40, 2006.

[3] P. Eskelinen, "Introduction to RF equipment and system design," Boston, MA: Artech House, 2004.

[4] Cameron, R. Kudsia, C. Mansour, R, "Microwave filters for communication systems: Fundamentals, design, and applications," 1st ed, Hoboken, New Jersey: John Wiley & Sons, Inc., 2007.

[5] R. Zhang and R. R. Mansour, "Low-cost dielectric-resonator filters with improved spurious performance," *IEEE Trans. Microwave Theory Tech.*, vol. 55, pp. 2168-75, 10, 2007.

[6] M. Memarian and R. R. Mansour, "Dual-mode half-cut dielectric resonator filters," in *2009 IEEE MTT-S International Microwave Symposium Digest (MTT)*, 2009, pp. 1465-8.

[7] I. C. Hunter and J. D. Rhodes, "Electronically tunable microwave bandstop filters," *IEEE Trans. Microwave Theory Tech.*, vol. MTT-30, pp. 1361-7, 1982.

[8] R. M. Young, C. R. Vale, T. T. Braggins, S. V. Krishnaswamy, C. E. Milton, D. W. Bever, L. G. Chorosinski, L. Chen, D. E. Crockett, C. B. Freidhoff, S. H. Talisa, E. Capelle, R. Tranchini, J. R. Fende, J. M. Lorthioir, A. R. Torres and J. Douglas Adam, "Low-loss bandpass RF filter using MEMS capacitance switches to achieve a one-octave tuning range and independently variable bandwidth," in *2003 IEEE MTT-S International Microwave Symposium Digest*, 2003, pp. 1781-1784.

[9] K. Entesari, "A differential 4-bit 6.5-10-GHz RF MEMS tunable filter," in *Microwave Theory and Techniques, IEEE Transactions on*, G. M. Rebeiz, Ed. 2005, pp. 1103-1110.

[10] M. F. Karim, A. Q. Liu, A. Alphones and A. B. Yu, "A tunable bandstop filter via the capacitance change of micromachined switches," *J Micromech Microengineering*, vol. 16, pp. 851-861, 2006.

[11] S. -. Park, M. A. El-Tanani, I. Reines and G. M. Rebeiz, "Low-Loss 4–6-GHz Tunable Filter With 3-Bit High- Orthogonal Bias RF-MEMS Capacitance Network," *Microwave Theory and Techniques, IEEE Transactions on,* vol. 56, pp. 2348-2355, 2008.

[12] A. B. Yu, A. Q. Liu and Q. X. Zhang, "Wide tuning range MEMS band-pass filter with inductance change," in *Digest of Technical Papers*, 2005, pp. 2061-4.

[13] G. L. Matthaei, L. Young, and E. M. T. Jones, "Microwave filters, impedance-matching networks, and coupling structures," Norwood, MA: Artech House, Inc, 1980.

[14] B. Yassini, Ming Yu, D. Smith and S. Kellett, "A Ku-Band High-Q Tunable Filter With Stable Tuning Response," *Microwave Theory and Techniques, IEEE Transactions on,* vol. 57, pp. 2948-2957, 2009.

[15] M. Hoeft, A. Kronberger and O. Bartz, "Tunable bandpass filters for multi-standard applications," in *Microwave Conference (GeMIC), 2008 German*, 2008, pp. 1-4.

[16] S. -. Chen, K. A. Zaki and R. G. West, "Tunable, temperature-compensated dielectric resonators and filters," *Microwave Theory and Techniques, IEEE Transactions on,* vol. 38, pp. 1046-1052, 1990.

[17] J. Uher and W. J. R. Hoefer, "Tunable microwave and millimeter-wave band-pass filters," *Microwave Theory and Techniques, IEEE Transactions on,* vol. 39, pp. 643-653, 1991.

[18] Tao Shen, K. A. Zaki and Chi Wang, "Tunable dielectric resonators with dielectric tuning disks," *Microwave Theory and Techniques, IEEE Transactions on,* vol. 48, pp. 2439-2445, 2000.

[19] C. Wang and W. D. Blair, "Tunable high-Q dielectric loaded resonator and filter," in *IEEE Radio and Wireless Conference*, 2002, pp. 249-52.

[20] K.Wakino, H. Tamura, and Isikawa, *"Dielectric resonator device,"* Available: U .Patent, Ed. US,Sept. 8, 1987.

[21] Tae-Yeoul Yun and Kai Chang, "Piezoelectric-transducer-controlled tunable microwave circuits," *Microwave Theory and Techniques, IEEE Transactions on,* vol. 50, pp. 1303-1310, 2002.

[22] M. Al-Ahmad, R. Matz and P. Russer, "Piezoelectric tuned LTCC bandpass filters," in *Microwave Symposium Digest, 2006. IEEE MTT-S International*, 2006, pp. 764-767.

[23] H. Joshi, H. H. Sigmarsson, D. Peroulis and W. J. Chappell, "Highly loaded evanescent cavities for widely tunable high-Q filters," in *2007 IEEE MTT-S International Microwave Symposium, IMS 2007,* 2007, pp. 2133-2136.

[24] F. Huang and R. R. Mansour, "Tunable compact dielectric resonator filters," in *Microwave Conference, 2009. EuMC 2009. European,* 2009, pp. 559-562.

[25] G. I. Panaitov, R. Ott and N. Klein, "Dielectric resonator with discrete electromechanical frequency tuning," *Microwave Theory and Techniques, IEEE Transactions on,* vol. 53, pp. 3371-3377, 2005.

[26] O. Y. Buslov, V. N. Keys, A. B. Kozyrev, I. V. Kotelnikov, P. V. Kulik, N. M. Alford and P. K. Petrov, "Tuneable piezoelectric filter based on a dual-mode dielectric resonator," in *Microwave and Telecommunication Technology, 2004. CriMico 2004. 2004 14th International Crimean Conference on,* 2004, pp. 410-411.

[27] Wenxing Tang and Jia-Sheng Hong, "Varactor-Tuned Dual-Mode Bandpass Filters," *Microwave Theory and Techniques, IEEE Transactions on,* vol. 58, pp. 2213-2219, 2010.

[28] E. E. Djoumessi, M. Chaker and K. Wu, "Varactor-tuned quarter-wavelength dual-bandpass filter," *Microwaves, Antennas & Propagation, IET,* vol. 3, pp. 117-124, 2009.

[29] Byung-Wook Kim and Sang-Won Yun, "Varactor-tuned combline bandpass filter using step-impedance microstrip lines," *Microwave Theory and Techniques, IEEE Transactions on,* vol. 52, pp. 1279-1283, 2004.

[30] S. R. Chandler, "Active varactor tunable microwave filters," in *European Microwave Conference, 1993. 23rd*, I. C. Hunter, Ed. 1993, pp. 244-245.

[31] T. S. Martin, F. Wang and K. Chang, "Theoretical and experimental investigation of novel varactor-tuned switchable microstrip ring resonator circuits," *Microwave Theory and Techniques, IEEE Transactions on,* vol. 36, pp. 1733-1739, 1988.

[32] A. R. Brown and G. M. Rebeiz, "A varactor-tuned RF filter," *Microwave Theory and Techniques, IEEE Transactions on,* vol. 48, pp. 1157-1160, 2000.

[33] A. R. Brown and G. M. Rebeiz, "Micromachined micropackaged filter banks and tunable bandpass filters," in *Wireless Communications Conference, 1997., Proceedings,* 1997, pp. 193-197.

[34] Y. -. Shu, J. A. Navarro and K. Chang, "Electronically switchable and tunable coplanar waveguide-slotline band-pass filters," *Microwave Theory and Techniques, IEEE Transactions on,* vol. 39, pp. 548-554, 1991.

[35] Jian Xu, Xiao-Peng Liang and K. Shamsaifar, "Full wave analysis and design of RF tunable filters," in *Microwave Symposium Digest, 2001 IEEE MTT-S International,* 2001, pp. 1449-1452 vol.3.

[36] X. Y. Zhang, C. H. Chan, Q. Xue and B. -. Hu, "RF Tunable Bandstop Filters With Constant Bandwidth Based on a Doublet Configuration," *Industrial Electronics, IEEE Transactions on,* vol. 59, pp. 1257-1265, 2012.

[37] A. M. E. Safwat, F. Podevin, P. Ferrari and A. Vilcot, "Tunable Bandstop Defected Ground Structure Resonator Using Reconfigurable Dumbbell-Shaped Coplanar Waveguide," *Microwave Theory and Techniques, IEEE Transactions on,* vol. 54, pp. 3559-3564, 2006.

[38] R. Zhang and R. R. Mansour, "Novel tunable lowpass filters using folded slots etched in the ground plane," in *2005 IEEE MTT-S International Microwave Symposium,* 2005, pp. 775-778.

[39] B. S. Virdee, "Effective technique for electronically tuning a dielectric resonator," *Electronics Letters,* vol. 33, pp. 301-302, 1997.

[40] B. S. Virdee, A. S. Virdee and L. A. Trinogga, "Novel invasive electronic tuning of dielectric resonators," in *Microwave Symposium Digest, 2003 IEEE MTT-S International,* 2003, pp. 51-54 vol.1.

[41] O. Y. Buslov, Chong-Yun Kang, V. N. Keis, I. V. Kotelnikov, A. Y. Shimko, M. F. Ivanova, A. V. Tumarkin, S. F. Karmanenko and A. B. Kozyrev, "Dielectric resonators loaded by ferroelectric varactors for tunable Ka band filter," *Integrated Ferroelectr.,* vol. 86, pp. 171-9, 2006.

[42] Manh-Tai Nguyen, W. D. Yan and E. P. W. Horne, "Broadband tunable filters using high Q passive tunable ICs," in *Microwave Symposium Digest, 2008 IEEE MTT-S International,* 2008, pp. 951-954.

[43] K. B. Kim, "Tunable dual-mode filter using varactor and variable ring resonator on integrated BST/TiO_2/Si substrate," *Electronics Letters,* vol. 46, pp. 509-511, 2010.

[44] Young-Hoon Chun, Jia-Sheng Hong, P. Bao, T. J. Jackson and M. J. Lancaster, "BST-varactor tunable dual-mode filter using variable ZC transmission line," *IEEE Microwave and Wireless Components Letters*, vol. 18, pp. 167-9, 03, 2008.

[45] Ken Zhang, T. Watson, A. Cardona and M. Fink, "BaSrTiO3-based 30–88MHz tunable filter," in *Microwave Symposium Digest (MTT), 2010 IEEE MTT-S International*, 2010, pp. 1492-1495.

[46] J. Nath, D. Ghosh, J. -. Maria, A. I. Kingon, W. Fathelbab, P. D. Franzon and M. B. Steer, "An electronically tunable microstrip bandpass filter using thin-film Barium-Strontium-Titanate (BST) varactors," *Microwave Theory and Techniques, IEEE Transactions on*, vol. 53, pp. 2707-2712, 2005.

[47] D. Kuylenstierna, A. Vorobiev and S. Gevorgian, "40 GHz lumped element tunable bandpass filters with transmission zeros based on thin Ba/sup 0.25/Sr/sup 0.75/TiO/sup 3/ (BST) film varactors," in *Silicon Monolithic Integrated Circuits in RF Systems, 2006. Digest of Papers. 2006 Topical Meeting on*, 2006, pp. 4 pp.

[48] Young-Hoon Chun, Jia-Sheng Hong, Peng Bao, T. J. Jackson and M. J. Lancaster, "Tunable bandstop filters using BST varactor chips," in *Microwave Conference, 2007. European*, 2007, pp. 110-113.

[49] Y. Chun, H. Shaman and J. Hong, "Switchable embedded notch structure for UWB bandpass filter," *IEEE Microwave and Wireless Components Letters*, vol. 18, pp. 590-592, 2008.

[50] A. Tombak, F. T. Ayguavives, J. Maria, G. T. Stauf, A. I. Kingon and A. Mortazawi, "Low voltage tunable barium strontium titanate thin film capacitors for RF and microwave applications," *IEEE MTT S Int. Microwave Symp. Dig.*, vol. 3, pp. 1345-1348, 2000.

[51] M. Ouaddari, S. Delprat, F. Vidal, M. Chaker and Ke Wu, "Microwave characterization of ferroelectric thin-film materials," *Microwave Theory and Techniques, IEEE Transactions on*, vol. 53, pp. 1390-1397, 2005.

[52] M. Sterns, M. Hrobak, S. Martius and L. -. Schmidt, "Magnetically tunable filter from 72 GHz to 95 GHz," in *German Microwave Conference, 2010*, 2010, pp. 82-85.

[53] B. K. Kuanr, V. Veerakumar, K. Lingam, S. R. Mishra, A. V. Kuanr, R. E. Camley and Z. Celinski, "Microstrip-Tunable Band-Pass Filter Using Ferrite (Nanoparticles) Coupled Lines," *Magnetics, IEEE Transactions on*, vol. 45, pp. 4226-4229, 2009.

[54] Zhou Hao-Miao, Xia Zhe-Lei and Deng Juan-Hu, "The research of dual-tunable magnetoelectric microwave filters: Numerical simulation of the magnetoelectric microwave filters based on theoretical model of electric tuning ferromagnetic resonance," in *Communications and Mobile Computing (CMC), 2011 Third International Conference on*, 2011, pp. 258-261.

[55] C. S. Tsai, G. Qiu, H. Gao, L. W. Yang, G. P. Li, S. A. Nikitov and Y. Gulyaev, "Tunable wideband microwave band-stop and band-pass filters using YIG/GGG-GaAs layer structures," *Magnetics, IEEE Transactions on*, vol. 41, pp. 3568-3570, 2005.

[56] J. Clarke and M. R. B. Dunsmore, "High-power tunable YIG filters," *Microwaves, Antennas and Propagation, IEE Proceedings H*, vol. 132, pp. 251-254, 1985.

[57] Guo-Min Yang, Jing Lou, Jing Wu, Ming Liu, Geyi Wen, Yaqiu Jin and N. X. Sun, "Dual H-and E-field tunable multiferroic bandpass filters with yttrium iron garnet film," in *Microwave Symposium Digest (MTT), 2011 IEEE MTT-S International*, 2011, pp. 1-4.

[58] A. N. Farr, G. N. Blackie and D. Williams, "NOVEL TECHNIQUES FOR ELECTRONIC TUNING OF DIELECTRIC RESONATORS." in *Conference Proceedings - 13th European Microwave Conference*. 1983, pp. 791-796.

[59] J. Krupka, A. Abramowicz and K. Derzakowski, "Magnetically tunable filters for cellular communication terminals," *Microwave Theory and Techniques, IEEE Transactions on*, vol. 54, pp. 2329-2335, 2006.

[60] J. Krupka, A. Abramowicz and K. Derzakowski, "Tunable dielectric resonator bandpass filter," in *MIKON-2000*, 2000, pp. 517-20.

[61] K. Entesari, "A 12–18-GHz three-pole RF MEMS tunable filter," in *Microwave Theory and Techniques, IEEE Transactions on*, G. M. Rebeiz, Ed. 2005, pp. 2566-2571.

[62] K. Entesari, "A 25–75-MHz RF MEMS tunable filter," in *Microwave Theory and Techniques, IEEE Transactions on*, K. Obeidat, Ed. 2007, pp. 2399-2405.

[63] E. Fourn, A. Pothier, C. Champeaux, P. Tristant, A. Catherinot, P. Blondy, G. Tanne, E. Rius, C. Person and F. Huret, "MEMS switchable interdigital coplanar filter," *Microwave Theory and Techniques, IEEE Transactions on*, vol. 51, pp. 320-324, 2003.

[64] L. Dussopt, "Intermodulation distortion and power handling in RF MEMS switches, varactors, and tunable filters," in *Microwave Theory and Techniques, IEEE Transactions on*, G. M. Rebeiz, Ed. 2003, pp. 1247-1256.

[65] C. L. Goldsmith, Z. Yao, S. Eshelman and D. Denniston, "Performance of low-loss RF MEMS capacitive switches," *IEEE Microwave Guided Wave Lett.*, vol. 8, pp. 269-271, 1998.

[66] S. -. Park, K. -. Lee and G. M. Rebeiz, "Low-Loss 5.15–5.70-GHz RF MEMS Switchable Filter for Wireless LAN Applications," *Microwave Theory and Techniques, IEEE Transactions on*, vol. 54, pp. 3931-3939, 2006.

[67] A. Abbaspour-Tamijani, L. Dussopt and G. M. Rebeiz, "Miniature and tunable filters using MEMS capacitors," *Microwave Theory and Techniques, IEEE Transactions on*, vol. 51, pp. 1878-1885, 2003.

[68] Sanghyo Lee, Jong-Man Kim, Jung-Mu Kim, Yong-Kweon Kim and Youngwoo Kwon, "Millimeter-wave MEMS tunable low pass filter with reconfigurable series inductors and capacitive shunt switches," *Microwave and Wireless Components Letters, IEEE*, vol. 15, pp. 691-693, 2005.

[69] D. Peroulis, S. Pacheco, K. Sarabandi and L. P. B. Katehi, "Tunable lumped components with applications to reconfigurable MEMS filters," in *Microwave Symposium Digest, 2001 IEEE MTT-S International*, 2001, pp. 341-344 vol.1.

[70] Hong-Teuk Kim, Jae-Hyoung Park, Yong-Kweon Kim and Youngwoo Kwon, "Low-loss and compact V-band MEMS-based analog tunable bandpass filters," *Microwave and Wireless Components Letters, IEEE*, vol. 12, pp. 432-434, 2002.

[71] Sang-June Park, I. Reines, C. Patel and G. M. Rebeiz, "High- RF-MEMS 4–6-GHz Tunable Evanescent-Mode Cavity Filter," *Microwave Theory and Techniques, IEEE Transactions on*, vol. 58, pp. 381-389, 2010.

[72] M. A. El-Tanani and G. M. Rebeiz, "High-Performance 1.5–2.5-GHz RF-MEMS Tunable Filters for Wireless Applications," *Microwave Theory and Techniques, IEEE Transactions on*, vol. 58, pp. 1629-1637, 2010.

[73] I. Reines, Sang-June Park and G. M. Rebeiz, "Compact Low-Loss Tunable -Band Bandstop Filter With Miniature RF-MEMS Switches," *Microwave Theory and Techniques, IEEE Transactions on*, vol. 58, pp. 1887-1895, 2010.

[74] Firas Sammoura and Liwei Lin, "A plastic W-band MEMS tunable filter," in *Microwave Symposium Digest, 2006. IEEE MTT-S International*, 2006, pp. 136-139.

[75] W. D. Yan and R. R. Mansour, "Micromachined millimeter-wave ridge waveguide filter with embedded MEMS tuning elements," in *2006 IEEE MTT-S International Microwave Symposium Digest,* 2006, pp. 1290-1293.

[76] W. D. Yan and R. R. Mansour, "Tunable Dielectric Resonator Bandpass Filter With Embedded MEMS Tuning Elements," *Microwave Theory and Techniques, IEEE Transactions on,* vol. 55, pp. 154-160, 2007.

[77] Fengxi Huang, S. Fouladi and R. Mansour, "A novel MEMS-based tunable dielectric resonator filter," in *Microwave Symposium Digest (MTT), 2011 IEEE MTT-S International,* 2011, pp. 1-4.

[78] F. Huang, S. Fouladi and R. R. Mansour, "High-Q Tunable Dielectric Resonator Filters Using MEMS Technology," *Microwave Theory and Techniques, IEEE Transactions on,* vol. 59, pp. 3401-3409, 2011.

[79] G. L. Matthaei, "Narrow-band, fixed-tuned, and tunable bandpass filters with zig-zag hairpin-comb resonators," *Microwave Theory and Techniques, IEEE Transactions on,* vol. 51, pp. 1214-1219, 2003.

[80] W. L. Jones, "Design of tunable combline filters of near-constant bandwidth," *Electronics Letters,* vol. 1, pp. 156-158, 1965.

[81] M. A. El-Tanani and G. M. Rebeiz, "Corrugated Microstrip Coupled Lines for Constant Absolute Bandwidth Tunable Filters," *Microwave Theory and Techniques, IEEE Transactions on,* vol. 58, pp. 956-963, 2010.

[82] L. Athukorala and D. Budimir, "Compact Second-Order Highly Linear Varactor-Tuned Dual-Mode Filters With Constant Bandwidth," *Microwave Theory and Techniques, IEEE Transactions on,* vol. 59, pp. 2214-2220, 2011.

[83] N. Zahirovic, S. Fouladi, R. R. Mansour and M. Yu, "Tunable suspended substrate stripline filters with constant bandwidth," in *Microwave Symposium Digest (MTT), 2011 IEEE MTT-S International,* 2011, pp. 1-4.

[84] Han-Ul Moon, Seung-Un Choi, Young-Ho Cho and Sang-Won Yun, "Size-reduced tunable hairpin bandpass filter using aperture coupling with enhanced selectivity and constant bandwidth," in *Microwave Symposium Digest, 2008 IEEE MTT-S International,* 2008, pp. 747-750.

[85] Hong-Lin Zhang, Xiu Yin Zhang and Bin-Jie Hu, "Tunable bandpass filters with constant absolute bandwidth," in *Antennas Propagation and EM Theory (ISAPE), 2010 9th International Symposium on,* 2010, pp. 1200-1203.

[86] H. Tanbakuchi, D. Nicholson, B. Kunz and W. Ishak, "Magnetically tunable oscillators and filters," in *1989 International Magnetics Conference, INTERMAG '89,* 1989, pp. 3248-53.

[87] B. Farhang-Boroujeny, "Filter bank spectrum sensing for cognitive radios," *IEEE Transactions on Signal Processing,* vol. 56, pp. 1801-11, 05, 2008.

[88] Walter Tuttlebee, "Software defined radio:Enabling technologies," in Anonymous Baffins Lane, Chichester, West Sussex, PO19 1UD, England: John Wiley & Sons Ltd, 2002, pp. 402.

[89] B. Noren, "Thin film barium strontium titanate (BST) for a new class of tunable RF components," *Microwave Journal, Euro-Global Edition,* vol. 47, pp. 210, 222, 214, 216, 218, 220, 05, 2004.

[90] M. K. Roy and J. Richter, "Tunable ferroelectric filters for software defined tactical radios," in *ISAF 2006,* 2007, pp. 348-51.

[91] N. M. Alford, O. Buslov, V. Keis, I. Kotelnikov, A. Kozyrev, P. Kulik and P. K. Petrov, "Tunable 4-pole piezoelectric filter based on two dielectric resonators," *Integrated Ferroelectr.,* vol. 77, pp. 123-8, 2005.

[92] T. Shen, C. Wang and K. A. Zaki, "Tunable dielectric resonators with dielectric tuning disks in rectangular enclosures," in *European Microwave Conference, 2000. 30th,* 2000, pp. 1-4.

[93] B. S. Virdee, "Tunable dielectric resonator bandpass filters," in *Proceedings of Asia-Pacific Microwave Conference,* 1998, pp. 1353-7.

[94] Chi Wang and W. D. Blair, "Tunable high-Q dielectric loaded resonator and filter," in *Radio and Wireless Conference, 2002. RAWCON 2002. IEEE,* 2002, pp. 249-252.

[95] K. Pance, "Multiband tunable dielectric resonator filters," in *Radio and Wireless Symposium, 2006 IEEE,* 2006, pp. 395-398.

[96] K. Derzakowski, J. Krupka and A. Abramowicz, "Magnetically tunable dielectric resonators and filters," in *34th European Microwave Conference,* 2004, pp. 1121-4.

[97] Xiaoguang Liu, L. P. B. Katehi, W. J. Chappell and D. Peroulis, "High-Q Tunable Microwave Cavity Resonators and Filters Using SOI-Based RF MEMS Tuners," *Microelectromechanical Systems, Journal of,* vol. 19, pp. 774-784, 2010.

[98] R. Stefanini, M. Chatras, A. Pothier, J. -. Orlianges and P. Blondy, "High Q tunable cavity using dielectric less RF-MEMS varactors," in *Microwave Conference, 2009. EuMC 2009. European,* 2009, pp. 1444-1447.

[99] S. -. Park, I. Reines and G. Rebeiz, "High-Q RF-MEMS tunable evanescent-mode cavity filter," in *Microwave Symposium Digest, 2009. MTT '09. IEEE MTT-S International,* 2009, pp. 1145-1148.

[100] D. Scarbrough, C. Goldsmith, J. Papapolymerou and Yuan Li, "Miniature microwave RF MEMS tunable waveguide filter," in *Microwave Integrated Circuits Conference, 2009. EuMIC 2009. European,* 2009, pp. 507-510.

[101] G. F. Craven and C. K. Mok, "The design of evanescent mode waveguide bandpass filters for a prescribed insertion loss characteristic," *IEEE Trans. Microwave Theory Tech.,* vol. MTT-19, pp. 295-308, 03, 1971.

[102] Y. C. Li and Q. Xue, "Tunable Balanced Bandpass Filter With Constant Bandwidth and High Common-Mode Suppression," *Microwave Theory and Techniques, IEEE Transactions on,* vol. 59, pp. 2452-2460, 2011.

[103] G. Tsuzuki, M. Hernandez, E. M. Prophet, S. Jimenez and B. A. Willemsen, "Ultra-selective constant-bandwidth electromechanically tunable HTS filters," in *Microwave Symposium Digest, 2006. IEEE MTT-S International,* 2006, pp. 693-696.

[104] M. A. Kunes and G. G. Connor, "A diqitally controlled tunable high power output filter for space apllications," in *Microwave Conference, 1989. 19th European,* 1989, pp. 681-686.

[105] S. Fouladi, F. Huang, W. D. Yan and R. Mansour, "Combline tunable bandpass filter using RF-MEMS switched capacitor bank," in *Microwave Symposium Digest (MTT), 2012 IEEE MTT-S International,* 2012, pp. 1-3.

[106]Piezoelectric ultrasonic motors, in, http://mmech.com/ultrasonic-motors/linear-motors.

[107] F. Huang, S. Fouladi and R. R. Mansour, "A Tunable Bandpass Filter with Absolute Constant Bandwidth Based on a Balanced Coupling Scheme," *To be submitted to Microwave Theory and Techniques, IEEE Transactions,* 2012.

[108] Fouladi, S. Huang, F. Yan, D. and Mansour, R., *"Tunable Bandpass Filter Device and Method,"* 2012 US Patent No.61/567,506.

[109] S. Fouladi, F. Huang, D. Yan and R. Mansour, "High-Q Narrowband Tunable Combline Bandpass Filters Using MEMS Capacitor Banks and Piezomotors," *Accepted by Microwave Theory and Techniques, IEEE Transactions,* September 2012.